Application of Modified Chitosan for Recovery of Heavy Metals Found in Spent Batteries

Ataollah Babakhani

Thesis Submitted to the University of Ottawa

in Partial Fulfillment of the Requirements for the Degree of

Doctor of Philosophy in Environmental Engineering*

Department of Civil Engineering

Faculty of Engineering

University of Ottawa

*The Doctor of Philosophy in Environmental Engineering is a Joint Program with Carleton University, administrated by the Ottawa-Carleton Institute for Environmental Engineering

Abstract

Finding economical and environmentally friendly processes to recover heavy metals (HMs) from spent batteries is a research priority to move toward sustainability. Adsorption seems an acceptable procedure to replace the current separation/purification stage of hydrometallurgical techniques. Chitosan is an efficient adsorbent for HM uptake from aqueous solutions. Nevertheless, in practice, chitosan modification is unavoidable to improve its physicochemical properties. Sodium tripolyphosphate is an environmentally benign crosslinker that can be used for chitosan modification. In addition, ion-imprinting technique could potentially enhance the adsorption efficiency and selectivity of crosslinked chitosan. Considering the above, the primary purposes of this research were: investigating the adsorption efficiency of chitosan for heavy metals uptake from synthetic solutions; modifying chitosan by crosslinking alone and combined with ion-imprinting techniques to improve the physicochemical properties as well as adsorption capacity and selectivity of chitosan; evaluating and comparing the adsorption efficiency of modified chitosan beads for the adsorption of Cd(II), Ni(II) and Co(II) in single and multicomponent batch adsorption systems.

Chitosan and sodium tripolyphosphate crosslinked chitosan beads were prepared to remove Cd(II) from aqueous solution in the first phase. FTIR and XRD of the synthesized beads showed partial consumption of chitosan amine groups and a decrease in crystallinity of chitosan structure over crosslinking reaction. The isotherm and thermodynamic studies showed that Langmuir isotherm was the best fit to the experimental data of Cd(II) adsorption on crosslinked chitosan and all the adsorption reactions were endothermic and spontaneous. A reduced quadratic model, constructed by the Response Surface Methodology (RSM), indicated that the Cd(II) adsorption uptake of 99.87 (mg/g) was achieved at 55 ℃ and 2.92 % (w/v) crosslinking degree. Then, chitosan and crosslinked chitosan beads by sodium tripolyphosphate were used for Ni(II) adsorption from aqueous media in the second phase. The BET characterization showed that increasing the crosslinking degree reduced the chitosan beads' surface area and their total pore volume. The Langmuir model described the experimental results best and showed that the maximum adsorption capacity of chitosan (80.00 mg/g) decreased after crosslinking (52.36 mg/g). In addition, a reduced quadratic model with a correlation coefficient of 0.96 was established to correlate the adsorption uptake of Ni(II) with pH and crosslinking degree. In the third phase, the

adsorption of Ni(II) and Cd(II) ions from single and binary metal ions solutions onto chitosan and crosslinked chitosan beads was studied. The extended Freundlich model fitted the adsorption equilibrium data in the binary system, implying the existence of preference in the order of Ni(II) > Cd(II). Desorption studies with a mixture of NaCl and H_2SO_4 were also conducted during this phase, demonstrating a desorption efficiency of greater than 85 %.

In the fourth phase, the removal of cadmium from aqueous solution was examined using a novel Cd(II)-imprinted crosslinked chitosan. SEM, FTIR, TGA, and BET characterizations revealed that the ion-imprinted chitosan beads had better physicochemical properties than chitosan beads and superior potential adsorption properties than non-imprinted crosslinked chitosan beads. The isotherm and thermodynamic studies revealed that the Langmuir isotherm fitted the Cd(II) experimental data the best, and the adsorption reactions were spontaneous and endothermic. The kinetics data were also best fitted by the pseudo-second-order equation. Finally, the ion-imprinted crosslinked chitosan beads were employed for the selective adsorption of Cd(II) in a competitive adsorption system of Cd(II)-Ni(II)-Co(II) in phase five. The characterization of the prepared adsorbents was performed using XRD and BET, showing a higher surface area of ion-imprinted crosslinked chitosan than non-imprinted crosslinked chitosan beads. The Extended Langmuir model fitted the experimental results obtained from the multi-component system, indicating that ion-imprinted crosslinked chitosan had a higher total metal uptake with better selectivity toward Cd(II) uptake compared to non-imprinted crosslinked chitosan. Studying the adsorption mechanism in a ternary system showed that the adsorption was governed by chemical binding and ion exchange mechanisms in the ternary system.

In conclusion, crosslinking by sodium tripolyphosphate improved chitosan physiochemical properties; however, it resulted in a decrease in HM adsorption uptake. The RSM was used to assess the effect of pH, temperature, and crosslinking degree and optimize the adsorption uptake of chitosan. Also, ion-imprinting was effective in enhancing the adsorption capacity and selectivity of crosslinked chitosan for the ion used as a template (Cd(II)) in preparing ion-imprinted crosslinked chitosan.

Keywords: Ni(II), Cd(II), Co(II), Heavy metals, Batch adsorption, Competitive adsorption, Chitosan, Adsorption mechanism, Isotherm study, Kinetics study, Thermodynamic study,

Characterization, Statistical analysis, Selectivity, Crosslinking, Ion-imprinting, Chitosan modification

Dedication

To my dear parents, Zahra and Javad

&

My beloved wife, Atefeh

Acknowledgement

It is an honour for me to thank those who made this thesis possible, and words fail to appreciate them in the way they should be. First and foremost, I would like to express my sincere gratitude and deepest appreciation to my supervisor Dr. Majid Sartaj for his valuable supervision, contribution and advice. The completion of this thesis would not have been possible without his encouragement, invaluable suggestions and continuous support throughout this research program.

My thanks are also extended to the technical officer of the environmental engineering laboratory, Patrick M. D'Aoust, and the materials characterization facility manager in the catalyst center, Dr. Yun Liu, for their technical assistance and expertise. I would like to acknowledge all my friends and colleagues in the Department of Civil Engineering at the University of Ottawa for their help. Finally, my highest appreciation goes to my family for their endless encouragement, especially my dear parents, Zahra and Javad, for their unconditional love and support during all these years. Special thanks to my wife, Atefeh, who has always supported me with patience and encouragement during this long journey.

Table of Contents

List of Tables

List of Figures

List of Acronyms and Abbreviations

AAS	Atomic Absorption Spectroscopy
Adj MS	Adjusted Mean Squares
Adj SS	Adjusted Sums of Squares
ANOVA	Analysis of Variance
ATR	Attenuated Total Reflectance
ATSDR	Agency for Toxic Substances and Disease Registry
BET	Brunauer–Emmett–Teller
BOD	Biological Oxygen Demand
CB	Chitosan Beads
CCD	Central Composite Design
COD	Chemical Oxygen Demand
Cyanex 272	Bis(2,4,4-trimethylpentyl) phosphinic acid
D2EHPA	Di-(2-ethylhexyl) phosphoric acid
DA	Degree of Acetylation
DD	Deacetylation Degree
DF	Degree of Freedom
D-R	Dubinin-Radushkevitch
EA	Elemental Analysis
ECH	Epichlorohydrin
EDTA	Ethylenediaminetetraacetic acid
EGDE	Ethylene Glycol Diglycidyl Ether
EL	Extended Langmuir
EPA	Environmental Protection Agency
FOG	Fat–Oil–Grease
FTIR	Fourier-Transform Infrared Spectroscopy
GLA	Glutaraldehyde
GO	Glyoxal

HM	Heavy Metal
IAST	Ideal Adsorption Solution Theory
II-CLCB	Ion-Imprinted Crosslinked Chitosan Beads
IIP-STPP-CB	Ion-Imprinted Crosslinked Chitosan Beads
IUPAC	International Union of Pure and Applied Chemistry
LIBs	Lithium-ion Batteries
MPSD	Marquardt's Percent Standard Deviation
MW	Molecular Weight
Ni-Cd	Nickel-Cadmium
NI-CLCB	Non-Imprinted Crosslinked Chitosan Beads
NiMH	Nickel-Metal Hydride
NMR	Nuclear Magnetic Resonance Spectroscopy
RMSE	Root Mean Square Error
RSM	Response Surface Methodology
SEM-EDS	Scanning Electron Microscopy and Energy Dispersive X-ray Spectroscopy
SRS	Sheindorf–Rebuhn–Sheintuch
STPP	Sodium Tripolyphosphate
STPP-CB	Sodium Tripolyphosphate Crosslinked Chitosan Beads
STPP-CLCB	Sodium Tripolyphosphate Crosslinked Chitosan Beads
TEM	Transmission Electron Microscopy
TGA	Thermogravimetric Analysis
TSS	Total Suspended Solids
USEPA	Environmental Protection Agency
WHO	World Health Organization
XPS	X-ray Photoelectron Spectroscopy
XRD	X-ray Powder Diffraction

Chapter 1

1 Introduction

1.1 General background

The production and consumption of batteries have increased due to enormous demand from both industrial activities and consumer usage. The total global battery market size is expected to reach over $100 billion in 2025 [1]. Generally, there are two common types of batteries: primary and rechargeable. The latter mainly includes nickel-cadmium (Ni-Cd), nickel-metal hydride (NiMH), lead-acid batteries, and lithium-ion batteries (LIBs). Ni-Cd batteries recycling has become a significant concern because they are classified as hazardous materials since they contain considerable amounts of nickel (Ni(II)), cadmium (Cd(II)), and cobalt (Co(II)). These batteries are also considered secondary sources of heavy metals (HMs) by having Ni(II), Cd(II), and Co(II) concentration levels of about 14%, 24.5%, and 2%, respectively [2,3].

The pyrometallurgical technique is the conventional technique that has been widely used to recycle used batteries and recover valuable and toxic metals. However, pyrometallurgical procedures are hazardous due to the high levels of pollution released into the atmosphere and secondary waste generation [4]. Consequently, it is preferable to find an economical and more environmentally friendly process to recover HMs from spent batteries. Hydrometallurgical routes are more economical and cleaner than pyrometallurgical methods; however, they are complex and require a higher number of steps [5,6]. The main disadvantages of hydrometallurgical technology come from the purification stages, preventing the development of an environmentally friendly approach toward battery recycling [7]. Therefore, it is crucial to devise a better recovery method to reduce the ecological footprint.

Adsorption is an alternative procedure to replace the current purification techniques of the hydrometallurgical route. Adsorption has some advantages such as flexibility in operation, feasibility in producing a high-quality product, economical viability in the context of initial capital cost and chemical requirement, and effectiveness in the purification process [8]. Among a wide range of adsorbents, low-cost natural materials or wastes from industry or agricultural operations have come to the attention and been implemented as adsorbents for HMs uptake [9]. Adsorbents from biological origins (bio-sorbents) have advantages over chemical sources; bio-sorbents are non-

toxic, biodegradable, available in the biosphere, cost-effective, and promote sustainable development strategies [10].

Wastes produced by the seafood industry have become a challenging environmental issue both in terms of quality and quantity [11]. In recent years, promoting and moving towards sustainable waste management and the interest in reusing waste materials have created a potential for seafood industry waste to be converted to useful materials such as chitin or chitosan [12]. By virtue of their high safety, non-toxicity, chemical and physical versatilities, numerous researches have been conducted on chitin and chitosan applications in medicine, agriculture, and the treatment of water and wastewater with different types of pollutants, either organics or inorganic species [13]. The presence of a large number of functional groups (such as amine and hydroxyl groups) on chitosan, the ease with which it may be modified, and the versatility of the chitosan chains all contribute to chitosan being considered an excellent adsorbent for HMs adsorption [14].

Chitosan is not suitable for practical use in its original form, mainly due to its solubility in acidic conditions and its relatively low physical strength. Therefore, physical or chemical modifications have been examined to increase chitosan stability [15]. Chitosan modification can also improve metal sorption performance, including sorption capacity and selectivity[16]. The chitosan-based adsorbents can be synthesized with relatively inexpensive chemical reagents, making them economically feasible and environmentally safe [17]. However, when it comes to chitosan modification methods, such as cross-linking and grafting, toxic or expensive chemical agents and mostly harsh conditions are essential. This increases the processing costs and generates secondary pollution due to the complicated chemical reactions. Therefore, chitosan modification via an eco-friendly pathway would be helpful in developing a sustainable biosorption system.

1.2 Research objectives

This study aimed to synthesize and modify chitosan by crosslinking and ion-imprinting to improve chitosan physicochemical properties and efficiency for Cd(II), Ni(II), and Co(II) uptake, as well as chitosan selectivity for Cd(II) adsorption. The specific objectives of this study are explained below.

- Synthesize and characterize chitosan, crosslinked chitosan and ion-imprinted crosslinked chitosan beads as a potential adsorbent for heavy metal ion adsorption.
- Assess the adsorbents' performance by changing operating conditions, including pH, adsorbent dosage, temperature, contact time, crosslinking degree, and initial metals concentration, and determine the optimum range values of these parameters.
- Investigate the adsorption of Cd(II), Ni(II), and Co(II) on chitosan, crosslinked chitosan and ion-imprinted crosslinked chitosan beads in single, binary, and ternary systems and quantify their competitive adsorption.
- Study the feasibility of regenerating the adsorbents by employing a suitable reagent.

1.3 Research hypotheses

According to the literature review, the following hypotheses were made:

- Chitosan, in the form of gel beads, is acceptable for batch and continuous adsorption tests [18].
- Chitosan beads are capable of adsorbing heavy metal ions, but the chitosan beads' chemical and physical stability are low.
- Crosslinking chitosan by sodium tripolyphosphate enhances its chemical and physical properties but reduces the adsorbent's efficiency for heavy metal ions uptake [19].
- Increasing initial pH, adsorbent dose, temperature, and time would improve the adsorption efficiency of chitosan-based adsorbents [20].
- Chitosan crosslinked by different concentrations of a crosslinking reagent shows different adsorption characteristics and physical/chemical properties [21].
- Ion-imprinting the crosslinked chitosan increases the adsorbent capacity and provides selectivity in a competitive system [22].
- NaCl can be used for ion-imprinting crosslinked chitosan and regenerating sorbent loaded by heavy metal ions [23].

1.4 Novelty or Significance

The novelty of this work comes from the following:

- Chitosan was employed to recover Cd(II), Ni(II), and Co(II) from the synthetic leach solution of used Ni-Cd batteries. This approach not only recovered heavy metals from waste batteries but also offered a new application for waste created by the seafood sector.
- Chitosan beads were synthesized and modified simultaneously in one step using an optimized amount of non-toxic crosslinker, suggesting an environmentally friendly and quick process to prepare low-cost and biodegradable adsorbent with acceptable chemical and physical properties for HM ions uptake with minimal chemical use.
- The ion-imprinting technique was used for the first time for chitosan crosslinked by sodium tripolyphosphate to improve its adsorption properties (such as adsorption uptake and selectivity) for HM ions adsorption.

1.5 Thesis organization and outline

This thesis is organized into nine chapters to present the research's key findings. Chapters 3 to 7 are in the form of technical papers. The content of these chapters is as follows:

- Chapter 1, Introduction, provides a brief overview and general information on batteries and the current battery recycling techniques. This chapter covers a general description of the problems associated with the battery recycling techniques, the novelty and the objectives of this research, and the thesis outline.
- Chapter 2, Literature Review, provides a literature review about batteries structure and the importance of battery recycling. The current techniques of battery recycling, along with their problems, are discussed in detail in this chapter. A literature review on adsorption as an alternative technique to recover HMs is also presented. In addition, this chapter covers the chitosan and chitin synthesis and modification processes, and the parameters affecting chitosan adsorption efficiency are discussed. In the last part of the chapter, the regeneration methods for loaded chitosan-based adsorbents are discussed.
- Chapter 3 (Technical Paper 1), Removal of Cadmium(II) from aqueous solution using tripolyphosphate crosslinked chitosan. This chapter focuses on cadmium adsorption by chitosan and sodium tripolyphosphate crosslinked chitosan beads. The effect of pH, adsorbent dose, temperature, and crosslinking degree was studied thoroughly in a batch

adsorption system, and response surface methodology (RSM) was applied to model and optimize cadmium adsorption onto crosslinked chitosan.*

- Chapter 4 (Technical Paper 2), Optimization of Nickel(II) adsorption by sodium tripolyphosphate crosslinked chitosan using response surface methodology (RSM). This chapter concentrates on Ni(II) adsorption on chitosan and chitosan crosslinked using sodium tripolyphosphate in a batch adsorption system. The effect of pH, temperature and crosslinking degree on Ni(II) adsorption was studied. Response surface methodology was employed to optimize the adsorption of Ni(II) on crosslinked chitosan beads.*
- Chapter 5 (Technical Paper 3), Competitive adsorption of nickel(II) and cadmium(II) ions by chitosan crosslinked with sodium tripolyphosphate. This chapter investigates the competitive batch adsorption system of Ni(II) and Cd(II) ions by chitosan and crosslinked chitosan beads. A comparison was drawn between mono- and binary systems by employing different adsorption isotherm models to evaluate coexisting metal ions effect. The regeneration of the loaded adsorbent was examined.*
- Chapter 6 (Technical Paper 4), Synthesis, characterization, and performance evaluation of ion-imprinted crosslinked chitosan (with sodium tripolyphosphate) for cadmium adsorption. This chapter evaluates the effect of ion-imprinting on Cd(II) adsorption on crosslinked chitosan in a batch adsorption system. The synthesized adsorbent properties were investigated for Cd(II) adsorption by altering pH and adsorbent dosage. The effect of time, temperature, and initial metal ions concentration on Cd(II) adsorption were also examined. The regeneration of loaded adsorbent was studied in this chapter as well.*
- Chapter 7 (Technical Paper 5), Competitive adsorption of Cd(II), Ni(II) and Co(II) onto ion-imprinted crosslinked chitosan: characterization and isotherm studies. This chapter investigates the competitive adsorption of Ni(II), Cd(II) and Co(II) on Cd-imprinted crosslinked Chitosan. A ternary system of Ni(II), Cd(II) and Co(II) was employed to investigate Cd-imprinted crosslinked chitosan performance. The effect of initial metal

concentration was studied in the mono and ternary adsorption systems, and the best-fitted isotherm models were determined.*

- Chapter 8, Synthesis, Integration and General Discussion of Results, presents a general discussion of the results and compares the results of each phase of this study.
- Chapter 9, Conclusions and Future Works, summarizes the main conclusions and provides possible recommendations for future studies.

Figure 1-1 shows the organization of this thesis.

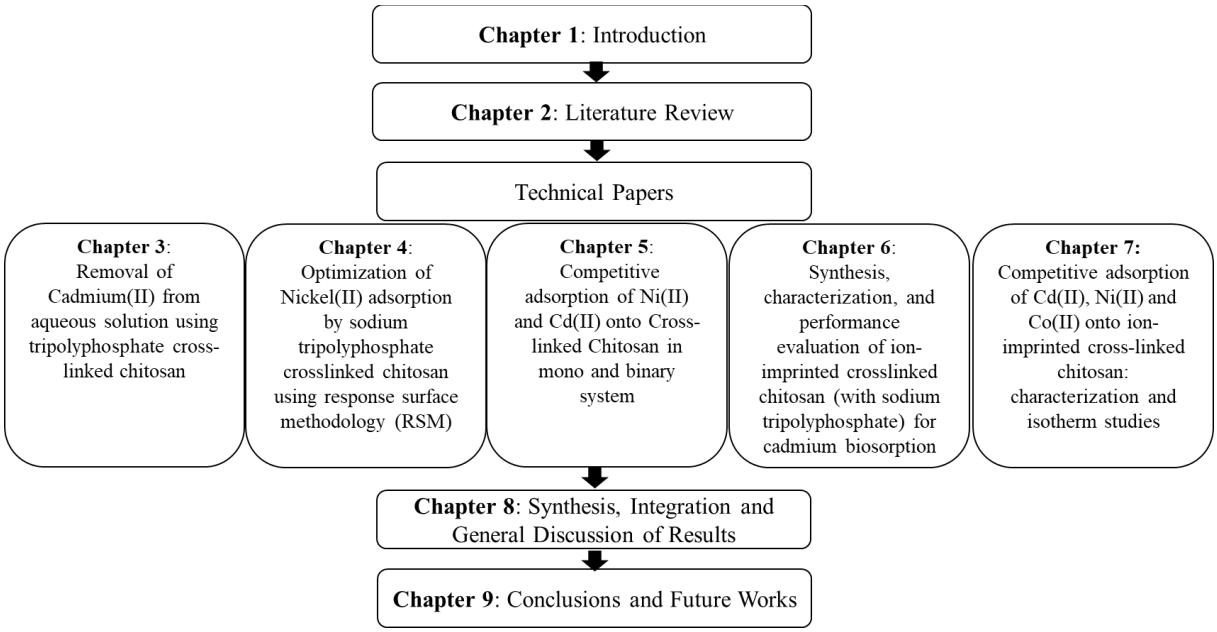

Figure 1-1. Organization of thesis

1.6 References

The references are merged with those of the other chapters' references and presented at the end of the thesis.

* Synthesized unloaded and loaded beads were characterized in each phase by different tools and tests, including solubility and swelling test, Brunauer–Emmett–Teller (BET) surface area, Scanning Electron Microscopy/ Energy-Dispersive X-ray Spectroscopy (SEM-EDS), Fourier transforms infrared (FTIR), Thermogravimetric Thermal Analysis (TGA), and X-ray Diffraction (XRD) to reveal valuable information regarding crystal and chemical structure as well as the topography of the beads.

Chapter 2

2 Literature Review

Since the 1900s, batteries have become a common power source for many household and industrial applications. In the last decades, batteries registered a significant consumption increase [24]. Battery technology has improved in different aspects over the past fifty years because of the growth in mobility and transportation systems (i.e., electric vehicles), communications and information technology, and electricity generation [25]. Although batteries are mostly simple in concept, it is surprising that their development has advanced more slowly than in other areas of electronics. Accordingly, they are often considered the heaviest, the costliest, and the least green component of any electronic device [26].

Depending on the materials used in their manufacturing, batteries are categorized into two groups: non-rechargeable primary and rechargeable secondary batteries. Primary batteries produce power through an irreversible chemical reaction; they include zinc-manganese (Zn–Mn), zinc-carbon (Zn–C), and primary-lithium or mercury batteries. However, rechargeable batteries, such as nickel-cadmium (Ni-Cd), nickel-metal hydride (Ni–MH) and lithium-ion (Li-ion) batteries, are more common and have found their applications in industry, particularly in portable electronic products [27,28]. Based on an assessment of the quantities of batteries sold in 2015 in Canada, the alkaline batteries (Zn-Mn) (74%) are the most popular non-rechargeable ones, followed by zinc-carbon batteries (15%), lithium dioxide manganese batteries (5%), zinc-air button cell batteries (4%) and silver oxide button cell batteries (2%). Among rechargeable batteries, nickel-metal hydride batteries (42%) are the most consumed type, followed by nickel-cadmium batteries (32%), lithium-ion batteries (22%), lithium polymer batteries (2%) and small sealed lead-acid batteries (2%) [29]. The main characteristics of the most frequently used batteries and their applications are presented in Table 2-1 [28].

Different metals are used in batteries, some of them are valuable (Ag, Ni, Zn and Co), and some are toxic (Hg, Cd and Pb). With the rapid expansion of the electronic vehicles market and the application of batteries, a considerable amount of batteries reach their end-of-life each year. Therefore, battery disposal is becoming critical, and an inappropriate method can pose threats to the environment and human health [30]. Different aspects of battery disposal are reviewed in this chapter, and two main approaches to battery recycling, including pyrometallurgy and

hydrometallurgy, are discussed in detail. After assessing each recycling method, the adsorption process is proposed as an alternative. Subsequently, the properties of chitosan as an environmentally friendly adsorbent for heavy metals uptake are discussed, followed by a review of the influential adsorption parameters and regeneration of loaded adsorbents.

Table 2-1. Main characteristics of commercial batteries

Battery Type	**Anode**	**Cathode**	**Electrolyte**	**Main Applications**
Zn-C	Zn	MnO_2	NH_3, $ZnCl_2$ and Water	Domestic general use
Ni-Cd	Cd	$Ni(OH)_2$	KOH	Wireless devices, cameras, laptops, pagers and mobile phones
Ni-MH	V, Ti, Zr, Ni, Cr, Co, and Fe	$Ni(OH)_2$ Cobalt oxides	KOH	Portable devices, mobile phones
Li-ion	C	$LiCoO_2$	Organic solvents or salt solutions	Portable devices, mobile phones, hybrid vehicles
Alakalike (Zn-Mn)	Zn	MnO_2	KOH	Domestic general use
Lead	Pb	PbO	H_2SO_4	Automotive use

2.1 Disposal of Used Batteries

Based on the guidelines/legislation in different countries, the appropriate disposal method for spent batteries may include landfill deposition, stabilization by incineration (with some controls) and recycling/recovery processes. In some countries, dumping used batteries at municipal solid waste landfills still occurs, increasing the toxic metal constituents in surface and groundwater streams due to leaching and infiltration [31]. The incineration process includes spent batteries collection followed by the mass-burn of the waste. As a result, the waste is converted to ash, gases and heat, causing environmental hazards due to releasing toxins such as mercury, cadmium and dioxins into the atmosphere. Meanwhile, safe disposal in landfills and spent-batteries stabilization processes have become increasingly expensive due to the increase in amounts of waste in addition to the limited sanitary landfill storage capacity. Therefore, in recent years landfilling and

incineration have been restricted by environmental legislation in most countries for spent battery disposal [32].

Considering the above, the most effective method of waste batteries management is recycling, which is of prime importance to environmental, economic and resource conservation concerns. As a result, different processes have been developed to recycle batteries and recover valuable and toxic metals. Canada's government adopted the Call2Recycle project to restrict the amounts of spent batteries entering landfill sites and encourage reusing the metals contained in used batteries as secondary raw materials [33].

2.2 Nickel-Cadmium Battery

The production of Ni-Cd batteries began in Europe and the United States in the 1950s [34]. Due to their high discharge efficiency and long service life, this battery type has been used for many decades. Despite its advantages, Ni-Cd batteries present environmental problems mainly because of cadmium. As a result, a decrease in Ni-Cd batteries consumption was observed in many countries, and they are currently classified as hazardous materials for disposal purposes [35]. The chemical composition of Ni-Cd batteries is approximately Fe (40%), Ni (22%), Cd (15%), plastic (5%), KOH (2%), Co (2%), others (16%). The schematic of the Ni-Cd battery components is shown in Figure 2-1 [36].

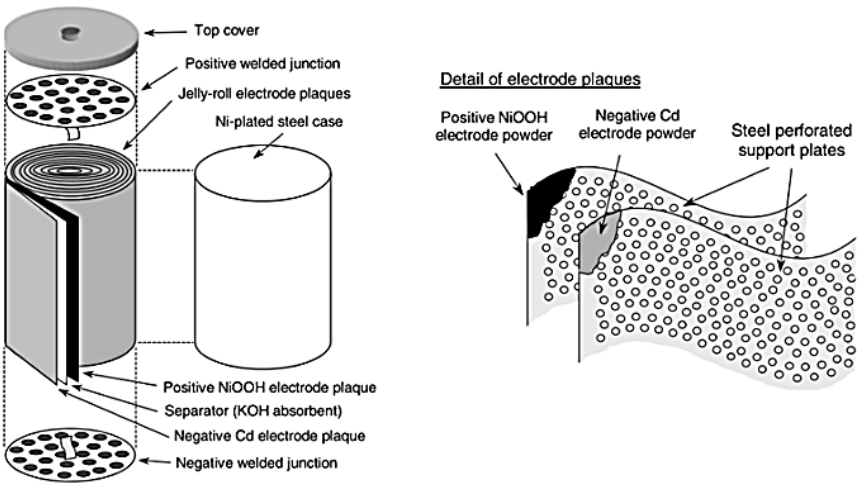

Figure 2-1. Schematic drawing of the Ni-Cd battery

The treatment of used Ni-Cd batteries, which are composed of a variety of assembled materials in addition to a wide range of compositions, requires a sophisticated approach. The simultaneous presence of metals in the electrodes, including nickel, cadmium, and cobalt, with different concentrations, justifies that the recycling process should be focused on the recovery of these metals first. Among numerous methods, mechanical, pyro-metallurgical, hydro-metallurgical and combined operations have been widely applied to recover valuable metals from used Ni-Cd batteries [37].

2.3 Pyrometallurgy

Pyrometallurgical methods are the most frequently used processes for recycling batteries with an acceptable yield. Generally, the pyrometallurgical method consists of roasting, smelting and refining. The pyrometallurgy is usually employed with the application of high temperatures to extract target metals and concentrates them by using physical transmission and chemical reactions such as decomposition of compounds, reduction and evaporation techniques [27,28]. Smelting and reduction are crucial parts of conventional pyrometallurgical approaches. Batteries are smelted by adding slag formers at high temperatures, usually higher than 1400 ℃ [38]. Concurrently, graphite is usually added as a reductant during the process, which may come from the anode material or an external source. Metals with low boiling points, such as Zn, Cd and Hg, evaporate at a high temperature and leave the molten phase. These vapours can either be reclaimed as metal after condensation or generate dust by reacting with oxygen [39].

2.3.1 Industrial Pyrometallurgical Processing of Ni-Cd Battery Recycling

The conventional recycling process of Ni-Cd batteries is based on cadmium distillation. Figure 2-2 shows a pyrometallurgical recycling process of Ni-Cd batteries. First, the decomposition of Ni(II) and Cd(II) hydroxides takes place according to the following reactions during heating and right after water evaporation;

$$Ni(OH)_2\,(s) \leftrightarrow NiO\,(s) + H_2O\,(g)\ T=230℃ \qquad 2\text{-}1$$

$$Cd(OH)_2\,(s) \leftrightarrow CdO\,(s) + H_2O\,(g)\ T=300℃ \qquad 2\text{-}2$$

The primary pyrometallurgical process of Ni-Cd batteries metals recovery is performed in temperatures of about 900 °C, under vacuum at inert or reducing atmosphere. Generally, cadmium is produced directly in the form of vapour above 767°C, which is the boiling point of metallic cadmium. A controlled atmosphere is required to avoid the oxidation of the produced metallic Cd(II). In the end, metallic cadmium with 99.9% purity is obtained, which can be used in various applications. Basically, Ni(II), Fe(II) and Co(II) remain solid during the treatment, which can be employed in stainless steel production [28].

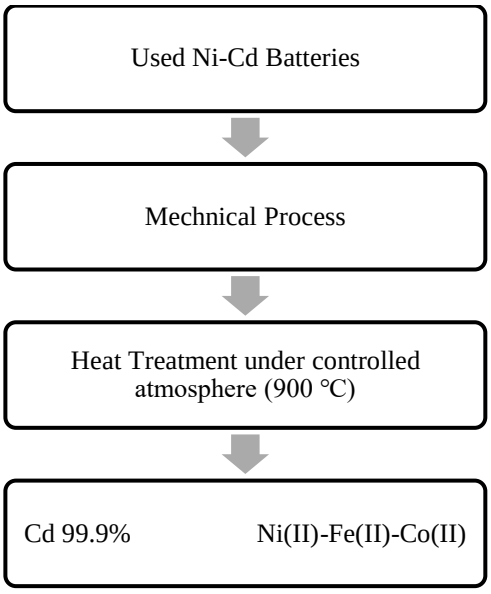

Figure 2-2. Schematic flow sheet of the pyrometallurgical method of Ni-Cd battery recycling

Recently, the recycling of Ni-Cd batteries is achieved by dedicated commercial battery recyclers such as Inmetco (United States), Accurec (Germany), SabNife (Sweden) and Snam-Savam (France), mostly through pyrometallurgical processes. Although highly pure cadmium (99.95%) is produced, most valuable metals such as cobalt and nickel are not fully recovered. Therefore, research on the thermal behaviour of electrode materials has been carried out to attain a better fundamental knowledge of the process [40]. Pyrometallurgical approaches have several important drawbacks, including a lack of flexibility and control, high costs, and a high energy requirement. Besides, pyrometallurgical processes are hazardous to the environment because of the detrimental generation of gaseous pollutants such as CO_2, dioxins, and other volatile materials [41].

Consequently, it is preferable to find an economical and environmentally friendly process to recycle batteries to recover the most valuable elements [42].

2.4 Hydrometallurgy

Hydrometallurgical methods are more economical and efficient compared to pyrometallurgical approaches. The hydrometallurgical process for metals recovery from used batteries was established in 1984. Soon after, hydrometallurgical routes became more common to treat spent batteries, containing several metals in their composition [43–45]. Recently, hydrometallurgical methods have attracted increasing attention because they have some advantages over pyrometallurgical techniques from the environmental perspective, i.e., the gas generation is relatively lower than for the pyrometallurgical methods. Also, this process's economic benefit is undeniable as selectivity, and high efficiency in recovering existing chemically similar metals are achievable [46]. The hydrometallurgical process's foundation is chemical reactions involving aqueous and organic solutions in the temperature range of 25-250℃ [47]. Hydrometallurgical systems are generally characterized by different pretreatment steps, including dismantling and crushing, followed by the dissolution of metal phases (leaching) [48]. The next step is purification/separation, which can be performed by precipitation or solvent extraction [49].

2.4.1 Leaching

Leaching is the primary step in the hydrometallurgical process. Both alkali and acid have been used as leaching agents to dissolve metals from spent batteries [50]. Sulphuric and hydrochloric acids are by far the most cited leaching agents that have been employed for battery leaching [45,49,51–53]. Concentrated solutions, high temperatures and long reaction times are usually needed for leaching, which are considered disadvantages of this stage. Researchers have carried out some studies to improve different leaching aspects and overcome these shortcomings [54].

2.4.2 Purification Methods

Purification can be accomplished by precipitation or solvent extraction. Precipitation is the formation of solids by the addition of a reagent to the leaching solution. The separation mechanism of chemical precipitation relies on the different solubilities of metal compounds at different pHs

[55]. Different reagents have been reported in the literature for precipitation, such as soda [56], ammonium oxalate [48], sodium carbonate [57] or carboxylate salts [58]. The precipitation method is commonly used on the industrial scale because of its simple operation and low cost. However, there are some limitations associated with this approach, including high sludge volume production, dewatering and disposal sludge problem and low metal selectivity [33].

Another purification approach in the hydrometallurgy process is liquid/liquid extraction, which involves the extraction of a metal ion from a liquid phase by an extractant. Solvent extraction is generally used to obtain pure metal or metal compounds by taking advantage of compounds' different relative solubilities in immiscible liquids. High purity of the metal could be achieved by this method, fulfilling the need for high-grade metals in industrial processes [59]. The solvent extraction method is considered simple and flexible; however, most extractants are expensive and harsh chemicals, creating a secondary source of pollution. As a result, the application of solvent extraction is limited once sustainable development is taken into account [60].

2.4.3 Industrial Hydrometallurgical Processing of Ni-Cd Batteries Recycling

The BATENUS process, established in Germany, is based on hydrometallurgical operations consisting of electrochemical and membrane techniques for metal separation [61]. The BATENUS method offers a solution for treating mixed battery waste, using sulphuric acid leaching and a combination of ion exchange and solvent extraction for purification. Collected batteries are sorted and then crushed, followed by physical separation of the structural elements. The powder is then leached with sulphuric acid. The leached liquors contain nickel and cadmium in significant amounts and some impurities such as cobalt and iron. The most frequently used technique for selective recovery of cadmium, nickel and cobalt is solvent extraction. After iron removal by hydroxide precipitation, cadmium is extracted using D2EHPA as an extractant diluted in kerosene. Cadmium extraction with D2EHPA involves the coextraction of nickel and cobalt, which needs a scrubbing stage with a pure cadmium solution [62]. In the next step, nickel is separated from cobalt through a solvent extraction system using CYANEX 272. The extracted metal is stripped by acid at each stage, and the solvent is regenerated and reused for the next cycle. Therefore, three concentrated solutions of each element are attained in which metals can be recovered either by

electrowinning or chemical precipitation [58]. The schematic flow sheet of the hydrometallurgical technique for Ni-Cd battery processing is shown in Figure 2-3.

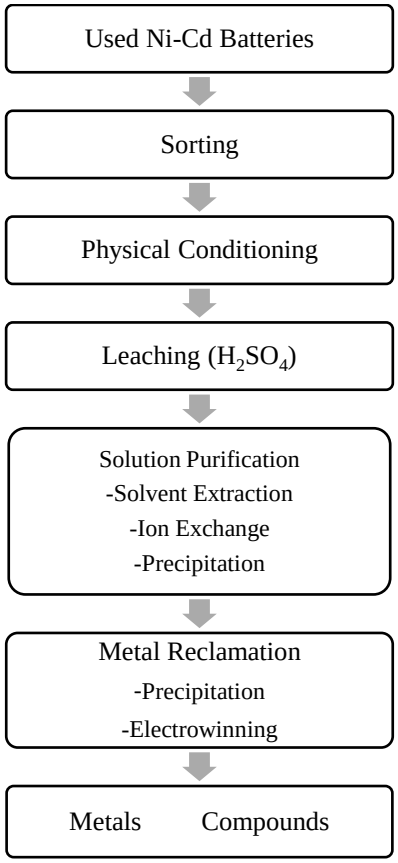

Figure 2-3. Schematic flow sheet of the hydrometallurgical method of Ni-Cd battery recycling

Hydrometallurgical technology has some disadvantages, particularly in the separation/purification stage [63]. While organic solvents can be regenerated and reused several times in the purification step, they are considered aggressive to the environment and harmful to human health. Moreover, their waste disposal and handling cost could be high [43]. Typically, the materials recovered through hydrometallurgy are mostly metallic compounds, and they should be processed further [64]. Table 2-2 shows the current recycling techniques in some developed countries.

Table 2-2. Summary of battery recycling process by the various company all over the world

Name of Technology	Recycling Method	Battery Type	Location of the Plant	References
BATREC	Pyrometallurgy	All types of batteries	Japan, Switzerland	https://batrec.ch/de-ch/
INMETCO	Pyrometallurgy	Ni-Cd, Ni-Fe, Ni-MH, Li-MH, Zn-C	USA	http://horsehead.net/inmetco/
SAB-NIFE	Pyrometallurgy	Ni-Cd	Sweden	https://www.saftbatteries.com
ZM SILESIA	Pyrometallurgy	Ni-Cd	Poland	http://hutaolawa.pl/en/index.html
TOXCO	Pyrometallurgy, Hydrometallurgy	Ni, Li-based	Canada, USA	https://www.retrievtech.com/
UMICORE	Pyrometallurgy, Hydrometallurgy	All types of battery	Belgium	https://csm.umicore.com/en/
BATENUS	Hydrometallurgy	All types of batteries except those containing lead	Germany	[61]

2.5 Adsorption

Different techniques, such as electrodeposition, adsorption, and crystallization, have been studied to overcome some of the aforementioned drawbacks associated with the hydrometallurgy purification step. Among them, adsorption has some advantages over others, including flexibility in terms of operation, feasibility in terms of production of high-quality product, economical viability in the context of initial capital cost and chemical requirement, and effectiveness in the purification process [65]. Adsorption is defined as a mass transfer process by which a compound is transferred and accumulates at the interface between two phases (liquid-solid or gas-solid). The target substance, the adsorbate, can bind to the surface of the solid phase called the adsorbent through physical/chemical interactions. Various adsorbents have been employed for HMs adsorption, such as activated carbons [66], zeolites [67], clay minerals [68], bio-sorbents [69], and nano adsorbents [70].

2.5.1 Activated Carbon

Activated carbon has been widely used to remove HMs from solutions containing Ni(II), Cd(II), and Co(II) [71,72]. However, their use is sometimes restricted mainly because of their high cost. Activated carbon sorbents derived from different natural materials have gained increasing attention over the last several years to overcome the limitations, but they are not viable for frequent use yet [73,74].

2.5.2 Zeolite

Zeolites are crystalline aluminosilicates that can occur naturally or be produced industrially on a large scale [75]. They are composed of hydrated aluminosilicate minerals, having exchangeable Na(I), K(I), Mg(II) and Ca(II) ions and water in their structural framework. Zeolites have gained considerable attention because of their low cost, excellent ion-exchange properties, high surface area, and hydrophilic character to adsorb metal ions from solution [67,76].

2.5.3 Clay Minerals

Clay minerals are hydrous aluminosilicates formed from soil and water colloid fractions. Generally, they are comprised of minerals such as metal oxides, carbonate and quartz [77]. The most common clays include montmorillonite, bentonite, and kaolinite. Bentonite has a high cation exchange capacity, is very selective, and is twenty times cheaper than activated carbon [78]. The negatively charged clay is neutralized by the uptake of positively charged species, resulting in clay's ability to attract and hold metal ions. Researchers have investigated the HMs uptake by clay minerals due to advantages over conventional adsorbents, including high surface area and excellent physical, chemical and structural/surface properties [79]. However, clay minerals are highly temperature-dependent, and variations in their structure at various temperatures affect their adsorption efficiency [80].

2.5.4 Bio-sorbent Materials

The need for the removal/recovery of HMs from the aqueous phase has directed some researchers' interest towards low-cost alternatives. Thus, natural materials or particular waste from industry and agricultural operations have come to attention and been implemented for HMs uptake

[81]. The frequently used term “low-cost adsorbents” suggests inexpensiveness and affordability as these materials should be easily and locally available in large quantities. Among them, adsorbents with biological origins (bio-adsorbents) have advantages over those from chemical sources. Typical bio-adsorbents can be derived from three sources: non-living biomass such as bark, lignin, shrimp, krill, squid and crab shells. The other two sources include algal biomass and microbial biomass such as bacteria, fungi and yeast [82].

Bio-adsorption of HMs from aquatic media is a relatively new and promising process. This approach is also suitable for treating solutions with a dilute concentration of HMs (2.5-25 mg/L) [69]. Chitosan has drawn substantial attention as a raw material for metal sorption purposes among different bio-adsorbents because of a large number of functional groups, such as amine and hydroxyl groups, and simple modification methods. Moreover, chitosan shows good biodegradability, biocompatibility and bioactivity, which justifies its broad range of applications [83]. Because of these benefits, the following sections present the literature on chitosan structure, properties, synthesis, modification, and application.

2.6 Chitin and Chitosan

Chitin is a white, hard, inelastic, nitrogenous polysaccharide with a high molecular weight. Chitin is a natural biopolymeric substance and consists of 2-acetamido 2-deoxy-b-D-glucose through a b-(1,4) linkage. After cellulose, this kind of linear mucopolysaccharide is the most abundant polymer on the earth [84]. In fact, it may be regarded as cellulose with the hydroxyl at position C-2 replaced by an acetamido group [85], which is depicted in Figure 2-4 [86]. Chitin occurs in a range of organisms, including crustacean shells, insects and fungi. However, wastes generated by the marine food processing industry are the principal source of industrial chitin [17,87]. Despite chitin's vast availability, its applications have been limited because of its intractability and insolubility, hindering physical and chemical modification [16].

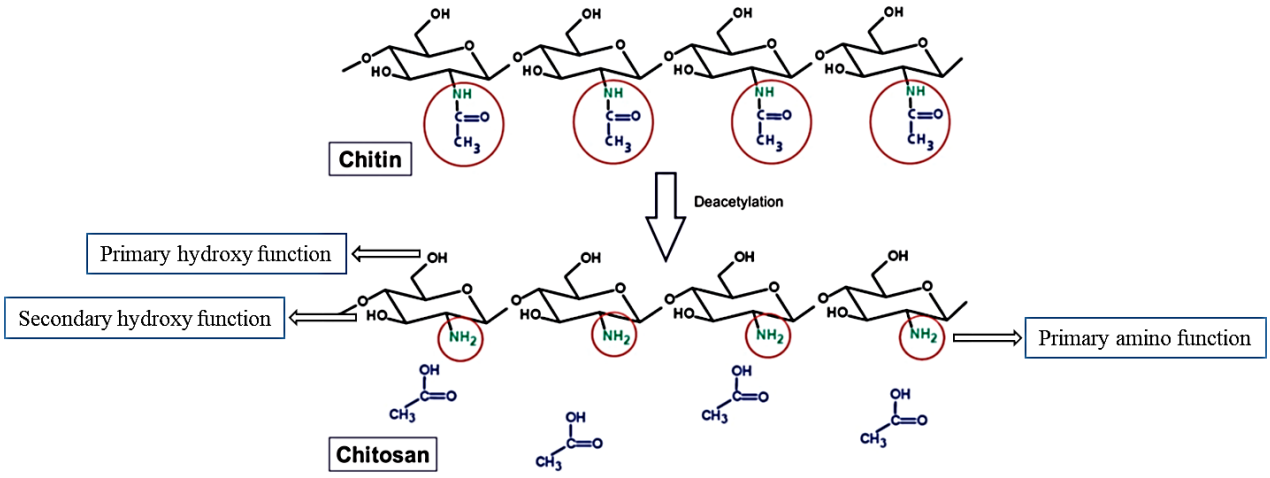

Figure 2-4. Chitin and chitosan structure

In 1859, Rouget published his discoveries that "modified chitin" could be prepared by treating chitin with boiling solutions of potassium hydroxide in water. This "Treated Chitin" was renamed "Chitosan" by Hoppe-Seiler in 1894, pronounced as "kite-O-san" [88]. Chitosan, poly [(1,4)-b-linked 2 amino-2-deoxy-D-glucose], is the N-deacetylated form of chitin with amino groups along with the chitosan structure (poly-glucosamine), shown in Figure 2-4. Chitosan is a semi-crystalline polymer in its solid-state, and the crystallinity of chitosan is lower than that of chitin. Although chitin and chitosan have the same chemical structure, the polymer's solubility in acidic solutions is considered a criterion for identifying chitin and chitosan. In dilute aqueous acids, the free amino groups at the C2 position of the chitosan backbone (D-glucosamine unit) are protonated, and the polymer becomes fully soluble below pH 3 [89]. The critical parameter for defining chitosan and chitin is the deacetylation degree (DD), defined as the ratio of 2-acetamido-2-deoxy-D-glucopyranose to 2-amino-2-deoxy-D-glucopyranose structural units [16]. The parameter of DD or degree of acetylation (DA) plays an important role in chitin/chitosan properties. In general, a polymer is usually called chitosan when it is soluble in dilute acidic solutions (1% dilute acetic acid or 1% dilute hydrochloric acid), corresponding to a deacetylation degree usually greater than 0.55. A typical DD for chitosan as an N-deacetylated derivative of chitin is larger than 0.65 or 0.70 [85].

2.6.1 Chitin/ Chitosan Production

The industrial processing of shellfish, such as shrimp, crab and krill for food production, has led to the generation of vast quantities of wastes [17]. Accumulation of this waste at high levels has turned into a significant problem in the seafood processing industry. Typically, a substantial amount of this biomass is dumped into the sea, resulting in pollution in coastal regions [90]. Fishery wastes result in adverse environmental effects because of their high biological oxygen demand (BOD), chemical oxygen demand (COD), total suspended solids (TSS), fat–oil–grease (FOG), pathogens, organic matters, and other nutrients. However, seafood processing waste might be regarded as a promising source for the processing and production of chitin and chitosan. The most abundantly available raw materials for chitin production are crab shells, shrimp and prawns [84,91]. The organisms containing chitin are composed of three basic elements: (1) chitin (20-30%), (2) minerals (30-60%) and (3) proteins (20-40%). Chitin works as a skeleton, while the minerals (mainly inorganic carbonate salts) impart the required strength to the structure, and proteins provide it with living tissue [17]. Therefore, chitin production requires the removal of mineral and protein constituents from the raw materials.

Chitin and chitosan are typically obtained by two types of extraction processes: chemical and biological methods. As shown in Figure 2-5, the prevalent chemical extraction of chitin involves demineralization (calcium carbonate and calcium phosphate separation), deproteinization (protein separation), and sometimes decolorization (removal of pigments) followed by deacetylation (acetyl groups removal) to form chitosan. The conversion of chitin to chitosan (deacetylation) is generally accomplished by treatment with concentrated sodium hydroxide (NaOH) solution (40-50%) at 100°C or higher temperature to remove some or all acetyl groups from the chitin [92].

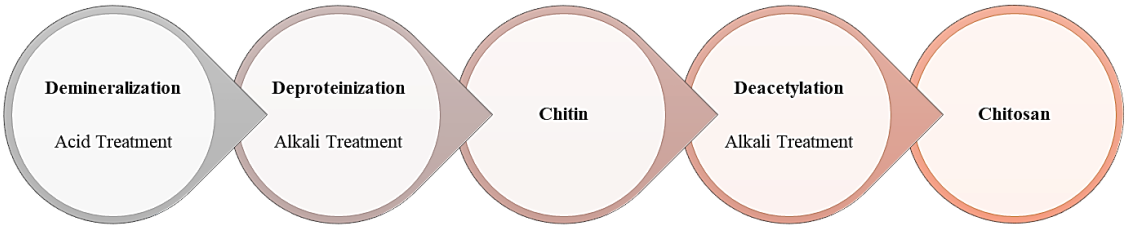

Figure 2-5. Chitin and chitosan chemical extraction procedure

Despite the many disadvantages of chemical processes, tabulated in Table 2-3, the short extraction time still makes it the most commercially used treatment [91]. The final product characteristic is considered the critical parameter in chitin and chitosan production, which is a function of the molecular weight (MW) and the deacetylation degree (DD).

Table 2-3. Comparison between chemical and biological extraction of chitin and chitosan

Extraction Method	Advantages	Disadvantages
Chemical	Short Processing time High DD% of the final product	Environmentally unfriendly
Biological	High quality of final product Environmentally safe	Long processing time

2.6.2 Chitosan Modification

In its original form, chitosan is not suitable for practical use as a bio-adsorbent mainly due to its solubility in acidic aqueous and relatively low physical strength [93]. Chitosan instability at low pHs is attributed to amine groups' presence on its surface, leading to the formation of protonated chitosan. Therefore, physical or chemical modifications have been extensively investigated to increase the stability of chitosan in acid media, improve its mechanical properties, and enhance the metal sorption performance, such as sorption capacity and metal selectivity [91,94].

2.6.2.1 Physical modifications

One of the most remarkable properties of chitosan is its adaptability, which means that it may be physically changed to produce a variety of polymer forms. Chitosan has been employed in the form of powder, nanoparticles [95], gel beads [96], membranes [97], and fibers [98] for various fields of application, including wastewater treatment, biomedical, and textiles. However, small particles have been shown to be ineffective in column systems due to their tendency to block the flow and impose significant hydrodynamic constraints. Employing chitosan gel beads as an alternative may be advantageous since they increase both diffusion characteristics (by increased porosity and decreased crystallinity) and hydrodynamic behaviour. However, it also decreases the volumetric sorption capacities because of the high water content of the beads [99]. However, drying the beads

can increase their volumetric sorption capacity and keep their kinetic characteristics for HMs uptake [98].

2.6.2.2 Chemical Modification

The chitosan chemical modification is often executed on the two active sites, including primary amino and primary (or secondary) hydroxyl groups, mainly to change the chemistry of chitosan [15]. The chitosan chemical modification is usually accomplished by grafting or crosslinking reactions, leading to the formation of chitosan derivatives with preferred properties. Crosslinking reaction consists of uniting the macromolecular chains to each other, which slightly decreases the adsorption capacity and selectivity since some functional groups of chitosan are occupied with the crosslinker and cannot interact with the pollutant [100]. In order to overcome the adverse impacts of crosslinking and boost selectivity for target metal ions, some other approaches have been examined, such as imprinting with target metal ions as a template or grafting [83]. In the grafting procedure, new functional groups are added onto the chitosan chain, which may increase the number of adsorption sites resulting in an adsorption capacity rise [101].

2.6.2.2.1 Chitosan Crosslinking

Crosslinking can be performed by chemical methods (using crosslinking agents) or physical processes (radiation or ultraviolet light) [102]. In general, crosslinking reinforces the chemical stability of chitosan in acidic solutions, enhances the mechanical resistance, modifies chitosan hydrophobicity, and stabilizes the chitosan at drastic pH change, which are essential aspects of an effective adsorbent. However, crosslinking decreases the number of free and available groups available in the chitosan backbone and decreases the accessibility to internal sites of the material, leading to a loss in the polymer chains' flexibility. Therefore, crosslinking may negatively impact the metal uptake efficiency and adsorption capacities, depending on the crosslinker type and crosslinking degree [103]. Different chemical reagents have been used for the crosslinking reactions with at least two reactive functional groups that allow the formation of bridges between polymer chains and active chitosan sites [89], shown in Figure 2-6.

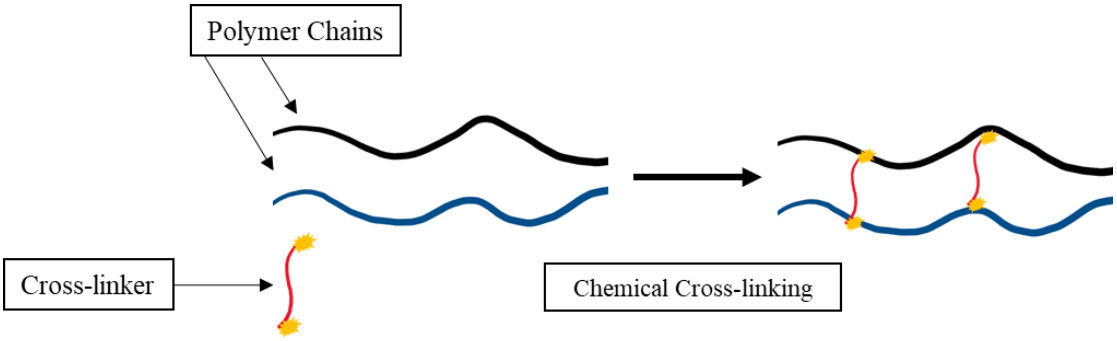

Figure 2-6. Schematic of the chemical crosslinking process

The crosslinking process may proceed via covalent or ionic bonds, depending on the type of crosslinking. The covalent crosslinking of chitosan is a chemical reaction, resulting in stable covalent bonds between the crosslinking agent and the polysaccharide chains. Any compound with at least two functional groups capable of condensation reaction with the polymer may be regarded as a covalent crosslinker [21]. The most common covalent crosslinkers employed for chitosan crosslinking is glutaraldehyde (GLA) [104]. Additionally, several covalent crosslinkers for chitosan crosslinking have been reported in the literature, including epichlorohydrin (ECH) [103] or ethylene glycol diglycidyl ether (EGDE) [105]. The covalent crosslinking of chitosan is an irreversible reaction, enabling chitosan sorbent to remain stable even in a very acidic medium (pH~1) [21]. In turn, the ionic crosslinking results in the chitosan chain's electrostatic attraction to the ionic crosslinkers, leading to the formation of electrovalent (ionic) bonds between them. Theoretically, chitosan may undergo ionic crosslinking with chemicals that possess at least two functional groups that generate a negative charge in water. Compared to chitosan crosslinked with covalent bonds, the ionically-crosslinked chitosan is less stable in acidic solutions. The most common ionic crosslinker type is sodium tripolyphosphate [106].

The crosslinked chitosan's properties are significantly affected by the type and dosage of the crosslinking agent and conditions of the crosslinking process (mainly pH and temperature) [107]. Although the crosslinking generally decreases the adsorption capacity of chitosan, several researchers have reported some improvements, primarily due to introducing new functional groups into their chain [105]. In essence, efforts have been made to maintain the degree of crosslinking as low as possible, followed by further chemical modifications such as grafting, imprinting or

functionalizing to minimize the adverse impact of crosslinking and improve selectivity as well as the adsorption capacity of chitosan [108]. The following compares the common covalent crosslinkers.

Covalent Crosslinkers

Epichlorohydrin (ECH)

2-(Chloromethyl) oxirane, C_3H_5ClO, is an abundant chemical intermediate applied in many fields. ECH is a relatively small organic molecule with a highly reactive three-membered oxirane ring and oxygen and chlorine heteroatoms. ECH is commonly referred to by many researchers as a suitable crosslinking agent to obtain more stable and durable chitosan [103,109]. Compared with other crosslinkers, the chitosan modified with ECH usually shows higher adsorption capacities. This behaviour is attributed to the fact that ECH mostly binds with the hydroxyl groups, and the major adsorption sites for heavy metals (amino groups) are not eliminated during the crosslinking process [110].

Glutaraldehyde (GLA)

Pentanedial, $C_5H_8O_2$, is also a relatively small compound, containing two aldehyde groups separated by a flexible chain of three methylene bridges. Crosslinking by glutaraldehyde happens via a Schiff's base reaction between the crosslinking agent's aldehyde ends and the amino moieties of chitosan to create imine functions. [100].

Ethylene Glycol Diglycidyl Ether (EGDE)

Ethylene glycol diglycidyl ether, $C_8H_{14}O_4$, has two epoxide functional groups located at both ends of the molecule [108]. The crosslinking reaction can be achieved by reacting the epoxide groups of EGDE with the amino groups ($–NH_2$) provided by the D-glucosamine units in the polymeric matrix of chitosan biopolymer [111].

Modified chitosan adsorbents are supposed to be environmentally friendly alternatives to commercial adsorbents such as activated carbon. However, modifying agents are usually considered toxic and hazardous, bringing adverse impacts to the environment. Considering covalent crosslinkers, ECH is one of the widely used crosslinkers. Substantial toxicology research has been conducted on it, showing that exposure to 30 ppm of ECH in laboratory rats results in severe kidney damage [108]. Table 2-4 shows the ECH structure, applications and safety/hazards

information. GLA also poses a significant threat to the aqua ecosystem at very high concentrations [112]. According to Sano et al. [113], long-term exposure to GLA with a concentration of at least 2.5 ppm reduces the reproduction rate of fishes. As it is tabulated in Table 2-4, GLA is also hazardous to human health like ECH, having a danger signal. As for EGDE, there are no reported data on the threshold toxicity limit of its concentration. However, upon long-term exposure to EGDE, respiratory and kidney systems might be affected [108].

Table 2-4. Covalent crosslinker agents' properties (https://pubchem.ncbi.nlm.nih.gov/)

Crosslinker	Structure	Applications	Safety and Hazards	Signal
Epichlorohydrin (ECH)		- Paint dissolvent - Fumigant against insects	- Flammable - Corrosive - Acute Toxic - Irritant - Health Hazard	Danger
Glutaraldehyde (GLA)		- Additive to glues - Disinfectant - Medical applications - Preserving and fixing agent	- Corrosive - Acute Toxic - Irritant - Health Hazard - Environmental Hazards	Danger
Ethylene Glycol Diglycidyl Ether (EDGE)	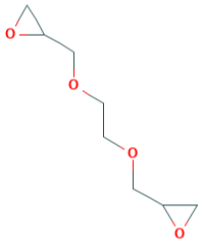	- Modifier of fibre, paper and resin - Crosslinker in biomaterial	- Irritate - Health Hazard	Warning

Ionic Crosslinker

Sodium Tripolyphosphate (STPP)

Penta sodium triphosphate, $Na_5P_3O_{10}$, is a polyanion and can interact with cationic chitosan by electrostatic forces [114] illustrated in Figure 2-7. The ionic interactions between the positively charged amino groups and negatively charged counter ion available in STPP form either

intermolecular or intramolecular linkages. Results show that chitosan beads crosslinked by ionic STPP are found to be more rigid, but chitosan beads crosslinked by covalent ECH show higher adsorption capacity [106]. Unlike covalent crosslinkers (ECH, GLA and EGDE), STPP is non-toxic to humans as it does not irritate skin and eyes upon exposure. However, it is the least reported crosslinker agent in the literature, implying that more research should be carried out on employing STPP as a crosslinker [108]. The chemical structure of Penta-sodium tripolyphosphate is shown in Figure 2-7 [115].

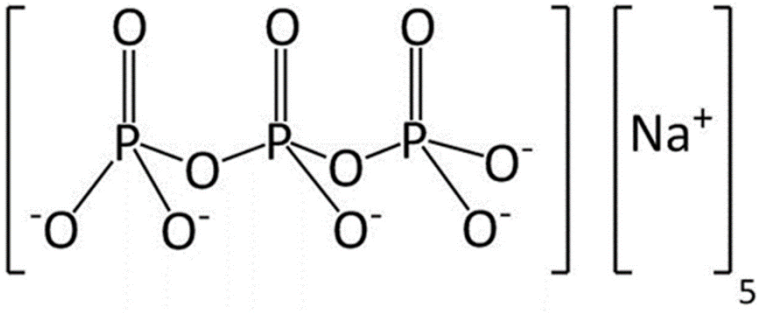

Figure 2-7. Chemical structure of Penta-sodium tripolyphosphate

2.6.2.2.2 Chitosan Grafting

Since crosslinking procedure may reduce the chitosan adsorption capacity because of the amine and hydroxyl groups consumption, grafting some functional groups is helpful to compensate for the crosslinking impact by introducing new functional groups [98,116]. Chitosan bears two types of reactive groups that can be grafted: the free amino groups on deacetylated units and the hydroxyl groups on the C3 and C6 carbons on acetylated or deacetylated units. Accordingly, the main chitosan grafting techniques can be categorized into N-substitution, O-substitution and free radical graft copolymerization [117]. The most common modification method includes N-substitution, in which the amino groups of chitosan are reacted by grafting agents [118]. In O-substitution, the hydroxyl groups of chitosan are targeted by designed small molecules or polymers. Generally, the protection and deprotection of primary amino groups play a significant role in this method because of the higher reactivity of amino groups over hydroxyl groups [119].

The most critical factors for the adsorption process to be acceptable are efficiency (high adsorption capacity), cost of the adsorbent in preparation and modification stages, and recently

sustainability. However, most research focuses on chitosan derivatives' technical performances, while their economic and eco-friendly aspects are usually neglected [120]. According to Bailey et al. [121], a sorbent can be considered low-cost if it requires little processing, is abundant in nature, or is a by-product or waste material from another industry. This being said, chitosan-based adsorbents production is economically feasible because they are easy to prepare with relatively inexpensive and quite harmless chemical reagents under mild conditions. However, when it comes to the modification of chitosan, particularly grafting, the chemical agents are an essential part that increases the system's cost and involves complicated chemical reactions, which generates secondary pollution, hindering the sustainability of adsorption operation. Therefore, an environmentally friendly and simple modification process is advantageous to the notion of low-cost adsorbent and sustainability.

2.6.2.2.3 Chitosan Imprinting

The previous attempts to overcome the lower adsorption capacity of crosslinked chitosan resulted in the development of new chitosan derivatives, grafted chitosan. Considering the drawbacks of grafting, such as secondary pollution generation and increased cost, several efforts have been made, culminating in introducing metal-imprinted crosslinked chitosan [83,122]. The surface imprinting technique is an emerging technology that has drawn much attention in developing recognition sites by reversible immobilization of template molecules on crosslinked polymer matrixes [123]. The imprinted adsorbents generally have specific recognition ability or selectivity for the corresponding metal ions in other metals' co-existence [124]. Generally, three steps are required to prepare imprinted crosslinked adsorbents: the formation of complexes or composites via chelation or electrostatic interaction between target ions (as a template) and functional monomers, followed by the addition of crosslinkers to initiate polymerization around the complexes or composites, and finally, the removal of template ions to form selective recognition sites [124], as shown in Figure 2-8. Any metal ions that can form a metal complex with chitosan can theoretically be implemented as a template. Metal-imprinted chitosan materials have been investigated in the literature, such as zinc [125], copper [126], nickel [127], lead [128], and cadmium [123], showing substantially remarkable adsorption capacity compared to non-imprinted crosslinked chitosan.

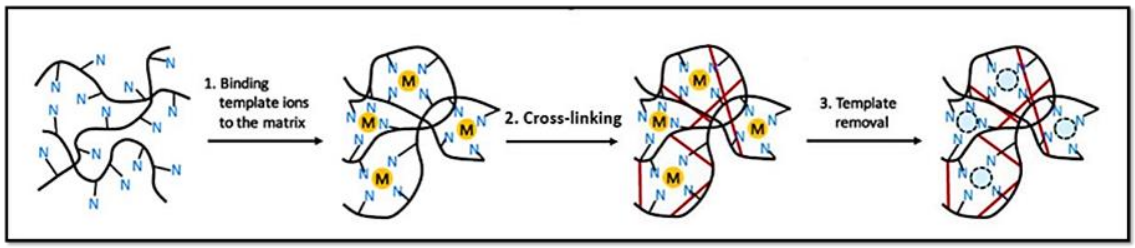

Figure 2-8. Schematic of the imprinting technique of chitosan by a metal template [129]

Various researchers have implemented modified chitosan to remove Ni(II) and Cd(II) from aqueous media, summarized in Table 2-5. It should be noted that comparing the adsorption capacities of the adsorbents reported in the literature is impossible unless the experimental conditions are the same. However, there is limited literature on imprinted chitosan-based composite and the competitive adsorption behaviour of Ni(II) and Cd(II).

Table 2-5. Nickel, cadmium, and cobalt adsorption on modified chitosan

Adsorbent	**Adsorbate**	**Adsorption Capacity (mg/g)**	**References**
Chitosan	Cd	6.07- 449.6	16,130
Magnetic chitosan grafted with α-ketoglutaric acid	Cd	201.2	131
GLA crosslinked chitosan	Cd	50.3	132
ECH-crosslinked chitosan	Cd	41.2	132
EGDE crosslinked chitosan	Cd	70.9	132
Cd-Imprinted chitosan	Cd	89.37	123
Chitosan	Ni	5.87 – 254.2	16
EDTA-Chitosan	Ni	71	133
ECH crosslinked-imprinted chitosan	Ni	29.23	19
GLA crosslinked metal-imprinted chitosan	Ni	35.80	134
Crosslinked magnetic chitosan-isatin Schiff's base	Ni	40.15	135
Magnetic chitosan/activated carbon	Co	44.5	136
Composite cryobeads based on chitosan	Co	74.01	137
Magnetic cyanoethyl chitosan Beads	Co	17.92	138

2.7 Characterization

The characterization of materials can provide valuable information about the adsorbents' structure and properties and the interaction mechanism between adsorbents and adsorbates. Characterization is a fundamental process in the application of chitosan-based adsorbents, without which no scientific understanding of the mechanism of chitosan modification and adsorption process can be obtained. With the rapid development of technology, more powerful characterization tools have arisen, including all forms of chemical, microscopic, and macroscopic analysis [86]. Table 2-6 shows different characterization tools utilized in the reports of chitosan-based adsorbents, including scanning electron microscope (SEM), Transmission electron microscopy (TEM), Fourier transforms infrared (FTIR), energy-dispersive X-ray spectroscopy (EDS), nuclear magnetic resonance spectroscopy (NMR), elemental analysis (EA), Brunauer–Emmett–Teller (BET) analyzer, X-ray diffraction (XRD), and X-ray photoelectron spectroscopy (XPS) [16,139].

Table 2-6. Characterization tools conducted for chitosan adsorbents

Chemical Analysis	Microscopic Analysis	Macroscopic Analysis
-Infrared spectroscopy (IR) -Fourier transform infrared spectroscopy (FTIR) -Attenuated total reflectance micro-Fourier transform infrared (ATR-FTIR) -X-ray diffraction (XRD) -X-ray photoelectron spectroscopy (XPS) -Nuclear magnetic resonance spectroscopy (NMR) -Elemental analysis (EA)	-Optical microscope -Transmission electron microscopy (TEM) -Brunauer-Emmett-Teller analyzer (BET) -Scanning Electron Microscopy coupled with Energy Dispersive X-ray (SEM-EDS)	-Thermogravimetric analyzer (TGA) -Magnetic testing -Mechanical testing -Compressive testing -Hardness testing

2.8 Adsorption Parameters

In the literature, it is not easy to find consistent information about the adsorption capacities of HMs on chitosan, as many parameters affect the adsorption efficiency. Two adsorbent materials (even for the same pollutant) cannot be compared without maintaining the same experimental conditions. Typically, batch adsorption tests are used to investigate the effect of various parameters

by adding a known mass of adsorbent to a fixed volume of liquid at a predetermined initial concentration and changing the influential parameters. Some of the basic parameters which greatly influence the adsorption process are (1) pH of the solution; (2) contact time; (3) initial pollutant's concentration; (4) temperature; (5) agitation speed; (6) volume of adsorbate; (7) ionic strength of solution; (8) adsorbent's dosage; (9) surface area of the adsorbent and (10) other available components in the system [140,141]. Having the above in mind, the only comparisons that can be realized are those for the same study's adsorbent/adsorbate systems.

2.8.1 Solution pH

During the adsorption process, the solution's pH is one of the most important variables affecting the speciation of metal, the degree of ionization, and the adsorbent's surface characteristics [142]. Thus, some research groups have investigated the effect of pH on HMs adsorption onto chitosan [133]. It was observed that the optimum pH mainly depends on the target HMs and types of modified chitosan. The inevitable precipitation of metal ions in the form of hydroxide ions usually occurs on pH greater than 7 or 8, depending on the adsorbate concentrations [96]. As a result, there is a pH range within which each metal ion can be adsorbed on a particular modified chitosan. It is shown in the literature that in acidic pHs, a mass of H^+ and H_3O^+ in the aqueous solution competes with the cationic metal ions for the available adsorption sites on chitosan and electrostatic repulsion occurs between cationic metal ions and positively charged chitosan surfaces which results in lower adsorption efficiency. With an increase in pH, the adsorption increases as long as the metal species are still positively charged or neutral and not precipitated [143,144]. This is true for most metal ions adsorption, although some metals, such as hexavalent chromium, exist in solution as negative species, showing an opposite behaviour [145].

2.8.2 Temperature

Temperature is perceived as an important parameter for the adsorption of metal ions by adsorbents. That is mostly because the solution's temperature may affect the solid/liquid interfaces, the swelling property of adsorbents, and metal ions' mobility. Generally speaking, the adsorption of HMs onto chitosan increases with temperature because high temperatures provide a faster rate of diffusion of adsorbate molecules (metals) from the solution to the adsorbent (chitosan) [146].

However, the adsorption process is not usually operated at high temperatures because this would increase operation costs [144]. Apart from the influence of solution temperature on adsorption efficiency, temperature changes may also be used to evaluate the thermodynamic parameters of an adsorption process. Thermodynamic parameters such as ΔG (Gibbs free energy change), ΔH (enthalpy change), and ΔS (entropy change) help investigate the nature of the adsorption process (spontaneity, randomness, endothermicity, or exothermicity). Evaluation of thermodynamic parameters gives an insight into the possible mechanisms of adsorption. These parameters can be calculated by using the thermodynamic equilibrium coefficient obtained at different temperatures [101].

At constant temperature and pressure, the ΔG value is the fundamental criterion of spontaneity, and a negative value for ΔG stands for the spontaneity of the reaction. By using the equilibrium constant obtained for each temperature, ΔG can be calculated according to the Gibbs expression, defined in Table 2-7. It is important to note that ΔG is estimated from the equilibrium adsorption data under the assumption that a molecule's adsorption is reversible and that an equilibrium condition is established in the batch system [144,147]. The ΔH and ΔS changes of an adsorption reaction can be determined using the Van't Hoff equation, indicated in Table 2-7, at different temperatures assuming these parameters to be independent of temperature. The positive values of ΔS could be explained as an increase in entropy due to the exchange of metal ions by more mobile ions during the adsorption process. The negative values of ΔG and ΔS, as known from thermodynamics, need a negative adsorption enthalpy (ΔH), meaning that the adsorption process is exothermic, as opposed to endothermic reactions with positive enthalpy. The ΔH value can also be used to measure the interaction force between adsorbate and adsorbent, indicating the bonding strength. Adsorption on solids is classified into physical or chemical adsorption, but the dividing line between the two is not sharp. Typically, ΔH for physical adsorption ranges from 4 to 40 kJ/mol, compared to chemical adsorption ranging from 40 to 800 kJ/mol [101,144,148].

Table 2-7. Thermodynamic equations and their parameters [149]

Expression	Linear Equation Form	Parameters
Sorption equilibrium constant	$K_L = \frac{C_{ad}}{C_e}$	C_{ad}: The adsorbed amount at equilibrium (mg/L) C_e: The equilibrium concentration in solution (mg/L)
Gibbs	$\Delta G° = -RT \ln k_L$	R: The universal gas constant (8.314 J/(mol.K)) T: The absolute temperature (K) k_L: The equilibrium constant
Van't Hoff	$\ln k_L = \frac{\Delta S^\circ}{R} - \frac{\Delta H^\circ}{RT}$	R: The universal gas constant (8.314 J/(mol.K)) T: The absolute temperature (K) k_L: The equilibrium constant

2.8.3 Adsorbent Dosage

To maximize the interactions between the metal ions and adsorption sites of adsorbents, finding an optimum dosage of the adsorbent is necessary. Thus, the effect of the adsorbent dosage of chitosan on metal ions adsorption has been investigated in the literature [150,151]. In general, the adsorption efficiency of an adsorbate increases with an increase in the adsorbent dosage because the increase in adsorbent dosage translates into more active exchangeable adsorption sites. However, the apparent adsorption uptake of the adsorbent decreases following the increase in adsorbent dosage. This observation is because the number of unoccupied active adsorption sites grows, and at the same time, nearly all the heavy metal ions in the aqueous solutions are adsorbed by the adsorbents, resulting in a decrease in the apparent adsorption capacity of the adsorbents [101,152].

2.8.4 Contact Time

Contact time is another governing factor in the adsorption process. The contact time directly reflects the process's economic efficiency, related to the adsorption kinetics [133,153]. An ideal adsorbent not only has a large adsorbate capacity but also has a fast adsorption rate. Therefore, the adsorption rate is another critical factor for selecting the adsorbent that must be considered. The most common kinetic models that have been widely used in the literature for adsorption processes are as follows: (i) pseudo-first-order kinetic model [154] (ii) pseudo-second-order kinetic model [155];

(iii) Elovich model [156], and (iv) intraparticle diffusion model [8] which are shown in Table 2-8. These kinetic models are also used to examine the controlling mechanism of the adsorption process.

Table 2-8. Frequently used kinetic models

Model	Equations	Nomenclature
Pseudo-first-order equation	$\log(q_e - q_t) = \log q_e - \frac{k_1}{2.303}\, t$	q_t: the amount of adsorbed on the adsorbent (mg/g) at time t (min) q_e: the amount of adsorbed on the adsorbent at equilibrium (mg/g) k_1: the rate constant of first-order adsorption (1/min)
Pseudo-second-order equation	$\frac{t}{q_t} = \frac{1}{k_2 q_e^2} + \frac{1}{q_e}\, t$	q_t: the amount of adsorbed on the adsorbent (mg/g) at time t (min) q_e: the amount of adsorbed on the adsorbent at equilibrium (mg/g) k_2: the rate constant of second-order adsorption (g/mg)/min
Elovich Equation	$q_t = \frac{1}{\beta}\ln(\alpha\beta) + \frac{1}{\beta}\ln t$	q_t: the amount of adsorbed on the adsorbent (mg/g) at time t (min) α: The initial sorption rate of Elovich kinetic model ((mg/g)/min) β: related to the extent of surface coverage (g/mg)
Intraparticle Diffusion	$q_t = k_m t^{1/2} + C$	q_t: the amount of adsorbed on the adsorbent (mg/g) at time t (min) k_m: the intraparticle diffusion constant ($mg/g/min^{1/2}$)

2.8.5 Metal Initial Concentration

The initial concentrations of metal ions have a substantial effect on the adsorption capacity of chitosan. Generally, adsorption capacity increases with increasing initial concentrations of metal ions. In fact, the initial concentration provides the driving force to overcome all mass transfer resistance of heavy metals between the aqueous and solid phases [133]. Adsorption properties and equilibrium data, commonly known as adsorption isotherms, describe how adsorbates interact with adsorbent materials, which are critical in optimizing the use of adsorbents. Therefore, it is crucial to establish the most appropriate correlation for the equilibrium curve. The equilibrium isotherms

show the amount of adsorbate that can be adsorbed by the adsorbent (q_e) in relation to the equilibrium concentration of the adsorbate in the fluid phase (C_e) [101]. Several isotherm models are available for analyzing experimental data and describing the equilibrium of the adsorption process, and some of them are listed in Table 2-9. The different equation parameters and the underlying thermodynamic assumptions of these models often provide insight into both the adsorption mechanism and the surface properties, along with the affinity of the adsorbent. Therefore, it is vital to establish the most appropriate correlation of equilibrium curves to optimize the condition for designing adsorption systems [10].

Table 2-9. Frequently used single-component isotherms models

Isotherm Types	Equations	Parameters	References
Langmuir	$q_e = \frac{q_{max}\, bC_e}{1 + bC_e}$	q_e: The equilibrium metal sorption capacity (mg/g) C_e: The equilibrium solute concentration in solution (mg/L) q_{max}: Langmuir constants related to maximum sorption capacity b: Bonding energy of adsorption (or affinity)	157
Freundlich	$q_e = K_f C_e^{1/n}$	q_e: The equilibrium metal sorption capacity (mg/g) C_e: The equilibrium solute concentration in solution (mg/L) K_f: Biosorption equilibrium constant representative of the sorption capacity n: Constant indicative of biosorption intensity	158
BET model (multilayer sorption)	$q_e = \frac{K_B Q_{MAx} C_e}{(C_s - C_e)[1 + (B-1)\,{}^{C_e}/_{C_s}]}$	q_e: The equilibrium metal sorption capacity (mg/g) C_e: The equilibrium solute concentration in solution (mg/L) C_s: The saturation concentration of the adsorbed component (mg/L) K_B: Constant indicating the energy of interaction between the solute and the adsorbent surface Q_{Max}: Constant indicating the amount of solute adsorbed forming a complete monolayer	159
Redlich– Peterson	$q_e = \frac{K_{RP}\, C_e}{1 + a_{RP} C_e^{\beta}}$	q_e: The equilibrium metal sorption capacity (mg/g) C_e: The equilibrium solute concentration in solution (mg/L) K_{RP}, a_{RP}, and β :Redlich–Peterson parameters	160
Sips	$q_e = \frac{q_m\, (K_L C_e)^{1/n}}{1 + (K_L C_e)^{1/n}}$	q_e: The equilibrium concentration of the solid phase (mg/g) C_e: The equilibrium concentration of liquid phase (mg/L) q_m , K_L, and $1/n$: The Sips parameters	161

2.8.6 Competitive Adsorption

The presence of other metal ions in the adsorption system can produce possible effects of synergism, antagonism or non-interaction, affecting the adsorption uptake of the metal ions

compared to their single-component systems [162]. The most desirable approach to model multi-component systems is an estimation of competitive isotherms solely based on the corresponding one-component isotherms parameters [163]. However, the individual adsorption parameters may not define interactions between competitive ions. Therefore, additional parameters for multi-component systems describing adsorbate interaction can be used along with the parameters of single-component system models to explain the adsorption in a competitive system. A summary of the most commonly used predictive isotherms is tabulated in Table 2-10.

Table 2-10. Summary of investigated multi-component adsorption isotherms

Isotherm	**Equation**	**Parameters**	**Reference**
Extended Freundlich	$q_{e,i} = \frac{K_{F,i}\, C_{e,i}^{(\frac{1}{n_i})+x_i}}{C_{e,i}^{x_i} + y_i C_{e,j}^{z_i}}$	$q_{e,i}$: The equilibrium solid phase of component i (mg/g) $C_{e,i}$: The equilibrium liquid phase of component i (mg/L) $K_{F,i}$, $1/n_i$: The single-component Freundlich parameters for component i	164,165
Modified Langmuir	$q_{e,i} = \frac{q_{m,i}\, K_{L,i}\, (C_{e,i}/\eta_i)}{1 + \sum_{j=1}^{N} (C_{e,j}/\eta_j)}$	$q_{e,i}$: The equilibrium solid phase of component i (mg/g) $C_{e,i}$: The equilibrium liquid phase of component i (mg/L) $q_{m,i}$ (mg/g), $K_{L,i}$ (L/mg): The single-component Langmuir parameters for component i $\eta_{i(j)}$: Langmuir correction coefficient for component i(j)	166,167
Extended Langmuir	$q_{e,i} = \frac{q_m\, K_{L,i}\, C_{e,i}}{1 + \sum_{j=1}^{N} K_{L,j}\, C_{e,j}}$	$q_{e,i}$: The equilibrium solid phase of component i (mg/g) $C_{e,i}$: The equilibrium liquid phase of component i (mg/L) $q_m(mg/g)$, $K_{L,i(j)}(L/mg)$: The single-component Langmuir parameters for component i(j)	168,169
Extended Sips	$q_{e.i} = \frac{q_{m,i}\, K_{L,i}\, C_{e,i} (\sum_{j=1}^{N} K_{L,j}\, C_{e,j})^{1/(n_i-1)}}{1 + (\sum_{j=1}^{N} K_{L,j}\, C_{e,j})^{1/n_i}}$	$q_{e,i}$: The equilibrium solid phase of component i (mg/g) $C_{e,i}$: The equilibrium liquid phase of component i (mg/L) $K_{L,i}$, $1/ni$: The single-component Sips parameters for component i $q_{m,i}$ (mg/g): The single-component Langmuir parameter for component i	161,163

2.9 Reusability

Adsorbent reusability or regeneration is considered essential to reduce the overall cost of the adsorption process. Regeneration is defined as the recycling or recovery of spent adsorbents using technically and economically feasible methods. Regeneration of loaded adsorbent could provide many advantages as follows: (i) recovery of pollutant, (ii) reusability of adsorbent, (iii) reducing the process cost, (iv) reducing secondary wastes, and (v) identifying the adsorption mechanism [101]. Desorption of adsorbed metal ions from chitosan-based adsorbents is one of the most important advantages of applying these adsorbents to the adsorption system. Nevertheless, chitosan may not be used continuously in the adsorption-desorption cycle because of its biodegradability and solubility in an acidic environment. Figure 2-9 shows the schematic of loaded chitosan adsorption and desorption.

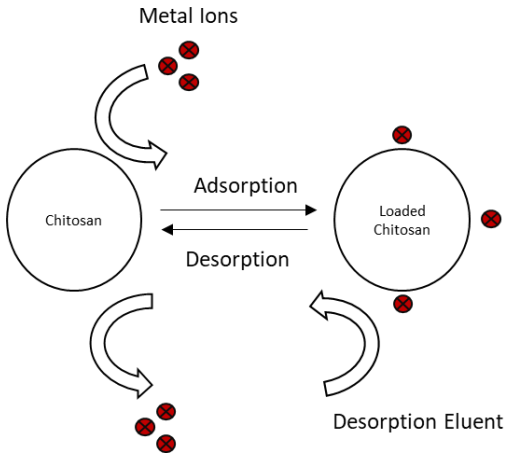

Figure 2-9. Schematic representation of the regeneration procedure of chitosan adsorbent

Different methods have been adopted in the literature for the regeneration of saturated chitosan, classified into three major groups: biological, thermal and chemical [170,171]. Some of the important advantages and disadvantages of these methods are summarized in Table 2-11 [172]. The desorption eluant must meet the following requirements: (i) non-damaging to the biomass, (ii) less costly, (iii) and environmentally friendly [173]. However, only a limited number of researches have been conducted about selecting an appropriate eluant and its optimal conditions for desorption of loaded chitosan.

Table 2-11. Classification of regeneration methods

Regeneration Method	Advantages	Disadvantages	References
Biological	-Complete recovery of adsorption capacity by biodegradation of adsorbed organic compound	-Suitable only for biodegradable contaminants -Toxicity of some pollutants to microorganism -Slow regeneration	174
Thermal	-Suitable for industrial scale	-Needs high temperature -Not cost-effective -Release of harmful gasses -Incapable of complete regeneration	175
Chemical	-Cost-effective -Fast regeneration -Very short process time	-Not environmentally friendly -Affecting the surface of adsorbents -Sludge production	176

The sorption mechanisms involved in metal ions uptake by chitosan can provide an orientation for designing the desorption strategy. Different reagents can be used in the regeneration method, such as solvents, organic and inorganic chemical compounds, electrical current, physical waves, and microorganisms [172]. Desorption and regeneration efficiencies of these methods may vary substantially, and the best option for the adsorbent and pollutants at hand should be identified. Taking into account the chemical compounds, various desorption agents, including acids, alkalis, salts, and chelating agents, have been applied to regenerate chitosan adsorbents after the adsorption of HMs. A summary of common desorption agents that have been used for Ni(II) and Cd(II) is shown in Table 2-12. The salt desorption agent suggests an environmentally friendly solution for regenerating loaded chitosan among the chemical compounds. The disposal of adsorbents at the end of operational life after several adsorption-desorption cycles is also a key aspect to reduce the environmental impact caused by solid waste generation. The use of spent adsorbents in other industrial applications is an attractive approach to waste minimization.

Table 2-12. Summary of desorption agents for recovering Ni(II) and Cd(II) from chitosan adsorbent

Adsorbate	Acid Agents	Chelator Agents	Salt Agents	References
Ni(II)	HCl, HNO_3, H_2SO_4	EDTA	NaCl	177–181
Cd(II)	HNO_3, HCl	EDTA	NaCl	146,151,180,182

Table 2-13 summarizes some recent research on Ni(II), Cd(II), and Co(II) adsorption on modified chitosan in a multi-component system, showing the fitted adsorption isotherm, kinetic model, investigated characterization methods, the temperature of operation and desorption agent.

Table 2-13. Summary of Ni(II), Cd(II), and Co(II) adsorption on chitosan-based-adsorbents

Metals	Isotherm Model	Kinetic Model	Characterization	Temperature (K)	Desorption	References
Cu, Pb, Ni	Langmuir	Pseudo-second-order	SEM, FTIR, XPS	293-313	HCl	183
Cu, Ag, Co, Zn, Ni, Mg	Multi-component Redlich–Peterson Unmodified Langmuir Langmuir-Freundlich	-	-	293	-	184
Cu, Ni, Zn, Cr, Fe	-	-	SEM, EDX	293	-	185
Cu, Ni	Langmuir	Pseudo-second order	TEM, XPS	298-343	-	186
Cd, Cu, Pb	Langmuir	Pseudo-second-order	FTIR, XPS, SEM, XRD	298-308	-	187
Co, Mn, Cd	Langmuir	Pseudo-second-order	SEM, FTIR, XPS	-	-	127
Cu, Zn, Ni, Cd, Cr	Langmuir	Pseudo-second-order	TEM,SEM-EDX, FTIR, XRD	293-327	HCl, EDTA	188
Cu, Ni, Co, Zn, Cd	Langmuir	-	FTIR	293	HCl, H_2SO_4, NH_3	129
Pb, Cu, Cd	-	Pseudo-second-order	XRD, FTIR	298-323	-	149
Cu, Cd	Langmuir	-	SEM,CHN, FTIR, TGA	298	HNO_3, EDTA	182

2.10 Summary and Research gap

Battery recycling and recovery HMs are becoming significant as the manufacturing, and use of electronic devices are escalating. Although hydrometallurgical processes are more environmentally friendly than pyrometallurgical ones, they generate secondary pollution in the environment and must be updated to ensure sustainable development. Adsorption seems an acceptable alternative procedure to recover HMs only if a low-cost adsorbent such as chitosan is employed. In essence, chitosan is an efficient adsorbent for HMs uptake from aqueous solutions, but its modification is inevitable because of the poor physical and chemical properties under harsh physical and chemical conditions. However, only sparse research has considered an environmentally friendly path for chitosan modification, and using non-toxic reagents has been barely examined for chitosan modification in the literature. Considering the shortcoming in a sustainable approach for cadmium, nickel, cobalt recovery from spent battery aqueous solution, the primary purpose of this research was to synthesize chitosan and modified chitosan using non-toxic reagent under mild chemical conditions and evaluate the efficiency of the fabricated adsorbents for the adsorption of cadmium(II), nickel(II), cobalt(II).

2.11 References

The references are merged with those of the other chapters' references and presented at the end of the thesis.

Chapter 3

Technical Paper 1

3 Removal of Cadmium (II) from aqueous solution using tripolyphosphate crosslinked chitosan[1]

Keywords: Heavy Metals; Adsorption; Ionic Crosslinker; Statistical Analysis; Cd(II)

3.1 Abstract

Finding an economical technique for Cadmium (Cd (II)) removal from aqueous solution through an environmentally friendly method has always been of great importance. To this aim, chitosan and sodium tripolyphosphate crosslinked chitosan beads were prepared for Cd (II) uptake from aqueous media. Chitosan with different crosslinking ratios was synthesized by changing the concentration of sodium tripolyphosphate solution (5, 10, and 15% (w/v)). Fourier-transform infrared (FTIR) spectroscopy and X-ray diffraction were then implemented to characterize chitosan and tripolyphosphate crosslinked chitosan beads. Investigating thermodynamic parameters proved the feasibility and spontaneity ($\Delta G^0 < 0$), endothermic nature ($\Delta H^0 > 0$) and randomness increase at solid/solution interface ($\Delta S^0 > 0$) of the adsorbents. The experimental adsorption data for crosslinked chitosan were fitted to isotherm models, out of which the Langmuir model showed the best fit. Lastly, factors influencing Cd (II) adsorption onto adsorbents, including temperature and crosslinking extent, were studied in detail by employing Response Surface Methodology (RSM). The quadratic regression model was in good agreement with experimental data (R^2 = 0.95). The designed model suggested that the maximum adsorption capacity of 99.87 (mg/g) is achievable at 55 ℃ and 2.92% (w/v) crosslinking degree, which was higher than the frequent crosslinked chitosan investigated by other researchers.

[1] A version of this chapter is published in Journal of Environmental Chemical Engineering (https://doi.org/10.1016/j.jece.2020.103842)

3.2 Introduction

The existence of heavy metals ions as environmental contaminants has become a worldwide concern in the last few decades due to their adverse and irreversible impacts. They pose severe threats to ecological systems, human health, and living resources, even at low concentrations, because of their toxic, non-biodegradable, and persistent nature [189]. Despite stringent regulations restricting their improper discharge, the level of heavy metal ions in the environment has steadily increased in recent years due to industrialization and urbanization [146].

Among heavy metals, cadmium (a natural element with trace quantities (0.1 mg/L) in the Earth's crust) has attracted attention substantially owing to its applications and high toxicity [190]. Cadmium is mainly found as a by-product of the chemical treatment of copper, lead, and zinc ores, and it has found applications in different industries, such as metal refineries, mining, smelting, printing, metal plating and the production of pigments, alloys, batteries [191]. Similar to other heavy metals, Cd (II) cannot be biodegraded in the environment; as a result, its concentration has grown steadily, mostly because of anthropogenic activities [62]. Cadmium accumulates in the kidneys and liver and is also found in skeletal and muscular systems leading to kidney damage, renal disturbances, and bone lesions [123]. Acute carcinogenic and teratogenic health impacts due to exposure to Cd (II) are well documented [192]. Considering its limited resources, adverse environmental impacts, and harmful effects on human health, recovery and/or removal of cadmium from various waste streams are crucial in terms of economy, environmental protection, health and safety.

Several techniques have been established for the recovery/removal of Cd (II) from the aqueous phase, such as coagulation and flocculation, chemical precipitation, oxidation/reduction, solvent extraction, electrochemical operations (mainly through redox reactions), membrane processes, ion-exchange and adsorption [44,62,193–195]. However, most of these approaches are not efficient enough when the metal concentration is not high, and the majority of them show some drawbacks such as secondary pollution production, elevated operating and investment costs. Hence, finding an economical and environmentally friendly method for the removal/recovery of Cd (II) has been of great importance when the solution's heavy metal concentration is low in the range (i.e., less than 100 mg/L). Nowadays, adsorption offers many advantages for removing/recovering heavy

metal from aqueous solutions since it is economically feasible (low cost) and ecologically friendly, simple in operation with fast kinetics, and not significantly affected by temperature change and shock-loadings [190,196–198].

Among commercial adsorbents, activated carbon has been the most extensively applied adsorbent for heavy metals uptake, including Cd(II), because of its vast surface area as well as having a porous structure. However, the practical applications of activated carbon are limited because of their high operating costs [22]. The other conventional and widely used adsorbents, such as activated alumina and cation-exchange resins, suffer from the same problem and remain relatively expensive materials. Thus, researchers have been looking for low-cost alternatives with high sorption capacities, such as natural materials or wastes from industrial/agricultural activities [143]. The commonly used term "low-cost adsorbents" implies inexpensiveness and affordability as they would be locally available in large quantities.

Adsorbents with biological origins (biosorbent) in general and biosorbents produced from organic wastes in particular offer advantages over those of chemical sources from different aspects such as promoting sustainable waste management. Metal biosorption is linked to the existence of functional groups in the framework of biosorbents (i.e., alcohol, aldehydes, ketones, carboxylic, ether, phenolic groups) which present binding spots with different affinity and specificity for heavy metal ions uptake [69,198–200]. Several biosorbents have been investigated for Cd (II) biosorption, such as industrial and municipal wastes [131,140,191,201–203], agricultural wastes [204,205], fungi and algae [206,207]. It has been shown that they have the capability of becoming a superior and sustainable technique for Cd (II) removal/recovery from aqueous solution. Among employed biopolymers, chitosan has been reported as an appropriate adsorbent for this aim in terms of operational efficiency and mainly sustainability as chitosan is derived from crustacean shells, which is a waste by-product of seafood processing industries [101,208].

Chitosan, the deacetylated form of chitin, which is an abundant and inexpensive biopolymer in nature, has sparked a significant interest to be utilized in different fields. These include the food industry, medicine, and wastewater treatment due to its unique biological and chemical characteristics, such as biocompatibility, non-toxicity, satisfactory chemical reactivity, hydrophilicity, and chelating in addition to its exceptional adsorption properties [185]. Chitosan has

currently obtained a reputation for its adsorption properties, which thereby offers a potential alternative to conventional adsorbents and also biosorbents [208]. Chitosan is an efficient ion-exchanger due to the existence of free amino and hydroxyl groups available on its backbone, responsible for the acceptable adsorption capacities [209,210]. As a result, its characteristics have been examined by researchers toward the recovery/removal of Cd(II) from aqueous media [191,202,211,212].

Although chitosan has been established as a proper biosorbent for heavy metals uptake, it suffers from poor chemical and physical properties such as low stability when exposed to low pH and high-temperature environments. Generally, chitosan dissolves in a solution through the acidic-to-neutral pH range; therefore, it does not show the required properties for the adsorption-desorption cycle. Consequently, it is imperative to enhance its properties through different techniques, such as crosslinking. The cross-linking process can be performed by chemical (cross-linking agents) or physical procedures (ultraviolet light or radiation) to improve the chemical/physical properties of chitosan, which enables it to be stable (insoluble) in acidic solutions with enhanced mechanical properties.

Several crosslinking agents have been investigated to improve the properties of chitosan, including Glutaraldehyde (GLA) [104,213], Glyoxal (GO) [104], Epichlorohydrin (ECH) [103,213], and Ethylene Glycol Diglycidyl Ether (EGDE) [105]. While these crosslinking agents are efficient in improving chitosan properties, they are considered toxic and hazardous, so they pose adverse effects to the environment. To address this issue, sodium tripolyphosphate (STPP), a non-hazardous and economically viable crosslinker, could be used [108]. Although the crosslinking technique can result in superior properties, it may also diminish the adsorption capacity of chitosan because some of the amine and hydroxyl groups on the chitosan surface are occupied through the crosslinking reactions. Characteristics of crosslinked chitosan are affected by the type and degree of the crosslinking agent, as well as the experimental conditions of performing the process, such as pH and temperature. However, information in the literature about the effect of crosslinking conditions on the adsorption properties of chitosan is limited [214].

Response surface methodology (RSM) is a statistical technique that contributes to the optimization of several variables with the minimum amount of data by offering a proper experimental design. Some researchers have applied RSM to examine and optimize the adsorption

efficiency and the effect of operational factors on the adsorption of different contaminants from aqueous phase [215,216]. Considering the limited existing literature about Cd (II) biosorption by crosslinked chitosan by Sodium Tripolyphosphate and the effect of operational parameters during crosslinking and adsorption processes, the aim of this study was to implement RSM to assess and optimize Cd (II) biosorption onto chitosan beads crosslinked by Sodium Tripolyphosphate as an efficient and non-toxic crosslinker. The effect of adsorbent dosage, pH, crosslinking degree, temperature, and initial concentration of metal was examined and discussed. Synthesizing crosslinked chitosan, accomplished in this study, offers the possibility of an environmentally benign method for chitosan modification and its application for Cd (II) removal from aqueous media.

3.3 Experimental

3.3.1 Materials

Chitosan (85% deacetylation degree) and cadmium sulfate hydrate ($3CdSO_4 \cdot 8H_2O$), and sodium tripolyphosphate ($Na_5P_3O_{10}$) were purchased from Fisher Scientific and Sigma (Canada), respectively. The other chemicals used included acetic acid (CH_3COOH), 99.9 wt %, purchased from VWR (Canada), sodium hydroxide (NaOH) purchased from Sigma (Canada), and sulphuric acid (H_2SO_4), N/50, purchased from Fisher Scientific (USA). All reagents were of analytical grade and used as received without further purification. The deionized water was used throughout the experimental work.

3.3.2 Instruments and Analytical Methods

The Cd (II) concentration was analyzed by atomic absorption spectroscopy (AAS) (PinAAcle 500, Perkin Elmer, Canada). The employed wavelength was 228.8 nm, and the calibration curve was prepared using standard solutions. pH was measured using a HACH (HQ40D) Instrument pH Meter. Fourier transform infrared spectroscopy (FTIR) was carried out for characterization in the range from 650 to 4000 cm^{-1} (Thermo Fischer, Nicolet 6700) using an attenuated total reflectance (ATR) sampling method. XRD patterns of adsorbents were obtained by the Rigaku Ultima IV

instrument with Cu Kα radiation. The voltage and current used were 40 kV and 44 mA, respectively, and the angle range was scanned from 10° to 30°.

3.3.3 Preparation of chitosan beads (CB)

1.60 g chitosan powder was dissolved into 40 mL of 5% (v/v) acetic acid solution on a stirrer and was left overnight. The solution was then dropped into a precipitation bath containing 300 mL of 0.50 M sodium hydroxide, which neutralized the acetic acid and thereby coagulated the chitosan gel to spherical chitosan beads (CB) having an average diameter of 1mm, as shown in Figure 3-1. Deionized water was used continuously to rinse the wet chitosan beads and wash away any sodium hydroxide from the surface of the beads. Following that, the beads were filtered using a glass microfiber filter and finally air-dried to remove the water from the structure.

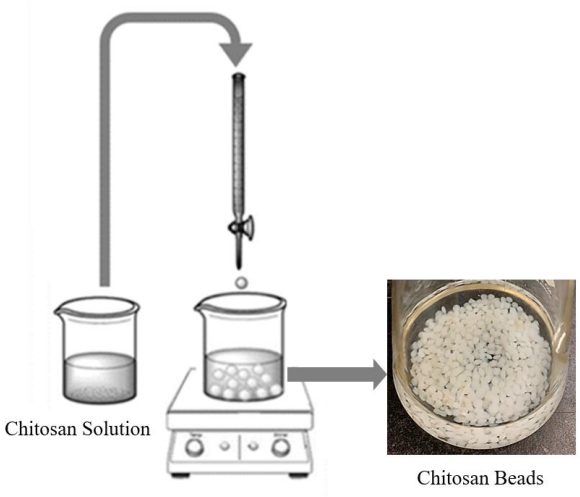

Figure 3-1. Schematic procedure of chitosan beads preparation

3.3.4 Preparation of sodium tripolyphosphate crosslinked chitosan beads (STPP-CLCB)

A similar process was applied by dissolving 1.60 g chitosan in 40 mL of 5% (v/v) acetic acid. Then, the sodium tripolyphosphate (STPP) solution was prepared at pH 8.5 with different concentrations (% (w/v)) to evaluate the effect of crosslinking degrees. Following that, the viscous solution of chitosan was gradually dropped into the STPP solution, which was being stirred continuously. The formed slightly yellowish crosslinked chitosan beads (STPP-CLCB) were left

in the solution overnight, followed by being filtered, rinsed with deionized water consistently, and subsequently air-dried. The interaction between the positively charged amino group of chitosan and phosphate groups of sodium tripolyphosphate as a polyanion is shown in Figure 3-2(c) schematically [217].

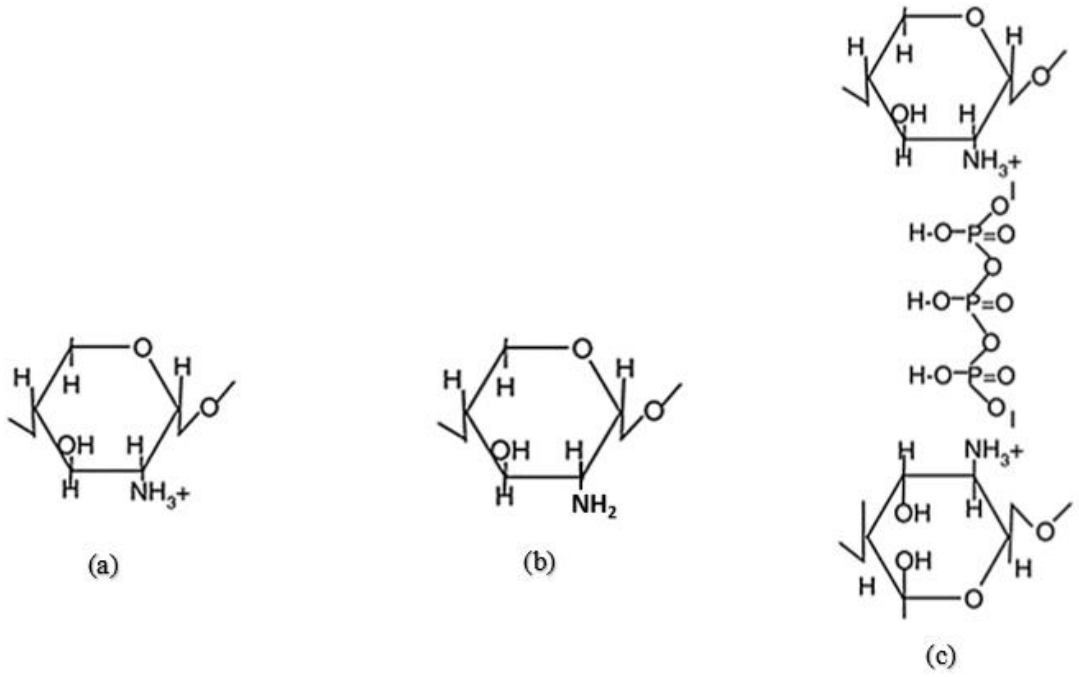

Figure 3-2. Schematic depiction of (a) chitosan, (b) deprotonated chitosan and (c) crosslinked chitosan by tripolyphosphate

3.4 Batch adsorption experiment

The batch adsorption tests were conducted in 125 mL Erlenmeyer flasks with 50 mL of Cd (II) solution, equilibrated at 225 rpm for 24 h to ensure equilibrium was achieved (no concentration change was observed after 18 h based on the preliminary tests). Stock solutions of Cd (II) ions (50 mg/L) were prepared using the analytical-reagent grade cadmium sulfate hydrate. A weighed amount of the adsorbent (either CB or STPP-CLCB) was added into Cd (II) solution. After giving enough time to the adsorption system, the amount adsorbed per unit mass of adsorbent at equilibrium, q (mg/g), was calculated by using the following equation:

$$q = \frac{(c_0 - c_e)V}{W} \qquad 3\text{-}1$$

Where c_0 and c_e (mg/L) are the initial and final concentration of a metal ion in the solution, V (L) is the volume of the solution, and W (g) is the weight of the dry adsorbent. Each test was conducted in triplicate unless otherwise stated, and the control experiments were also conducted to monitor any weight loss due to precipitation.

3.4.1 The effect of adsorbent dosage

The impact of adsorbent dosage on the Cd (II) ions uptake was assessed by changing the amount of adsorbent from 12.5 to 50 mg at a constant initial concentration of 50 mg/L of Cd (II) in 50 mL solution with the initial pH of 7.5 and agitation period of 24 h at 25℃.

3.4.2 The effect of pH

22.5 mg of the adsorbent samples (equivalent to a dosage of 0.45 g/L) was placed in a series of flasks that contained 50 mL of a Cd (II) solution with the initial concentration of 50 mg/L at 25℃. The stirring rate was fixed at 225 rpm for 24 h. The initial pH value of the Cd (II) solution of flasks was adjusted in the range of 4 to 8.5 by using 0.1 M sodium hydroxide/sulfuric acid solutions.

3.4.3 The effect of temperature

Batch adsorption tests were conducted by placing 22.5 mg of dry beads in a series of flasks having 50 mL of Cd (II) solution (50 mg/L) at pH 7. The containers were agitated in a shaker at 225 rpm while the temperature was adjusted at 25, 40, and 55℃ for 24 h.

3.4.4 The effect of initial concentration

22.5 mg of adsorbent with different crosslinking degrees (5, 10, and %15) were employed to study the distribution of Cd (II) between solid adsorbent and liquid phase at equilibrium. The experiments were conducted in 50 mL of Cd (II), having initial concentrations in the range of 0 to 1500 mg/L at an initial pH of 6.5 while stirring for 24 h at 25℃. Various isotherm equations,

including Freundlich, Langmuir, and Dubinin–Radushkevich (D–R), have been investigated to describe the equilibrium characteristics of adsorption.

3.5 Statistical analysis and optimization

Conventional optimization methods include one variable change at a time, which is pretty laborious, particularly when different variables are examined at the same time. Instead, response surface methodology (RSM) attempts to optimize the response surface shaped through the effect of the operating variables. RSM is an empirical modelling technique that can be employed to assess the correlation between a set of adjustable experimental parameters and obtained results. Furthermore, designing experiments is usually included in RSM to provide satisfactory measurements of the response, being able to establish a mathematical model with an acceptable fit to the data attained from the design of experiments [216,218]. Once the model is achieved, various statistical analysis methods are normally implemented to assess the error possibility, the fittingness of the model, and the statistical significance of the parameters in the model. The Central Composite Design (CCD) of experiments for two independent variables, including temperature and crosslinking degree (concertation of STPP crosslinking agent), was selected for the design of experiments of this research to determine the values of each variable, contributing to the optimization of the responses (adsorption efficiency).

Two factors, temperature and crosslinking extent, were selected in this research as the independent variables, shown as T and STPP, respectively, each having five levels (±1, 0, and ±α, for the factorial, center, and axial points, respectively), as presented in Table 3-1 (star point (α) was considered as 1.4142). In a system having two independent variables (X_1 and X_2), the mathematical correlation of the response Y to the defined variables can be predicted by the full quadratic (second-degree) polynomial equation (Eq. (3-2)):

$$Y = \beta_0 + \beta_1 X_1 + \beta_2 X_2 + \beta_{12} X_1 X_2 + \beta_{11} X_1^2 + \beta_{22} X_2^2 \qquad 3\text{-}2$$

Where Y is the predicted yield, β_0 is constant, β_1 and β_2 are linear coefficients, β_{12} is the cross-product coefficient, and β_{11} and β_{22} are quadratic coefficients.

Table 3-1. The levels of variables chosen for the experiment runs.

Independent Variables		Coded Value				
	Symbol	-α	-1	0	+1	+α
Temperature (°C)	T	19.82	25	37.5	50	55.17
STPP Solution Conc. (% w/v)	STPP	2.93	5	10	15	17.01

The total number and arrangement of experimental tests were defined by using MINITAB 19 Software for Windows. Considering the suggested design, 13 experiments were carried out with three replicates to assure the accuracy of the results.

3.6 Results and discussion

3.6.1 Effect of adsorbent dosage on Cd(II) adsorption onto chitosan

Finding the ideal adsorbent dosage is important so as to increase the interactions between Cd (II) ions and adsorption sites of adsorbent in the solution and, at the same time, maintain high removal efficiency. The adsorption capacity and the removal percentage of Cd (II) on chitosan beads (CB) as a function of adsorbent dosage are presented in Figure 3-3. The obtained results showed a sharp increase in removal percentage from 57.4 to 99.8 %, reaching a plateau by changing the CB dosage from 0.25 to 1 g/L, which is in agreement with other researchers' findings [151,219]. This observation is the result of the increase in the existence of the available adsorption sites for Cd (II) and chitosan interaction. However, adsorption capacity witnessed a reverse trend, declining from 101.1 to 43.9 mg/g with an increase in the adsorbent dosage, which concurs with Ren et al. and Salah et al. [219,220] results. This behaviour is considered a result of the fact that some of the adsorption sites remain unused when the adsorbent dosage increases, leading to a reduction in the adsorption capacity of the adsorbent. Within the range studied in this set of experiments, the removal efficiency and adsorption capacity for Cd (II) ions were simultaneously at their optimum level when the CB dosage was 22.5 mg (0.45 g/L). Hence, this dosage was chosen for subsequent experiments.

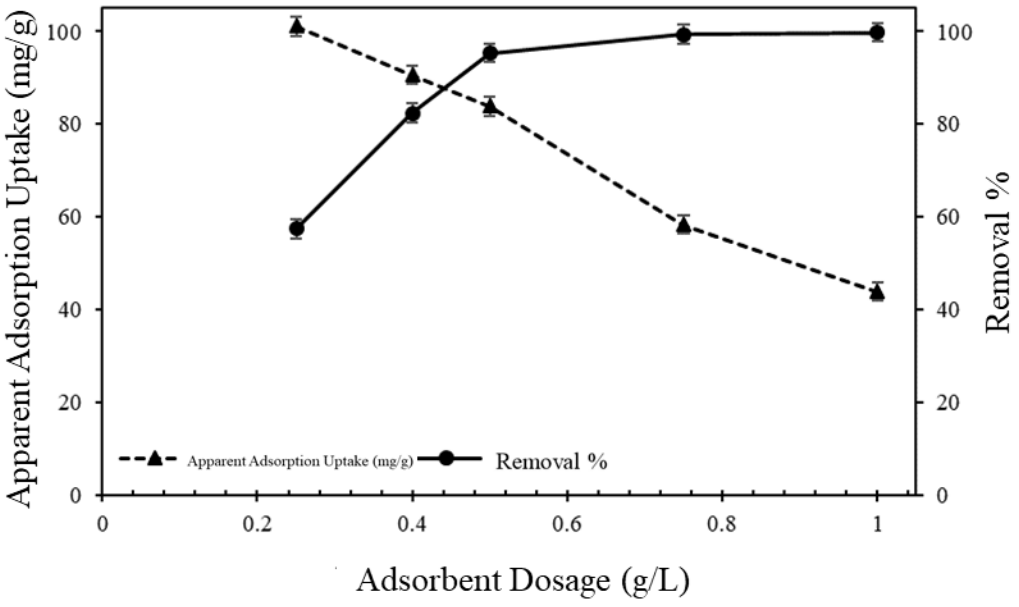

Figure 3-3. Effect of adsorbent dosage on the adsorption of Cd (II) onto CB at 25°C, pH 7.5 and Cd(II) concentration 50 mg/L

3.6.2 Effect of pH on Cd(II) adsorption onto chitosan

The adsorption efficiency of adsorbents depends on the pH of aqueous media. The influence of the initial pH of the solution is more important than the final, as it affects not only the protonation of the adsorbent functional groups but also the speciation of heavy metal ions in the solution. Figure 3-4 illustrates the effect of initial pH within the range of 4.0 to 8.5 on the adsorption capacity of CB toward Cd (II) uptake when the adsorbent dosage was 0.45 g/L. It was observed that the higher adsorption capacity (Cd (II) uptake) occurred at higher pHs, and the maximum adsorption capacity, 141.3 mg/g, took place at pH 8.5. However, at low pHs (pH<6), the amine groups of the chitosan beads begin to protonate, preventing the complex formation on the chitosan surface, which can explain the reduction in the Cd (II) adsorption onto CB. While the same pattern was observed by other researchers [101,221,222], the reported maximum adsorption capacity and the corresponded pH varies with each other since different factors have an impact on the adsorption reaction, such as temperature, pH of the solution, initial concentration of metal, adsorbent dosage and adsorbent functional groups.

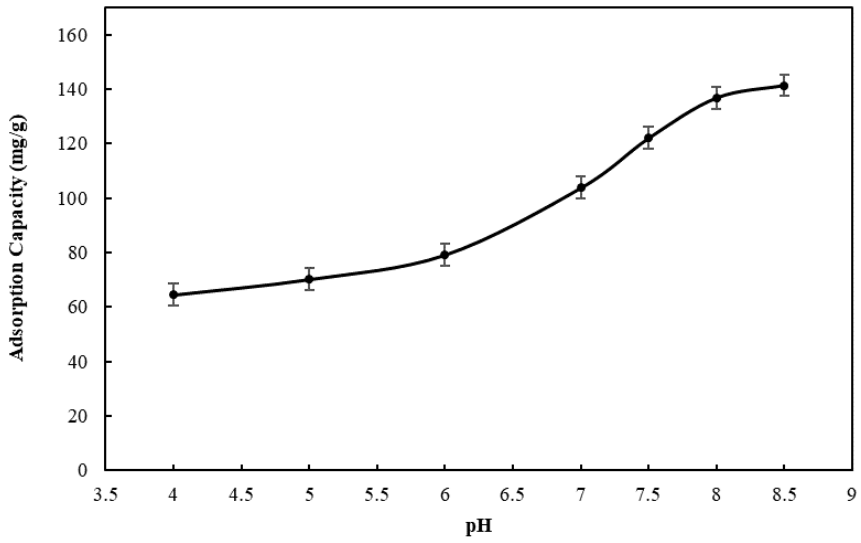

Figure 3-4. Effect of pH on the adsorption of Cd(II) onto CB at 25℃, dosage 0.45 g/L and Cd(II) concentration 50 mg/L

Based on the chelation mechanism, increasing the pH facilitates the amino group of chitosan to become free from the protonation and available for metal adsorption. However, the metal solubility decreases with a further increase in pH, leading to metals precipitation as hydroxides. At low metal concentrations, the precipitation is controlled by Eq. (3-3) [223];

$$[OH^-] = \frac{\sqrt{K_{SP}}}{[M^{2+}]} \quad 3\text{-}3$$

$$pH = \log\frac{1}{[H^+]} \quad 3\text{-}4$$

$$[H^+][OH^-] = 10^{-14} \quad 3\text{-}5$$

Where $[M^{2+}]$ is the metal ion concentration (g/L) and K_{SP} is the solubility product constant, which is 2.50×10^{-14} for $Cd(OH)_2$ at 25℃. Taking into account Eq. (3-4) and (3-5), the hydroxide precipitation of Cd(II) having a concentration of 50 mg/L would start at pH 8.5. Due to a slight difference between Cd(II) uptake at pH 7 and 8 and the fact that working in the neutral pH range is usually preferred since the need for chemicals for pH adjustment is obviated, pH 7 was selected for subsequent tests, and no precipitation was observed.

3.6.3 Crosslinking and Characterization of CB and STTP-CLCB

Three different adsorbents, including none-crosslinked (CB), lower and higher degrees of crosslinked beads (STPP-CLCB) at a constant pH 8.5, were prepared for characterization. The concentration of the STPP solution of lower and higher were 5 and 15% (w/v), respectively. Considering the conducted preliminary tests, if STPP concentration is much greater than 15% (w/v), sodium tripolyphosphate solution becomes saturated, and precipitation starts which hinders the chitosan crosslinking, and on the other hand, at low concentrations much lower than 5% (w/v), the crosslinking process may not complete.

The synthesized CB and STPP-CLCB were characterized using FTIR spectroscopy, which is presented in Figure 3-5. For chitosan (Figure 3-5(a)) shows a broad band centred at 3200–3500 cm^{-1} corresponds to the combined peaks of the NH_2 and OH group stretching vibration, which disappeared after crosslinking by STPP (Figure 3-5(b) and (c)). The absorption peak at 2875 cm^{-1} is attributed to the asymmetric and symmetric stretching vibrations of -CH groups of chitosan, which was weakened and finally vanished by increasing the crosslinking degree to 15% (w/v) [224,225]. The peak at 1602 cm^{-1} was assigned to the characteristic N-H absorption of NH_2, which was shifted to the lower wavenumber at~1580 cm^{-1} on 5 and 15% STPP-CLCB, which could be a result of the reaction between phosphoric and ammonium ions [226]. The other regular absorption peak on chitosan is 1078 cm^{-1}, which is ascribed to the bending vibration of the C–O stretching group, which disappeared after crosslinking. In its place, additional new peaks were observed in Figure 3-5(b) and (c) at ~1200 and ~900 cm^{-1}, corresponding to P=O stretching and deformation, which suggests the occurrence of crosslinking by STTP [227]. The strength of absorbance at these wavelengths is related to the STPP solution concentration, having a sharper peak at a higher crosslinking degree (15% (w/v)) [214].

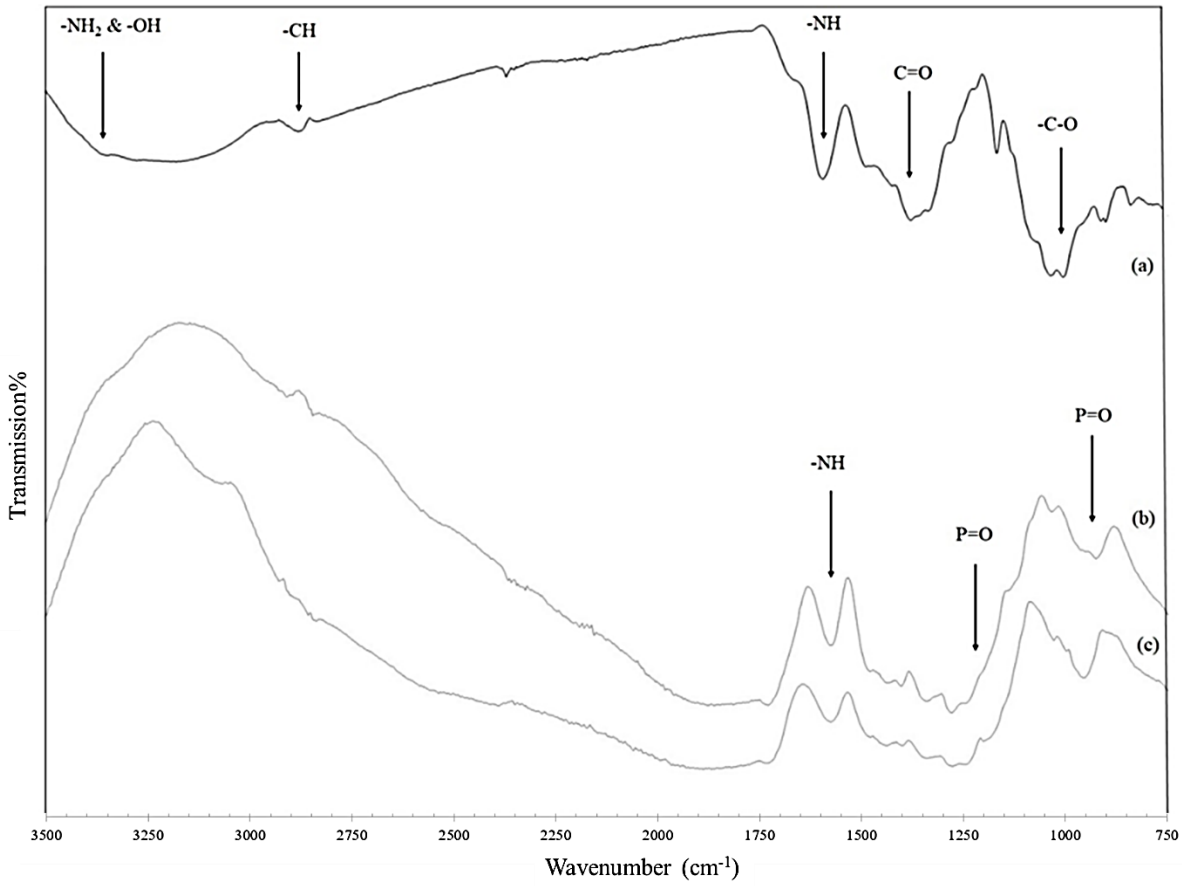

Figure 3-5. FTIR spectra of (a) chitosan (b) 5% STPP-CLCB and (c) 15% STPP-CLCB

The crystallographic structure of chitosan and crosslinked chitosan by STPP (5 and 15% (w/v)) were examined by XRD; they are presented in Figure 3-6. Chitosan characterization, Figure 3-6(a), confirms the presence of the crystalline region by exhibiting a peak at 20° which was also reported by other researchers [228,229]. The peak is allocated to the crystal lattice of chitosan, showing chitosan crystallized in an orthorhombic unit cell [230]. After crosslinking by STTP with two different concentrations of 5 and 15% (w/v), the broader peaks are obtained at 20° which is shown in Figure 3-6 (b) and (c). It is widely accepted that the width of the XRD peak reveals information regarding the size of the crystallite; the broadened peak usually arises from imperfect crystals. Therefore, it is concluded that the increase of imperfect crystal of STTP-CLCBs is related to sodium tripolyphosphate concentration, leading to a decrease in crystallinity [231].

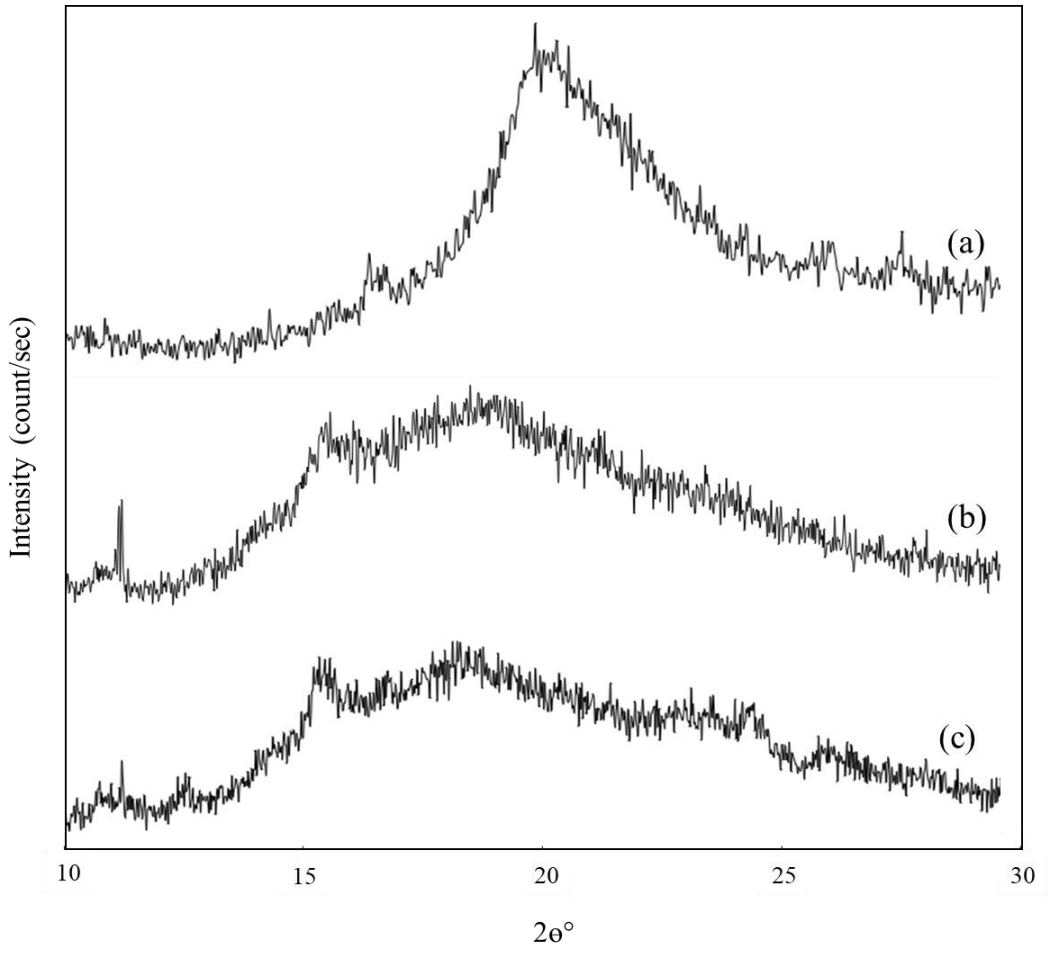

Figure 3-6. XRD patterns of (a) chitosan, (b) 5% STPP-CLCB and (c) 15% STPP-CLCB.

Chitosan crosslinking by an ionic crosslinker (i.e., sodium tripolyphosphate) depends on the availability of positively and negatively charged groups in the solution [232]; because dissolved chitosan in acid is polycationic and presents $-NH^{+}_{3}$ groups, while STTP dissolved in water, dissociates to hydroxyl (OH^{-}) and phosphoric ions (PO_4^{3-}), both presenting negative charges. Dissociated sodium tripolyphosphate to OH^{-} and $-P_3O_{10}^{5-}$ compete with each other to interact with $–NH_3^{+}$ groups of chitosan through either deprotonation or ionic interaction, respectively, which is shown in Figure 3-2(b) and (c). This interaction between the positively charged amino sites and negatively charged counterion (originating from the sodium tripolyphosphate dissociation) is responsible for the formation of the chitosan-tripolyphosphate pellets [217]. Since heavy metals adsorption primarily takes place on chitosan functional groups, including amino and hydroxyl

groups, a decrease in the density of either of them due to crosslinking would lead to lowering the chitosan adsorption capacity toward metal uptake.

3.6.4 Effect of degree of crosslinking and temperature on Cd(II) adsorption

Temperature has been identified as an influential factor for the adsorption of heavy metals, mainly because the solution temperature can affect the solid/liquid interfaces, the swelling property of adsorbents, and the mobility of metal ions. The crosslinking extent is also a critical parameter that influences the adsorption capacity, and generally, an increase in the extent of crosslinking reduces adsorption capacity. Figure 3-7 presents the results of Cd(II) adsorption on CB and two STPP-CLCBs at three different temperatures (25, 40 and 55°C) and crosslinking extent when pH and adsorbent dosage were 7 and 0.45 g/L, respectively. At ambient temperature, CB adsorption capacity was 91.6 mg/g, whereas it was 71.1 and 43.1 mg/g for lower and higher STPP-CLCB (5 and 15% (w/v)), respectively. Cd(II) uptake by CB changed from 91.6 to 122.9 (mg/g) (34% increase), as the temperature increased from 25 to 55°C. Both STPP-CLCBs showed the same behaviour and witnessed a surge in adsorption capacity as the temperature increased. The adsorption capacity of the lower STPP-CLCB experienced an increase of 30.1 mg/g, achieving 101.2 mg/g, while the adsorption capacity of the higher STPP-CLCB showed a more significant shift, hitting 81.4 mg/g from 43.0 mg/g when temperature increased from ambient temperature to 55°C. The observed results were consistent with the work by Liu et al. and Shaker [123,142], and increasing temperature enhanced the adsorption of Cd(II) crosslinked and non-crosslinked beads because high temperatures supply a faster diffusion rate of Cd (II) from the solution onto the adsorbent. Under similar experimental conditions, beads with a higher degree of crosslinking (15% STPP-CLCB) showed the lowest adsorption capacity for Cd (II) uptake at all temperatures, and the adsorption capacity of CB was significantly higher than both STPP-CLCBs. Consequently, the temperature and the degree of crosslinking are essential factors affecting Cd(II) adsorption, and investigation of these parameters together offers interesting results.

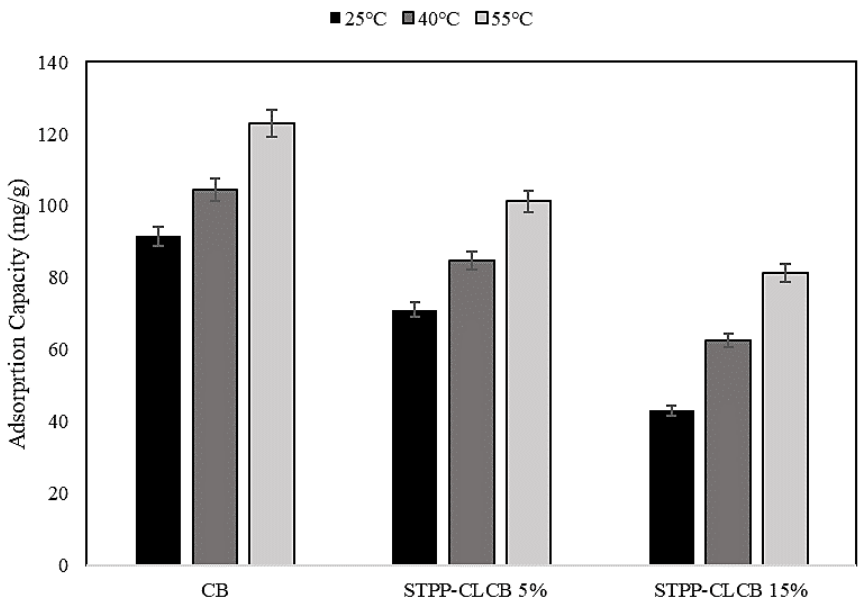

Figure 3-7. Effect of temperature and crosslinking on the adsorption of Cd(II) at pH 7, dosage 0.45 g/L and Cd (II) concentration 50 mg/L.

3.6.5 Thermodynamic analysis

Thermodynamic parameters of an adsorption process are investigated to comprehend the nature of the adsorption reaction, such as spontaneity, randomness, endothermicity, or exothermicity, which are helpful in the practical application of the adsorption process. The thermodynamic parameters can be estimated by the thermodynamic equilibrium coefficients (ΔG°, ΔH°, and ΔS°) obtained at different temperatures. From the thermodynamic point of view, the relationship between Gibbs Free Energy of the adsorption process and sorption equilibrium constant can be described as:

$$\Delta G^\circ = -RT \ln k_C \qquad 3\text{-}6$$

Where ΔG° is the Gibbs Free Energy (J/mol), k_C is the sorption equilibrium constant, T is the absolute temperature (K), and R is the universal gas constant (8.314 J/(mol.K)). The equilibrium constant of the adsorption process, k_C, is calculated by Eq. (3-7) [148] at 298.15, 313.15 and 328.15 K.

$$k_C = \frac{C_{ad}}{C_e} \qquad 3\text{-}7$$

Where C_{ad} is the concentration of solute adsorbed (Cd(II)) on adsorbent at equilibrium (mg/L), and C_e is the equilibrium concentration of cadmium ion in the solution (mg/L). By employing the equilibrium constant calculated for each temperature, ultimately, ΔG◦ can be obtained by Eq. (3-6). It is crucial to note that the calculated ΔG◦ assumes that the adsorption of Cd(II) ions is reversible, and the system reaches the equilibrium state at all temperatures.

Reactions proceed spontaneously at a given temperature if ΔG◦ is a negative quantity. According to the magnitude of ΔG◦, it is feasible to categorize the nature of the adsorption process as physical sorption (described as an ion exchange) when ΔG◦ is higher than −20 kJ/mol [233]. Based on Table 3-2, showing the thermodynamic parameters of CB and STPP-CLCBs, except for higher degree STPP-CLCB (15% (w/v)) at room temperature, the other beads experienced negative ΔG◦ values (higher -20 kJ/mol) at all temperatures. The obtained data suggest the spontaneous physical Cd(II) adsorption, whereby no energy input from outside of the system is needed. ΔG◦ of Cd(II) adsorption onto CB and STTP-CLCB became more negative with increasing temperature, which implies that the adsorption process is more favourable, and the driving force is greater at higher temperatures. Cd(II) uptake by CB at 328.18 K showed the lowest value of ΔG◦ (-7.77 kJ/mol), which explains its highest adsorption capacity among the investigated adsorbents. In contrast, the positive value of ΔG◦ (1.33 kJ/mol) for higher STPP-CLCB at ambient temperature explains its lowest adsorption capacity, discussed earlier.

The standard enthalpy (ΔH◦) and entropy (ΔS◦) changes of an adsorption system can be calculated by using the Van't Hoff Equation (Eq. (3-8)) at different temperatures, supposing these parameters to be independent of temperature. By taking into account Eq. (3-8) and plotting ΔG◦ vs. T, the values of ΔH◦ and ΔS◦ can be calculated from the slope and intercept if the plots show linear behaviour.

$$\ln k_C = \frac{\Delta S^\circ}{R} - \frac{\Delta H^\circ}{RT} \qquad 3\text{-}8$$

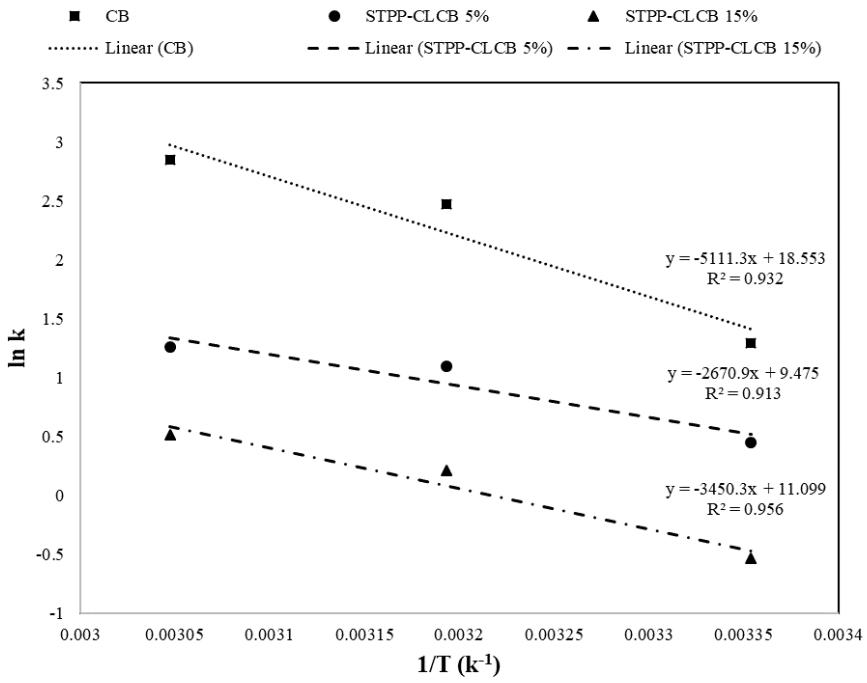

Figure 3-8. Plot of ln k versus 1/T for estimation of thermodynamic parameters for the adsorption of Cd(II) ions onto CB and STPP-CLCB beads at pH 7, dosage 0.45 g/L and Cd (II) concentration 50 mg/L.

The values of ΔH◦ and ΔS◦ from the slope and intercept of the Van't Hoff plot, shown in Figure 3-8, are given in Table 3-2. The positive value of ΔH◦ of all three chitosan beads types reveals that the adsorption reactions were endothermic and implies strong binding of Cd(II) to the adsorbents. The magnitude of ΔH◦ can provide a vision of the interactions happening between the adsorbent and adsorbate. The reported range in the literature varies; however, they all agree that ΔH° > 80 kJ/mol is associated with chemisorption [8]. while ΔH◦ less than 20 (kJ/mol) is an indication of physisorption. In this study, the calculated enthalpy changes were between the above limits, 22.20 and 42.49 kJ/mol; however, considering the aforementioned ΔG◦ discussion, it could be concluded that adsorption was due to physisorption rather than chemisorption. The positive values of ΔS◦ reflect the good affinity of adsorbents for Cd(II) and show that the randomness increases at the solid/solution interface over the sorption process [234]. While most of the conducted research by other scientists regarding Cd(II) adsorption on chitosan derivatives show spontaneous adsorption, a variety of ΔS◦ and ΔH◦ has been reported, revealing the employed crosslinker makes a considerable effect on the mechanism of adsorption leading to different thermodynamic parameters.

Table 3-2. Thermodynamic parameters for Cd(II) adsorption onto CB and STPP-CLCB at pH 7, dosage 0.45 g/L and Cd (II) concentration 50 mg/L.

	Equilibrium Constant			ΔG° (kJ mol^{-1})			ΔH°(kJ mol^{-1})	ΔS° (J mol^{-1} K^{-1})
Temperature (K)	293.15	313.15	328.15	293.15	313.15	328.15		
Chitosan (CB)	3.65	11.88	17.28	-3.20	-6.44	-7.77	42.49	154.25
5% STPP-CLCB	1.56	2.98	3.52	-1.10	-2.84	-3.43	22.20	78.77
15% STPP-CLCB	0.58	1.24	1.67	1.33	-0.55	-1.40	28.68	92.28

3.6.6 Equilibrium isotherms

Establishing an appropriate correlation between the equilibrium curves and adsorption isotherm is imperative to enhance the design of an adsorption system for the adsorbate uptake. The isotherm models can present helpful information regarding the distribution of adsorption sites available on the adsorbent surface and the characteristic of adsorbents, such as surface properties and their capacities [8]. While several theoretical and empirical correlations have been investigated and reported in the literature to model the adsorption isotherms, this study examined Langmuir, Freundlich, and Dubinin–Radushkevich (D-R) isotherm models. Although microcomputers and advanced statistical software can be employed for curve fitting, linear regression is still broadly used as a practical and straightforward way for this purpose. The models' equation and their linear forms are provided in Table 3-3.

Table 3-3. Langmuir, Freundlich, and Dubinin–Radushkevich isotherm models

Isotherm Types	Equation	Parameters	Linear Form	References
Langmuir	$q_e = \frac{q_{max}\, bC_e}{1 + bC_e}$	q_e: The equilibrium metal sorption capacity (mg/g) C_e: The equilibrium solute concentration in solution (mg/L) q_{max}: Langmuir constant related to maximum sorption capacity (mg/g) b: Bonding energy of adsorption (or affinity)	$\frac{C_e}{q_e} = \frac{1}{q_{max}\, b} + \frac{C_e}{q_{max}}$	157
Freundlich	$q_e = K_f C_e^{1/n}$	q_e: The equilibrium metal sorption capacity (mg/g) C_e: The equilibrium solute concentration in solution (mg/L) K_f: Biosorption equilibrium constant representative of the sorption capacity ((mg/g).(L/mg)$^{1/n}$) n: Constant indicative of biosorption intensity	$\log q_e = \log K_f + \frac{1}{n}\log C_e$	158
Dubinin–Radushkevich	$q_e = (q_{max})e^{(-K_{ad}\varepsilon^2)}$	q_e: The equilibrium metal sorption capacity (mg/g) q_{max}: The D-R constant related to maximum sorption capacity (mg/g) K_{ad}: The D-R constant related to mean sorption free energy (mol^2/kJ^2) ε: Polanyi potential	$\ln q_e = \ln q_{max} - K_{ad}\varepsilon^2$	235

The Langmuir isotherm assumption is according to monolayer adsorption on homogenous sites, suggesting that adsorption can only take place at a fixed number of specific localized sites which are equivalent and identical with no lateral interaction and steric hindrance between the adsorbed molecules [236] whereas Freundlich isotherm hypothesis is based on a heterogeneous surface with a non-uniform distribution of active adsorption sites. The D-R isotherm describes the adsorption with Gaussian energy distribution onto heterogeneous surfaces, which is usually employed to distinguish between physical and chemical adsorption.

After fitting the isotherm models to experimental data, the adsorption isotherm parameters and their correlation coefficients (R^2) were calculated and listed in Table 3-4. From R^2 values, it is evident that the Langmuir model predicts experimental data of STPP-CLCBs better than the D–R model. In contrast, the Freundlich model does not fit the experimental data properly. Considering the highest R^2 value belonging to the Langmuir model, it can be concluded that the adsorbents' (STPP-CLCB) surfaces were homogeneous with equivalent energy in its site, and adsorbent sites were equally distributed across the adsorbent. The maximum uptake for Cd(II) at 25˚C and pH of 6.5, using 5, 10, and 15% STTP-CLCB, were found to be 90.09, 101.01, and 109.89 mg/g based on the Langmuir model. The Langmuir constant (b) corresponds to the initial slope of the isotherm curve, and a high affinity for the adsorbate is suggested by the high value of b [237]. While 15%

STPP-CLCB had the highest maximum adsorption capacity, the Langmuir constant (b) of this adsorbent had the lowest affinity for Cd(II) ions, showing 0.50. The adsorption capacity of 5% STPP-CLCB was lower than the maximum adsorption capacity of 10 and 15% STPP-CLCB; however, its b value was higher than 10 and 15% STPP-CLCB values. This observation implies that 5% STPP-CLCB had a higher affinity for Cd(II) ions at low concentrations, but less tendency to adsorb more Cd(II) ions at higher concentrations.

Table 3-4. Langmuir, Freundlich, and Dubinnin-Radushkevich isotherms constants

Constants	**5% STPP-CLCB**	**10% STPP-CLCB**	**15% STPP-CLCB**
Langmuir isotherm			
q_{max} (mg/g)	90.09	101.01	109.89
b (L/mg)	1.06	0.88	0.50
R^2	0.99	0.98	0.99
Freundlich isotherm			
K_f $((mmol/g).(L/mmol)^{1/n})$	3.10	3.24	5.61
n	1.96	1.91	2.19
R^2	0.72	0.75	0.76
Dubinnin-Radushkevich isotherm			
q_{max} (mg/g)	68.43	75.44	81.19
K_{ad} (mol^2/kJ^2)	4×10^{-5}	4×10^{-5}	2×10^{-5}
E	111.80	111.80	158.11
R^2	0.93	0.90	0.79

3.6.7 Response Surface Methodology

In the present study, Central Composite Design (CCD) for two variables (crosslinking level (STPP) and temperature (T)) was applied as the experimental design model. After conducting 13 experiments, each with three replicates at pH 7 and an adsorbent dosage 0.45 g/L, a full quadratic equation was determined to formulate the adsorption capacity as a function of the crosslinking extent and temperature. The full quadratic model was obtained as follows:

$$Q\,(mg/g) = 102.6 - 1.70\,T - 1.87\,STPP + 0.0280\,T*T - 0.0652\,STPP*STPP + 0.0324\,T*STPP \qquad 3\text{-}9$$

Where Q (mg/g) is the adsorption capacity, T is the temperature of the batch adsorption test, and STPP is the concentration of the crosslinking agent used for the preparation of the beads. In addition to the linear impacts of the studied variables on Cd(II) adsorption capacity, the model also provides valuable information about the quadratic and interaction impacts of the parameters such as T*T, STPP*STPP, and T*STPP. The coefficient of the model (Eq. (3-9)) was investigated through the analysis of variance of regression (ANOVA) included in the RSM, and the result of this is given in Table 3-5.

Table 3-5. Analysis of variance for the full quadratic model.

Source	DF	Adj SS	Adj MS	F-Value	P-Value
Model	5	1607.57	321.515	57.71	<0.001
T	1	655.87	655.868	117.73	<0.001
STPP	1	767.49	767.494	137.76	<0.001
T*T	1	133.52	133.525	23.97	0.002
STPP*STPP	1	18.51	18.506	3.32	0.111
T*STPP	1	16.36	16.358	2.94	0.130
Error	7	39.00	5.571		
Lack-of-Fit	3	37.14	12.380	26.68	0.004
Pure Error	4	1.86	0.464		
Total	12	1646.57			
R^2=97.63%	R^2(predicted)= 95.94%		R^2(adjusted)=83.78%		

As a general rule, high Fischer's '$F_{statistics}$' value accompanied by a low probability 'P' value (<0.05) suggests a high significance of the regression model/parameters. Conducted variance analysis for the full quadratic model shows the model is significant, having a high F-Value (57.71) and low P-Value (<0.001). However, the P-Value of lack-of-fit (0.004) was also significant, meaning that there could be some systematic deviation unaccounted for in the designed model [238]. Considering the model terms, such as the linear, square and interaction, it was observed that the interaction of crosslinking degree and temperature term (T*STPP) and square term of crosslinking degree (STPP*STPP) were insignificant, presenting low F-Values (2.94 and 3.32, respectively), and high P-Values (0.130 and 0.111, respectively). Therefore, the T, STPP, T*T elements only

suggested significant effects on the adsorption capacity of the adsorbent. Thus, the model was reduced to the below form by omitting the insignificant terms;

$$Q\,(mg/g) = 97.79 - 1.481\,T - 1.959\,STPP + 0.02940\,T*T \qquad 3\text{-}10$$

The outcomes of the reduced quadratic model for adsorption capacity in the form of analysis of variance (ANOVA) are provided in Table 3-6.

Table 3-6. Analysis of variance for the reduced quadratic model.

Source	**DF**	**Adj SS**	**Adj MS**	**F-Value**	**P-Value**
Model	3	1572.71	524.237	63.88	<0.001
T	1	655.87	655.868	79.92	<0.001
STPP	1	767.49	767.494	93.52	<0.001
T*T	1	149.35	149.348	18.20	0.002
Error	9	73.86	8.207		
Lack-of-Fit	5	72.00	14.401	31.03	0.003
Pure Error	4	1.86	0.464		
Total	12	1646.57			
R^2=95.51%	R^2(predicted)= 87.27%		R^2(adjusted)=94.02%		

Considering Table 3-6, it is evident that the F-Value of the reduced quadratic model (63.88) is greater compared to the full quadratic model (57.71), implying the adsorption capacity equation can be described by the reduced model better. The model P-Value (<0.001) shows that it is statistically significant at the 99% confidence level. The results of variance analysis were used to estimate the parameters' statistical significance, revealing that the linear effect of the variables (T and STPP) beside the square term of temperature (T) was significant, having P lower than 0.05. Figure 3-9 shows the plot of calculated adsorption capacities by the reduced model versus data from conducted experiments for Cd(II) adsorption. The figure suggests that the model can predict the adsorbent behaviour successfully as the points are located close to the line of equality.

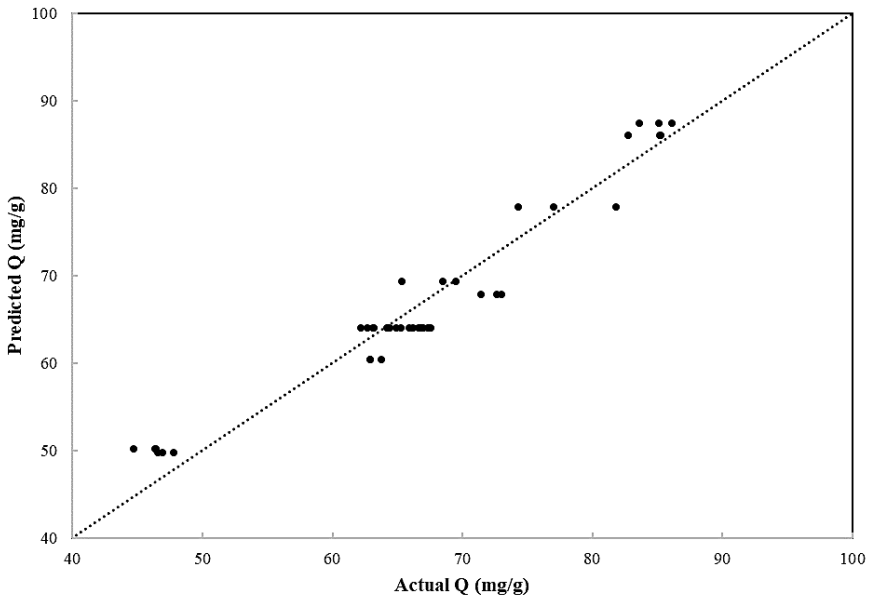

Figure 3-9. Actual vs predicted values of Q(mg/g) based on the reduced model for Cd(II) adsorption

The goodness of fit for the predicted outcomes by the model and the observed data within the range of experiments can be examined by the regression coefficient (R^2). The regression coefficient happened to drop to 0.95 from 0.97 when insignificant terms were eliminated from the model; however, the predicted regression coefficient witnessed a rise reaching 0.87, which was 0.83 initially in the full quadratic model. The value of R^2 and adjusted R^2 of the reduced model are almost close to 1.0, confirming an acceptable description of the relationship between the independent variables (temperature and crosslinking extent) and the response (adsorption capacity). The results of ANOVA revealed that the lack of fit of the reduced model was significant ($P<0.05$). It could arise from some missing systematic variations in the model, and developing a more complex model with a higher number of terms by introducing a higher-order term could lead to an insignificant lack of fit [238]. To confirm that the reduced model presents acceptable approximation, the diagnostic plot of residuals was also generated and plotted in Figure 3-10. According to the figure, it is verified that the model was fairly precise, and there was no need to doubt any violation of the independence or constant variance assumption in all runs since all the standardized residuals were randomly spread within the range (−2 to +2) through the graph [239].

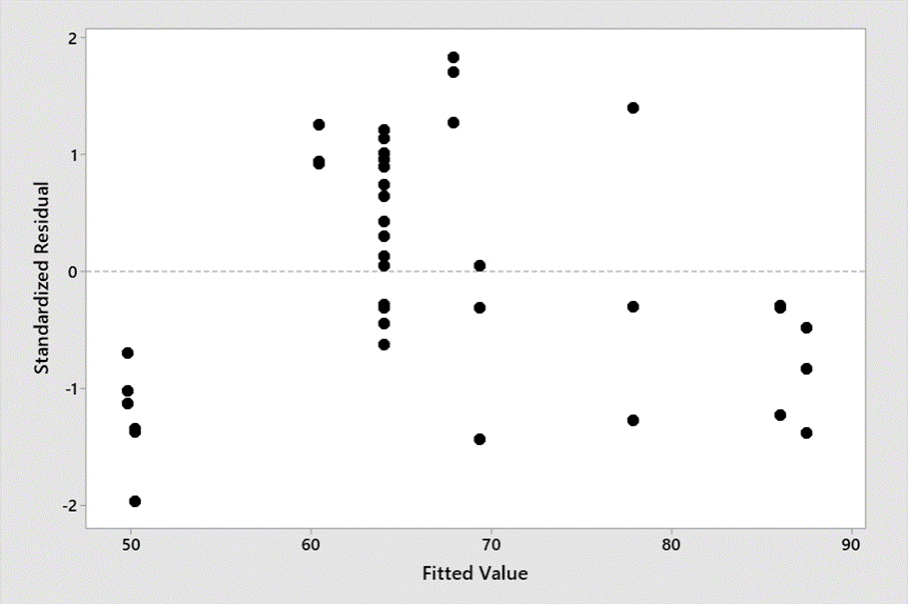

Figure 3-10. Diagnostic plot of the reduced model for Cd(II) adsorption onto STPP-CLCB.

The three-dimensional surface plot (a) and the two-dimensional contour plot (b) of the reduced model are shown in Figure 3-11 to examine the combined effect of temperature and crosslinking level on Cd(II) adsorption onto STPP-CLCB. From Figure 3-11(a), it is perceptible that increasing the temperature and reducing the crosslinking degree boost the adsorption capacity of STPP-CLCB for Cd(II) uptake. The impact of the crosslinking degree was more considerable than temperature, and by increasing the crosslinking degree, the adsorption capacity declined to below 40 mg/g at low temperatures.

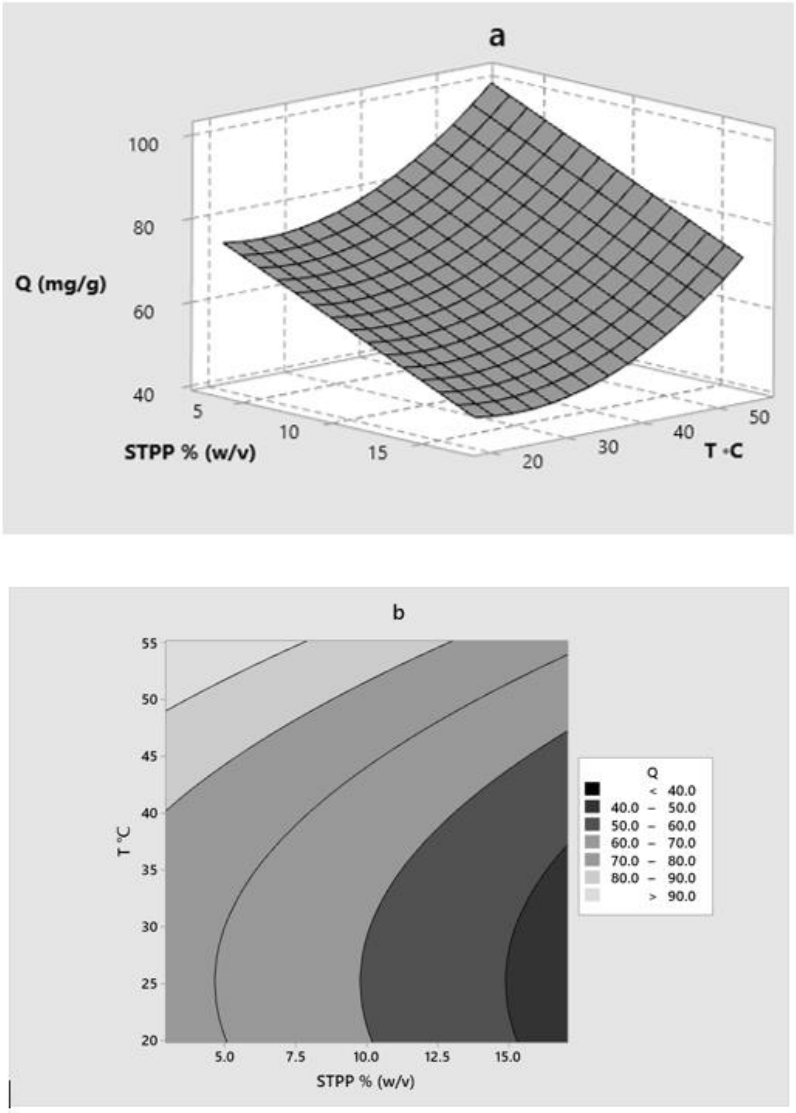

Figure 3-11. (a) Surface plot and (b) contour plot by response surface methodology for temperature-crosslinking degree pair effect on adsorption capacity.

Figure 3-11(b) can facilitate finding the optimum region for the adsorption process of Cd(II) onto STTP-CLCB. Considering the adsorbent behaviour by the reduced model, the maximum predicted adsorption capacity at optimum adsorption variables was calculated by the model, being 99.87 mg/g at temperature 55.17 °C and STPP solution concentration 2.92% (w/v). A test with three replicates was conducted to verify the optimized data obtained by the statistical model under the same defined conditions, and the results were compared to the outcome of the model. Observed

data revealed the adsorption capacity of 93.43 mg/g at the same conditions, which showed a variance of 6.44% from the model prediction. Although applying a 2.92% (w/v) STPP solution resulted in the greatest adsorption of crosslinked chitosan for Cd(II) uptake, it should be mentioned that the formation of the beads took longer than the case with a 5 %(w/v) solution, and some of the formed beads were broken during water rinsing. The maximum adsorption capacities of Cd(II) ions with different conventional crosslinkers are included in Table 3-7 [132]. Considering the table, the adsorption performance of Cd(II) onto STPP-CLCB at the optimum condition was higher (93.43 mg/g) than other commonly employed crosslinkers, while epichlorohydrin (ECH) crosslinked chitosan exhibited the lowest adsorption capacity (41.2 mg/g).

Table 3-7. Comparison of Cd(II) adsorption capacity onto different crosslinked chitosan

Adsorbents	**Sorption Capacity (mg/g)**	**Initial Concentration (mg/L)**	**Reference**
Chitosan crosslinked with GLA	50.3	5-500	132
Chitosan crosslinked with ECH	41.2	5-500	132
Chitosan crosslinked with EDGE	70.9	5-500	132
Chitosan crosslinked with STPP (this study)	93.43 (at the optimum point)	50	

3.7 Conclusions

The most critical factors for the adsorption process to be acceptable are efficiency (high adsorption capacity), cost of the adsorbent used, and sustainability of the process, including the preparation and modification stages. Chitosan beads synthesized by sodium tripolyphosphate were employed in this study as a cost-effective and environmentally benign adsorbent for the adsorption of Cd (II) from aqueous solution. Temperature and crosslinking degree were shown to have a significant impact on the adsorption capacity of crosslinked chitosan. Among the investigated adsorption isotherms, Langmuir showed the best fit to the observed data. The adsorption capacity of STTP-CLCB was identified to be higher for lower crosslinked chitosan beads at low metal concentrations, while higher crosslinked chitosan showed higher adsorption capacity at high metal concentrations. The adsorption capacity was boosted by increasing temperature, which was confirmed by the thermodynamic analysis, showing that almost all of the adsorption processes

were spontaneous at high temperatures. The application of the response surface method predicted the reduced quadratic model with a high correlation coefficient (0.95), suggesting acceptable model prediction and fit to the observed data. The optimization based on the reduced model indicated that the maximum adsorption capacity of 99.87 (mg/g) is feasible at the temperature of 55.17 ℃ when sodium tripolyphosphate solution concentration is 2.92% (w/v), which was inspected and confirmed by performing some experiments under the defined conditions.

3.8 References

The references are merged with those of the other chapters' references and presented at the end of the thesis.

Chapter 4

Technical Paper 2

4 Optimization of Nickel(II) adsorption by sodium tripolyphosphate crosslinked chitosan using response surface methodology (RSM)[2]

Keywords: Batch adsorption study; Heavy metals; Statistical analysis; Ni(II)

4.1 Abstract

The purpose of this study was to synthesize chitosan and crosslinked chitosan hydrogel beads by sodium tripolyphosphate for Ni(II) adsorption from aqueous media. The BET characterization showed that increasing the crosslinking degree reduced the surface area and total pore volume. Increasing temperature and the initial pH of the solution improved the adsorption capacity of the fabricated adsorbents. The calculated thermodynamic parameters indicated the endothermic character of Ni(II) adsorption and randomness increase at the solid/solution interface during adsorption processes. The Langmuir model was more appropriate to analyze Ni(II) experimental data with maximum adsorption capacity in the order of chitosan beads > crosslinked chitosan beads. Two independent experimental factors, including pH and crosslinking degree, were correlated to the adsorption capacity using Response Surface Methodology (RSM), and the model was well-aligned with the experimental data having R^2 = 96.05%. The developed linear model proposed that the adsorption capacity of 31.94 mg/g is feasible at pH 7.21 and crosslinking degree of 2.93% (w/v) for Ni(II) uptake. The adsorption and crosslinking mechanism were investigated using FTIR and SEM-EDS techniques; it appears that the amine groups were the primary sites for metal ions uptake and crosslinking.

[2] A version of this chapter is submitted for publication

4.2 Introduction

Nickel (Ni(II)) has been classified as a high-risk heavy metal due to its bioaccumulative properties, posing a serious threat to human health and animal species [189]. Acute exposure to Ni(II) is linked to several negative health consequences, including diarrhea, kidney disease, and cancer [240]. Apart from these challenges, Ni(II) demand is increasing globally, underscoring the necessity of nickel recovery from industrial waste streams before being released into the environment [241]. As a result, different techniques have been studied to remove heavy metals (HMs), including Ni(II), from aqueous media, such as solvent extraction, ultrafiltration, reverse osmosis, ion exchange, chemical precipitation, adsorption, and electrodialysis [62,193,198,242–245]. Each strategy has distinct advantages and disadvantages, and a detailed evaluation of the relative merits and demerits has been reviewed in the literature [193,198,246]. Nonetheless, the associated costs and the effluent concentration play the primary role in the technique's selection. Among the methods explored, adsorption has gained recognition as a promising technique because of its ease of use, flexibility, adaptability, versatile design, low energy consumption, and cost-effectiveness [8,247]. Accordingly, various adsorbents have been introduced and employed in the literature for HMs adsorption, such as activated carbons [248], zeolites [249], clay minerals [68], and bio-sorbents [69].

The need to remove HMs from the aqueous phase through a sustainable approach has directed researchers' interest to low-cost adsorbents. Thus, natural materials and wastes from industry/agriculture have been brought to light and applied for this purpose [9,250]. Among the investigated adsorbents, biologically-derived adsorbents (bio-adsorbents) have several advantages over those derived from chemicals, such as their availability and renewable nature [251]. Lignin, chitin/chitosan, and cellulose are the most abundant biopolymers. They contain hydroxyl, carboxyl, and amine groups that can bind metal ions and create surface complexes by contributing an electron pair [16]. Of these alternatives, chitosan has garnered considerable attention for heavy metals sorption for multiple reasons, including the presence of different functional groups in its structure (amine and hydroxyl groups) and its modifiability [252,253]. Furthermore, chitosan is largely synthesized by the deacetylation of chitin, which is derived mostly from fishery wastes such as shrimp, lobster, and crab shells [9]. As a result, the use of chitosan in wastewater treatment promotes the sustainable management of seafood sector wastes as well.

Despite chitosan's remarkable characteristics, it is unsuitable for practical use in its natural form due to the solubility in acidic aqueous and comparatively lack of physical strength [94]. Therefore, researchers have investigated different modification techniques to improve chitosan mechanical strength and resistance under different experimental conditions [101,254]. Chemical crosslinking is a common technique for chitosan modification, resulting in chitosan derivatives with desirable physicochemical characteristics [21]. In crosslinking reactions, chitosan macromolecular chains are bonded together, boosting chitosan chemical and physical strength at the expense of reducing the adsorption capacity since crosslinkers occupy particular functional groups of chitosan, rendering them unavailable for metal ions uptake [100]. Hence, various methods such as grafting and ion-imprinting have been developed to counteract the negative effect of crosslinking, leading to an increase in the adsorption system's cost and generating secondary pollution via complex chemical reactions [197,255]. According to the literature, the type of crosslinker used and the conditions of the crosslinking reaction have a significant effect on chitosan's adsorption capacity, as well as its chemical and physical properties; thus, complex modification reactions involving environmentally hazardous chemicals (i.e., in grafting) can be avoided by selecting an appropriate crosslinker and optimizing the experimental conditions [21,89].

Among different ionic crosslinkers employed for chitosan modification, sodium tripolyphosphate is the most often used reagent because of its low cost and environmental friendliness. Our previous study [96] showed that crosslinking of chitosan and the hydrogel beads formation could be accomplished in a single step using sodium tripolyphosphate, resulting in a chitosan-based adsorbent with superior chemical and physical properties. The results demonstrated that altering the variables involved in the crosslinking and adsorption process can mitigate the negative effect of crosslinking on Cd(II) uptake efficiency. Generally, observing the simultaneous effect of factors on adsorption capacity and their optimization have been challenging, requiring additional time, chemicals, and expenses [256]. Hence, Response Surface Methodology (RSM), a collection of statistical and mathematical techniques, has been widely employed in environmental studies for modelling and optimization purposes [257–259].

Given the scarcity of available data on Ni(II) biosorption on chitosan crosslinked with sodium tripolyphosphate, the purpose of this study was to synthesize crosslinked chitosan and employ

response surface methodology to optimize crosslinking degree and adsorption operational parameters to increase Ni(II) adsorption capacity. In this work, the swelling/solubility test and Brunauer−Emmett−Teller (BET) characterization were conducted to evaluate the effect of crosslinking on chitosan hydrogel beads' properties. The effect of pH, the degree of crosslinking, temperature, and metal ions' initial concentration was studied, followed by an attempt to examine thermodynamic parameters and isotherms models. Moreover, different characterization techniques were applied to examine the adsorbents' characteristics before and after Ni(II) adsorption for mechanism investigation.

4.3 Experimental

4.3.1 Materials

Chitosan with a deacetylation degree of 85%, nickel sulphate hydrate ($NiSO_4.6H_2O$), and sulphuric acid (H_2SO_4, N/50) were bought from Fisher Scientific (Canada/USA). Sodium tripolyphosphate ($Na_5P_3O_{10}$) and sodium hydroxide (NaOH) were obtained from Sigma (Canada). Acetic acid (CH_3COOH, 99.9 wt. %) was purchased from VWR (Canada). All reagents were of analytical grade and used as received without further purification. The deionized water was used throughout the experimental work.

4.3.2 Instruments and Analytical Method

HACH Instrument pH Meter (HQ40D) was employed to monitor the pH of the solution, and Atomic Absorption Spectroscopy (AAS, PinAAcle 500, Perkin Elmer) was used to determine the equilibrium concentration of Ni(II). The employed wavelength was 232.2 nm, and the calibration curve was prepared using standard solutions. The adsorbents' specific surface area and total pore volume were calculated using N_2 adsorption-desorption isotherms at temperature 77 K by the Accelerated Surface Area and Porosimetry Analyzer (ASAP 2020, Micromeritics Co.). Fourier Transform Infrared Spectroscopy (FTIR, Thermo Fischer, Nicolet 6700) equipped with the Attenuated Total Reflectance (ATR) sampling method was used to study the adsorbents bands before and after adsorption in the range 450-3500 cm^{-1}. The surface topography and elemental analysis of adsorbents after adsorption was studied using Scanning Electron Microscopic (SEM,

JEOL JSM-7500F), equipped with Oxford EDS INCA 350 spectrometer for Energy Dispersive Spectroscopy (EDS) characterization.

4.3.3 Preparation of chitosan beads (CB)

To synthesize chitosan hydrogel beads, a similar process to that used previously was followed [96]. 1.60 g chitosan powder was dissolved into 40 mL acetic acid solution at a concentration of 5% (v/v) stirred for 24h. Afterwards, the solution was added to a precipitation bath filled with 300 mL of 0.50M sodium hydroxide and left overnight, resulting in spherical chitosan hydrogel beads (CB) formation. CBs were rinsed continuously with deionized water for 3-5 minutes to remove any sodium hydroxide from the surface. The beads were ultimately dried by air to eliminate the remaining moisture from the structure.

4.3.4 Preparation of sodium tripolyphosphate crosslinked chitosan beads (STPP-CB)

Chitosan powder was dissolved into the acetic acid solution, similar to the CB preparation procedure. Then, the viscous chitosan solution was progressively added to the sodium tripolyphosphate solution with different concentrations (5, 10, 15% (w/v)) prepared at pH 8.5 to form sodium tripolyphosphate crosslinked chitosan beads (STPP-CB). The beads were kept in the solution for 24h and then filtered, washed with deionized water on a consistent basis, and dried in the air [96].

4.3.5 Swelling and solubility test

100 mg of CB, STPP-CB5% and 15% (w/v) were immersed in 5% (v/v) acetic acid (pH~2.5), distilled water (pH~6.8) and 0.5 M sodium hydroxide solution (pH~13.0), shaking at 100 rpm at room temperature to evaluate their solubility and swelling properties. After 24h, the beads were removed from the solutions (if they were not dissolved), and the surface was wiped with filter paper to absorb the remaining moisture. The swollen samples were promptly weighed, and the swelling percentage was calculated using the following equation (Eq. (4-1)):

$$\text{Percentage of swelling} = \frac{W_s - W_0}{W_0} \times 100\% \qquad 4\text{-}1$$

where W_s and W_0 (mg) are the weight of swollen and dry beads, respectively.

4.3.6 Batch adsorption studies

Ni(II) stock solution (50 mg/L) was prepared using nickel sulphate hydrate of analytical grade. Batch adsorption experiments were performed in 125 mL glass conical flasks with 50 mL of Ni(II) solution, equilibrated at 225 rpm for 24h (equilibrium was achieved in 18h based on the preliminary tests). The optimum amount of adsorbent (0.55 g/L) was added to the solution. The solution's initial pH was changed from 4.0 to 7.5 ± 0.2 using 0.10M sodium hydroxide/sulfuric acid solution to determine the effect pH. After reaching equilibrium, the loaded beads were filtered, and Ni(II) concentration in the solution was determined using AAS. The equilibrium adsorption amount, q (mg/g), was calculated using the following equation (Eq. (4-2)):

$$q = \frac{(C_0 - C_e)V}{W} \qquad 4\text{-}2$$

where C_0 and C_e are the initial and equilibrium concentrations (mg/L) of the metal ions in the solution; W (g) is the weight of the dry adsorbent, and V (L) is the solution volume. Each test was conducted in triplicate unless otherwise stated, and the control experiments were also conducted to monitor any weight loss.

4.3.6.1 Thermodynamic study

A set of flasks containing 50 mL of Ni(II) solution (50 mg/L) at pH 6.5 was prepared. A weight of 27.5 mg of dry beads (equivalent to 0.55 g/L) was added to the flasks, agitated in an incubator shaker running at 225 rpm for 24h with different temperatures (25, 40, and 55°C) to study the effect of temperature and compute the thermodynamics parameters.

4.3.6.2 Isotherm model study

The batch adsorption experiments were run at room temperature in 50 mL of Ni(II) solutions with different initial concentrations ranging from 10 to 1500 mg/L over a 24-hour period. The

hydrogel beads with the dosage of 0.55 g/L were added to the solutions, and the pH was adjusted to 6.5. Among different theoretical and empirical isotherm models, Langmuir, Freundlich, and Sips, provided in Table 4-1, were employed in this study to investigate the adsorption isotherms. Regression coefficient (R^2) and root mean square error (RMSE) were used to assess the isotherm models' fitness to experimental equilibrium data.

Table 4-1. Langmuir, Freundlich, and Sips isotherm models

Isotherm	Equation	Isotherm Parameters	References
Langmuir	$q_e = \frac{q_{max}\, bC_e}{1 + bC_e}$	q_e: The amount of adsorbate per unit mass of adsorbent weight (mg/g) C_e: The equilibrium concentration of adsorbate (mg/L) q_{max}: The maximum adsorption capacity (mg/g) b: Bonding energy of adsorption (or affinity) (L/mg)	157
Freundlich	$q_e = K_f C_e^{1/n}$	q_e: The amount of adsorbate per unit mass of adsorbent weight (mg/g) C_e: The equilibrium concentration of adsorbate (mg/L) K_f: The Freundlich constant related to the adsorption capacity ((mg/g).(L/mg)$^{1/n}$) n: The Freundlich constant related to the adsorption intensity	158
Sips	$q_e = \frac{q_m\, (K_L C_e)^{1/n}}{1 + (K_L C_e)^{1/n}}$	q_e: The amount of adsorbate per unit mass of adsorbent weight (mg/g) C_e: The equilibrium concentration of adsorbate (mg/L) q_m: The Sips maximum adsorption capacity (mg/g) K_L: The Sips equation constant (L/mg) 1/n: The sips equation exponent related to the index of the heterogeneity	260

4.3.7 Statistical analysis and optimization

RSM includes designing experiments to gather adequate and accurate response measurements to build a mathematical model that best fits the experimental data. Once the model is constructed, several statistical analysis techniques are often applied to determine the likelihood of error, the model's fit, and the statistical significance of the model's parameters [261,262]. If model parameters are not significant for an accurate interpretation of the experimental data, a subset of the model with fewer terms is frequently used [263]. The Central Composite Design (CCD) of experiments was used in this study to analyze the effect of two independent experimental factors: pH and crosslinking level (concertation of sodium tripolyphosphate solution) on Ni(II) adsorption capacity. A full quadratic polynomial equation can be employed in a system with two independent

factors (X_1 and X_2) to estimate the correlation between the response (Y) and the variables, given in Eq. (4-3) [264]:

$$Y = \beta_0 + \beta_1 X_1 + \beta_2 X_2 + \beta_{12} X_1 X_2 + \beta_{11} X_1^2 + \beta_{22} X_2^2 \qquad 4\text{-}3$$

where β_0 is the offset term, β_1 and β_2 are linear coefficients, β_{11} and β_{22} are quadratic coefficients, and β_{12} is the interaction coefficient. MINITAB 19 Software for Windows was used to define the total number and order of experiments, and the proposed experimental design is summarized in Table 4-2. Accordingly, 13 experiments with triplicate were conducted to ensure the precision of the results.

Table 4-2. Detail scope of experiments and range of the operating parameters

Variable	Symbol	Coded Value				
		-α	-1	0	+1	+α
pH	pH	5.7	6.0	6.5	7.0	7.2
Conc. of STPP Solution (% (w/v))	STPP	2.9	5	10	15	17.1

4.4 Results and discussion

4.4.1 Characterization

The BET surface area and total pore volume of CB, STPP-CB5% and STPP-CB15% were recorded in Table 4-3. As indicated, chitosan crosslinking reduced CB's BET surface area from 6.50 to 5.60 and 5.08 (m^2/g) after using 5 and 15% (w/v) sodium tripolyphosphate solution corresponds to 13.8 and 21.8% decrease, respectively. This observation can be attributed to the crosslinker's binding of chitosan functional groups [220], validated subsequently by FTIR in this work. The table also indicates that the total pore volume decreased following chitosan crosslinking by 5 and 15% (w/v) sodium tripolyphosphate solution, implying that STPP-CB would show a lower adsorption efficiency compared to CB. Repo et al. [133] also reported the same observation after crosslinking chitosan with EDTA and DTPA and concluded that chitosan crosslinking reduces the area and pore sizes.

Table 4-3. BET surface area and total pore volume of CB, STPP-CB5%, and STPP-CB15%

	BET surface area (m^2/g)	Total pore volume (cm^3/g)
CB	6.50	4.07×10^{-3}
STPP-CB5%	5.60	3.63×10^{-3}
STPP-CB15%	5.08	2.93×10^{-3}

Regardless of the greater BET surface area and total pore volume of CB, the literature has indicated that chitosan shows hydrophilic characteristics and low physiochemical strength in acidic, neutral and basic solutions, mainly because of the presence of amine groups in chitosan structure [226]. Therefore, solubility and swelling tests were conducted to evaluate the physicochemical properties of CB, STPP-CB5% and STPP-CB15% in solutions having different pHs, including 2.5, 6.8 and 13.0, and the results are tabulated in Table 4-4. As seen in the table, crosslinking chitosan by sodium tripolyphosphate successfully strengthened the chitosan structure since STPP-CBs were insoluble in 5% (v/v) acetic acid, whereas chitosan was dissolved in the acidic solution after 24h. Additionally, increasing the degree of crosslinking was effective in reducing the swelling percentage of chitosan hydrogel beads in the acidic and alkaline media as well as distilled water. In distilled water, the swelling percentage of CB was about six times that of STPP-CB15%. This observation validated the STPP-CBs network's low accessibility and hydrophobic nature, enabling it to function in a wide range of pH. Hence, crosslinking enhanced the physicochemical properties of chitosan hydrogel beads at the expense of decreasing their surface area and total pore volume, which can be minimized by optimizing crosslinking degree and adsorption process parameters [265].

Table 4-4. Solubility and swelling properties of CB, STPP-CB5%, and STPP-CB15%

Beads	Solubility - Swelling (%)		
	5% (v/v) Acetic Acid	Distilled Water	0.5 M NaOH
CB	Soluble - N/A	Insoluble - 118.2	Insoluble - 109.1
STPP-CB5%	Insoluble - 36.4	Insoluble - 27.3	Insoluble - 18.2
STPP-CB15%	Insoluble - 24.2	Insoluble - 19.1	Insoluble - 14.6

4.4.2 Effect of pH and crosslinking

The effect of initial pH on Ni(II) adsorption onto CB, STPP-CB5%, 10%, and 15% was investigated by changing the pH, and the results are shown in Figure 4-1. As seen, an increase in the pH value resulted in a greater adsorption uptake, which can be explained by the fact that at higher pHs, the amino groups of chitosan become deprotonated and available for metal ions uptake [266]. On the other hand, the lower metal ions uptake at acidic pHs was due to the inability of protonated amine groups to form the metal ion-adsorbent complex as the primary binding sites [267]. It is shown that as the pH increases, the solubility of metal ions decreases; thereby, metal ions precipitate as hydroxides [268]. Thus, pHs higher than 7.5 were not examined in this research because of the precipitation of nickel hydroxide [269].

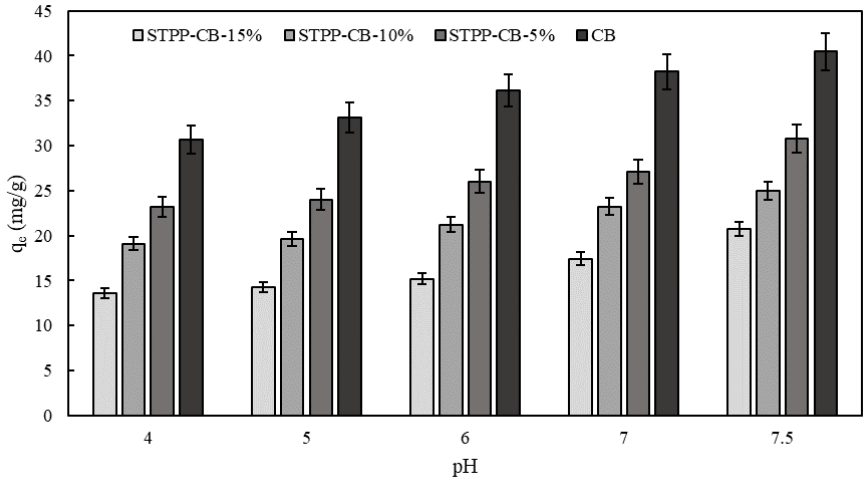

Figure 4-1. Effect of pH on the adsorption of Ni(II) with the concentration of 50 mg/L and adsorbent dosage of 0.55 g/L

As shown in Figure 4-1, Ni(II) uptake on STPP-CBs were lower than CB, following the order of STPP-CB5% > STPP-CB10% > STPP-CB15%. This observation can be explained by the mechanism of ionic crosslinking with sodium tripolyphosphate and metal ions adsorption on chitosan-based adsorbents. Chitosan-tripolyphosphate pellets are normally formed due to the interaction between chitosan's positively charged NH_3^+ groups and negatively charged $P_3O_{10}^{5-}$ groups originating from sodium tripolyphosphate dissociation [270]. Given that heavy metals are adsorbed largely on the amino and hydroxyl groups of chitosan, a drop in the densities of any of these functional groups owing to crosslinking would decrease chitosan adsorption efficiency [100].

Taking this into account, the Ni(II) adsorption on STPP-CBs decreased as the degree of crosslinking increased because more chitosan functional groups were engaged in the crosslinking reaction at a more concentrated sodium tripolyphosphate solution.

4.4.3 Effect of temperature and thermodynamic study

The adsorption of Ni(II) on CB and STPP-CBs was investigated at three temperatures (25, 40, and 55°C), and the results are shown in Figure 4-2. As seen, the adsorption uptake of all adsorbents was improved by increasing the temperature from 25 to 55°C, which was in agreement with the work by Rouhi Broujeni et al. [271]. Figure 4-2 also shows that CB adsorption capacity was higher than that of STPP-CBs at all temperatures, in the sequence of STPP-CB5% > STPP-CB10% > STPP-CB15%, which is in agreement with the previous section's findings. It should be noted that STPP-CB15% showed the lowest adsorption capacity enhancement after increasing temperature to 55°C (23.24% increase), presumably due to an insufficient number of adsorption sites on its surface due to crosslinking by a concentrated sodium tripolyphosphate solution.

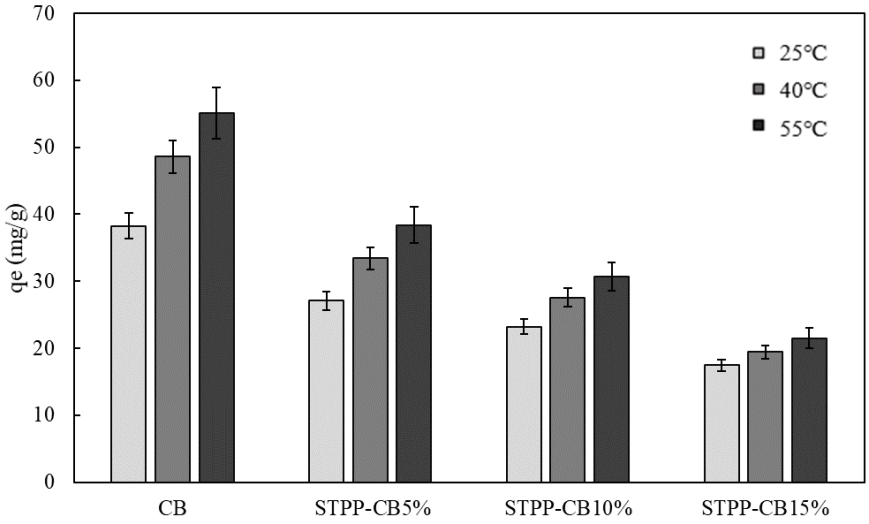

Figure 4-2. Effect of temperature and crosslinking on the adsorption of Ni(II) with the concentration of 50 mg/L and adsorbent dosage of 0.55 g/L

Thermodynamic parameters were also examined to study the adsorption reaction's nature, including spontaneity, randomness, and endothermicity/exothermicity. The thermodynamic parameters (ΔG°, ΔH°, and ΔS°) were computed using the following equations (Eq. (4-4), (4-5), and (4-6)) [149]:

$$k_C = C_{ad}/C_e \quad (4\text{-}4)$$

$$\Delta G° = -RT \ln k_C \quad (4\text{-}5)$$

$$\ln k_C = {\Delta S^\circ}/{R} - {\Delta H^\circ}/{RT} \quad (4\text{-}6)$$

where R is the universal gas constant (8.314 J/mol/K), and T is the absolute temperature (K). k_C is the sorption equilibrium constant; C_{ad} and C_e are the metal ions' equilibrium concentration (mg/L) on the adsorbent and in the solution, respectively.

The thermodynamic parameters of the studied adsorbents are listed in Table 4-5. As shown in the table, ΔG° values of Ni(II) uptake by CB and STPP-CBs were positive except for CB at 40 and 55℃, implying that the adsorption process at these two temperatures was thermodynamically spontaneous with minimal requirements of the activation energy [272]. Ni(II) adsorption onto CB showed the lowest ΔG° value (-0.84 kJ/mol) at 55°C; conversely, the maximum ΔG° value (3.73 kJ/mol) was observed on STPP-CB15% at ambient temperature, confirming the former's superior and the latter's inferior adsorption capacity, presented in earlier sections. The standard enthalpy (ΔH°) and entropy (ΔS°) of the adsorption processes were obtained using Van't Hoff (Eq. (6)) on the assumption that they are temperature-independent. The positive values of ΔH° indicated that Ni(II) adsorption on CB and STPP-CBs was endothermic. The metal ions binding becomes stronger as the ΔH° value increases, and as seen in the table, CB had the greatest ΔH° value, implying a higher affinity of CB for Ni(II). Meanwhile, the positive ΔS° values implied the increase of randomness at the solid-solute interface during Ni(II) adsorption [271].

Table 4-5. Thermodynamic parameters for Ni(II) adsorption with the concentration of 50 mg/L and adsorbent dosage of 0.55 g/L

	Equilibrium Constant			ΔG◦ (kJ/mol)			ΔH◦(kJ/mol)	ΔS◦ (J/mol K)
Temperature (K)	293.15	313.15	328.15	293.15	313.15	328.15		
CB	0.66	1.14	1.36	1.03	-0.34	-0.84	19.83	63.48
STPP-CB5%	0.39	0.58	0.67	2.32	1.42	1.08	14.68	41.73
STPP-CB10%	0.32	0.43	0.47	2.83	2.18	2.04	10.82	27.04
STPP-CB15%	0.22	0.27	0.29	3.73	3.40	3.37	7.40	12.35

4.4.4 Response surface methodological approach

4.4.4.1 Development of the regression model equation

The current work applied Central Composite Design (CCD) as the experimental design method to examine the effect of two independent variables: pH of the solution (pH) and crosslinking extent (STPP) on Ni(II) adsorption capacity (Q). The reason for employing CCD was to facilitate the examination of the interaction between the parameters affecting the response and to determine the parameters' optimum values to maximize the response. The relationship between the response (Q) and the input values yielded the following full quadratic equation as follows (Eq. (4-7)):

$$Q\ (mg/g) = 10.50 + 4.70\ pH - 1.11\ STPP - 0.20\ pH * pH - 0.01\ STPP * STPP + 0.03\ pH * STPP \quad 4\text{-}7$$

where Q (mg/g) is the adsorption capacity, pH is the initial pH of the solution, and STPP stands for the crosslinking solution concentration (% (w/v)) used in the formation and crosslinking of the beads. The analysis of variance (ANOVA) was used to compute all the statistical controls (R^2, adjusted R^2, p-value, F-value, and lack of fit) to evaluate the model's accuracy, and the results are tabulated in Table 4-6.

Table 4-6. Analysis of variance for the quadratic models

	Full quadratic					**Reduced quadratic**				
Source	DF	Adj SS	Adj MS	F-value	p-value	DF	Adj SS	Adj MS	F-value	p-value
Model	5	902.62	180.52	173.51	<0.001	2	899.96	499.98	437.94	<0.001
pH	1	33.85	33.85	32.54	<0.001	1	33.85	33.85	32.95	<0.001
STPP	1	866.11	866.11	832.44	<0.001	1	866.11	866.11	842.93	<0.001
pH*pH	1	0.05	0.05	0.05	0.82	-	-	-	-	
STPP*STPP	1	2.59	2.59	2.49	0.124	-	-	-	-	
pH*STPP	1	0.06	0.06	0.06	0.081	-	-	-	-	
Error	33	34.33	1.04			36	36.99	1.02		
Lack-of-Fit	3	17.68	5.89	10.62	<0.001	6	20.34	3.39	6.11	<0.001
Pure Error	30	16.65	0.55			30	16.65	0.55		
	R^2=96.34% R^2(predicted)= 95.78% R^2(adjusted)=94.78%					R^2=96.05% R^2(predicted)= 95.83 R^2(adjusted)=95.33%				

The ANOVA computed for the full quadratic model (Eq. (4-7)) revealed that the model was statistically significant at the F-value of 173.51 and the corresponding p-value of <0.001 [273]. Examining the model coefficients showed that the square terms, including STPP*STPP and pH*pH and the interaction between crosslinking degree and pH (STPP*pH) were insignificant, exhibiting low F-value and high p-value. Thus, the insignificant terms were eliminated from the model, and the reduced model was simplified to the below form (Eq. (4-8)):

$$Q\,(mg/g) = 18.34 + 2.37\,pH - 1.20\,STPP \qquad 4\text{-}8$$

The ANOVA results for the reduced model are also given in Table 4-6. The 95% interval confidence level range of coefficients were (2.80,1.95) and (-0.78,-1.62) for pH ad STPP, respectively. Taking the table into account, it is clear that the F-value of the linear model (437.94) was greater than the full quadratic model (173.51), suggesting that the equation can adequality represent the adsorption capacity of Ni(II). The p-values of the reduced model and the terms were lower than 0.001, showing that they were statistically significant at the 99% confidence level. The linear model's lack of fit was also significant, indicating that some systematic variation might have been neglected in the proposed model, and adding a higher-order term to construct a more complicated model may result in an insignificant lack of fit [238]. The diagnostic plots of residuals were created to determine the model's reliability, shown in Figure 4-3. The results indicated that

the model was accurate, as all standardized residuals were randomly distributed among the graphs in the range (-2 to +2) [239].

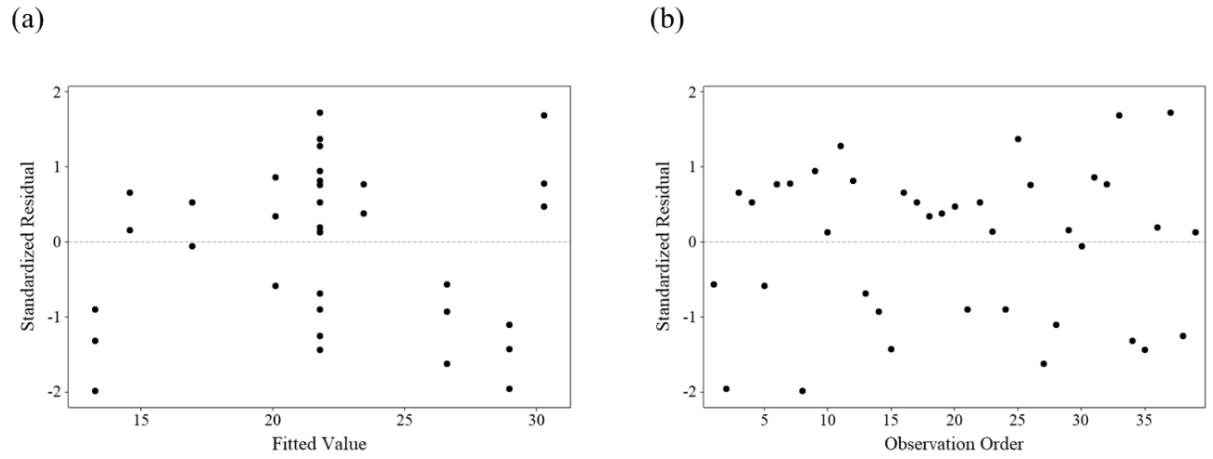

Figure 4-3. Diagnostic plots of the linear model for Ni(II) adsorption (a) standardized residual vs. fitted value (b) standardized residual vs observation order

The regression coefficient (R^2) can be used to verify the goodness of fit between the model's predicted outcomes and the observed data. Comparing the obtained R^2 values, listed in Table 4-6, showed a slight decrease from 96.3% to 96.1% by changing the model from the full quadratic to linear. However, the adjusted R^2 increased marginally from 94.8% to 95.3% after removing the insignificant terms from the full quadratic model. The linear model's predicted R^2 value was very close to 1.0, indicating a good fit between the values predicted by the model and actual values. Figure 4-4 displays a plot of the predicted Ni(II) adsorption capacities against experimental data. The figure indicates that the model can accurately predict the response (Q) as a function of independent variables (pH and STPP) since the points were uniformly scattered close to the 45◦ line.

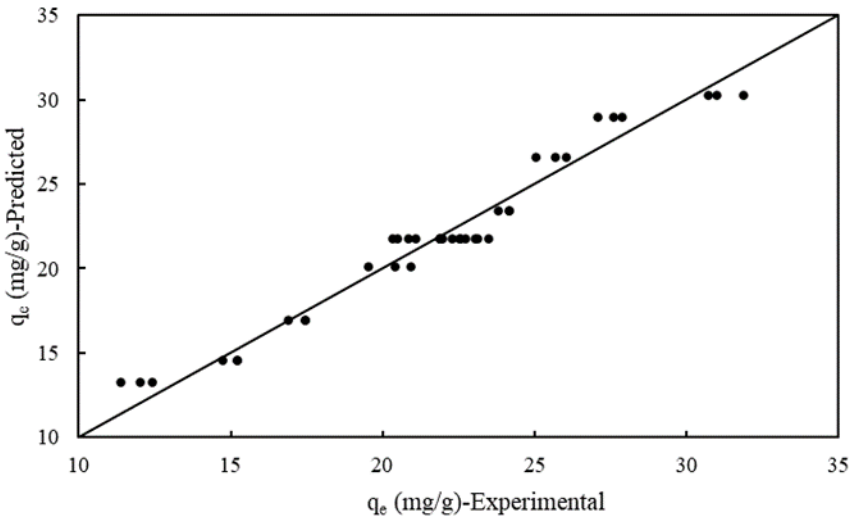

Figure 4-4. Predicted vs experimental values of adsorption capacity based on the linear model for Ni(II) adsorption

4.4.4.2 Estimation for maximum Ni(II) removal

The three-dimensional surface and contour plots, showing the interactive effects of the independent parameters on adsorption capacity, are shown in Figure 4-5-a and Figure 4-5-b. As demonstrated, increasing the pH and decreasing the crosslinking extent improved the adsorption capacity of STPP-CBs for Ni(II) adsorption. The figures also suggest that STPP had a greater effect on Ni(II) uptake compared to pH, consistent with ANOVA results because of its higher F-value. The RSM technique can be employed to predict adsorption capacity for different values of the variables and optimize them to obtain a maximum response. Accordingly, the numeric optimization was performed, and the maximum adsorption capacity of 31.94 mg/g was estimated at the optimal adsorption variables: pH 7.21 and 2.93% (w/v) sodium tripolyphosphate solution. A three-replicate test was conducted to validate the statistical model's optimized adsorption capacity under the same defined conditions. The obtained result indicated the adsorption capacity of 33.59 mg/g, showing a 5.17% error between the value predicted by the model and the actual value. This discrepancy was because the model was being used in an extrapolative fashion to predict the optimal conditions.

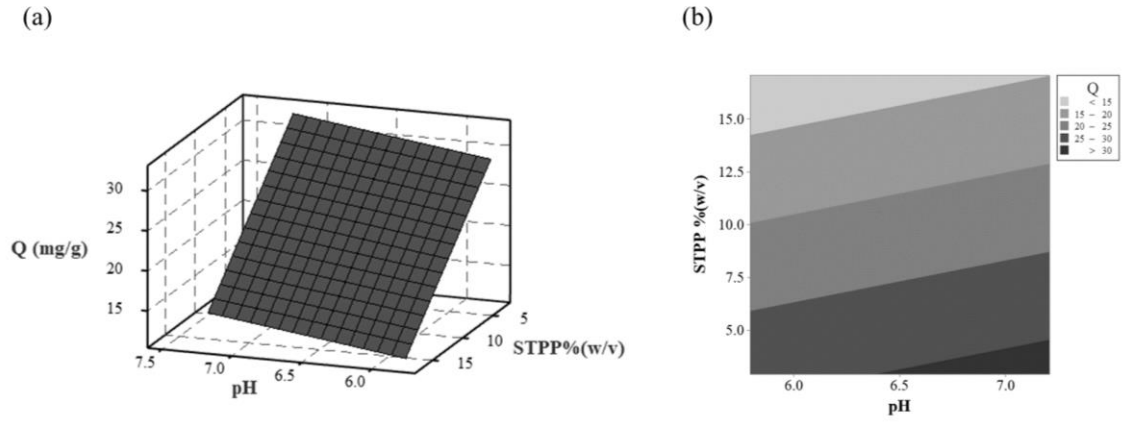

Figure 4-5. (a) 3-D surface plot (b) contour plot for pH-crosslinking degree pair effect on Ni(II) adsorption uptake

4.4.5 Batch adsorption isotherm study

Isotherm models can be quite useful in determining the distribution of adsorption sites on the adsorbent surface, as well as adsorbent characteristics, including surface properties and capacities [8]. Accordingly, the initial Ni(II) concentration was changed between 10 and 1500 mg/L, and the adsorption capacity data were recorded and fit by the Langmuir, Freundlich, and Sips isotherm models. Figure 4-6 shows the applied isotherm models and the collected experimental data for Ni(II) adsorption on CB (Figure 4-6-a) and STPP-CB5% (Figure 4-6-b). As indicated, the adsorption uptake of investigated adsorbents increased gradually by increasing the Ni(II) initial concentration reaching saturation, giving the maximum Ni(II) adsorption capacity, in the order of CB > STPP-CB5%.

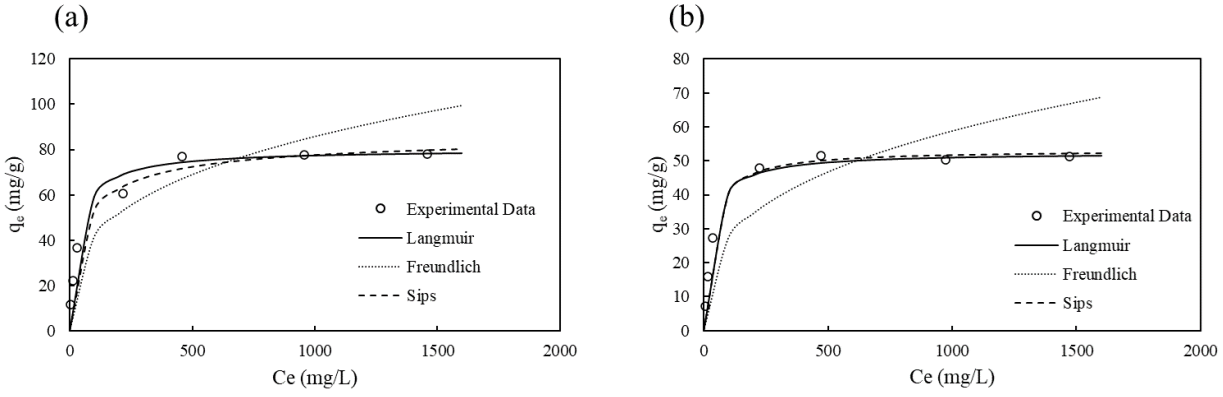

Figure 4-6. Experimental data and adsorption isotherm models of Ni(II) on (a) CB, (b) STPP-CB5%, with dosage of 0.55 g/L at room temperature

The isotherm models were fitted to the experimental data, and the adsorption isotherms parameters along with the regression coefficient (R^2) and root mean square error values (RMSE) were calculated in Table 4-7. The examination showed that the Ni(II) adsorption data were fitted properly by the two-parameter Langmuir and three-parameter Sips models, having high R^2 and low RMSE values. The good fit of the Sips model can be attributed to the addition of a third fitting parameter (1/n), enabling the model to present a combination of Langmuir and Freundlich isotherms. In general, using two-parameter isotherm models is preferred; additionally, the RMSE values for the Langmuir model were comparable to those for Sips. As a result, the Langmuir isotherm was chosen to compare the adsorbents' maximum adsorption capacity [274]. According to the Langmuir model, the maximum Ni(II) adsorption capacity (q_{max}) onto CB was 80.00 mg/g, which diminished to 52.36 mg/g after crosslinking with 5% (w/v) sodium tripolyphosphate solution in order to improve the physicochemical and mechanical properties of chitosan hydrogel beads. The higher adsorption capacity of CB was due to the presence of more functional groups on its surface and higher surface area compared to crosslinked chitosan beads. The empirical Freundlich model, applied to non-ideal and reversible adsorption with heterogeneous surfaces, failed to fit the experimental data by showing a low R^2 and high RMSE compared to Langmuir and Sips isotherms.

Table 4-7. Langmuir, Freundlich, and Sips isotherm models constants for Ni(II) adsorption with the adsorbent dosage of 0.55 g/L

Isotherm Constants	CB	STPP-CB5%
Langmuir isotherm		
q_{max} (mg/g)	80.00	52.36
b (L/mg)	0.03	0.03
R^2	0.99	0.99
RMSE	3.66	1.61
Freundlich isotherm		
K_f $((mmol/g).(L/mmol)^{1/n})$	9.76	5.98
1/n	0.31	0.33
R^2	0.94	0.86
RMSE	9.49	8.93
Sips isotherm		
q_m (mg/g)	87.74	53.05
K_L (L/mg)	0.01	0.03
1/n	0.70	1.07
R^2	0.99	0.99
RMSE	2.60	0.95

The adsorption capacity of some chitosan-based adsorbents from the literature is listed in Table 4-8 for comparison purposes. As shown in the table, the adsorption capacities of CB and STPP-CB5% were within the range of the other chitosan-based adsorbents. However, the hydrogel beads fabricated in this study were formed and crosslinked concurrently in a single step using a non-toxic crosslinker, resulting in a cleaner and simpler crosslinking technique than the others. It is worth mentioning that several parameters affect the maximum adsorption capacity of adsorbents, including temperature, contact time, initial metal ions concentration, adsorbent dosage, and pH. As a result, comparing reported maximum adsorption capacities is complicated unless the system is subjected to identical experimental circumstances.

Table 4-8. Adsorption capacity of Ni(II) onto chitosan-based adsorbents

Adsorbent	pH	Maximum adsorption capacity (mg/g)	Reference
Grafted hydrazinyl amine magnetite-chitosan	5	254.12	[275]
Histidine modified chitosan beads	5	140.8	[276]
Chitosan crosslinked by epichlorohydrin	6-7	32.36	[277]
Ion-imprinted chitosan crosslinked by epichlorohydrin	4	29.55	[278]
Chitosan-modified montmorillonite crosslinked by tripolyphosphate	-	25.82	[279]
Chitosan crosslinked by sodium tripolyphosphate 5% (w/v)	6.5	52.36	This study
Chitosan hydrogel beads	6.5	80.00	This study

4.4.6 Adsorption mechanism

4.4.6.1 FTIR analysis

FTIR spectroscopy was used to characterize the synthesized CB and STPP-CB15 % before and after Ni(II) adsorption, and the results are shown in Figure 4-7 and Figure 4-8, respectively. CB spectrum before adsorption is presented in Figure 4-7-a, indicating broadband between 3150 and 3450 cm^{-1} assigned to the stretching vibrations of the NH_2 and OH groups coupled, which became narrower after Ni(II) adsorption (Figure 4-7-b). The peak at ~2950 cm^{-1} corresponded to the asymmetric and symmetric stretching vibrations of chitosan -CH groups remained unchanged after adsorption, implying that the C-H bond was not involved in the adsorption process [224,225]. The absorption peak at ~1530 cm^{-1} attributed to the characteristic N-H was shifted to a lower wavenumber with reduced intensity after Ni(II) uptake, as seen in Figure 4-7-b, suggesting the contribution of amine groups in metal ions adsorption [226]. Another impacted absorption peak on CB was observed at ~1190 cm^{-1}, ascribed to bending vibration of the C–O stretching group, in which the density decreased following Ni(II) adsorption [96].

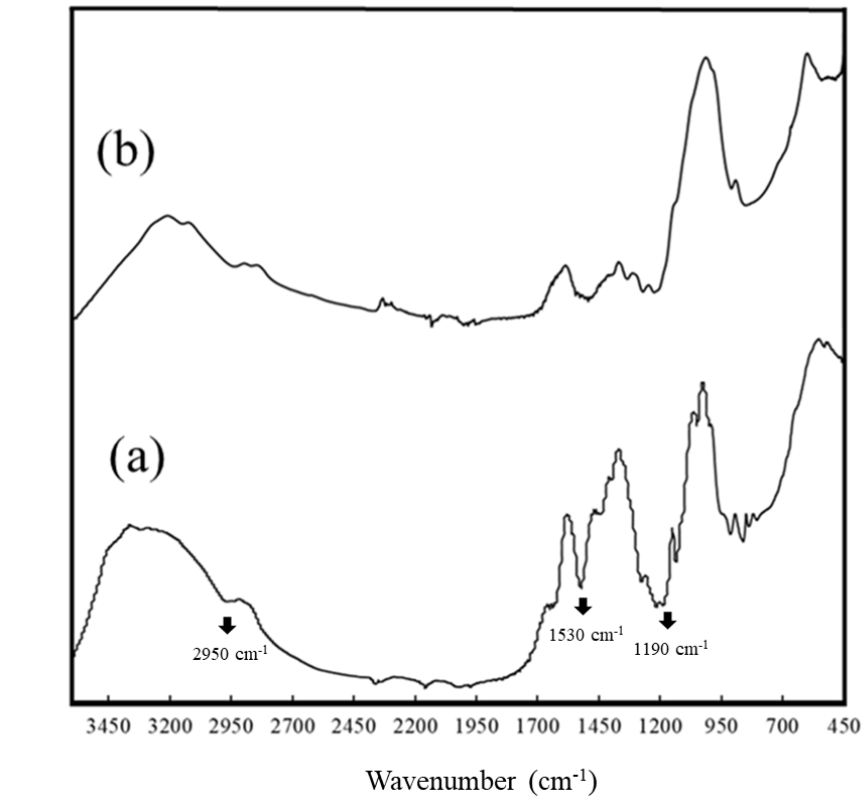

Figure 4-7. FTIR spectra of CB (a) before and (b) after adsorption of Ni(II)

Figure 4-8-a shows FTIR spectra of STPP-CB15% before adsorption. As seen, a peak was observed at ~1210 cm^{-1}, ascribed to P=O stretching, indicating the occurrence of crosslinking by sodium tripolyphosphate [227]. The peak detected at ~1580 cm^{-1} on STPP-CB15% can be attributed to the shifted N-H bond with less strength compared to the CB spectrum (Figure 4-7-a), demonstrating the amine group's role in the crosslinking reaction. Comparing the spectra of STPP-CB15% before and after adsorption revealed that the peak corresponding to the N-H bond was lowered and shifted further after adsorption of Ni(II) (Figure 4-8-b). This observation verified that amine groups were required for both crosslinking and adsorption of metal ions [214]. The peak at ~2950 cm^{-1} detected on CB ascribed to -CH groups asymmetric and symmetric stretching vibrations remained unaffected after crosslinking and Ni(II) adsorption, indicating that -CH groups neither participated in crosslinking nor Ni(II) uptake.

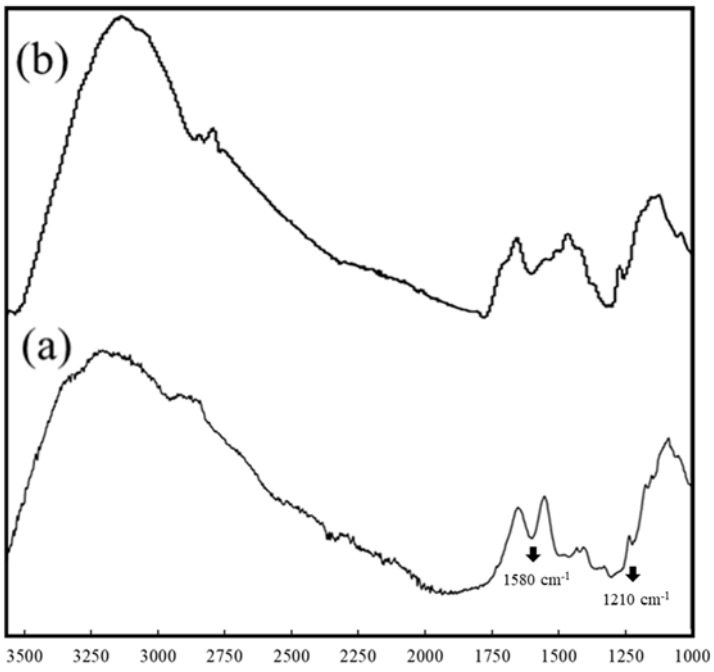

Figure 4-8. FTIR spectra of STPP-CB15% (a) before and (b) after adsorption of Ni(II)

4.4.6.2 SEM-EDS analysis

The SEM-EDS analysis of CB and STPP-CB15% after Ni(II) adsorption are shown in Figure 4-9-a and Figure 4-9-b, respectively. The EDS analysis showed the presence of carbon and oxygen, both of which are components of the chitosan structure, and the Au peaks in the obtained spectra were caused by the samples being coated with gold. The success of crosslinking with sodium tripolyphosphate was confirmed by the appearance of the P peak on STPP-CB15%, as shown in Figure 4-9-b. The EDS data indicated the presence of Ni(II) signals on both adsorbents, confirming Ni(II) adsorption on their surfaces. STPP-CB15% EDS data exhibited a lower Ni(II) peak intensity than CB, implying CB had a greater affinity for Ni(II) adsorption. This examination is in agreement with the findings of the sections mentioned above, underlying the fact that the crosslinking reagent overran chitosan amino groups, and as a result, the remaining amino groups were the primary metal ion binding sites, leading to lower Ni(II) uptake by STPP-CB15% compared to CB.

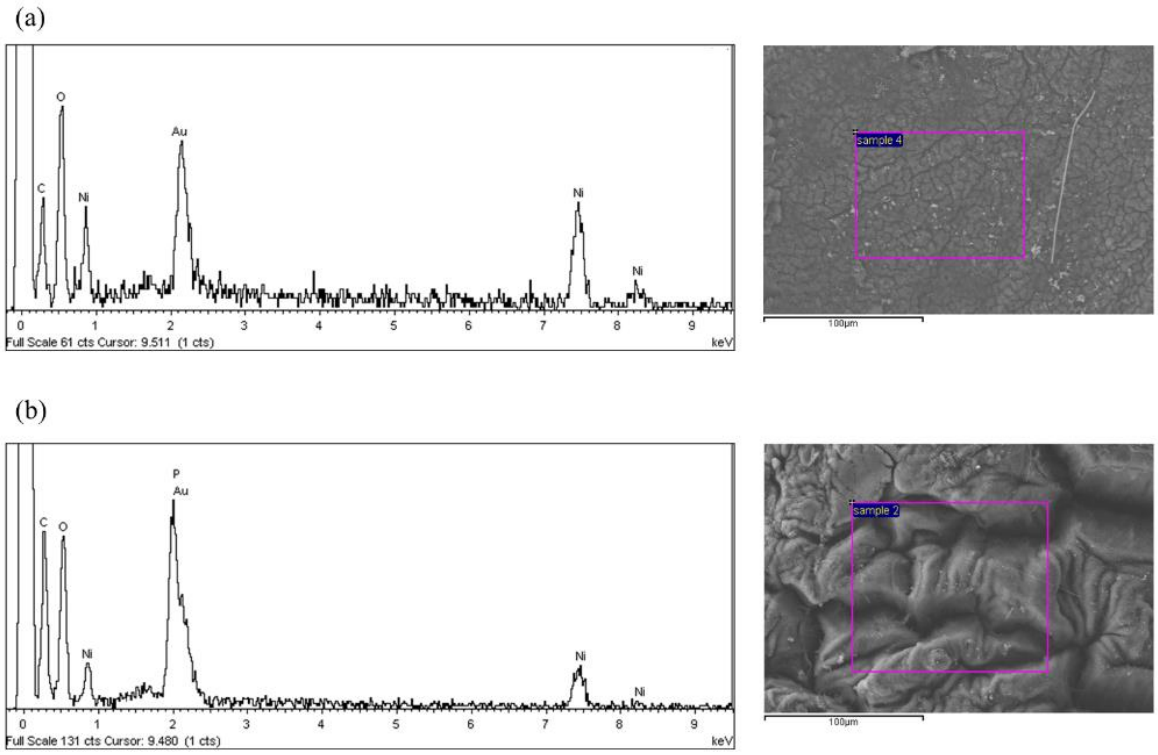

Figure 4-9. SEM-EDS analysis of (a) CB and (b) STPP-CB15% after adsorption of Ni(II)

4.5 Conclusions

Chitosan hydrogel beads crosslinked by sodium tripolyphosphate were examined in this work as a cost-effective and ecologically friendly bio-sorbent for Ni(II) adsorption from aqueous media. The characterization results indicated that increasing the crosslinking degree reduced the adsorbents' surface area and total pore volume at the cost of obtaining beads with higher physiochemical properties. The effect of pH and temperature on Ni(II) adsorption revealed that Ni(II) adsorption uptake was greater at higher pHs and temperatures. A linear model with a high magnitude of the coefficient of determination was developed by RSM to correlate Ni(II) adsorption capacity to pH and the crosslinking degree. The model computed the maximum adsorption capacity of 31.94 mg/g at 7.21 pH and 2.92% (w/v) sodium tripolyphosphate solution concentration. The Langmuir and Sips isotherms, the best-fitted models to the experimental data, showed maximum adsorption capacity in the order of CB > STPP-CB5%. FTIR and SEM-EDS

characterizations showed that amine groups were the main sites for crosslinking by sodium tripolyphosphate and metal ions adsorption.

4.6 References

The references are merged with those of the other chapters' references and presented at the end of the thesis.

Chapter 5

Technical Paper 3

5 Competitive adsorption of nickel(II) and cadmium(II) ions by chitosan crosslinked with sodium tripolyphosphate[3]

Keywords: binary adsorption; adsorption isotherms; biosorption; heavy metals; selectivity; desorption

5.1 Abstract

This study investigated the adsorption of Ni(II) and Cd(II) ions from single and binary metal ion solutions onto chitosan and crosslinked chitosan beads, which were prepared using an environmentally-friendly crosslinker, sodium tripolyphosphate. The synthesized adsorbents were characterized by swelling test, BET and SEM, and tested for Ni(II) and Cd(II) uptake after optimizing experimental factors, including adsorbent dosage (0.55 g/L) and initial pH (6.5). The single-ion equilibrium adsorption data fitted well with the Langmuir model. In the binary system, a decrease in adsorption capacity was observed, implying the existence of preference in the order of Ni(II) > Cd(II). Among the studied models for competitive adsorption, the extended Freundlich model fitted the adsorption equilibrium data successfully. Characterization of loaded crosslinked chitosan beads showed amino and phosphate groups were responsible simultaneously for the metal ions uptake. Desorption experiments were also conducted using a mixture of NaCl and H_2SO_4, showing acceptable results.

[3] A version of this chapter is published in Journal of Chemical Engineering Communications (https://doi.org/10.1080/00986445.2021.1966424)

5.2 Introduction

Heavy metals (HMs) are pollutants with a significant environmental burden because of their toxicity and endurance. They can contaminate the environment by industrial discharge entering into streams, lakes, rivers, and groundwater [71,280]. HMs are transformed into hydrated ionic form in the aqueous phase, where they become highly toxic compared to their metal atom counterparts. The formed hydrated ions interrupt the enzymatic process, which causes the end of aquatic life. The toxic effects of heavy metals do not end there, and they can also affect human life via bioaccumulation in the food chain [281]. Due to these adverse impacts, health authorities such as the World Health Organization (WHO) and the U.S. Environmental Protection Agency (EPA) have established strict regulations and guidelines for the discharge of the effluents containing HMs into the environment [86].

Among heavy metals, transition metals, such as nickel (Ni(II)) and cadmium (Cd(II)), are essential raw materials for manufacturers [62]. The widespread industrial applications of cadmium and nickel imply that large amounts of them are likely to find their way into the environment. Exposure to low amounts of Ni(II) cannot be avoided since it is ubiquitous in the environment, and health problems typically result from exposure to high dosages of Ni(II). These health problems include severe lung and kidney damage, gastrointestinal distress, skin dermatitis, chest pain, and shortness of breath [282]. Conversely, cadmium is not regarded as an essential element to the human being, and it is notorious for being extremely toxic even at low concentrations [191]. Persistent Cd(II) intake, even minute amounts, leads to severe damage to human bodies. The possible role of cadmium in human carcinogenesis has been documented in detail [283].

Apart from these concerns, the current demand scenario for Ni(II) and Cd(II) has surged, which highlights the importance of their recovery from industrial waste streams [284]. Solid wastes such as spent batteries, catalysts, alloy scrap and also aqueous solutions generated by industrial activities contain large quantities of Ni(II) and Cd(II). Therefore, researchers have concentrated on developing different techniques to remove/recover them from effluents or industrial wastes [285]. To date, different technologies have been developed and emerged for this aim, including membrane filtration [286], coagulation/flocculation [287], flotation [288], electrochemical reduction/oxidation [289], ion-exchange [243], chemical precipitation [290], and adsorption [291]. The majority of conventional

techniques suffer from some limitations, such as low efficiency, sensitive working conditions, high operating costs, and secondary waste production [168]. Therefore, an effective, clean and economical technique has been demanded to overcome the drawbacks of current technologies.

Among the various processes, adsorption has come to attention as a promising and economical approach [79,215]. The adsorption process offers several advantages such as economic viability in the context of the capital cost and chemical requirement, sustainability in the context of zero waste production, flexibility in terms of operation, along with efficiency in terms of treating pollutants at low concentrations [71,191]. Various adsorbents have been employed and introduced in the literature for heavy metals adsorption, including activated carbon [292], zeolites [293], carbon nanotubes [294], and low-cost adsorbents such as agricultural wastes or industrial by-products/wastes [295,296]. Recently, there has been an increasing interest in using low-cost biosorbents because of their abundance and renewable nature. In this context, using biosorbents has gained much attention for heavy metals removal and recovery [69,190,297]. Biosorption not only can reduce the cost of waste disposal by converting them to adsorbents but also offer a sustainable adsorption system for HMs uptake [10].

Considering the studied biosorbents, chitosan properties have encouraged researchers to invest in it as a green adsorbent to remove organic or inorganic pollutants, the first research on this topic was initiated in 1969 [298–300]. The conducted research showed that chitosan is an effective biosorbent for Ni(II) and Cd(II) adsorption even at low concentrations because of the existence of amino and hydroxyl groups in its structure [186,301,302]. However, chitosan modification is necessary to enhance its sorption performance, such as sorption capacity and metal selectivity, and increase its chemical/mechanical resistance to extreme media conditions [94]. Modification of chitosan with grafting (inserting new functional groups) or crosslinking (uniting the macromolecular chains to each other) reactions have been studied and reported by other researchers to prepare desirable chitosan-based materials [16,303].

Different crosslinkers have been reported for chitosan modification, such as Glyoxal (GO) [180], Glutaraldehyde (GLA) [213], Epichlorohydrin (ECH) [304], and Ethylene Glycol Diglycidyl Ether (EGDE) [305]. Most of the examined crosslinkers (i.e., ECH and GLA) are toxic and hazardous to the environment and human health. Hence, a non-hazardous and low-cost crosslinker, such as

sodium tripolyphosphate (STPP), can be a good alternative for chitosan crosslinking to reduce the environmental footprint. The feasibility of using STPP and its impact on chitosan adsorption capacity was investigated in the previous research as a proof of concept for a single-metal adsorption system [96]. Most of the existing studies involving chitosan–metal bonding examined a single-metal adsorption system. However, the presence of only one kind of metal ion is a rare situation. Therefore, the study of competitive adsorption of Ni(II)-Cd(II) by a low-cost biosorbent is attractive as different metal species can impact the removal efficiency of other existing metals.

The primary objective of this study was to modify chitosan by a non-hazardous crosslinker, sodium tripolyphosphate, and examine the feasibility of using it for the individual and simultaneous removal of Ni(II) and Cd(II) ions from an aqueous solution. Swelling/solubility experiments, Brunauer− Emmett−Teller (BET) and SEM characterization were carried out to confirm crosslinking occurrence and enhancement of modified chitosan chemical properties. Several isotherm models were employed and compared with each other in a single- and binary component system to interpret the Ni(II) and Cd(II) adsorption data and study the sorbent selectivity. Different characterization techniques, including SEM-EDS and FTIR, were also implemented to understand the adsorption mechanism of modified chitosan in the binary system.

5.3 Experimental and Method

5.3.1 Chemicals and instruments

Chitosan (85% deacetylation degree), sulphuric acid (H_2SO_4, N/50), sodium chloride (NaCl), cadmium sulphate hydrate ($3CdSO_4 \cdot 8H_2O$), and nickel sulphate hydrate ($NiSO_4.6H_2O$) were purchased from Fisher Scientific (Canada). Sodium tripolyphosphate ($Na_5P_3O_{10}$) and sodium hydroxide (NaOH) were acquired from Sigma (Canada), and acetic acid (CH_3COOH, 99.9 wt. %) was bought from VWR (Canada). All chemicals used in this study were of analytical grade and used without further treatment or purification.

5.3.2 Batch adsorption test

An analogous process to previous work [96] was employed to prepare chitosan beads (CB) and crosslinked chitosan beads (STPP-CB) by 5% (w/v) sodium tripolyphosphate solution. Stock

solution of metal ions with different concentrations was prepared using cadmium/nickel sulphate hydrate, followed by adding a weighed amount of the adsorbent (either CB or STPP-CB). The batch adsorption experiments were conducted using 125 mL Erlenmeyer flasks containing 50 mL of metal ion(s) solution, shaking at room temperature at 225 rpm for 24 h, as no metal concentration changes were measured after 18 h based on the preliminary tests. Once the adsorption system reached equilibrium, the concentration of metal ion(s) was analyzed by Atomic Absorption Spectroscopy (AAS) (PinAAcle 500, Perkin Elmer), and the amount adsorbed per unit mass of adsorbent at equilibrium, q (mmol/g), was calculated by using the following equation:

$$q = \frac{(C_{0,i} - C_{e,i})V}{W} \qquad 5\text{-}1$$

where C_0 and C_e (mmol/L) are the initial and final concentrations of the metal ion in the solution, V (L) is the volume of the solution, and W (g) is the weight of the dry adsorbent. It should be noted that each test was conducted with three replicates, and the average was used. The control experiments were also conducted to monitor any weight loss.

5.3.2.1 Effect of adsorbent dosage

The amount of adsorbent changed from 12.5 to 50 mg in 50 mL of metal ion solution with the initial concentration of 50 mg/L to assess the impact of adsorbent dosage on metal ion uptake.

5.3.2.2 Effect of pH

To study the effect of pH, 27.5 mg of the adsorbent (equivalent to the dosage of 0.55 g/L) was added to 50 mL of metal ion solution (Ni(II)/Cd(II)) with the initial concentration of 50 mg/L. Sodium hydroxide or sulfuric acid solutions (0.1 M) were used to adjust the solution pH in the range of 4.0 to 8.5, monitored by HACH (HQ40D) pH meter.

5.3.2.3 Effect of initial concentration of metal ions

27.5 mg of adsorbent was placed in 50 mL of metal ions solution at pH 6.5 with different initial concentrations of each metal ranging from 10 to 1500 mg/L in the monocomponent system. The same conditions and concentration range with the mass ratio of 1:1 (Ni(II):Cd(II)) were used in

the binary system to examine the distribution of metal ions between solid adsorbent and liquid phase at equilibrium.

5.3.3 Desorption studies

15 mg loaded STPP-CB were used for the binary system of Ni(II) and Cd(II) with a mass ratio of 1:1 in which the concentration of each metal was 50 mg/L under the optimum conditions. The loaded beads were separated, washed gently with de-ionized water to remove any unadsorbed metal ions, and air dried. Then, 2.5 mg of the dried beads were equilibrated for 48 h with 50 mL H_2O and a mixed solution of NaCl (0.2 mol/L) and H_2SO_4 (0.01 mol/L). The quantity of desorbed metal ions was determined by AAS. All experiments were conducted in triplicates, and the average values were presented. The following equation was used to calculate the percentage of desorption:

$$\text{Desorption} = \frac{\text{amount of metal ions desorbed}}{\text{amount of metal ions adsorbed}} \times 100\% \qquad 5\text{-}2$$

5.3.4 Characterization techniques

The specific surface area and total pore volume of CB and STPP-CB were measured by N_2 adsorption-desorption isotherms using the Accelerated Surface Area and Porosimetry Analyzer (ASAP 2020, Micromeritics Co.) and calculated by Brunauer–Emmett–Teller (BET) method (by the Micromeritics Software). The surface topography was analyzed with a JEOL JSM-7500F Scanning Electron Microscopic (SEM), operating at an acceleration voltage of 3.0 kV. Energy Dispersive Spectroscopy (EDS) was carried out using an Oxford EDS INCA 350 spectrometer. The specimens were coated with gold before the SEM and EDS analyses to prevent charging. Fourier transform infrared spectroscopy (FTIR) was performed in the range from 650 to 4000 cm^{-1} (Thermo Fischer, Nicolet 6700) using the attenuated total reflectance (ATR) sampling method. The adsorbents' solubility and swelling behaviour were also tested by immersing 0.10 g of each adsorbent (CB and STPP-CB) in 5% (v/v) acetic acid (pH~2.5), distilled water (pH~6.8) and 0.5 M sodium hydroxide solution (pH~13.0), shaking at 100 rpm for 24 h at 25 °C. Following that, the beads were removed and blotted using filter paper to absorb excess water on the surface. The swollen samples were weighed immediately, and the swelling percentage for each sample was calculated by using the following equation:

$$\text{Percentage of swelling} = \frac{W_s - W_0}{W_0} \times 100\% \qquad 5\text{-}3$$

where W_s (g) is the weight of swollen beads, and W_0 (g) is the weight of dry beads.

5.3.5 Single and multi-component adsorption equilibrium isotherm models

Several isotherm models, such as Langmuir, Freundlich, and Sips, and their extension or modified versions have been developed and employed to describe the adsorption equilibrium data. The isotherm models summarized in Table 5-1 were used in this study to evaluate the sorption performance in the single and multicomponent systems.

Table 5-1. Summary of the employed isotherm models for mono and multicomponent system

Isotherm	Equation	Parameters	Reference
Langmuir	$q_e = \frac{q_m K_L C_e}{1 + K_L C_e}$ $(5-4)$	q_e: The equilibrium concentration of the solid phase (mmol/g) C_e: The equilibrium concentration of liquid phase (mmol/L) $q_m (mmol/g)$, $K_L (L/mmol)$: The single-component Langmuir parameters	157
Modified Langmuir	$q_{e,i} = \frac{q_{m,i} K_{L,i} \left(C_{e,i}/\eta_i\right)}{1 + \sum_{j=1}^{N} \left(C_{e,j}/\eta_j\right)}$ $(5-5)$	$q_{e,i}$: The equilibrium concentration of solid phase of component i (mmol/g) $C_{e,i(j)}$: The equilibrium concentration of liquid phase of component i(j) (mmol/L) $q_{m,i} (mmol/g)$, $K_{L,i}$ $(L/mmol)$: The single-component Langmuir parameters of component i $\eta_{i(j)}$: Langmuir correction coefficient of component i(j)	166,167
Extended Langmuir	$q_{e,i} = \frac{q_m K_{L,i} C_{e,i}}{1 + \sum_{j=1}^{N} K_{L,j} C_{e,j}}$ $(5-6)$	$q_{e,i}$: The equilibrium concentration of solid phase of component i (mmol/g) $C_{e,i(j)}$: The equilibrium concentration of liquid phase of component i(j) (mmol/L) $q_m (mmol/g)$, $K_{L,i(j)}$ $(L/mmol)$: The multi-component Langmuir parameters of component i(j)	169

Freundlich	$q_e = K_F C_e^{1/n}$ $(5-7)$	q_e: The equilibrium concentration of the solid phase (mmol/g) C_e: The equilibrium concentration of liquid phase (mmol/L) $K_F((\mathrm{mmol/g}).(\mathrm{L/mmol})^{1/n}), 1/n$: The single-component Freundlich parameters	158
Extended Freundlich	$q_{e,i} = \frac{K_{F,i}\, C_{e,i}^{\left(\frac{1}{n_i}\right)+x_i}}{C_{e,i}^{x_i} + y_i C_{e,j}^{z_i}}$ $(5-8)$	$q_{e,i}$: The equilibrium concentration of solid phase of component i (mmol/g) $C_{e,i(j)}$: The equilibrium concentration of liquid phase of component i(j) (mmol/L) $K_{F,i}((\mathrm{mmol/g}).(\mathrm{L/mmol})^{1/n}), 1/n_i$: The single-component Freundlich parameters of component i x_i, y_i, z_i : The multi-component Freundlich fitting parameters	164,165
Sips	$q_e = \frac{q_m\,(K_L C_e)^{1/n}}{1+(K_L C_e)^{1/n}}$ $(5-9)$	q_e: The equilibrium concentration of the solid phase (mmol/g) C_e: The equilibrium concentration of liquid phase (mmol/L) $q_m\ (\mathrm{mmol/g}), K_L(\mathrm{L/mmol}), 1/n$: The single-component Sips parameters	161
Extended Sips	$q_{e.i} = \frac{q_{m,i}\, K_{L,i}\, C_{e,i} \left(\sum_{j=1}^{N} K_{L,j}\, C_{e,j}\right)^{1/(n_i)-1}}{1+\left(\sum_{j=1}^{N} K_{L,j}\, C_{e,j}\right)^{1/n_i}}$ $(5-10)$	$q_{e,i}$: The equilibrium concentration of solid phase of component i (mmol/g) $C_{e,i(j)}$: The equilibrium concentration of liquid phase of component i(j) (mmol/L) $q_{m,i}\ (\mathrm{mmol/g}), K_{L,i(j)}(\mathrm{L/mmol}), 1/n_i$: The single-component Sips parameters of component i(j)	161,163

5.3.5.1 Ideal Adsorption Solution Theory (IAST)

The IAST, proposed by Radke and Prausnitz [306], is a gas mixtures model and was later developed for dilute multicomponent liquid solutions to predict the adsorption isotherms using single-solute equilibrium data. The IAST is based on two assumptions; first, the components of the adsorption system behave as ideal components according to Raoult's law, which means there is no interaction between adsorbent and adsorbate. Secondly, the chemical potential of each component is equal in solution and adsorbed phases, which interprets as the fact that the spreading pressure of a single solute, π (the decrease of surface tension as a result of adsorption), is unchanged after adding other components to the solute in the multicomponent adsorption system [307]. In IAST, the following

equations (Eq. (5-11) to (5-15)) are needed to understand a multicomponent adsorption system behaviour from single-solute isotherms:

$$q_T = \sum_{i=1}^{N} q_i \qquad 5\text{-}11$$

$$Z_i = {q_i}/{q_T} \qquad 5\text{-}12$$

$${1}/{q_T} = \sum_{i=1}^{N} {Z_i}/{q_i^0} \qquad 5\text{-}13$$

$$C_i = Z_i C_i^0 \qquad 5\text{-}14$$

$${\pi A}/{RT} = \int_0^{C_i^0} {q_i^0}/{C_i^0}\ dC_i^0 \qquad 5\text{-}15$$

where q_T (mmol/g) is the total solid-phase concentration, q_i (mmol/g) is the equilibrium solid-phase concentration of component i, Z_i is the mole fraction of adsorbate i in the adsorbed phase, and q^0_i (mmol/g) is the adsorption capacity of component i in a single-solute solution. C_i and C^0_i (mmol/L) are the liquid-phase concentration of component i in multi- and single-component solutions, respectively. Also, A (m^2/g) is the specific surface area of the sorbent, π is the spreading pressure, R (kJ/g K) is the universal gas constant, and T (K) is the temperature.

The IAST can be combined with other adsorption equations of the single-solute system, such as Langmuir, Freundlich and Sips, to determine the values for two variables, including the mole fraction of the adsorbed phase components (Z_i) and the spreading pressure (π). In the case of using the Langmuir equation (Eq. (5-4)), the reduced spreading pressure equation, Π, can be presented as follows (Eq. (5-16)).

$$\prod = {\pi A}/{RT} = \int_0^{C_i^0} {q_i^0}/{C_i^0}\ dC_i^0 = q_{m,i} \ln\left(1 + K_{L,i}\, C_i^0\right) \qquad 5\text{-}16$$

Hence, depending on the number of the components, a system of non-linear equations needs to be solved to determine the unknowns (c^0_i, q^0_i, Z_i and Π) stated in the above equations (Eq. (5-10) to Eq. (5-15)). If there are two components in the system, six unknowns exist, including c^0_1, q^0_1, c^0_2, q^0_2, Z_1 and Π; therefore, six non-linear equations are needed to find the unknowns.

5.3.5.2 Determination of isotherm parameters and selectivity coefficient

In this study, the parameters of isotherm models were determined via data fitting and minimizing Marquardt's Percent Standard Deviation (MPSD) error (Eq. (5-17)) using the solver add-in function of the MS excel [133]

$$\mathrm{MPSD} = \sum_{i=1}^{n} \left(\frac{q_{i,exp} - q_{i,cal}}{q_{i,exp}} \right)^2 \qquad \textit{5-17}$$

In the above equation, q (mmol/g) is the equilibrium solid-phase concentration; the subscript "exp" and "calc" display the experimental and calculated values of q, and n is the number of the components in the system.

In a binary system, distribution coefficient is used to evaluate adsorbent selectivity toward the available components, defined as Eq. (5-18) [187]:

$$K_d = q_e / C_e \qquad \textit{5-18}$$

where q_e (mmol/g) and C_e (mmol/L) represent the equilibrium adsorption capacity and component concentration in the solution, respectively. Selectivity coefficient (α) can be defined according to Eq. (5-19) to evaluate the competitive adsorption in the binary system [187]:

$$\alpha_{m1/m2} = K_d(m_1) / K_d(m_2) \qquad \textit{5-19}$$

where $K_d(m_1)$ and $K_d(m_2)$ are distribution coefficients of the adsorbates (m_1 and m_2) in the binary system. The selectivity coefficient implies selectivity toward m_1 (or m_2) if it is greater (or less) than unity.

5.4 Results and discussion

5.4.1 Adsorption of metal ions in the mono-component system

5.4.1.1 Effect of solution initial pH

MEDUSA-HYDRA chemical equilibrium software [308] was employed simultaneously in this study to draw Ni(II), Cd(II), and their species distribution diagrams as a function of pH presented in Figure 5-1(a) and (b). As shown in Figure 5-1(a), various species of cadmium can be formed by changing the pH of the solution, including Cd^{2+}, $Cd(OH)^{+}$, $Cd(OH)_2$, and $Cd(OH)_3^{-}$. It is evident that $Cd(OH)_{2(S)}$ formation starts at pH>8.5, in which cadmium precipitation begins. Similarly, different species of Ni(II), such as Ni^{2+}, $Ni(OH)_2$, $Ni(OH)_3^{-}$ are formed by increasing pH. As presented in Figure 5-1(b), Ni^{2+} is the only ionic species in a solution from acidic pHs up to almost 8.0. Hence, the pH range between 4.0 and 8.5 was selected to evaluate the pH effect on Ni(II) and Cd(II) adsorption, and higher values of pHs were avoided to prevent metal ions precipitation in the form of hydroxide. The conducted experiments indicated that Cd(II) adsorption uptake increased steadily by increasing the initial pH of the solution and reached 0.92 mmol/g at pH 8.5, while it was 0.60 mmol/g at pH 4.0. Comparably, Ni(II) uptake increased from 0.57 to 1.37 mmol/g by increasing pH to 8.5, and a similar trend was reported by other researchers. Considering Figure 5-1(b), the increase in apparent Ni(II) adsorption uptake at pHs above 7.5 might be due to $Ni(OH)_{2(S)}$ formation and a combination of both precipitation and adsorption. It is widely acknowledged that the active sites of chitosan beads become protonated in the acidic medium due to high H^{+} concentrations [186]. As a result, electrostatic repulsion between chitosan chains and the metal ions led to lower metal ions uptake at pHs below 6.5. Since working close to neutral pH is desirable, pH 6.5 was selected as optimal for the subsequent experiments, in which the only removal mechanism was adsorption with acceptable efficiency.

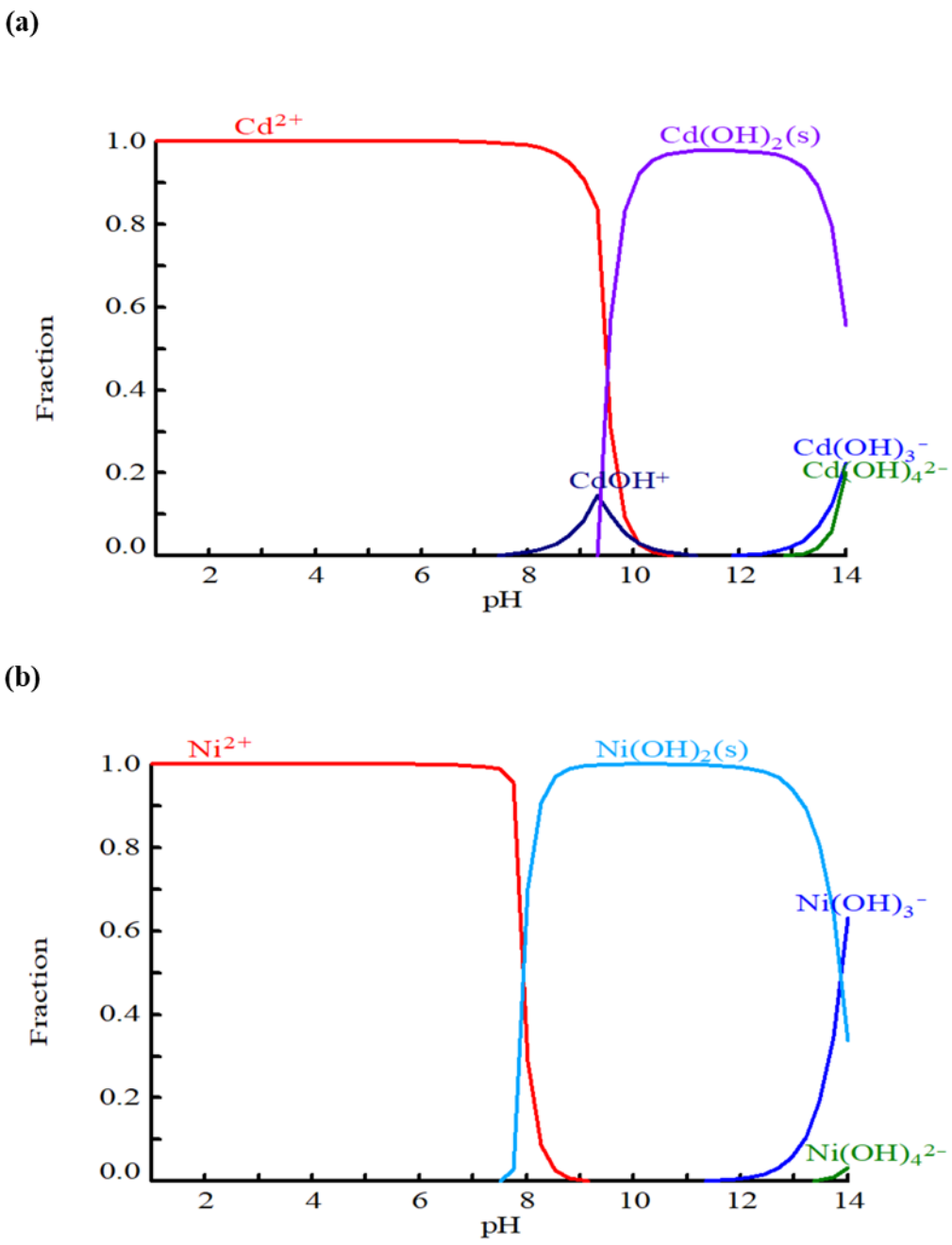

Figure 5-1. Speciation of (a) Cd^{2+} and (b) Ni^{2+}as a function of pH in dilute aqueous solution.

5.4.1.2 Effect of adsorbent dosage

Our previous research indicated that the optimum dosage of CB for Cd(II) removal is 0.45 g/L [96]. Similarly, the effect of CB dosage on Ni(II) adsorption was investigated in the current research by adding a specific amount of adsorbent, varied from 0.25 to 1 g/L. Results revealed that the

removal percentage increased from 26.90% to 69.52%, with an increase in adsorbent dosage. Conversely, the calculated apparent adsorption uptake decreased by 0.35 mmol/g, being equal to 0.63 mmol/g, when the CB dosage changed from 0.25 to 1 g/L. Other researchers observed similar behaviour with this justification that increasing the adsorbent dosage increases the number of unoccupied active adsorption sites on the surface of the adsorbent leading to a decrease in apparent adsorption capacity [151]. Hence 0.55 g/L was chosen as a suitable dosage within the studied range for all upcoming sorption experiments.

5.4.1.3 Characterization and crosslinking mechanism

Among investigated crosslinkers for chitosan modification, sodium tripolyphosphate (STPP) can be beneficial owing to its effectiveness and non-toxicity. According to chitosan pK (~6.3), dissolved chitosan in acidic media presents $-NH^{+3}$ sites. On the other hand, sodium tripolyphosphate, as an ionic crosslinker and weak acid, dissociates to hydroxyl (OH^-) and phosphoric ions (PO_4^{3-}) after dissolution in water. Therefore, crosslinked particles (STPP-CB) can be formed through ionic interaction by adding chitosan to the STPP solution [89], discussed and characterized in detail in the literature [96,309].

The Brunauer–Emmett–Teller (BET) specific surface area and the total pore volume of CB were found to be 6.50 m^2/g and 4.07×10^{-3} cm^3/g. Crosslinking of chitosan by sodium tripolyphosphate reduced the surface area and the total pore volume to 5.60 m^2/g and 3.63×10^{-3} cm^3/g, respectively. The reduction in the surface area and the total pore volume after crosslinking could be attributed to the fact that some amino groups of chitosan were crosslinked by sodium tripolyphosphate [220], which was confirmed by FTIR characterization. Scanning electron microscopy was used to visualize the surface morphology of CB and STPP-CB (Figure 5-2). Figure 5-2(a) shows a smooth surface for CB, whereas the SEM image of crosslinked chitosan revealed a different surface morphology for the STPP-CB surface. As shown in Figure 5-2(b), the surface of STPP-CB is rougher than CB, indicating the occurrence of crosslinking on the CB surface. XRD patterns of CB and STPP-CB, conducted in our previous work, showed a decrease of crystallinity after crosslinking chitosan by sodium tripolyphosphate [96].

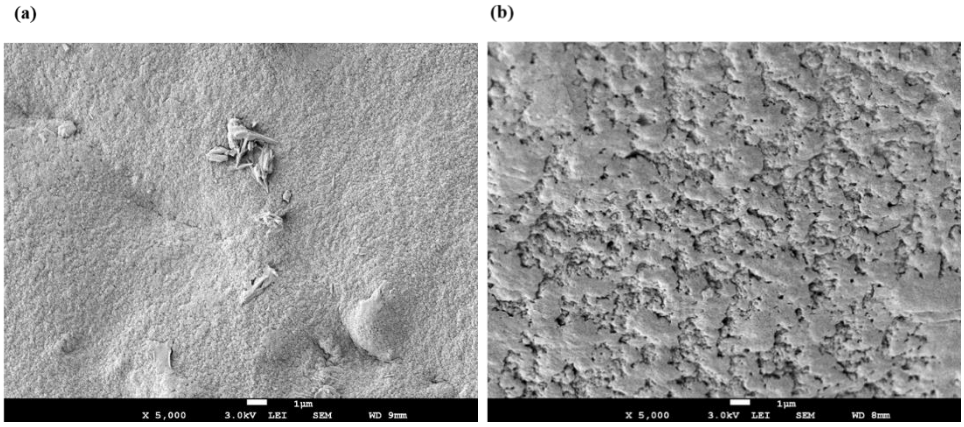

Figure 5-2. SEM images of (a) CB and (b) STPP-CB

Chitosan beads show hydrophilic character because of the primary amine group presence in the chitosan structure [226]. Most of the amine groups of chitosan undergo protonation at pHs below 4.0, and the positively charged polysaccharide chains of chitosan start repulsing one another. This electrostatic interaction becomes more intense at lower pHs, leading to the dissolution of chitosan beads in dilute acetic acid solution [21]. Therefore, the solubility test was required to examine the stability of CB and STPP-CB by changing pH from acidic to alkaline, and the results are given in Table 5-2. The observations indicated that CB suffered from weak chemical resistance and lack of sorption capability in acidic environments since it became dissolved in the solution by reducing pH to 2.5. However, the results showed crosslinking was able to reinforce the chemical strength of CB; as a result, STPP-CB was insoluble in the acidic and alkaline medium as well as distilled water. Table 5-2 also shows the swelling percentages for both CB and STPP-CB decreased by increasing solution pH, which is generally ascribed to the hydration or ionization of unbound -NH_2 sites of chitosan [107]. As seen in Table 5-2, the swelling percentage of STPP-CB was lower than CB in distilled water and alkaline medium. This observation confirmed lower accessibility to the STPP-CB network and its hydrophobic character, offering good physicochemical properties and making it a suitable adsorbent to work in a wide range of pH [265].

Table 5-2. Swelling and solubility properties of CB and STPP-CB

Beads	Solubility - Swelling (%)		
	5% (v/v) Acetic Acid	Distilled Water	0.5 M NaOH
CB	Soluble - N/A	Insoluble - 118.2	Insoluble - 109.1
STPP-CB	Insoluble - 36.4	Insoluble - 27.3	Insoluble - 18.2

5.4.1.4 Modelling adsorption isotherms for a single-component system

The adsorption data obtained from seven different initial concentrations of Ni(II) and Cd(II) in a monocomponent system were analyzed in the present study by using Langmuir, Freundlich, and Sips equations (Eq. (5-4), (5-7), and (5-9)) to model the metal ions adsorption onto CB and STPP-CB. MSPD and/or R^2 were calculated and used to evaluate each model's accuracy for interpreting the experimental data. The calculated isotherms parameters, along with the regression coefficient (R^2) and MPSD values, are listed in Table 3. Considering R^2 as a goodness of fit criterion, it was observed that the monolayer Langmuir equation provided the best fit (R^2 = 0.99) to the experimental data of Ni(II) and Cd(II) on both CB and STPP-CB. According to the Langmuir model, the maximum adsorption capacity (q_m) values varied considerably depending on the employed adsorbent and metal ions in the solution. By comparison, the maximum adsorption capacity of CB for Ni(II) uptake was almost 30% higher than Cd(II), 1.36 mmol/g compared to 1.06, and both were approximately reduced by 40% after crosslinking by 5% (w/v) STPP (0.89 and 0.61 mmol/g, respectively). The reduction in the adsorption capacity resulted from less available amino groups as adsorption sites for metals uptake [265]. The Langmuir constant (K_L), which is related to the affinity of binding sites, indicated that the binding sites of both CB and STPP-CB were higher and stronger for Cd(II) ions than Ni(II) [152].

Table 5-3. Langmuir, Freundlich, and Sips isotherms constants for the adsorption of Cd(II) and Ni(II) onto CB and 5% STTP-CB in the mono-component system.

Adsorption Parameters		Langmuir model			Freundlich model			Sips model			
		q_m (mmol/g)	K_L (L/mmol)	R^2 MPSD	1/n	K_F ((mmol/g).(L/mmol)$^{1/n}$)	R^2 MPSD	q_m (mmol/g)	K_L (L/mmol)	1/n	R^2 MPSD
Ni(II)	CB	1.36	1.66	0.99 0.14	0.31	0.6	0.94 0.22	1.49	1.07	0.7	0.99 0.01
	STPP-CB	0.89	1.99	0.99 0.03	0.33	0.4	0.86 0.51	0.9	1.72	1.07	0.99 0.00
Cd(II)	CB	1.06	17.03	0.99 0.62	0.21	0.82	0.8 0.59	1.05	34.78	0.87	0.97 0.05
	STPP-CB	0.61	2.82	0.99 0.23	0.4	0.33	0.85 0.51	0.65	2.05	0.96	0.96 0.16

By focusing on MPSD, the Sips isotherm model, a combination of the Langmuir and Freundlich models, presented a reasonable fit to the experimental data of Cd(II) uptake onto CB and STPP-CB. The interpretation of Ni(II) adsorption onto CB and STPP-CB by the Sips model showed the best fit having the lowest MPSD (~0.00) and highest R^2 (0.99). The corresponding parameters of the Sips equation, including q_m, K_L, and 1/n, are also presented in Table 5-3. Similar to Langmuir isotherm parameters, the maximum adsorption capacity of CB and STPP-CB (q_m) for Ni(II) uptake (1.49 and 0.90 mmol/g) obtained from the Sips model was higher than that of Cd(II) (1.05 and 0.65). Some of the Ni(II) and Cd(II) biosorption capacity onto chitosan and chitosan-based materials reported in the literature are presented in Table 5-4. It should be noted that the maximum adsorption capacity of adsorbents depends on different factors such as temperature, time, initial concentration, adsorbent dosage, and pH. Hence drawing a comparison between the reported maximum adsorption capacities is not simple unless the same experimental conditions are employed for the adsorption system [310].

Table 5-4. Studies of the adsorption of Ni(II) and Cd(II) as single solutes using chitosan-based adsorbents

Adsorbent	Metal	pH	Adsorption Capacity (mmol/g)	Reference
Chitosan	Cd(II)	6	0.09	[221]
Epichlorohydrin crosslinked chitosan-clay composite	Cd(II)	4.5	0.64	[311]
Epichlorohydrin-triphosphate crosslinked chitosan	Cd(II)	7	0.74	[227]
Formaldehyde crosslinked chitosan-pheylthiourea resin	Cd(II)	5	1.06	[211]
5% Tripolyphosphate crosslinked chitosan beads	Cd(II)	6.5	0.61	This Study
Ether crosslinked chitosan	Ni(II)	5.5	0.90	[83]
Epichlorohydrin crosslinked Chitosan	Ni(II)	5.5	0.44	[83]
Imprinted glutaraldehyde-crosslinked chitosan	Ni(II)	5	0.61	[134]
5% Tripolyphosphate crosslinked chitosan beads	Ni(II)	6.5	0.89	This Study

5.4.2 Adsorption of metal ions in the binary-component system (Ni(II) and Cd(II))

5.4.2.1 Modelling adsorption isotherms for Ni(II)-Cd(II) uptake by CB

The concept of multicomponent adsorption is highly important because having aqueous media with one component occurs so rarely. Interactions between the system's components play a critical role in the adsorption properties of adsorbents. Since finding the model parameters in multicomponent systems is not simple, some adsorption isotherm models have been developed based on the information from adsorption equations of monocomponent systems. The adsorption data of Ni(II) and Cd(II) onto CB and STPP-CB in the competitive adsorption system was investigated with five multicomponent adsorption models, including modified and extended Langmuir, extended Freundlich, extended Sips, and IAST (Eq. (5-5), (5-6), (5-8), (5-10), and Eq. (5-11) to (5-16), respectively). The experimental and calculated qe values of Cd(II) and Ni(II) ions in a binary system onto CB are presented in the parity plots, Figure 5-3(a) and (b). The closer data

points to the bisecting line (45°line) show that the corresponding model fits the experimental data better. Also, the models' fitting parameters, along with their MPSD and R^2 values, are listed in Table 5-5.

Table 5-5. Parameter values of multicomponent isotherm models obtained from data of the binary system of Ni(II) and Cd(II) on CB

	CB																			
	Modified Langmuir				Extended Langmuir				Extended Freundlich						Extended Sips				IAST
	$q_{m,i}$ (mmol/g)	$K_{L,i}$ (L/mmol)	η_i	R^2	q_m (mmol/g)	$K_{L,1}$ (L/mmol)	$K_{L,2}$ (L/mmol)	R^2	$K_{F,i}$ ((mmol/g).(L/mmol)$^{1/n}$)	n_i	x_i	y_i	z_i	R^2	$q_{m,i}$ (mmol/g)	$K_{L,i}$ (L/mmol)	n_i	R^2	R^2
Ni(II)	1.36	1.66	1.00	0.49	1.51	1.27	4.09	0.71	0.60	3.18	0.38	5.35	0.40	0.94	1.49	1.08	1.41	0.04	0.78
Cd(II)	1.06	17.03	2.52	0.93		4.09	1.27	0.92	0.82	4.65	0	0.30	0.09	0.93	1.05	34.78	1.15	0.97	0.97
Model MPSD	0.92				0.64				0.22						13.14				0.67

The modified Langmuir model, with two interaction terms (η_1 and η_2) for Cd(II) and Ni(II), in addition to the single component Langmuir parameters, projected a fair prediction for Cd(II). However, Ni(II) interpretation was not acceptable, and it was underestimated by this model, particularly at high concentrations, leading to deviation from experimental results (R^2 = 0.49). Extended Langmuir with three fitting parameters (q_m, $K_{L,1}$, and $K_{L,2}$) in a binary system was examined in this study to find the maximum adsorption capacity. All the parameters of this model were estimated by fitting the competitive adsorption data, and information from the single-metal Langmuir isotherm was not used. The overall metal ions (Cd(II) and Ni(II)) uptake (q_m) by CB was calculated via this model as 1.51 mmol/g, which was lower than the sum of the maximum adsorption capacity of Cd(II) and Ni(II) (2.42 mmol/g) obtained by the Langmuir model in the monocomponent system. This observation may suggest that there was a variety of binding sites with an overlap for Cd(II) and Ni(II) uptake in the binary system, which is in contrast to the Langmuir model hypothesis, assuming a homogeneous adsorbent surface [312]. It is reported in the literature that the presence of other components in the solution changes the isotherm curve shape by affecting the apparent affinity of the components for the active sites, as well as the maximum adsorption capacity of each component [281].

The Sips equation provided the worst fit in the competitive adsorption system, presenting high MPSD (13.14) and significant error among the studied models. At the same time, the Sips equation

presented a proper interpretation of the single-metal isotherms of both Cd(II) and Ni(II), discussed in the previous section. On the other hand, the extended Freundlich isotherm with three fitting parameters (x_i, y_i, z_i) calculated from the binary system plus two parameters from the monocomponent system ($K_{F,i}$ and n_i), showed an acceptable fitting in competitive adsorption of both metals, having satisfactory MPSD (0.22) and error less than 20%. This observation implies that heterogeneous adsorption was expected in the competitive system of Ni(II)-Cd(II) onto CB. It should be noted that the Freundlich model could not provide accurate prediction in the monocomponent system, and the homogeneous adsorption assumption based on the Langmuir isotherm was the primary mechanism in that system.

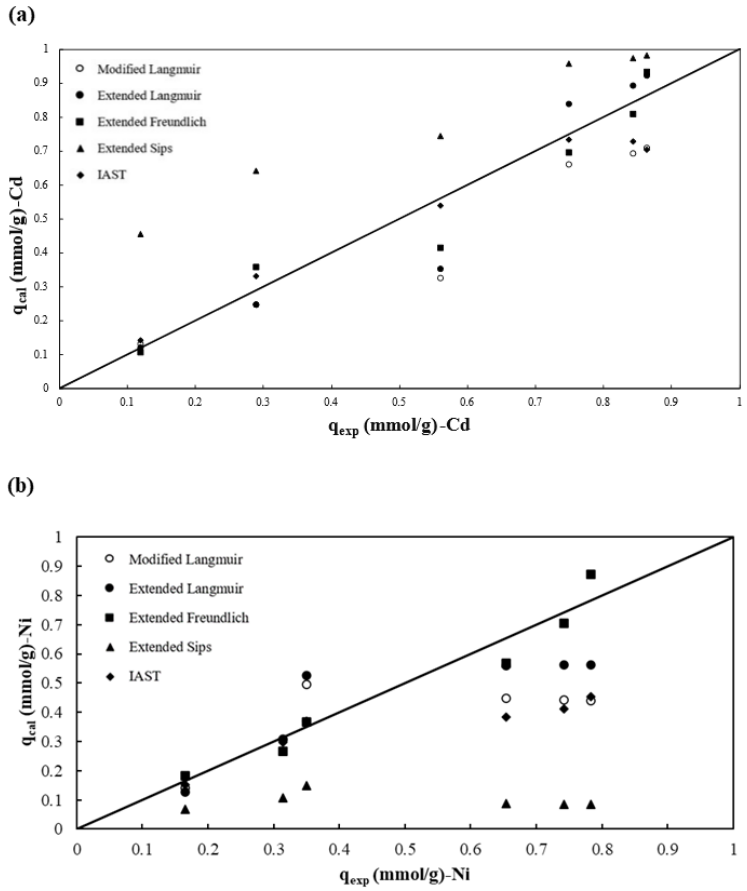

Figure 5-3. Comparison of the experimental and calculated q_e values of (a) Cd(II) and (b) Ni(II) ions in the binary system on CB

By incorporating the Langmuir isotherm as the best-fit isotherm for the single-component system in the IAST, the behaviour of metal ions in the binary system was examined by this model. While IAST provided a reasonable curve fitting to Cd(II) experimental data with 0.97 R^2 and an error less than 20%, Ni(II) equilibrium experimental data were underpredicted, except for very low concentrations, leading to high MPSD and error. There might be several reasons for this failure, such as ignoring the physical characteristics of the process in the model or neglecting the interaction between metal ions and the sorbent at high concentrations [307]. Unlike the other models investigated in this study, the IAST model uses the initial metal concentrations to interpret the equilibrium solid- and liquid-phase concentrations. This model assumes that the solutes in a competitive adsorption system act independently of each other with no interaction, displacement effects, and competition. Therefore, providing accurate prediction in the binary adsorption system is less likely [281].

5.4.2.2 Modelling adsorption isotherms for Ni(II)-Cd(II) uptake by STPP-CB

Figure 5-4(a) and (b) compare the predicted data of Cd(II)-Ni(II) adsorption onto STPP-CB with the experimental data, and the models' parameters are listed in Table 5-6. As shown in Figure 5-4(a) and (b), most of the data points are spread out around the 45◦ line, revealing that the experimental adsorption data for the binary systems onto STPP-CB could be represented by the studied multicomponent isotherm models with varying degree of fit. Similar to adsorption onto CB in the binary system, the Sips isotherm model was not reliable to fit the metal ions adsorption onto STPP-CB and showed the worst result for modelling the competitive adsorption system, having MPSD of 5.64 and high error. Even though this model could successfully fit Ni(II) experimental data in the monocomponent system, the Ni(II) projection by this model was poor, particularly at low concentrations, with an error exceeding 30%.

Table 5-6. Parameter values of multicomponent isotherm models obtained from data of the binary system of Ni(II) and Cd(II) onto STPP-CB

	STPP-CB																			
	Modified Langmuir				Extended Langmuir				Extended Freundlich						Extended Sips				IAST
	$q_{m,i}$ (mmol/g)	$K_{L,i}$ (L/mmol)	η_i	R^2	q_m (mmol/g)	$K_{L,1}$ (L/mmol)	$K_{L,2}$ (L/mmol)	R^2	$K_{F,i}$ ((mmol/g).(L/mmol)$^{1/n}$)	n_i	x_i	y_i	z_i	R^2	$q_{m,i}$ (mmol/g)	$K_{L,i}$ (L/mmol)	n_i	R^2	R^2
Ni(II)	0.89	1.99	2.8	0.99	0.77	0.81	1.4	0.99	0.39	3.02	0.12	1.4	0.0	0.79	0.91	1.72	0.94	0.96	0.98
Cd(II)	0.62	2.82	1.55	0.96		1.40	0.81	0.96	0.82	4.65	0.0	0.14	86	0.99	0.65	2.05	1.03	0.98	0.12
Model MPSD	0.71				0.69				0.49						5.64				5.98

The modified Langmuir isotherm model provided adequate reproduction of the experimental data at low concentrations of metals to a certain extent, having MPSD of 0.71 and 0.96 and 0.99 R^2, for Cd(II) and Ni(II), respectively. According to this model, the K_L values, reflecting the affinity between the adsorbent and the metals in the binary systems, were 2.82 and 1.99 l/mmol for Cd(II) and Ni(II). The modified Langmuir interaction coefficients, η_i, were greater than 1.0, confirming that there were interactions between Cd(II) and Ni(II) in the binary system. The overall metal ions uptake (q_m) in the binary system onto STPP-CB was calculated using the extended Langmuir model as 0.77 mmol/g. The obtained value was noticeably lower than the sum of the maximum total capacities of Cd(II) and Ni(II) ions (1.48 mmol/g) resulting from the single-component adsorption system based on the Langmuir isotherm. This examination indicated that Cd(II) and Ni(II) adsorption sites might be partially overlapped in the studied binary system. Furthermore, this observation violated the Langmuir model's fundamental assumptions, stating that there is no lateral interaction between the adsorbate molecules, and the affinity of each binding site for the adsorbate molecules remains uniform [313].

The IAST model incorporated by the Langmuir model from the single-metal system produced a good fit to Cd(II) experimental points only in dilute solutions. However, the error increased at higher concentrations, and the model underpredicted the estimated values of Cd(II). The IAST also failed to predict Ni(II) behaviour in the binary system with high MPSD and more than 30% error. The IAST's poor fit can be explained by the heterogeneity of the adsorption sites and the probability of the interaction of the adsorbates, which are not included in this model [314]. A comparison of MPSD values for different isotherm models showed that the extended Freundlich model (MPSD = 0.49) exhibited excellent simulation of the experimental data at the whole

concentration range of Cd(II) and Ni(II) ions in binary system onto STPP-CB. This model assumes multilayer coverage, and as a result, the presence of heterogeneous adsorbent sites on the surface of the crosslinked chitosan was expected.

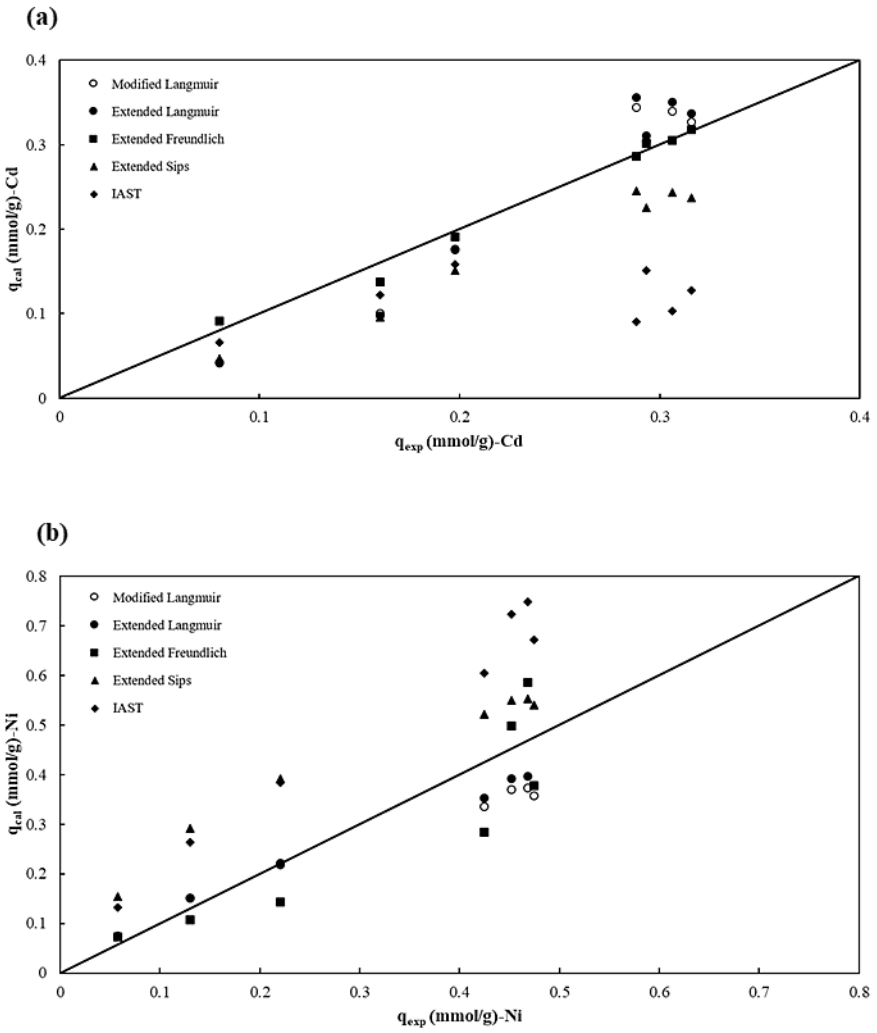

Figure 5-4. Comparison of the experimental and calculated q_e values of (a) Cd(II) and (b) Ni(II)ions in the binary system on STPP-CB

5.4.2.3 Characterization and adsorption mechanism for Ni(II)-Cd(II) uptake

Figure 5-5 shows the SEM-EDS analysis of (a) CB and (b) STPP-CB after adsorption in the binary system of Ni(II) and Cd(II). The EDS results clearly showed signals corresponding to Ni(II) and Cd(II) on both adsorbents, verifying metal ions uptake on their surface. The EDS spectra confirmed the existence of carbon and oxygen on the adsorbents belonging to the chitosan

structure, and Au peaks identified in their EDS spectra corresponded to the sample coating. P peak, detected on STPP-CB (Figure 5-5(b)), validated the success of crosslinking with STPP. Cd(II) peak intensity was lower in STPP-CB than CB, which could be specified that CB had a better affinity for Cd(II) uptake. This observation is in good agreement with the previous section's findings and the fact that the crosslinker occupied some amino groups of chitosan, and the residual amino groups of chitosan were the primary binding sites for metal ions [309]. The SEM images of loaded CB and STPP-CB in the binary system are also shown in Figure 5-5(a) and (b), indicating changes in the surface morphology of the studied adsorbents after adsorption of Ni(II) and Cd(II) in comparison to Figure 5-2(a) and (b) (SEM images before adsorption). The crystal-like structure in Figure 5-5(a) and different morphology in Figure 5-5(b) compared to Figure 5-2(b) can be attributed to the presence of Ni(II) and Cd(II) on the surface of the adsorbents and their interaction with CB and STPP-CB functional groups [106,315].

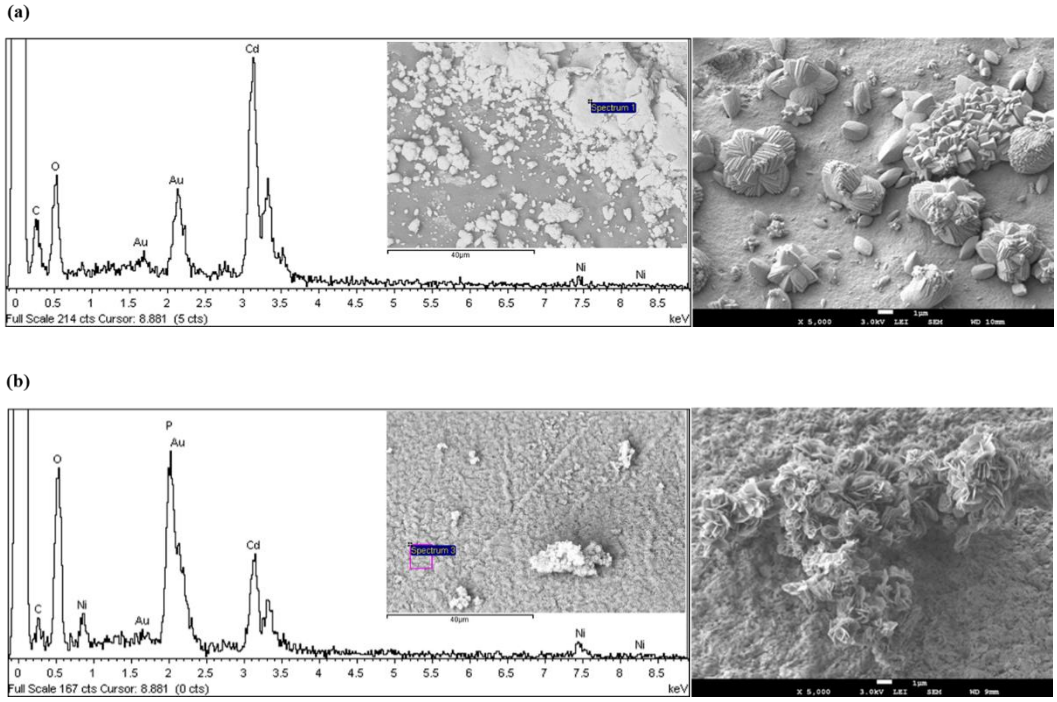

Figure 5-5. SEM-EDS element distribution images of (a) CB and (b) STPP-CB after adsorption in the binary system of Ni(II)-Cd(II)

While the leading functional group responsible for metals uptake is amino groups, sodium tripolyphosphate might occupy some of them because of the ionic interaction between the positively charged amino groups of chitosan and the negatively charged groups of sodium

triphosphate [214]. Thus, the residual amino groups and the new phosphate groups could be responsible for the metal ions adsorption on STPP-CB. FTIR can reveal valuable information about the active sites on the adsorbent surface involved in metal ions adsorption in the binary system. FTIR spectra of the STPP-CB were recorded before and after the adsorption of Ni(II) and Cd(II) in the binary system, shown in Figure 5-6. A decrease and shift in the peak at ~1150 cm^{-1} corresponding to P=O stretching vibration occurred in the spectrum after adsorption of metal ions, indicating that phosphate groups were affected by the adsorption process; thus, they participated in metal ions adsorption. A remarkable change in the FTIR spectrum was also detected in the region of 1300-1350 cm^{-1}, attributed to C-N stretching vibration and N-H deformation vibration (amide III groups), which was lowered significantly after adsorption. Another vivid change related to the nitrogen atom bond happened in the wavenumber at ~1600 cm^{-1} corresponding to N-H. There were no other considerable changes in the peak positions of any other peaks. Considering the lower adsorption capacity of STPP-CB and the results from FTIR characterization, it is reasonable to assume nitrogen atoms were the main adsorption sites responsible for the coordinated binding of Ni(II) and Cd(II) to STPP-CB.

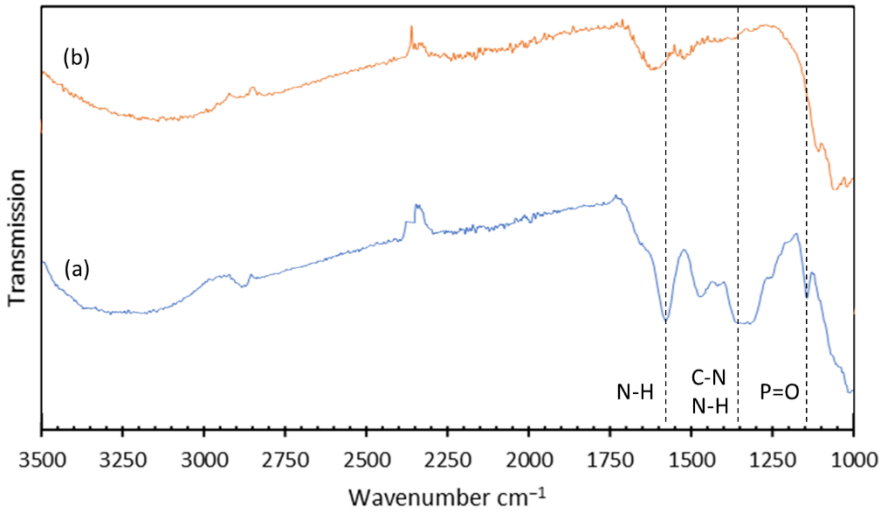

Figure 5-6. FTIR spectra of STPP-CB beads (a) before and (b) after adsorption of Ni(II) and Cd(II) in the binary system of Ni(II)-Cd(II)

5.4.2.4 Selectivity study of STPP-CB for Ni(II)-Cd(II) uptake

As discussed earlier, the presence of other metals in the solutions changes the apparent metal affinity for the active sites compared to the monocomponent system. It means the available components in the binary adsorption system with different adsorption affinity should compete with each other for adsorption on the same site. Finding a standard rule to determine how metal properties influence competitive sorption is generally complicated due to possible adsorbate-adsorbate and adsorbate-adsorbent interactions [316]. Among various influential factors that determine the sorption preferences of a sorbent, it seems that the binding of metal ions on sorbents mainly depends on the physicochemical characteristics of metals, including ionic radii, atomic weight, electronegativity, hydrolysis constant, and softness of metals in the system [317]. Some of the physicochemical properties of Cd(II) and Ni(II) ions are tabulated in Table 5-7 [185,318]. While a combination of mentioned properties affects the metal ions competitive adsorption, some studies concluded that metal ions with higher electronegativity and hydration energy could be adsorbed at the adsorption site more readily [319]. Selective separation of Cd(II) from Ni(II) in a binary system onto STPP-CB was investigated in this study by calculating the selectivity coefficient presented in Eq. (5-19). The selectivity coefficient for Ni(II) ($\alpha_{Ni/Cd}$) varied from 1.18 to 4.28, confirming that the modified chitosan bead had better selectivity for Ni(II) rather than Cd(II) as all the values were above unity. Different behaviour was also reported in the literature depending on the available components and employed adsorbent, where Cd(II) and Ni(II) presented in the adsorption system [127,151,320,321].

Table 5-7. Metal ion characteristic parameters

Metal	Ionic radius (pm)	Electronegativity (Pauling)	Hydrolysis constant	Hydration enthalpy (kJ/mol)
Ni(II)	69	1.91	9.9	-2,106
Cd(II)	95	1.69	10.1	-1,806

Constructing a three-dimensional plot may be a suitable graphical method to evaluate the experimental data of both single and binary adsorption systems in which the metal uptake (z-axis) is plotted as a function of the final equilibrium concentrations of two metal ions (x- and y-axis). The results of this examination are depicted in Figure 5-7. The isotherms of each metal in a monocomponent system can be seen in the corresponding vertical planes, where the other metal concentration is zero. As shown in Figure 5-7, the presence of co-ion in the system diminished the

adsorption uptake of metal ions compared to a single-component adsorption system, and this decrease was roughly 54% for Ni(II) (Figure 5-7(b)) compared to 49% for Cd(II) (Figure 5-7(a)). Generally, the extent of reduction in the uptake in a binary adsorption system is affected by several factors, including the adsorbent initial concentration as well as its characteristics and molecular structure [322].

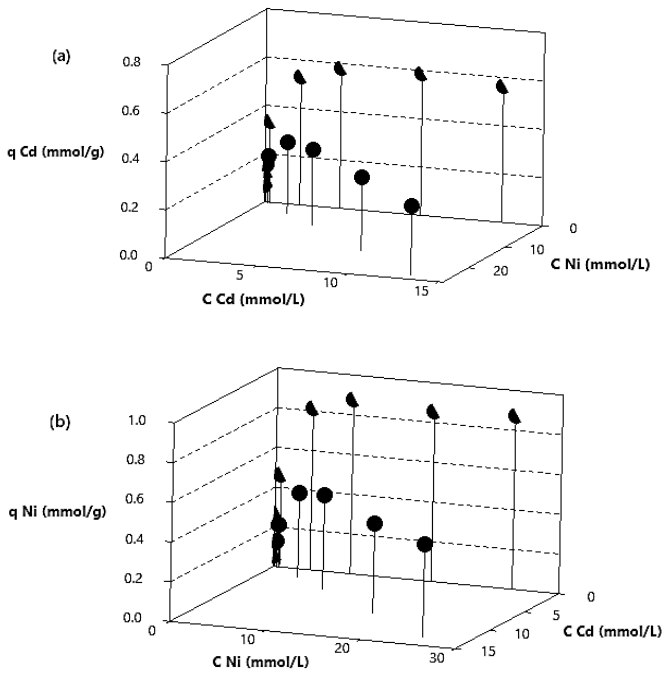

Figure 5-7. Mono and binary adsorption data of (a) Cd(II) and (b) Ni(II) on STPP-CB

5.4.3 Desorption

Desorption studies are necessary to assess the feasibility of recovering adsorbed metals and regenerating the adsorbent for further usage. Different eluents have been studied for the desorption of chitosan-based adsorbents loaded by Ni(II) and Cd(II), including acidic eluents such as HCl, HNO_3, H_2SO_4 [177,179], chelators (i.e. EDTA) [180], and salt agents (i.e. NaCl) [151]. In this study, H_2O and a mixture of NaCl and H_2SO_4 solutions were used as eluents for the desorption of loaded STPP-CB in the binary system. The desorption percentage of Ni(II) and Cd(II) (Eq. (2)) are tabulated in Table 5-8. The mixture of 0.2 mol/L NaCl and 0.01 mol/L H_2SO_4 showed good desorption results for Ni(II) and Cd(II), showing 87.6% and 90.1%, respectively. It should be noted that the desorption was complete around 48 h, indicating that desorption was a slow process.

Table 5-8. Desorption percentage of Ni(II) and Cd(II) ion from STPP-CB

Eluent	Desorption (%)	
	Ni(II)	Cd(II)
H_2O	0.42	0.35
NaCl (0.2 mol/L) + H_2SO_4 (0.01 mol/L)	87.6	90.1

5.5 Conclusion

A non-toxic crosslinker, sodium tripolyphosphate, was employed to crosslink synthesized chitosan beads. SEM analysis and solubility/swelling tests were conducted, which confirmed the crosslinking reaction occurrence. The optimum conditions for adsorption tests were determined, including the adsorbent dosage (0.55 g/L) and pH (6.5). Mono and binary component adsorption systems of Cd(II)-Ni(II) on CB and STPP-CB were investigated under optimum conditions. The results indicated that Langmuir could accurately fit the experimental data in the monocomponent system. The obtained maximum adsorption capacity of Cd(II) and Ni(II) onto CB were 1.06 and 1.36 mmol/g, respectively, which decreased to 0.61 and 0.89 mmol/g after crosslinking. Extended Freundlich provided a reasonable estimation for the binary system of Cd(II)-Ni(II) onto CB and STPP-CB, suggesting a heterogeneous adsorption system. The selectivity coefficient ($\alpha_{Ni/Cd}$) of STPP-CB was greater than unity in the range of concentrations studied, showing selectivity in Ni(II) adsorption. From the SEM-EDS and FTIR characterizations, before and after adsorption, it was concluded that two binding sites were involved in Cd(II) and Ni(II) adsorption on STPP-CB surface, including NH_2 and $P\text{-}O^-$. A mixture of NaCl and H_2SO_4 was found to be an appropriate eluent for the desorption of Ni(II) and Cd(II) from loaded STPP-CB, having a desorption efficiency of 87.6 and 90.1%, respectively.

5.6 References

The references are merged with those of the other chapters' references and presented at the end of the thesis.

Chapter 6

Technical Paper 4

6 Synthesis, characterization, and performance evaluation of ion-imprinted crosslinked chitosan (with sodium tripolyphosphate) for cadmium biosorption[4]

Keywords: Heavy Metals; Cd(II); Adsorption Isotherm; Thermodynamics; Kinetics; Desorption

6.1 Abstract

This study examined the removal of cadmium from aqueous solution using novel Cd(II)-imprinted chitosan hydrogel beads crosslinked by sodium tripolyphosphate. The synthesis of ion-imprinted and non-imprinted crosslinked chitosan beads was confirmed using Scanning Electron Microscopy (SEM), Fourier Transform Infrared Spectroscopy (FTIR), and Thermogravimetric Thermal Analysis (TGA). Brunauer-Emmett-Teller (BET) analysis showed an increase in surface area after the ion imprinting process. Batch adsorption tests were performed to determine the adsorption process parameters such as initial pH (7.0), adsorbent dosage (0.65 g/L), and contact time (48h). Isotherm investigation showed that the Langmuir model could describe Cd(II) adsorption well, and the maximum adsorption capacity of the ion-imprinted chitosan was 21% ± 5 higher than that of the non-imprinted one. The computed thermodynamic parameters at three different temperatures (25, 40, 55 ℃) showed the spontaneity and endothermic nature of Cd(II) adsorption on the synthesized bio-sorbents. The kinetics data were best fitted by the pseudo-second-order equation with a coefficient of determination of 0.99. Additionally, desorption tests employing a solution of NaCl and H_2SO_4 were undertaken, yielding acceptable results.

[4] A version of this chapter is published in Journal of Environmental Chemical Engineering (https://doi.org/10.1016/j.jece.2022.107147)

6.2 Introduction

The quality of water resources has deteriorated over the last decades due to human activities and the discharge of industrial effluents [247,323]. Dyes, oil spills, pharmaceuticals, pesticides, and heavy metals are among the top priority pollutants [108,199,324,325]. Among them, aquatic system pollution by heavy metals (HMs) has become a severe global issue because of their adverse impact on aquatic life, human health and the environment [247,326]. HMs are discharged to the environment from different sources such as mining operations, electroplating, ore refining, and the usage of batteries and fertilizers. Chromium (Cr), Cadmium (Cd), Mercury (Hg), Copper (Cu), Lead (Pb), and Arsenic (As) are classified by the United States Environmental Protection Agency (USEPA) as the main HMs of concern due to their persistence and irreversible toxic properties [327]. Therefore, multiple approaches such as ion flotation [261], chemical precipitation [328], chemical coagulation/flocculation [329], ion exchange [330], catalysis [331], membrane filtration [332], and adsorption [333] have been extensively studied in the literature to remove heavy metals from industrial effluents. The literature indicates that conventional treatment methods have several drawbacks and shortcomings, including high energy and capital requirements, incomplete removal, and secondary waste production [65,334]. As a result, recent research studies have been directed towards developing more sustainable, affordable and efficient techniques, concluding that adsorption could be a viable alternative because of its technical, economic, and environmental advantages over the others [193,335].

Various adsorbents such as activated carbon [333], polymer-based materials [252], biomaterials [336], industrial residues [337], and agricultural wastes [338], have been widely applied for heavy metals removal [334]. Given the high surface area and adsorption capacity of activated carbon, this adsorbent has been the primary choice for wastewater treatment for many years. However, its application has been steadily restricted because of its high production and regeneration costs [247,339]. Consequently, the utilization of abundant biomaterials, such as agricultural and industrial waste products, has received substantial attention due to their economic feasibility and environmental significance [69,340]. As a result, the adsorption capacity of different adsorbents derived from agricultural residues such as rice husk [338], nutshells [341], fruit peels [342], as well as marine industry wastes, i.e., alga/chitosan-based materials [197,269,338], have been reported in the literature for Cd(II) uptake, the seventh most toxic HMs based on Agency for Toxic Substances and Disease Registry (ATSDR)

ranking [343]. According to the literature, chitosan offers several advantages such as non-toxicity, biodegradability, reusability, and ease of synthesis and modification [97]. Chitosan can be obtained by partial deacetylation of chitin, the second most abundant biopolymer in nature after cellulose. Chitin is commonly found in crab, shrimp, and lobster shells, which are normally discarded by the seafood processing industry [91]. Hence, converting seafood wastes to chitosan can provide an effective bio-sorbent and, at the same time, serves as a sustainable solution for managing seafood sector wastes [199,344].

Despite chitosan's excellent adsorption properties, it shows low mechanical and chemical stability, especially in acidic media, limiting its application in large-scale treatment systems [86]. As a result, several chemical and physical modification techniques have been developed to improve chitosan physiochemical properties [15,16]. The majority of employed procedures involve crosslinking reactions, in which chitosan chains are connected to one another, resulting in chitosan which has a low solubility in dilute organic and mineral acids [21]. In this context, different crosslinkers have been introduced in the literature, including Glyoxal [345], Epichlorohydrin [265], Glutaraldehyde [100], and Ethylene Glycol Diglycidyl Ether [346]. However, most of the investigated crosslinkers are environmentally hazardous and costly, preventing the use of chitosan as a low-cost, green bio-sorbent for HMs adsorption. Therefore, using a non-toxic, low-cost crosslinker, such as sodium tripolyphosphate, is more desirable [347]

In previous work, the ionic crosslinking of chitosan was successfully accomplished using sodium tripolyphosphate to strengthen the chitosan structure. The results indicated that the adsorption efficiency of the crosslinked chitosan decreased by increasing the crosslinking degree [96]. This observation can be explained by the fact that crosslinking reduces the number of amino and hydroxyl groups in chitosan, which serve as the main sites for metal ion adsorption [348]. Thus, researchers have investigated different strategies to mitigate this issue [255]. Recently, ion imprinting technology has been introduced to produce crosslinked chitosan with enhanced adsorption capacity [19,127]. This technique has been successfully applied to different polymers, resulting in adsorbents with high recognition properties based on the coordination geometry, charge, and size of the template ion used [134,349]. Preparing ion-imprinted crosslinked adsorbents involves three stages:

attaching template ions to the adsorbent matrix, crosslinking, and finally removing the template ions using a desorption agent [129].

Different ion-imprinted chitosan-based adsorbents have been synthesized and employed to remove HM ions from drinking water, surface water, and wastewater, demonstrating considerably higher adsorption capacity compared to non-imprinted crosslinked adsorbents [83,278]. Additionally, it has been demonstrated that ion-imprinted adsorbents show predetermined selectivity for the given target ion in mixed ions solutions because of the interaction between monomers and templates [123,188]. Rahangdale and Kumar [197] employed acrylamide grafted chitosan-based ion-imprinted polymer to recover cadmium from nickel-cadmium battery waste, reporting an enhanced affinity towards Cd(II) uptake because of ion imprinting and grafting. Although some studies have been conducted on synthesizing Cd(II)-imprinted adsorbent for cadmium uptake, Cd(II)-imprinted chitosan crosslinked with sodium tripolyphosphate as a non-toxic reagent has not been reported in the literature [123,350].

In view of the above, the present study aimed to synthesize ion-imprinted chitosan crosslinked by sodium tripolyphosphate for cadmium adsorption. Different techniques, including SEM, BET, FTIR, and TGA, were employed to characterize the synthesized novel ion-imprinted and non-imprinted crosslinked chitosan hydrogel beads. The effect of adsorbent dosage, initial pH, initial metal ions concentration, temperature, and contacting time was examined on Cd(II) adsorption. Different kinetic and isotherm models were employed to study the experimental equilibrium adsorption data. The thermodynamic parameters, including ΔG^o, ΔH^o, and ΔS^o were calculated for the biosorption process. Desorption tests were also conducted to determine the adsorbents' reusability.

6.3 Experimental

6.3.1 Materials

Chitosan (deacetylation degree = 85%), sulphuric acid (H_2SO_4, N/50), sodium chloride (NaCl), and cadmium sulphate hydrate ($3CdSO_4 \cdot 8H_2O$) were obtained from Fisher Scientific Co. (Canada). Acetic acid (CH_3COOH, 99.9 wt. %) was supplied by VWR (Canada), and sodium tripolyphosphate ($Na_5P_3O_{10}$), as well as sodium hydroxide (NaOH), were purchased from Sigma

Chemical Co. (Canada). All chemicals were of analytical grade and used directly without further treatment or purification.

6.3.2 Preparation of ion-imprinted (II-CLCB) and non-imprinted (NI-CLCB) crosslinked chitosan beads

Cd(II)-imprinted chitosan hydrogel beads were prepared using the procedures reported in the literature with some minor changes to reduce the usage of chemicals harsh to the environment [197]. Cadmium sulphate hydrate was dissolved in 40 mL dilute acetic acid solution (5% v/v) to give a Cd^{2+} solution of 12.5 mg/L. Then 1.6 g chitosan (dry weight) was added to the same solution, and the batch was placed on a magnetic stirrer and mixed for 24h to obtain a homogeneous solution. The solution was then added dropwise into a flask containing sodium tripolyphosphate (5% w/v), which was determined to be the optimal concentration based on the previous study [96]. Spherical Cd(II) complexed chitosan beads were precipitated and left in the solution for 24h. Subsequently, the beads were separated, washed with deionized water, and transferred to a mixture of sulfuric acid (0.01 M) and sodium chloride (0.2 M) solution under constant shaking at 150 rpm for three days in 45 °C ± 5 to extract the template Cd^{2+} from the synthesized hydrogel beads. The resulting ion-imprinted beads were then washed with deionized water until no Cd^{2+} was detected. Regeneration of binding sites of ion-imprinted crosslinked chitosan beads (II-CLCB) was performed by rinsing the adsorbent with sodium hydroxide (0.5 M) followed by deionized water and then air-dried. The same procedure was carried out in the absence of the template ion (Cd^{2+}) addition and removal steps to prepare non-imprinted crosslinked chitosan beads (NI-CLCB). Figure 6-1 shows a schematic drawing of the II-CLCB structure.

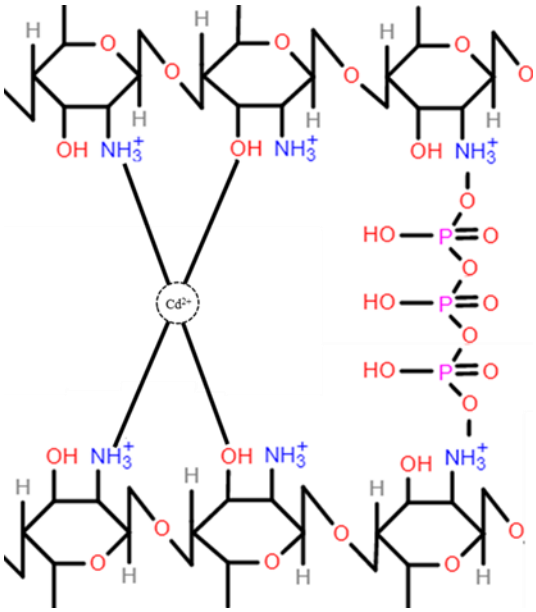

Figure 6-1. Schematic illustration of Cd(II)-imprinted chitosan crosslinked with sodium tripolyphosphate (II-CLCB)

6.3.3 Characterization of synthesized adsorbents

The surface topography was analyzed with a JEOL JSM-7500F Scanning Electron Microscopic (SEM), operating at an acceleration voltage of 3.0 kV. The specimens were coated with gold before the SEM analyses to prevent charging. The adsorbents' specific surface area, total pore volume, and pore diameter were measured by N_2 adsorption-desorption isotherms at 77 K using an Accelerated Surface Area and Porosimetry Analyzer (ASAP 2020, Micromeritics Co.) and computed using Brunauer–Emmett–Teller (BET) method by the Micromeritics Software. Fourier transform infrared spectroscopy (FTIR) was performed for the characterization of NI-CLCB and II-CLCB bands in the range from 450 to 4000 cm^{-1} (Thermo Fischer, Nicolet 6700) with the support of the attenuated total reflectance (ATR) sampling method. Thermal gravimetric analysis (TGA) was performed with Q5000 SA analyzer in the temperature range of 25–700 °C at a heating rate of 10 °C/min to obtain information about the thermal stability of the synthesized adsorbents.

6.3.4 Batch adsorption experiment

The batch adsorption experiments were carried out in 125 mL Erlenmeyer flasks filled with 50 mL of Cd(II) solution to investigate the effect of different factors on Cd(II) adsorption. A specified

amount of the adsorbent (either NI-CLCB or II-CLCB) was placed into the solution, shaking at an agitation speed of 225 rpm for 48h, at room temperature, unless otherwise stated. The initial pH effect on the cadmium(II) (50 mg/L) adsorption process was investigated in the range of 4.0-8.0 ± 0.2 (monitored by HACH (HQ40D)), and the pH was adjusted by sodium hydroxide/sulfuric acid solution (0.1 M). The adsorbent dosage effect was also examined by varying the amount of the adsorbent from 0.25 to 1 g/L. Once the adsorption system reached the equilibrium, the residual concentration of Cd(II) in the solution was analyzed by an AAS (PinAAcle 500, Perkin Elmer), and the amount adsorbed per unit mass of adsorbent, q_e (mmol/g), was calculated as follows:

$$q_e = \frac{(C_0 - C_e)\,V}{W} \qquad 6\text{-}1$$

where C_0 (mmol/L) is the initial, and C_e (mmol/L) is the equilibrium concentrations of adsorbate in the solution, V (L) is the solution volume, and W (g) represents the weight of the dry adsorbent. Each test was carried out with three replicates, and the mean was used unless otherwise stated. The control experiments were also conducted to monitor any weight loss.

6.3.4.1 Batch adsorption isotherm studies

A weighed amount of the adsorbent (equivalent to 0.65 g/L) was added to flasks containing 50 mL Cd(II) solution, with different initial concentrations ranging from 10 to 1500 mg/L. The flasks were shaken at 225 rpm for 48h at room temperature (~25 ℃). After reaching equilibrium, samples were filtered, and the adsorption capacity was calculated using Eq. (6-1). Different isotherm models, including Langmuir [157], Freundlich [158], Temkin [351], and Dubinin–Radushkevich (D–R) [235], were employed to describe adsorption isotherm data. The linearized forms of the isotherm models are listed in Table 6-1 [141]. Coefficient of determination (R^2) and Root Mean Square Error (RMSE) were calculated to assess the best-fit isotherm model.

Table 6-1. Linear forms of isotherm models and their parameters

Isotherm equations	Isotherm parameters
Langmuir $\frac{C_e}{q_e} = \frac{1}{K_L q_m} + \frac{C_e}{q_m}$	q_e: The amount of adsorbate per unit mass of adsorbent weight (mmol/g) C_e: The equilibrium concentration of adsorbate (mmol/L) q_m: The maximum adsorption capacity (mmol/g) K_L: The Langmuir constant related to the adsorption energy (L/mmol)
Freundlich $\log q_e = \log K_F + \frac{1}{n} \log C_e$	q_e: The amount of adsorbate per unit mass of adsorbent weight (mmol/g) C_e: The equilibrium concentration of adsorbate (mmol/L) 1/n: The Freundlich constant related to the adsorption intensity K_F: The Freundlich constant related to the adsorption capacity ((mmol/g).(L/mmol)$^{(1/n)}$)
Temkin $q_e = \frac{RT}{b_T} \ln K_T + \frac{RT}{b_T} \ln C_e$ $B = \frac{RT}{b_T}$	q_e: The amount of adsorbate per unit mass of adsorbent weight (mmol/g) C_e: The equilibrium concentration of adsorbate (mmol/L) b_T: The Temkin constant related to the heat of adsorption (J/mol) K_T: The Temkin constant related to the binding energy (L/mmol) R: The universal gas constant (8.314 J/mol/K) T: The absolute temperature B: The Temkin constant
Dubinin-Radushkevich $\ln q_e = \ln q_m + K\varepsilon^2$ $\varepsilon = RT \ln(1 + \frac{1}{C_e})$ $E = (2K)^{-1/2}$	q_e: The amount of adsorbate per unit mass of adsorbent weight (mmol/g) C_e: The equilibrium concentration of adsorbate (mmol/L) q_m: The maximum adsorption capacity (mmol/g) K: The activity coefficient related to the adsorption mean free energy (mol^2/kJ^2) Ɛ: The Polanyi potential (J/mol) E: The mean free energy of adsorption per mole of the adsorbate (kJ/mol) R: The universal gas constant (8.314 J/mol/K) T: The absolute temperature

6.3.4.2 Effect of temperature

To evaluate the effect of temperature on Cd(II) adsorption on NI-CLCB and II-CLCB, 0.65 g/L of dry beads was added to a series of flasks filled with 50 mL of the metal ions solution (50 mg/L) with the initial pH of 7.0 ± 0.2. The flasks were agitated in an incubator shaker running at 225 rpm for 48h, at different temperatures including 25, 40, and 55 ℃. The Cd(II) uptake was calculated at equilibrium using Eq. (6-1).

6.3.4.3 Effect of contact time

The effect of contact time on Cd(II) adsorption onto NI-CLCB and II-CLCB was investigated by placing 0.65 g/L of the adsorbent in a series of flasks containing 50 mL of Cd(II) solution (50 mg/L). The mixture pH was adjusted to 7.0 ± 0.2 and kept in constant agitation at 225 rpm and room temperature for 5, 10, 20, 30, 60, 180, 360, 680, 1440, 2880 and 4320 min. Sampling was performed from each beaker, and the adsorption capacity was calculated using Eq. (6-1). The adsorption kinetics of Cd(II) adsorption was evaluated using pseudo-first and second-order kinetic models, and the intra-particle model tested diffusion impact.

6.3.5 Desorption Studies

After loading the adsorbents with 50 mg/L Cd(II) solutions, they were separated through filtration, gently rinsed with de-ionized water, and air-dried. The dried beads were equilibrated with 50 mL NaCl (0.2 M) and H_2SO_4 (0.01 M) solution for 48h, and AAS was employed to determine the amount of desorbed metal ions. Each experiment was conducted in duplicate, and the average value was used. The percentage of desorption was calculated using the following equation (Eq. (6-2)):

$$\text{Desorption\%} = \frac{\text{amount of metal ions desorbed}}{\text{amount of metal ions adsorbed}} \times 100\% \qquad \textit{6-2}$$

6.4 Results and discussion

6.4.1 Characterizations of NI-CLCB and II-CLCB

6.4.1.1 Surface analysis

The BET surface area and total pore volume of NI-CLCB were computed as 5.60 (m^2/g) and 3.63×10^{-3} (cm^3/g), respectively. For II-CLCB, greater values were obtained (6.20 (m^2/g) and 4.04×10^{-3} (cm^3/g)), implying that the ion imprinting process enhanced the surface area of crosslinked chitosan to some extent. The average pore diameters of NI-CLCB and II-CLCB were

nearly identical, measured at 2.59 and 2.60 nm, respectively, categorized as mesopores, according to the IUPAC classification [352]. The surface morphologies of II-CLCB and NI-CLCB were also examined using a scanning electron microscope, and the images are shown in Figure 6-2(a) and (b). As can be seen, the II-CLCB surface showed a porous structure compared to the non-granular surface of NI-CLCB. The morphological change seen after the ion imprinting process can be explained by the removal of the template ions from the II-CLCB surface and the subsequent formation of imprinted cavities. Other researchers have also documented the porous surface morphology of the ion-imprinted chitosan-based adsorbents [353].

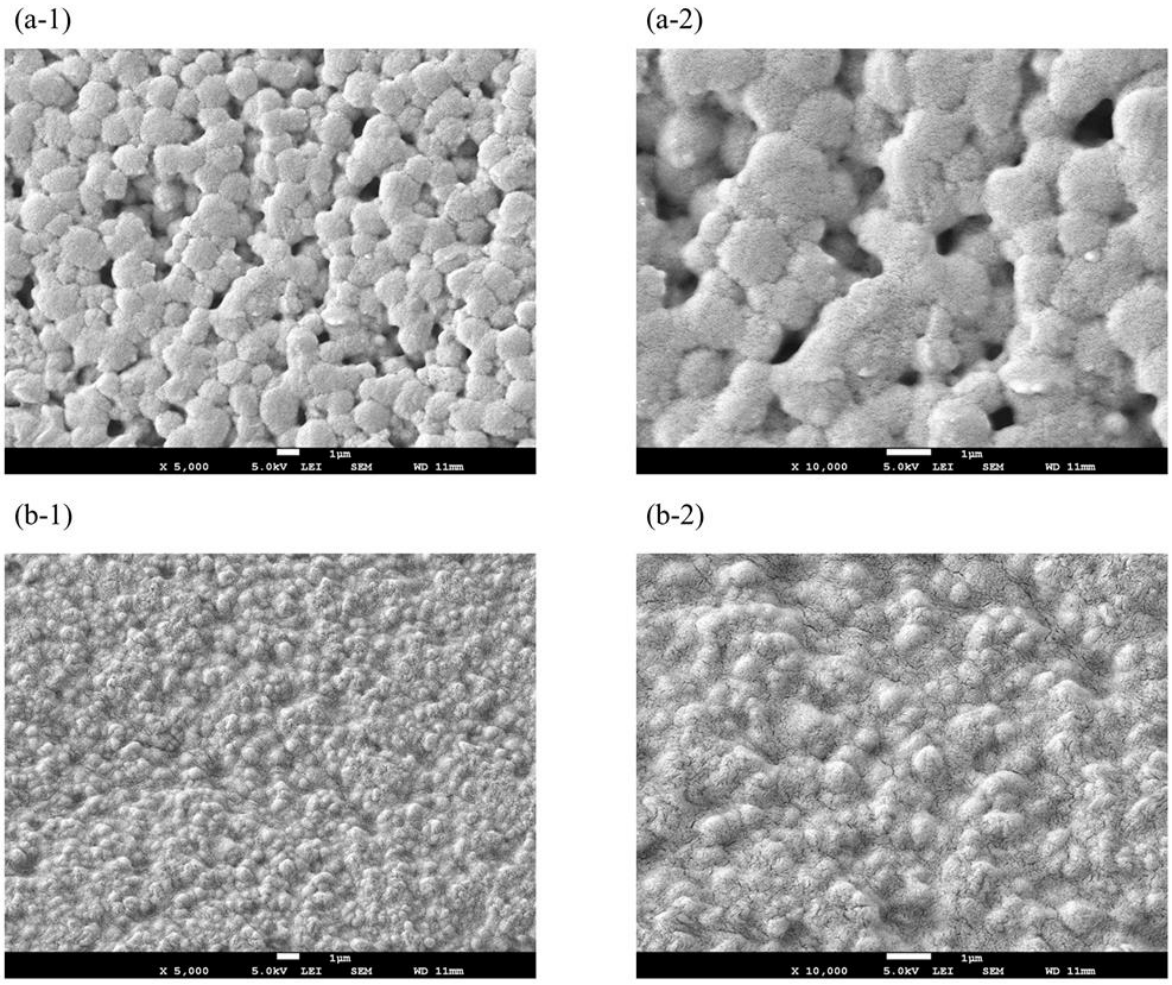

Figure 6-2. SEM analysis of II-CLCB (a-1)×5000, (a-2)×10000 and NI-CLCB (b-1)×5000, (b-2)×10000

6.4.1.2 FTIR analysis

FTIR spectroscopy has been widely used as an analytical technique to characterize chitosan and sodium tripolyphosphate. Their identified characteristic peaks reported in the literature are summarized in Table 6-2 [21,107,354–357]. The FTIR technique was employed to characterize the commercial sodium tripolyphosphate and chitosan (85% DD) used in this study, and the results are presented in Figure 6-3. Additionally, Figure 6-3 provides the FTIR spectra of NI-CLCB and II-CLCB to identify the functional groups involved in crosslinking and imprinting processes.

Table 6-2. FTIR characteristic bands of chitosan and sodium tripolyphosphate

Material	Wavenumber (cm^{-1})	Functional Groups
Chitosan	3273	N-H and O-H stretching vibration
	2921 and 2877	C-H symmetric and asymmetric stretching
	1650	C=O of amide group
	1590	Bending vibration of N−H of the primary amine
	1430	Bending vibration of O−H deformation
	1370	Bending vibration of C−H group
	1153	C−O-C asymmetric stretching
	1066 and 1028	C-O stretching
Sodium tripolyphosphate	1210	Stretching vibration of P=O
	1130	Symmetric and anti-symmetric stretching vibration of O−P=O
	1090	Symmetric and anti-symmetric stretching vibration of PO3
	800	Stretching vibration of P−O−P bridge

A comparison between the FTIR spectra of chitosan (Figure 6-3(b)) and NI-CLCB (Figure 6-3(c)) indicated that the peak corresponding to bending vibration of N−H at 1525 cm^{-1} disappeared after crosslinking, which can be attributed to the interaction between the negatively charged triphosphate groups and the positively charged amino groups of chitosan [358]. Moreover, new sharp peaks were detected on chitosan after crosslinking (Figure 6-3(c)) at ~750 and 1000 cm^{-1} assigned to the stretching vibration of P-O, which were also identified in the spectrum of sodium tripolyphosphate (Figure 6-3(a)), verifying the presence of the phosphate groups in crosslinked chitosan structure [359]. FTIR spectra of chitosan (Figure 6-3(b)) and II-CLCB (Figure 6-3(d)) were nearly identical with a few differences, indicating that the preparation of Cd(II)-imprinted

crosslinked chitosan hydrogel beads did not significantly impact chitosan functional groups. As seen in Figure 6-3(b) and (d), a band at about 3000 cm^{-1} associated with the stretching vibration of N-H and O-H was observed on both II-CLCB and chitosan, whereas it was not identified on NI-CLCB (Figure 6-3(c)) most likely as a result of their involvement in the crosslinking reaction [124]. Peaks detected at around 850 and 1550 cm^{-1} in the spectrum of II-CLCB corresponding to the stretching vibration of P-O and bending vibration of N-H, respectively, confirmed the occurrence of partial crosslinking with sodium tripolyphosphate as well as the existence of more amino groups on the II-CLCB surface compared to NI-CLCB [226].

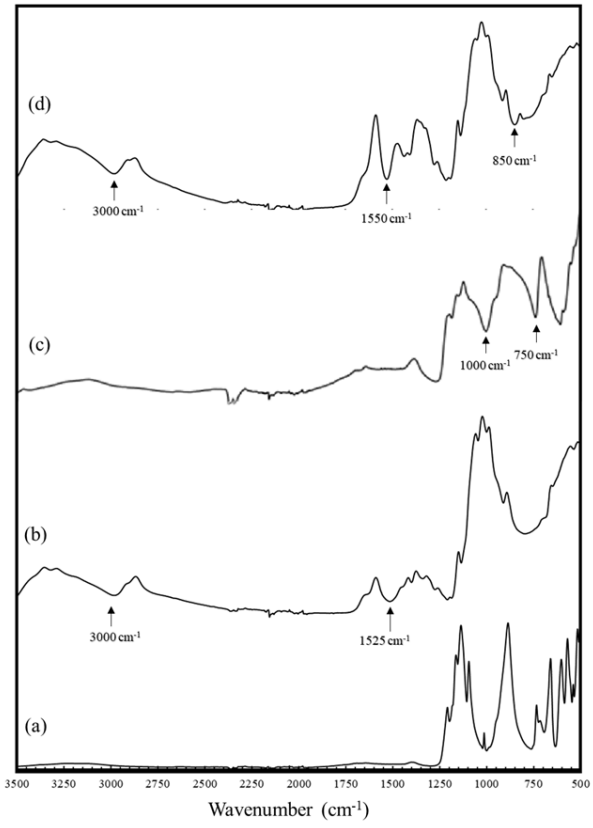

Figure 6-3. FTIR spectra of (a) sodium tripolyphosphate, (b) chitosan, (c) NI-CLCB, and (d) II-CLCB

6.4.1.3 TGA analysis

TGA technique was used to evaluate the thermal properties of commercial chitosan and sodium tripolyphosphate, as well as NI-CLCB and II-CLCB, and the results are shown in Figure 6-4. As demonstrated, commercial chitosan (Figure 6-4(a)) degraded in two steps. The initial weight loss

of 9-10% in the 30–125 ℃ range is attributed to eliminating water molecules adsorbed on the polysaccharides. The second mass loss began at 230 ℃ and accounted for 49% of the total weight loss, attributed to chitosan glycosidic bond breakdown [360]. Also, the temperature of 50% weight loss of chitosan was found to be ~350 ℃. It is worthwhile to highlight a considerable difference in the thermal behaviour of sodium tripolyphosphate (Figure 6-4(d)) and chitosan (Figure 6-4(a)), as the former did not decompose or lose weight except for the evaporation of moisture water at ~110 ℃, indicating the high thermal stability of sodium tripolyphosphate [227].

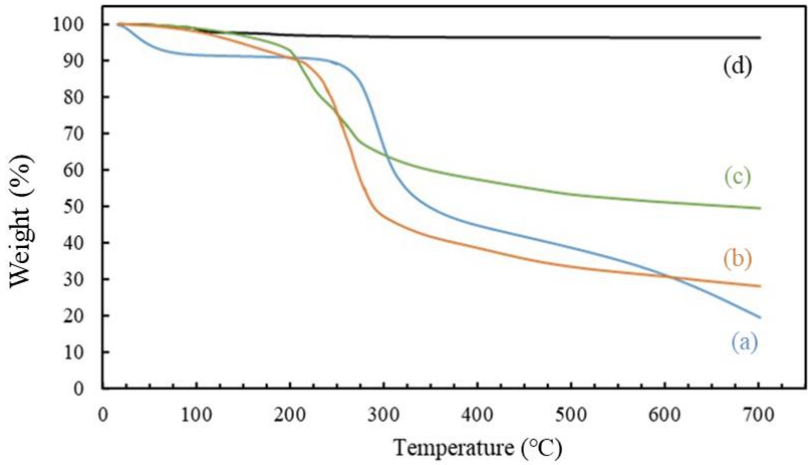

Figure 6-4. TGA thermographs of (a) chitosan, (b) II-CLCB, (c) NI-CLCB, and (d) sodium tripolyphosphate

Drawing a comparison between TGA profiles of chitosan/sodium tripolyphosphate (Figure 6-4(a) and Figure 6-4(d)) and NI-CLCB (Figure 6-4(c)) could provide insight into the role of sodium tripolyphosphate in crosslinking [361]. As shown in Figure 6-4(c), after the free water evaporation stage, the second weight loss of NI-CLCB (~28%) started at 200℃ and was completed in two steps at 296℃, which can be corresponded to the destruction of the ionic bond between chitosan molecules and sodium tripolyphosphate followed by chitosan chains degradation. 50% weight loss of NI-CLCB took place at 650℃, which was significantly higher than chitosan, implying that chitosan thermal stability was improved after crosslinking [362]. Meanwhile, the II-CLCB thermograph (Figure 6-4(b)) showed a two-stage degradation similar to chitosan. The three-dimensional network formed by ion imprinting and crosslinking proposed retaining more water than the initial chitosan water content [270]. Therefore, the first stage of II-CLCB weight loss, attributed to the evaporation of free water, was slightly higher than chitosan (~3%), which started

at 90 ℃. The second stage accounting for 42% between 210 and 300℃, was due to chitosan and crosslinker bond destruction and chitosan decomposition. The 50% degradation temperature of II-CLCB (~290℃) was lower than that of chitosan and NI-CLCB, indicating that the Cd(II)-imprinted adsorbent was less thermally stable. This may be explained by the fact that imprinting created a mesopore structure, resulting in low thermal stability due to the pores between polymer chains [363].

6.4.2 Cd(II) adsorption study

6.4.2.1 Effect of pH and adsorbent dosage

One of the most important factors influencing metal adsorption at solid–water interfaces is the pH of the aqueous solution. In fact, different pHs change the availability of metal ions in the solution as well as the metal-binding sites on the adsorbent surface [364]. As indicated in the literature, cadmium remains present in the form of Cd^{2+} at pH < 8.0 in dilute solutions and the precipitation of Cd(II) as hydroxide starts at higher pHs [130]. Hence, the effect of hydrogen ion concentration on the extent of Cd(II) adsorption on NI-CLCB and II-CLCB was investigated in a pH range of 4.0 to 8.0 ± 0.2, shown in Figure 6-5. Experiments were not carried out at pHs below 4.0 because the amino groups of chitosan as the primary sites for metal ions uptake undergo protonation, hindering the metal ions interaction with binding sites [365]. Quite the opposite, at higher pHs, the presence of free lone pair of electrons on nitrogen atoms of chitosan amino groups serves as the active adsorption site with a high affinity for metal ions adsorption [100]. It can be seen from Figure 6-5 that the adsorption uptake of both adsorbents increased by increasing pH. Kumar et al. [366] also reported a similar trend in the adsorption of Cd(II) on crosslinked chitosan/polyvinyl alcohol blend beads. The results indicated that Cd(II) adsorption on II-CLCB was approximately 25% higher than NI-CLCB in the pH range examined. This observation was expected because the larger surface area of II-CLCB compared to NI-CLCB provided a greater number of bindings sites for Cd(II) adsorption [348]. In addition, the lower removal efficiency of NI-CLCB can be ascribed to crosslinking reaction, in which the available free binding sites responsible for metal ions sorption were occupied by sodium tripolyphosphate, which is consistent with FTIR results [96]. Considering the results and the tendency to work in neutral pH, pH 7.0 was selected for the following adsorption experiments.

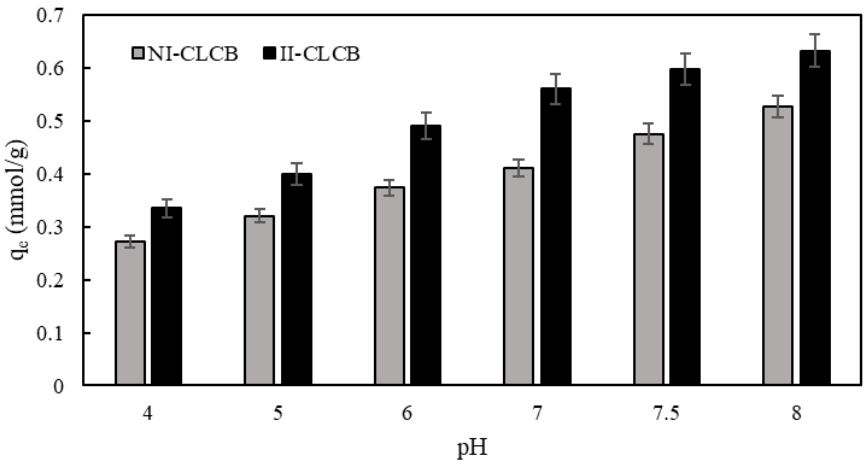

Figure 6-5. Effect of pH on the adsorption of Cd(II) (50 mg/L) onto NI-CLCB and II-CLCB with dosage 0.65 g/L at room temperature

The quantity of bio-sorbent in the solution can also affect the extent of metal ions uptake [346]. The dependence of Cd(II) adsorption on adsorbent dosage was investigated by changing the amount of the II-CLCB from 0.25 to 1 g/L. The results indicated that the percentage of Cd(II) removal increased with increasing adsorbent dosage. This observation was expected because a higher dosage of II-CLCB in the solution provided more available sites for the metal ions' adsorption. On the other hand, the apparent adsorption capacity calculated by Eq. (6-1) decreased with an increase in adsorbent dosage. The reduction in adsorption capacity can be explained by the fact that some adsorption sites remained unsaturated by increasing the adsorbent mass [366]. Therefore, the optimum dosage of II-CLCB was determined as 0.65 g/L in which the Cd(II) removal percentage and adsorption capacity were maximum concurrently.

6.4.2.2 Adsorption isotherm study

Investigating the influence of Cd(II) concentration on the adsorption uptake was necessary to develop the applications of the adsorbents [305]. Hence, the initial Cd(II) concentration varied from 10 to 1500 mg/L, and the adsorption uptake of Cd(II) onto NI-CLCB and II-CLCB were recorded. Each test was conducted in duplicate, and the mean was used. Isotherm models can help explain how the adsorbate interacts with the adsorbent; therefore, different equilibrium models have been developed and used in the literature [150,234]. Searching for an equilibrium model that interprets the experimental data of this work satisfactorily was accomplished by fitting the data to Langmuir,

Freundlich, Temkin and Dubinin-Radushkevich isotherm models. Figure 6-6 shows the employed isotherm models and the collected experimental data for Cd(II) adsorption on NI-CLCB (Figure 6-6(a)) and II-CLCB (Figure 6-6(b)). As depicted in the figure, the adsorption uptake of both adsorbents increased progressively as the Cd(II) initial concentration increased and reached saturation, giving the maximum Cd(II) adsorption capacity. The maximum Cd(II) adsorption of II-CLCB was found to be 21% ± 5 higher than that of NI-CLCB, indicating that the synthesis of ion-imprinted adsorbent successfully enhanced the adsorption properties of II-CLCB.

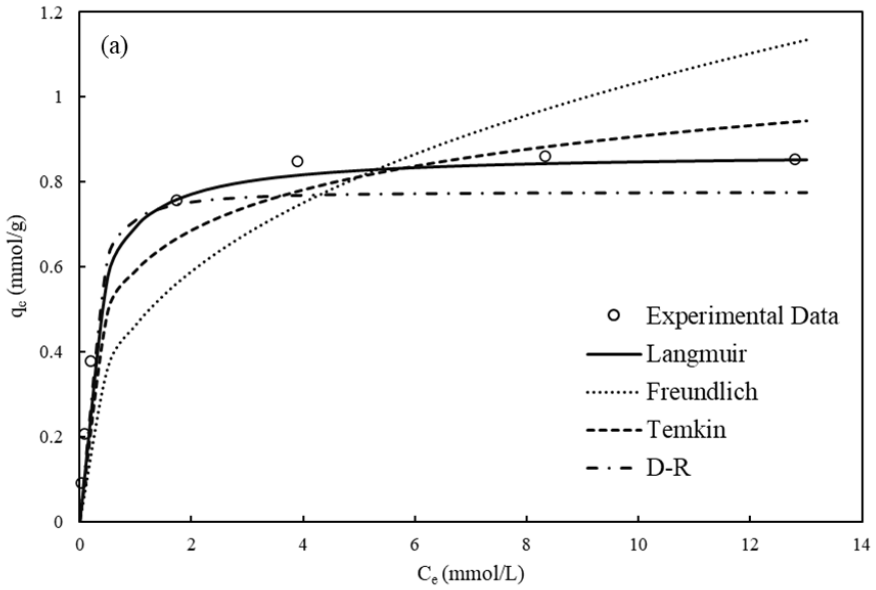

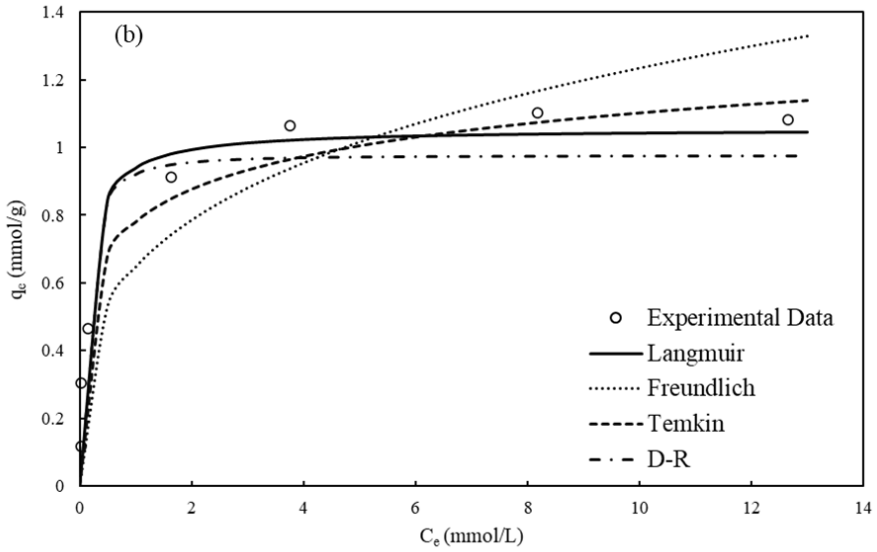

Figure 6-6. Experimental data and adsorption isotherm models of Cd(II) on (a) NI-CLCB and (b) II-CLCB with dosage 0.65 g/L at room temperature

Table 6-3 lists the computed isotherm models parameters, their linear fitting correlation coefficients (derived from the intercept and slope) as well as RMSE. The results indicated that the Langmuir isotherm model provided the best correlation ($R^2 = 0.99$) between the experimental data and theoretical predictions for NI-CLCB and II-CLCB with RMSE less than 0.1 mmol/g. Therefore, the monolayer adsorption played the main role in Cd(II) adsorption onto the studied adsorbents with finite biosorption sites [146]. The maximum adsorption capacity of NI-CLCB and II-CLCB calculated using the Langmuir model was in the order of II-CLCB (1.05 mmol/g) > NI-CLCB (0.87 mmol/g), demonstrating the greater adsorption efficiency of the synthesized ion-imprinted adsorbent. In comparison, the Freundlich model did not match the adsorption data, showing lower determination coefficients ($R^2 = 0.87$ and 0.89) and higher RMSE values (0.17 and 0.16 mmol/g). Also, the Freundlich plot failed to display the plateau at high aqueous concentrations, denoting the maximum saturation shown in the figure. The equilibrium data were also examined with the Dubinin-Radushkevich (D-R) and Temkin isotherm models. Temkin empirical isotherm model is characterized by a uniform distribution of the binding energies. This model is based on indirect adsorbate/adsorbent interaction, assuming that the heat of adsorption of all the molecules in the layer decreases linearly with coverage [141]. Dubinin-Radushkevich isotherm is generally employed to characterize the mechanism of the adsorption process based on the mean

biosorption energy value (E) [367]. Considering the estimated R^2 and RMSE values, Temkin and D-R isotherm models could not provide a good fit to the experimental data of NI-CLCB and II-CLCB compared to Langmuir.

Table 6-3. Isotherm parameters and determination coefficients for biosorption of Cd(II) on NI-CLCB and II-CLCB

Isotherm Constants	NI-CLCB	II-CLCB
Langmuir		
q_m (mmol/g)	0.87	1.05
K_L (L/mmol)	3.96	8.06
R^2	0.99	0.99
RMSE	0.07	0.09
Freundlich		
1/n	0.35	0.28
K_F ((mmol/g).(L/mmol)$^{1/n}$)	0.46	0.65
R^2	0.87	0.89
RMSE	0.17	0.16
Temkin		
K_T (L/mmol)	79.05	263.59
b_T (J/mol)	17.99	17.72
R^2	0.91	0.94
RMSE	0.10	0.09
Dubinin-Radushkevich		
q_m (mmol/g)	0.78	0.97
K (mol^2/kJ^2)	3.00×10^{-8}	2.00×10^{-8}
E (kJ/mol)	4.08	5.00
R^2	0.92	0.95
RMSE	0.09	0.11

The adsorption capacity of some chitosan-based adsorbents from the literature is listed in Table 6-4 for comparison purposes. As shown in the table, the adsorption capacity of II-CLCB was within the range of the reported adsorption capacities of other chitosan-based adsorbents, modified under sophisticated processes and complex chemical reactions. However, the chitosan hydrogel beads fabricated in this study were formed and crosslinked simultaneously in a single step by a non-toxic crosslinker. Moreover, ion-imprinting was accomplished under mild experimental conditions, enabling the preparation of an efficient bio-sorbent for Cd(II) uptake in a simple and clean method. It is worth noting that various factors impact the maximum adsorption capacity of adsorbents, including temperature, time, initial concentration, adsorbent dosage, and pH. As a result, drawing a comparison between the reported maximum adsorption capacities is difficult unless the adsorption system is subjected to the same experimental conditions.

Table 6-4. Adsorption capacity of Cd(II) onto chitosan-based adsorbents

Adsorbent	pH	Adsorption Capacity (mmol/g)	Reference
Magnesium oxide biochar-chitosan	5	0.26	[368]
Phosphorylated chitosan/$CoFe_2O_4$ composite	5.9-6.1	0.63	[369]
Magnetic kaolinite immobilized chitosan	6	0.79	[370]
Magnetic Cd(II)-imprinted aminoethyl chitosan	6	0.23	[22]
Chitosan-based hydrogel	6	0.80	[252]
Crosslinked chitosan by sodium tripolyphosphate	7	0.83	[96]
Surfactant-modified chitosan using sodium dodecyl sulphate	6.5-7	1.11	[371]
CS_2-modified chitosan encapsulated magnetic Fe_3O_4 nanoparticles	6	1.76	[212]
Thiourea-modified magneticion-imprinted chitosan/TiO_2 composite	6-7	2.28	[372]
Cd(II)-imprinted chitosan crosslinked by sodium tripolyphosphate	7	1.10	This work

6.4.2.3 Effect of temperature and thermodynamic study

The adsorption uptake of cadmium(II) on NI-CLCB and II-CLCB was also assessed at three different temperatures, 25, 40 and 55 °C, and the results are shown in Figure 6-7. As seen, the Cd(II) uptake by NI-CLCB and II-CLCB increased sharply by changing the temperature from 25 °C to 40 °C, reaching 0.51 and 0.59 mmol/g, respectively, and marginally increased by further raising the temperature from 40 °C to 55 °C. The results are consistent with those of Deng et al. [187], who studied the effect of temperature on competitive adsorption of Pb(II), Cd(II) and Cu(II) onto chitosan-pyromellitic dianhydride modified biochar. The enhancement in adsorption uptake at elevated temperatures might be attributable to a variety of factors, such as improving Cd(II) mobility towards the active sites and enlarging pores [373].

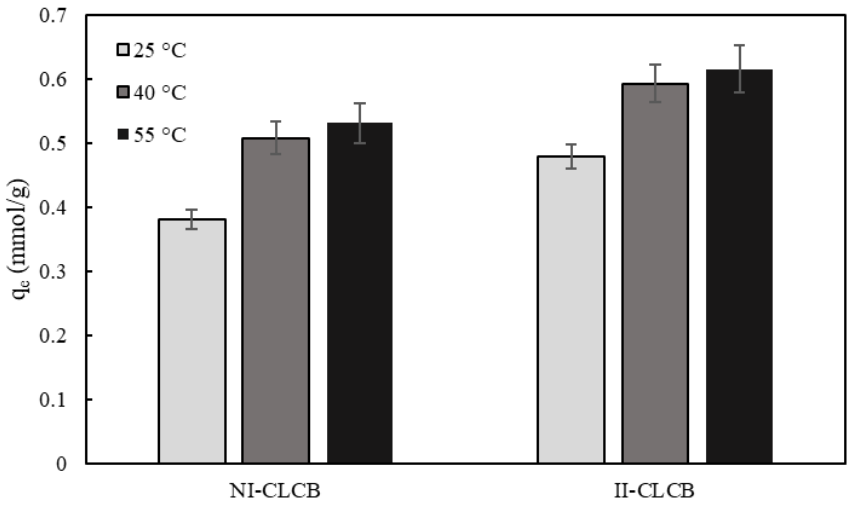

Figure 6-7. Effect of temperature on the adsorption of Cd(II) (50 mg/L) onto NI-CLCB and II-CLCB with dosage 0.65 g/L

Thermodynamic parameters of an adsorption process, including free energy ΔG^o, enthalpy ΔH^o, and entropy ΔS^o, help understand the nature of the adsorption reaction, such as spontaneity, randomness, and endothermicity/exothermicity [142]. Hence, the following equations (Eq. (6-3), (6-4), and (6-5)) were used to calculate the thermodynamic parameters:

$$k_C = C_{ad}/C_e \qquad 6\text{-}3$$

$$\Delta G° = -RT \ln k_C \qquad 6\text{-}4$$

$$\ln k_C = {\Delta S^\circ}/{R} - {\Delta H^\circ}/{RT} \qquad 6\text{-}5$$

where C_{ad} and C_e are the equilibrium concentration of the adsorbate (mmol/L) on the adsorbent and in the solution, respectively, and k_C is the sorption equilibrium constant. T is the absolute temperature (K), and R is the universal gas constant (8.314 J/mol/K). The computed thermodynamic parameters of Cd(II) adsorption on NI-CLCB and II-CLCB are presented in Table 6-5.

Table 6-5. Thermodynamic parameters for Cd(II) adsorption onto NIP-STPP and IIP-STPP

Temperature (K)	293.15	313.15	328.15	293.15	313.15	328.15		
	Equilibrium Constant (k_c)			ΔG° (kJ/mol)			ΔH°(kJ /mol)	ΔS° (J/mol/K)
NI-CLCB	1.36	3.30	4.04	-0.75	-3.11	-3.81	29.83	103.43
II-CLCB	2.60	8.50	13.15	-2.37	-5.57	-7.03	44.21	157.13

As seen in Table 6-5, the estimated values of ΔG^o were negative for both adsorbents, indicating that Cd(II) adsorption on NI-CLCB and II-CLCB occurred spontaneously, whereby no energy input was required to drive the reactions. At higher temperatures, the ΔG^o values of the adsorbents became more negative, meaning that the adsorption process was more feasible with a larger degree of spontaneity in the order of II-CLCB>NI-CLCB [187]. The estimated positive values of ΔH^o confirmed that the adsorption process onto NI-CLCB and II-CLCB was endothermic. Some other chitosan-based adsorbents used for Cd(II) adsorption have also exhibited an endothermic adsorption process [366,374]. The magnitude of ΔH^o can reveal valuable information about interactions between the adsorbent and adsorbate. The heat evolved during physical adsorption, such as van der Waals interaction, is usually lower than 20 kJ/mol; electrostatic interaction falls into the range of 20-80 kJ/mol; chemisorption bond strength varies between 80-450 kJ/mol [8,375]. The obtained ΔH^o values of NI-CLCB and II-CLCB were 29.83 and 44.21 kJ/mol, respectively, indicating electrostatic interaction was dominant in this study. The positive entropy values for NI-CLCB and II-CLCB (103.43 and 157.13 J/mol/K) suggested randomness increase at the adsorbent/adsorbate interface during the adsorption processes [185].

6.4.2.4 Kinetics study

Different kinetic models have been employed to simulate the experimental data and investigate the rate-limiting step of the adsorption process. The pseudo first-order and pseudo-second-order equations are primarily used to simulate metals biosorption, where electrons are shared or exchanged between metal ions and functional groups [133]. The intraparticle diffusion model, which emphasizes the role of mass transfer in hydrogel beads, has also been successfully applied in the literature for describing the kinetics of metal ions sorption [376]. The equations of the models are presented below (Eq. (6-6), (6-7), (6-8)):

Pseudo first-order equation:

$$q_t = q_e(1 - \exp(-k_1 t)) \qquad 6\text{-}6$$

Pseudo second-order equation:

$$q_t = \frac{k_2\, q_e^2\, t}{1 + k_2\, q_e\, t} \qquad 6\text{-}7$$

The intraparticle diffusion equation:

$$q_t = k_m t^{1/2} + C \qquad 6\text{-}8$$

where q_t and q_e (mmol/g) are the amounts of adsorbate on the adsorbents at time t and equilibrium, respectively. k_1 (1/min) and k_2 (g/mmol/min) are the rate constants of pseudo first-order and pseudo-second-order kinetic models and k_m (mmol/g/min$^{1/2}$) is the intraparticle diffusion constant.

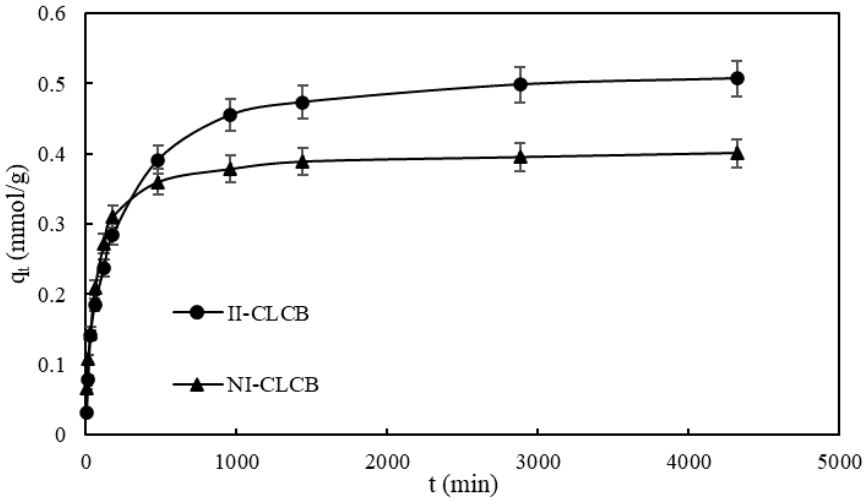

Figure 6-8. Effect of the contact time on the adsorption of Cd(II) (50 mg/L) onto NI-CLCB and II-CLCB with dosage 0.65 g/L

Figure 6-8 depicts the influence of contact time on Cd(II) adsorption on NI-CLCB and II-CLCB. As seen from the figure, both adsorbents' adsorption rates were initially fast, then gradually slowed until they reached equilibrium. The availability of abundant adsorption sites can explain the fast

adsorption rate at the beginning, which declined slowly as the number of active sites decreased after becoming occupied during adsorption [377]. The adsorption capacity of NI-CLCB remained stable after 18h; however, II-CLCB continued to increase until 48h. Consequently, this period was selected in this work to ensure ample time to attain adsorption equilibrium.

The linear form of pseudo first-order and pseudo second-order were employed to simulate the adsorption data and the corresponding kinetics parameters. The correlation coefficients computed from the slopes and intercepts of the plots are given in Table 6-6. As indicated, R^2 values of NI-CLCB and II-CLCB from the pseudo-second-order kinetic model were 0.99, which exceeded the results obtained by the pseudo-first-order kinetic model. Moreover, the theoretical q_e values calculated using the pseudo second-order were remarkably close to the experimental data in the order of II-CLCB>NI-CLCB, shown in Table 6-6. These observations suggested that the pseudo-second-order model was more suitable than the pseudo-first-order kinetic model to describe the experimental data, implying that the surface reaction might be the rate-limiting step [378].

Table 6-6. Adsorption kinetics parameters for Cd(II) adsorption onto NI-CLCB and II-CLCB

Isotherm Constants	NI-CLCB	II-CLCB
Pseudo-first-order model $\ln(q_e - q_t) = \ln q_e - k_1 t$		
Measured q_e (mmol/g)	0.40	0.51
Calculated q_e (mmol/g)	0.17	0.61
k_1 (1/min)	1.40×10^{-3}	6.00×10^{-4}
R^2	0.84	0.94
Pseudo-second-order model $t/q_t = 1/k_2 q_e^2 + t/q_e$		
Measured q_e (mmol/g)	0.40	0.51
Calculated q_e (mmol/g)	0.40	0.52
K_2 (1/min)	0.05	0.02
R^2	0.99	0.99
Intraparticle diffusion model $q_t = k_m t^{1/2} + C$		
$k_{m,1}$ (mmol/g/min$^{1/2}$)	2.21×10^{-2}	2.22×10^{-2}
$k_{m,2}$ (mmol/g/min$^{1/2}$)	3.80×10^{-3}	9.60×10^{-3}
$k_{m,3}$ (mmol/g/min$^{1/2}$)	6.00×10^{-4}	1.50×10^{-3}

The adsorption mechanism on a porous adsorbent is usually a multi-step process, and it is critical to understand the steps involved in the adsorption process [152]. These steps may include adsorbate transfer from the bulk solution, intraparticle diffusion in the pores and solid phase, followed by adsorption on the adsorption sites (chemical reactions) [379]. The intraparticle model was adopted to investigate the rate-controlling step, and therefore the plot of q_t versus $t^{1/2}$ was drawn, shown in Figure 6-9. If intraparticle diffusion is involved in the biosorption process, the plot of uptake should be linear, and intraparticle diffusion controls the rate if the line goes through the origin [302]. However, the Cd(II) adsorption plots indicated three consecutive steps during the adsorption process. NI-CLCB showed a slightly faster process than II-CLCB for the first stage corresponding to the boundary layer or external film diffusion. However, the NI-CLCB rate was slower than II-CLCB in the second portion attributed to metal diffusion in adsorbent pores and regions. This observation is supported by the fact that metal ions found it more difficult to access the active sites of NI-CLCB due to crosslinking, as opposed to II-CLCB, which has mesopores on its surface [378]. The adsorption rate started to slow down in the last stage, belonging to diffusion in micropores or chemical equilibration, because of the low concentration of adsorbate concentration in the solution,

and the adsorption reached equilibrium 109. According to the obtained data, it was concluded that chemical sorption controlled the adsorption rate of Cd(II) on NI-CLCB and II-CLCB since the intraparticle diffusion step line (stage 2) did not pass through the origin, which is in agreement with the pseudo-second-order assumptions as of the best fit model to the experimental data [135,380].

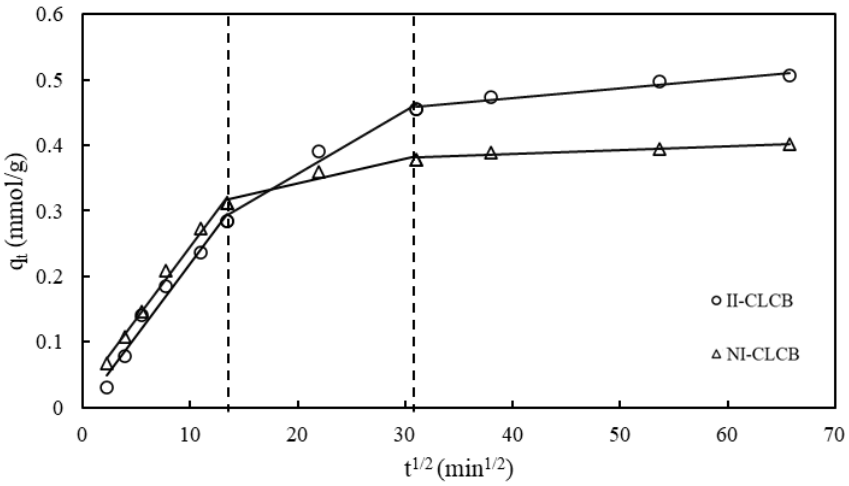

Figure 6-9. Intraparticle diffusion kinetics of the adsorption of Cd(II) on NI-CLCB and II-CLCB

6.4.2.5 Adsorption mechanism

Different mechanisms have been reported in the literature for HMs adsorption on chitosan-based adsorbents, such as chemical interactions (i.e. chelation) and electrostatic interactions (i.e. ion exchange), depending on the surface functional groups and pH of the solution [130,187,381,382]. Normally, the lone pair of electrons on the N and O atoms on chitosan (from amino and hydroxyl groups) can be provided to the metal ions' vacant atomic orbitals to form coordination complexes, subject to the availability of amino and hydroxyl groups [130]. However, the FTIR analysis showed that ionic crosslinking with sodium tripolyphosphate partially consumed chitosan amino and hydroxyl groups, thus not completely available for cadmium(II) binding. On the other hand, Sureshkumar et al. [214], who studied the adsorption of uranium uptake on chitosan crosslinked with sodium tripolyphosphate, reported that phosphate groups of sodium tripolyphosphate contributed to metal ions' adsorption in addition to the remaining amino groups of chitosan, confirmed by Babakhani and Sartaj [269]. According to the obtained results from the isotherm and kinetics studies, it was concluded that chemisorption on the monolayer surface controlled Cd(II) adsorption onto

NI-CLCB and II-CLCB. Also, the thermodynamic studies suggested that electrostatic reaction was dominant. Taking everything into account, it is plausible to suppose that Cd(II) adsorption onto NI-CLCB and II-CLCB occurred on two different binding sites: the remaining amino groups of chitosan and phosphate groups of sodium tripolyphosphate. The former is attributed to chemical reactions, and the latter to ion exchange.

6.4.3 Cd(II) desorption study

Desorption studies are necessary from environmental, economic, and practical points of view to recover metal ions adsorbed on the adsorbent surface and regenerate the adsorbent for future reuse. Hence, different eluents have been adopted in the literature for the desorption of chitosan-based adsorbents saturated with heavy metals, such as acidic eluents [177], chelators [211], and salt regents [309]. Choosing an appropriate desorption agent is critical for chitosan-based adsorbents; the desorption agent should be inexpensive, non-toxic to the environment, and non-destructive to the chitosan, as well as capable of restoring the chitosan's physical and adsorption properties to near-original levels. All things considered, a solution of NaCl (0.2 M) and H_2SO_4 (0.01 M) was used in this study for the desorption of loaded NI-CLCB and II-CLCB. The Cd(II) desorption rates calculated using Eq. (6-2) are tabulated in Table 6-7, showing acceptable results in the order of NI-CLCB > II-CLCB.

Table 6-7. Desorption percentage of Cd(II) ion from NI-CLCB and II-CLCB

Eluent	Desorption%	
	NI-CLCB	II-CLCB
$NaCl+H_2SO_4$	91.2	86.4

6.5 Conclusions

Ion-imprinted and non-imprinted crosslinked chitosan hydrogel beads were synthesized and examined for cadmium adsorption from aqueous solution. The SEM, BET, FTIR, and TGA were applied to characterize the adsorbents and confirm the successfulness of crosslinking and imprinting processes. The cadmium(II) adsorption rate was investigated by changing the initial pH and adsorbent dosage, and their optimum values were determined. Among different isotherm models examined for fitting to the experimental data, Langmuir was found to be more suitable.

This model Cd(II) maximum adsorption capacity onto NI-CLCB and II-CLCB were 0.87 and 1.05 mmol/g, respectively, demonstrating the better removal efficiency of the latter. The thermodynamics study revealed that the Cd(II) adsorption was spontaneous and endothermic. The kinetics assessment showed pseudo-second-order rate equation governed the kinetics adsorption of Cd(II) on both adsorbents, and electrostatic interaction was the dominant adsorption mechanism. The obtained results suggested that the amino and phosphate groups were the main biding sites for Cd(II) uptake. Using a mixture of NaCl and H_2SO_4 was effective for the desorption of loaded adsorbents.

6.6 References

The references are merged with those of the other chapters' references and presented at the end of the thesis.

Chapter 7

Technical Paper 5

7 Competitive adsorption of Cd(II), Ni(II) and Co(II) onto ion-imprinted crosslinked chitosan: characterization and isotherm studies[5]

Keywords: Heavy Metals, Chitosan, Multicomponent, Adsorption, Ion-imprinting, Crosslinking

7.1 Abstract

The purpose of this research was to synthesize a green chitosan-based adsorbent for the selective adsorption of Cd(II) from a multi-solutes phase containing competitive ions of Ni(II) and Co(II). Accordingly, chitosan beads were synthesized and modified in two steps, including crosslinking and ion imprinting, to improve physicochemical properties, adsorption capacity, and selectivity of the adsorbents. The characterization of the prepared bio-adsorbents was performed using XRD and BET, confirming the superior properties of modified chitosan beads. The adsorption efficiency of the synthesized adsorbents was studied in mono- and multi-component batch adsorption systems. The Langmuir isotherm showed the best fit for the mono-component system's experimental data, and the maximum adsorption capacity of ion-imprinted crosslinked chitosan was in the order of Cd(II) (1.06 mmol/g) > Co(II) (0.68 mmol/g) > Ni(II) (0.38 mmol/g). The Extended Langmuir model fitted the experimental results from the multi-component system, indicating that ion-imprinted crosslinked chitosan had a higher total metal uptake (1.33 mmol/g) with better selectivity toward Cd(II) uptake compared to non-imprinted crosslinked chitosan ($\beta > 1.35$). The adsorption mechanism was investigated using SEM-EDS and FT-IR techniques, suggesting that the adsorption was governed by chemical binding and ion exchange mechanisms in the ternary system.

[5] A version of this chapter is submitted for publication

7.2 Introduction

The manufacture of electronic devices, such as cellphones, tablets, laptops, has increased significantly because of technological innovation and market development, leading to the production of several billion units of batteries across the world [383]. Among the different rechargeable batteries, nickel-cadmium batteries (Ni-Cd) offer some advantages over other kinds, such as high efficiency at low temperatures, higher charge-discharge rates, and a long lifespan [197]. However, Ni-Cd batteries contain a significant amount of heavy metals (HM), such as cadmium and nickel, accounting for 12–15 wt.% and 15-20 wt.% of the battery, which are notorious for toxicity [48]. This has resulted in restrictions on using these batteries and replacing them with Nickel-Metal hydride (Ni-MH) and Lithium-ion (Li-ion) batteries in many countries due to their severe impacts on the environment and human health [55]. In recent years, several studies have been undertaken to evaluate the environmental impact of Ni-Cd battery waste disposal [30]. If not properly managed, the scrap nickel-cadmium batteries would end up in landfills, resulting in infiltration into groundwater and soil, and if they enter surface water or accumulate in the soil, they will adversely affect the plants, animals, and human beings [384]. Apart from the environmental concerns, the demand for metals present in Ni-Cd batteries such as nickel and cobalt (accounts for 0.6-1 wt.% of Ni-Cd batteries) is increasing, highlighting the importance of recycling waste batteries and recovering these HMs [385,386]. There are scarce resources that will not be sufficient to meet future demand. Recycling materials can help conserve resources and delay the depletion of virgin natural resources, which is a step toward sustainability.

As a result, several HMs recycling methods have been introduced and developed in the literature, including pyrometallurgical and hydrometallurgical processes, to recover valuable metals from Ni-Cd batteries [387]. Pyrometallurgical procedures, which are the conventional techniques, are expensive and energy-intensive and pollute the environment by releasing fine particles and hazardous chemicals into the air [48,388]. On the other hand, hydrometallurgical processes, which are based on chemical reactions in aqueous solutions at ambient temperature, have gained growing interest due to their higher efficiency, along with economic and environmental benefits [389]. Among common purification/separation techniques implemented in hydrometallurgical, biosorption has attracted increasing attention due to the advantages over the traditional processes such as solvent

extraction and chemical precipitation [43], by offering low operating costs and high efficiency [251,321]. The critical point in biosorption is to choose a bio-adsorbent that is both efficient and cost-effective with an excellent adsorption capacity. In this context, chitosan has received substantial interest because of its biocompatibility and nontoxic nature, as well as good adsorption characteristics owing to the presence of free amino and hydroxyl groups in its structure [101,390]. Additionally, chitosan can be derived from the seafood processing sector wastes, such as shrimp, lobster, and crab shells, which are abundant [11,91]. Thus, converting seafood waste to chitosan and leveraging it as a bio-adsorbent for heavy metals recovery would also contribute to sustainable waste management.

Chitosan application has been restricted due to several problems, such as solubility in dilute acidic solutions, low selectivity for metal ions, and poor physical strength [391]. However, recent studies have demonstrated that these problems can be resolved by crosslinking followed by grafting an active agent onto its structure, resulting in modified chitosan with enhanced physicochemical properties [94,108]. Chemical agents are an essential part of grafting that increases the system's cost and generates secondary pollution, hindering the development of a sustainable metals recovery [392]. Therefore, a cost-effective and clean technique is needed to boost the adsorption capacity of crosslinked chitosan since some of the active sites are occupied during crosslinking. Lately, the ion imprinting technique has been developed and employed by which unique recognition sites are introduced on the crosslinked chitosan surface, resulting in higher adsorption capacity and selectivity to target metal ions [266,393]. Some researchers have studied the effect of the ion imprinting technique on the adsorption efficiency of precious metal ions from aqueous solutions [394,395]. However, most of the research was conducted in a single-component system [396,397], while the presence of other metal ions produces potential effects of synergism, antagonism or non-interaction [162,229], highlighting the need for and the importance of studying modified chitosan in a competitive adsorption system.

The main aim of this research was to attempt to develop a techno-economically feasible and sustainable method to adsorb and separate Cd(II) from Ni(II) and Co(II) from synthetic solution using Cd(II)-imprinted chitosan crosslinked by sodium tripolyphosphate. In the present paper, chitosan, crosslinked chitosan and Cd(II)-imprinted crosslinked chitosan beads were synthesized

and characterized by XRD and BET analysis. Their performance for adsorption was investigated in single and ternary systems of Cd(II), Ni(II), and Co(II) under different initial pHs and metal ions concentrations. Equilibrium isotherms were investigated in the mono- and multi-component system to deduce the adsorption process. Furthermore, the possible adsorption mechanisms in the ternary system were explored through different characterization techniques, including FTIR and SEM-EDS.

7.3 Experimental and methods

7.3.1 Materials

Chitosan with a deacetylation percentage of 85%, sulphuric acid (H_2SO_4, N/50), cadmium sulphate hydrate ($3CdSO_4 \cdot 8H_2O$), nickel sulphate hydrate ($NiSO_4.6H_2O$), and cobalt sulphate hydrate ($CoSO_4.7H_2O$) were purchased from Fisher Scientific Co. (Canada). Sodium tripolyphosphate ($Na_5P_3O_{10}$) and sodium hydroxide (NaOH) were obtained from Sigma Chemical Co. (Canada). Acetic acid (CH_3COOH, 99.9 wt. %) was provided by VWR (Canada). All chemicals were of analytical grade and used directly without further treatment or purification.

7.3.2 Instruments and Analytical Methods

The metal ions concentration was determined using atomic absorption spectroscopy (AAS) (PinAAcle 500, Perkin Elmer, Canada). The following wavelengths were employed: cadmium, 228.8 nm; nickel, 232.2 nm; cobalt, 240.7 nm, and the calibration curves were prepared using standard solutions. pH was monitored by a HACH (HQ40D) Instrument pH Meter. The adsorbents' specific surface area, total pore volume, and pore diameter were evaluated by N_2 adsorption-desorption isotherms at 77 K using an Accelerated Surface Area and Porosimetry Analyzer (ASAP 2020, Micromeritics Co.) and computed by Brunauer–Emmett–Teller (BET) method. The X-ray diffraction (XRD) patterns were recorded using a Rigaku Ultima IV instrument with Cu Kα radiation. The applied voltage and current were 40 kV and 44 mA, respectively, and the angle range scanned was between 10° and 50°. The surface topography of adsorbents before and after adsorption was investigated by Scanning Electron Microscopic (SEM) JEOL JSM-7500F, running at an acceleration voltage of 3.0 kV. Energy Dispersive Spectroscopy (EDS) was conducted by

Oxford EDS INCA 350 spectrometer. The specimens were coated with gold prior to the SEM-EDS analysis to avoid charging. Fourier transform infrared spectroscopy (FTIR) was used to characterize adsorbents before and after adsorptions in the range from 500 to 3750 cm^{-1} using attenuated total reflectance (ATR) sampling method (Thermo Fischer, Nicolet 6700).

7.3.3 Preparation of the adsorbents

Chitosan beads (CB), sodium tripolyphosphate crosslinked chitosan beads (STPP-CB), and ion-imprinted crosslinked chitosan beads (IIP-STPP-CB) with cadmium templates were prepared based on the literature [96,397]. The procedure was as follows. 1.60 g chitosan powder was dissolved into 40 mL of 5% (v/v) acetic acid solution. The chitosan solution was added dropwise into different precipitation baths, including 0.50 M sodium hydroxide solution and 5% w/v sodium tripolyphosphate solution prepared at pH 8.5, which neutralized the acetic acid and thereby coagulated the chitosan gel to spherical chitosan (CB) and crosslinked chitosan beads (STPP-CB), respectively.

To synthesize the cadmium imprinted crosslinked chitosan (IIP-STPP-CB), a weighed amount of cadmium sulphate hydrate was dissolved in 40 mL diluted acetic acid (5% v/v) to give a solution concentration of 12.5 mg/L Cd^{2+}. Then, 1.6 g chitosan was added to the same solution. Later, the solution was transferred dropwise into a flask containing 5% w/v sodium tripolyphosphate solution to form spherical beads having an average diameter of 1 mm. The beads were then separated, rinsed with deionized water, and moved to a solution containing sulfuric acid (0.01 M) and sodium chloride (0.2 M) for three days at 45±2°C to remove the template Cd^{2+}. To regenerate the binding sites of the beads, they were rinsed with sodium hydroxide (0.5 M) followed by deionized water.

7.3.4 Batch adsorption experiment

Adsorption experiments were carried out in 125 mL Erlenmeyer flasks containing 50 mL of metal ion(s) solution at room temperature. Metal sulphates were employed to prepare stock solutions of the individual metals (Cd(II), Ni(II), Co(II)) and their ternary system (Cd(II)/Ni(II)/Co(II)). A weighed amount of dried adsorbent (0.65 g/L) was placed into each solution, shaking with the oscillation frequency of 225 rpm. The solutions were then filtered after

48h, and AAS was used to determine the equilibrium concentration of metal ions, and the solid phase concentration, q_e (mmol/g), was calculated as follows:

$$q_e = \frac{(C_0 - C_e)\,V}{W} \qquad 7\text{-}1$$

where C_0 (mmol/L) and C_e (mmol/L) are the initial and the equilibrium concentrations of adsorbate in the solution, V (L) is the solution volume, and W (g) represents the weight of the dry adsorbent. Each test also included two blank solutions containing no adsorbent as a control. Each test was conducted in triplicate, and the average was used unless otherwise stated.

7.3.4.1 Effect of pH in single-component solution systems

The initial solutions' pH was changed from 4.0 to 7.5 ± 0.2 using 0.1M sodium hydroxide or sulfuric acid solutions to evaluate the effect of the initial pH on the adsorption uptake of metal ions in the unary system with the concentration of 50 mg/L. After reaching equilibrium (48h), the solutions were filtered and analyzed, and Eq. (7-1) was used to determine the solid phase concentration.

7.3.4.2 Single-component and multi-component isotherm studies

In the mono-component system (Cd(II), Ni(II), Co(II)), the initial concentration of metal ions was changed from 0.089 to 8.89 mmol/L, and equimolar solutions of Cd(II)/Ni(II)/Co(II) were employed in the same concentration range in the ternary system. The pH of the solutions was adjusted to 6.5 using 0.1M sodium hydroxide/sulfuric acid. After 48h, the solutions were filtered, and the solid phase concentration was calculated using Eq. (1). Different isotherm models were employed to fit the experimental data, including Langmuir and Freundlich for the single-component system and extended Langmuir and Sheindrof-Rebhun-Sheintuch for the ternary system.

7.4 Results and discussion

7.4.1 Characterization of CB, STPP-CB, and IIP-STPPCB

The X-ray diffraction patterns of chitosan and sodium tripolyphosphate powders, STPP-CB and IIP-STPP-CB, are shown in Figure 7-1. Chitosan powder (Fig.7-1(a)) exhibited a semi-crystalline nature because of diffraction at $2\theta \approx 20°$, which was also reported in the literature [398,399]. Sodium tripolyphosphate powder (Fig.7-1(b)) showed multiple sharp peaks between 10 and 50° diffraction angles, indicating its crystalline structure [400]. The chitosan characteristic peak at $2\theta \approx 20°$ was weakened significantly after crosslinking CB by sodium tripolyphosphate, as shown in Fig.7-1(c) (STPP-CB). The broadened characteristic peak of chitosan detected in the STPP-CB pattern can be attributed to the rupture of hydrogen bonds of the polysaccharide chains and the presence of interpenetrating phosphoric ions after treatment by sodium tripolyphosphate [393,398]. As seen in Fig.7-1(c), a sharp peak was observed in the XRD spectra of STPP-CB at $2\theta \approx 45°$, which was detected in the diffraction pattern of sodium tripolyphosphate powder (Fig.7-1(b)), suggesting the successful completion of crosslinking. Different diffraction patterns of STPP-CB and chitosan powder demonstrated that the arrangement of molecules within the crystal lattice changed after crosslinking [400]. The X-ray diffraction patterns of IIP-STPP-CB (Fig.7-1(d)) showed two peaks at $2\theta \approx 20°$ and 45°, inherited from chitosan and sodium tripolyphosphate powder, respectively. The detected chitosan characteristic peak in IIP-STPP-CB spectra indicated that the imprinting technique successfully protected the chitosan structure during the crosslinking process.

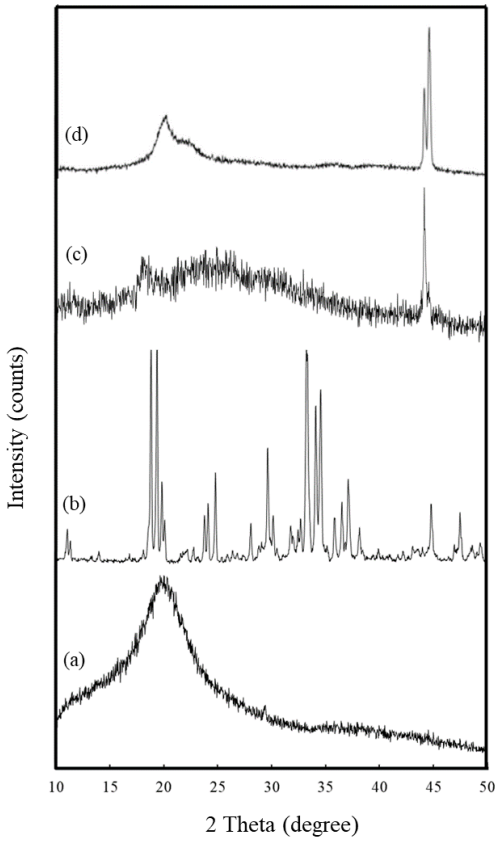

Figure 7-1. XRD patterns of (a)chitosan powder, (b) sodium tripolyphosphate powder, (c)STPP-CB, and (d)IIP-STPP-CB

BET technique was employed to evaluate the surface area and the total pore volume of the sorbent materials, and the results are indicated in Table 7-1. According to the table, crosslinking chitosan reduced CB's BET surface area and total pore volume by 14% and 11%, respectively, which could be attributed to chitosan amino groups' occupation by the crosslinking reagent, sodium tripolyphosphate [220]. However, the BET surface area and total pore volume increased by 11% after ion-imprinting the crosslinked chitosan beads. The extraction of Cd(II) ions from the polymer matrix and the presence of new sites after the ion-imprinting process can explain this improvement [401].

Table 7-1. BET surface area and total pore volume of CB, STPP-CB, and IIP-STPP-CB

	BET surface area (m^2/g)	Total pore volume (cm^3/g)
CB	6.50	4.07×10^{-3}
STPP-CB	5.60	3.63×10^{-3}
IIP-STPP-CB	6.20	4.04×10^{-3}

7.4.2 Effect of pH in single metal solutions

The binding of metal ions to functional groups on the adsorbent surface is substantially pH-dependent because the solution's initial pH influences both the protonation of adsorbent functional groups and the speciation of heavy metal ions [222]. The effect of pH on the sorption of Cd(II), Ni(II), and Co(II) on CB and STPP-CB in a mono-component system is shown in Figure 7-2. The high concentration of hydrogen ions competing with metal ions at low pH values prevented the metal ions from approaching the adsorbents' binding sites [366]. As a result, the sorbed amounts of all metal ions were low at acidic pHs. The improvement in metal ions uptake at higher pHs can be explained by a decrease in positive surface charge on the adsorbents, resulting in less electrostatic repulsion between the surface and the metal ions, thus increasing metal ions adsorption [96,402]. However, the solubility of the metals decreases by increasing pH, leading to the precipitation of metals as hydroxides [96]. Therefore, pHs above 7.5 were not investigated to avoid metal ions precipitation, and pH = 6.5 was selected for the experiments in the following sections.

Since heavy metals adsorption primarily takes place on chitosan functional groups, including amino and hydroxyl groups, a decrease in the metal ions uptake was expected after chitosan crosslinking due to a decrease in the density of functional groups [226]. As shown in Fig.7-2(a) and (b), the adsorption capacity of Cd(II) and Ni(II) on STPP-CB was lower than CB, which can be attributed to the occupation of amino groups as the main binding sites by the crosslinker and lower BET surface area of crosslinked chitosan beads. However, Fig.7-2(c) shows Co(II) uptake increased after chitosan crosslinking by sodium tripolyphosphate, which can be ascribed to the participation of the phosphate groups on STPP-CB surface in Co(II) adsorption, which was confirmed later by FTIR.

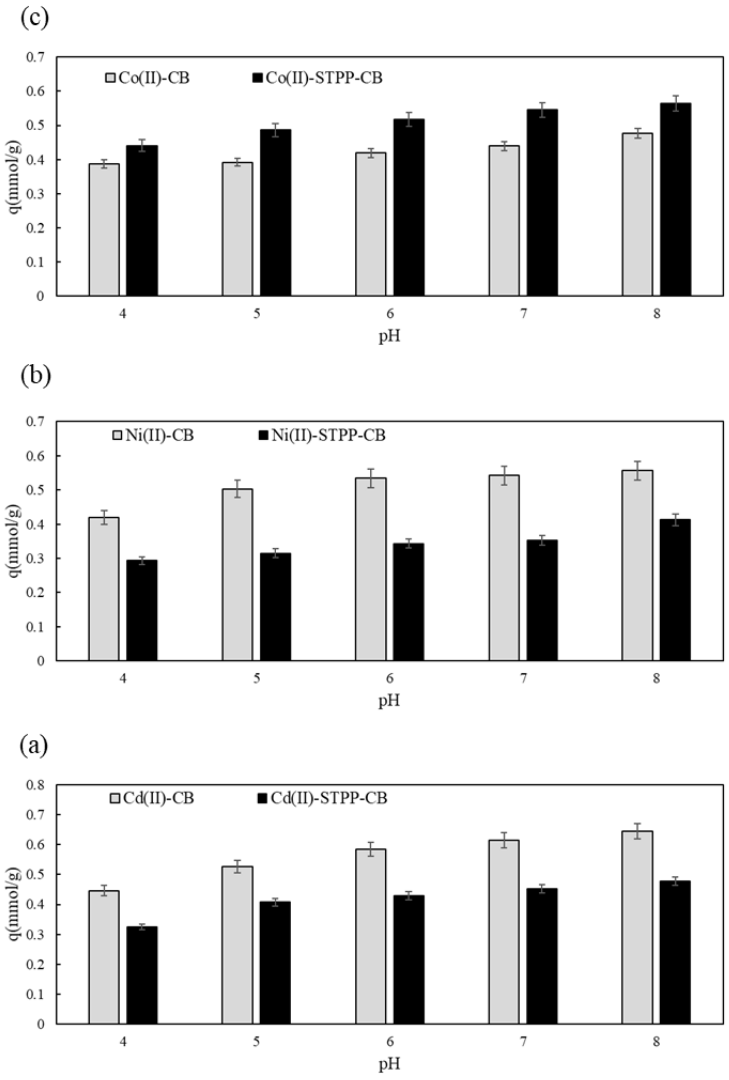

Figure 7-2. Effect of pH on the adsorption of (a)Cd (II), (b)Ni(II), and (c)Co(II) onto CB and STPP-CB with dosage 0.65 g/L at room temperature and metal concentration of 50 mg/L

7.4.3 Adsorption isotherm studies

7.4.3.1 Single metal solutions

The adsorption capacity of CB, STPP-CB, and IIP-STPP-CB was investigated for Cd(II), Ni(II), and Co(II) uptake by changing their initial concentration from 0.089 to 8.89 mmol/L in the mono-component system. The results indicated an increase in metal ions adsorption by increasing the metal ions concentrations because of high ion intensity and a large concentration gradient [272]. Langmuir and Freundlich isotherm models were employed in this study to describe the

experimental data of the metal ions' adsorption. A linear form of the Langmuir isotherm is given by Eq. (7-2) as follows [157]:

$$\frac{C_e}{q_e} = \frac{1}{q_m K_L} + \frac{C_e}{q_m} \qquad 7\text{-}2$$

where q_e (mmol/g) and C_e (mmol/L) are equilibrium solid-phase and liquid-phase concentrations in the bulk solution. K_L (g/mmol) is the Langmuir constant related to adsorption energy, and q_m (mmol/g) is the maximum adsorption capacity for monolayer formation on the adsorbent. The isotherm constants, including q_m and K_L, can be calculated from the slope and the intercept of the plot between $1/q_e$ and $1/C_e$. The K_L parameter is proportional to the sorbent–sorbate affinity; a higher K_L value more favourable adsorption [403].

The Freundlich isotherm is generated by assuming a heterogeneous surface with a non-uniform heat of adsorption distribution [404]. The linear form of the Freundlich isotherm can be expressed by Eq. (7-3) as follows [404]:

$$\log q_e = \log K_f + \frac{1}{n} \log C_e \qquad 7\text{-}3$$

where K_F ((mmol/g).(L/mmol)$^{(1/n)}$) is adsorption capacity at unit concentration, and 1/n is an empirical constant related to the heterogeneity of the adsorbent surface. The isotherm constants K_F and 1/n can be obtained from the slope and the intercept of the plot log q_e versus log C_e.

As listed in Table 7-2, the Langmuir isotherm model matched better with the experimental data of CB, STPP-CB and IIP-STPP-CB rather than the Freundlich because the former's coefficient of determination (R^2) was greater than the latter for all adsorbents and metals. Thus, the Langmuir assumptions could be dominant in the mono-component system; all the adsorption sites had a similar adsorption affinity, and the adsorption at one site had no effect on adsorption at an adjacent site [403].

Table 7-2. Langmuir and Freundlich isotherms constants for the adsorption of Cd(II), Ni(II), Co(II) onto CB, STPP-CB, IIP-STPP-CB in the unary system with dosage 0.65 g/L

		The Langmuir isotherm constants			The Freundlich isotherm constants		
		K_L (g/mmol)	q_m (mmol/g)	R^2	K_F ((mmol/g).(L/mmol)$^{(1/n)}$)	1/n	R^2
Cd(II)	CB	11.08	1.17	0.99	0.88	0.28	0.84
	STPP-CB	7.15	0.86	0.99	0.59	0.33	0.81
	IIP-STPP-CB	9.53	1.06	0.99	0.78	0.29	0.82
Ni(II)	CB	3.55	0.90	0.99	0.54	0.33	0.95
	STPP-CB	3.39	0.44	0.99	0.26	0.36	0.85
	IIP-STPP-CB	1.86	0.38	0.99	0.19	0.40	0.87
Co(II)	CB	2.95	0.61	0.99	0.36	0.31	0.96
	STPP-CB	5.22	0.73	0.99	0.48	0.30	0.91
	IIP-STPP-CB	3.58	0.68	0.99	0.42	0.30	0.92

As seen, the Langmuir isotherm constants (q_m and K_L) of CB followed the order of Cd(II) > Ni(II) > Co(II), whereas it changed to Cd(II) > Co(II) > Ni(II) after chitosan crosslinking (STPP-CB) and ion-imprinting (IIP-STPP-CB). Hence, it could be concluded that all of the adsorbents had a greater affinity for Cd(II) than for Ni(II) or Co(II). Figure 7-3 (a) and (b) illustrate the Langmuir isotherms of Cd(II), Ni(II) and Co(II) adsorption on STPP-CB and IIP-STPP-CB. As shown, q_m of STPP-CB for Cd(II) uptake was 43% and 15% higher than those for Ni(II) and Co(II), respectively, and this difference increased to 64% and 36% after ion imprinting, suggesting that ion imprinting and using Cd^{2+} as template effectively enhanced the adsorption capacity of crosslinked chitosan for Cd(II) uptake.

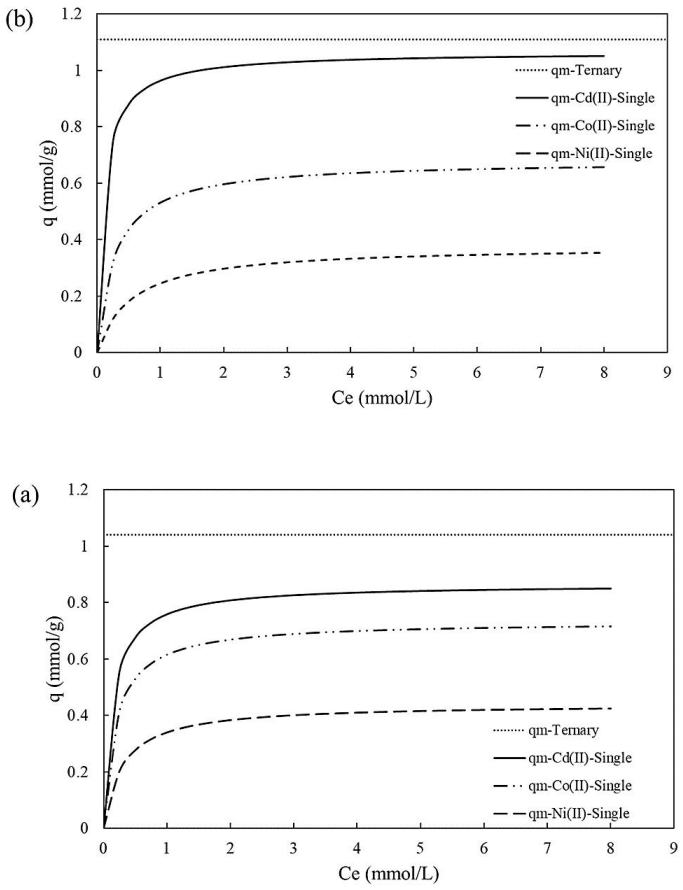

Figure 7-3. Langmuir isotherm models of Cd(II), Ni(II), Co(II) adsorption in mono-component systems and the total metal ions uptake in the ternary system on (a)STPP-CB and (b)IIP-STPP-CB

The q_m and K_L values of CB for Ni(II) adsorption (Table 7-2) dropped by 51% and 4% following crosslinking chitosan by sodium tripolyphosphate. However, Co(II) witnessed an opposite trend, and the Langmuir model parameters (q_m and K_L) enhanced by 20% and 77% after the crosslinking reaction. This observation implied the participation of the phosphate groups of sodium tripolyphosphate in addition to the amino groups of chitosan in Co(II) adsorption on STPP-CB. Comparing the Cd(II) parameters of the Langmuir model revealed that CB had the greatest q_m and K_L values, 1.17 mmol/g and 11.08 g/mmol, respectively, which decreased by 26% and 35% after crosslinking chitosan beads by sodium tripolyphosphate, at the expense of increasing the physiochemical properties of chitosan. However, the maximum adsorption capacity (q_m) and the adsorbent affinity (K_L) of crosslinked chitosan beads improved after ion-imprinting, reaching 1.06

mmol/g and 9.53 g/mmol. This examination suggested that the ion-imprinting technique could effectively protect some functional groups of chitosan during the crosslinking reaction and provide recognition sites on the IIP-STPP-CB surface for Cd(II) uptake [214]. The maximum adsorption capacity of some adsorbents for Cd(II) uptake is listed in Table 7-3. Comparing the adsorption capacity of II-STPP-CB to that of other adsorbents in the literature revealed that it is within the range of the others and is comparable to them.

Table 7-3. Adsorption capacity of Cd(II) onto different adsorbents

Adsorbent	pH	Adsorption Capacity (mmol/g)	Reference
Polyacrylic acid-based hydrogel	6	1.8	[405]
Polyampholyte hydrogel	6	1.4	[406]
Graphene oxide	6	1.2	[407]
Surfactant-modified chitosan using sodium dodecyl sulphate	6.5-7	1.11	[371]
β-cyclodextrin-based hydrogel	5	0.88	[408]
Orange peel	7	0.53	[409]
Cd(II)-imprinted chitosan crosslinked by sodium tripolyphosphate	6.5	1.06	This Study

7.4.3.2 Ternary metal solutions

Adsorption is more complicated in a multicomponent system because of ion-ion competition and ion-surface interactions, leading to a different capacity for the adsorbates compared to the mono-component system [187]. Some studies have employed the original Langmuir and Freundlich isotherm equations for a ternary system to investigate the impact of co-existing metal ions on the isotherm constants [410,411]. However, this approach fails to consider the system's non-ideality, resulting from metal ion-metal ion and metal ion-surface interactions [412]. Therefore, in the present study, the extended Langmuir model (EL) and Sheindorf–Rebuhn–Sheintuch model (SRS) were applied to describe adsorption in a multi-solute system. The extended Langmuir equation is given by Eq. (7-4) [169].

$$q_{e,i} = \frac{q_m K_{L,i} C_{e,i}}{1 + \sum_{j=1}^{N} K_{L,j} C_{e,j}} \qquad 7\text{-}4$$

where $q_{e,i}$ (mmol/g) is the equilibrium concentration of solid phase of component i. $C_{e,i}$ (mmol/L) indicates the equilibrium concentration of liquid phase of component i. q_m (the total metal ions uptake, mmol/g) and K_L (g/mmol) are the multi-component Langmuir parameters of component i.

SRS equation is a multi-component Freundlich type equation, based on the assumption of exponential distribution of adsorption energies available for each solute, and a general form of SRS equation is given by Eq. (7-5) [404]:

$$q_{e,i} = K_{F,i} C_{e,i} \left(\sum_{j=1}^{N} \left(a_{ij} C_{e,j} \right)^{\left(\frac{1}{n_i} - 1 \right)} \right) \qquad 7\text{-}5$$

where $q_{e,i}$ (mmol/g) and $C_{e,i}$ (mmol/L) are the equilibrium concentration of the solid phase and liquid phase of component i. $K_{F,i}$ and 1/n are the mono-component Freundlich constants for solute i. a_{ij} is the competitive coefficient in the multi-component system, which must be determined experimentally. The nonlinear optimization was adopted to minimize Marquardt's Percent Standard Deviation (MPSD) error between the experimental data and the modelled isotherms using the "Solver add-in" of Microsoft Office Excel to estimate the models fitting parameters [413]. MPSD equation is given as follows (Eq. (7-6)):

$$\text{MPSD} = \sum_{i=1}^{n} \left(\frac{q_{i,exp} - q_{i,cal}}{q_{i,exp}} \right)^2 \qquad 7\text{-}6$$

In the above equation, q_i (mmol/g) is the equilibrium solid-phase concentration of component i; the subscript "exp" and "calc" show the experimental and calculated values of q, and n is the number of the components in the system.

Table 7-4. Extended Langmuir and Sheindorf–Rebuhn–Sheintuch model parameters in the ternary system of Cd(II), Ni(II), Co(II))

		CB			STPP-CB			IIP-STPP-CB		
	q_m (mmol/g)	1.33			1.04			1.11		
EL parameters		Cd(II)			Ni(II)			Co(II)		
		CB	STPP-CB	IIP-STPP-CB	CB	STPP-CB	IIP-STPP-CB	CB	STPP-CB	IIP-STPP-CB
	$K_{L,i}$ (g/mmol)	1.48	1.32	1.45	0.79	0.46	0.31	0.52	0.92	0.67
	R^2	0.95	0.96	0.90	0.95	0.96	0.98	0.96	0.99	0.97
	Model MPSD	0.28	0.21	0.48	0.28	0.21	0.48	0.28	0.21	0.48
SRS parameters	K_F ((mmol/g).(L/mmol)$^{(1/n)}$)	0.88	0.59	0.78	0.54	0.26	0.19	0.36	0.48	0.42
	1/n	0.28	0.33	0.30	0.33	0.36	0.40	0.31	0.30	0.30
	a_{ij}	0.14	2.36	2.05	0.77	3.61	0.99	3.26	0.71	0.13
	a_{ik}	2.87	0.14	0.40	2.19	0.59	3.70	0.47	2.00	2.56
	R^2	0.76	0.77	0.69	0.93	0.93	0.85	0.91	0.89	0.94
	Model MPSD	1.67	1.52	2.05	1.67	1.52	2.05	1.67	1.52	2.05

The comparison of the experimental and calculated q_e values of Cd(II), Ni(II), and Co(II) in the ternary system are shown in the parity plots Figure 7-4(a), Figure 7-4(b), and Figure 7-4(c). If the model matches the experimental data better, the data points were closer to the bisecting line. Considering this, the figures suggest that the EL model was in good agreement with the experimental data. The EL and SRS isotherm constants for Cd(II)-Ni(II)-Co(II) system, as well as MPSD and R^2, were computed and listed in Table 7-4. As indicated, the EL model with four parameters fitted the Cd(II), Ni(II), and Co(II) data better than SRS with twelve parameters because of having a higher coefficient of determination ($0.99 > R^2 > 0.90$ vs. $0.94 > R^2 > 0.69$) and lower MPSD value (<0.48 vs. <2.05), confirming the superiority of EL model. All EL parameters (q_m, $K_{L,Cd}$, $K_{L,Ni}$, $K_{L,Co}$) were calculated by fitting multi-component adsorption equilibrium data, and no data were incorporated from the single-metal Langmuir isotherm. However, only half of the SRS model parameters were estimated using multi-component adsorption equilibrium data ($a_{Cd/Ni}$, $a_{Cd/Co}$, $a_{Ni/Cd}$, $a_{Ni/Co}$, $a_{Co/Ni}$, $a_{Co/Cd}$), and the rest was obtained

from the single-metal Freundlich isotherm ($K_{F,Cd}$, $K_{F,Ni}$, $K_{F,Co}$, $1/n_{Cd}$, $1/n_{Ni}$, $1/n_{Co}$), which might be the reason for deviation of this model from the experimental data [318].

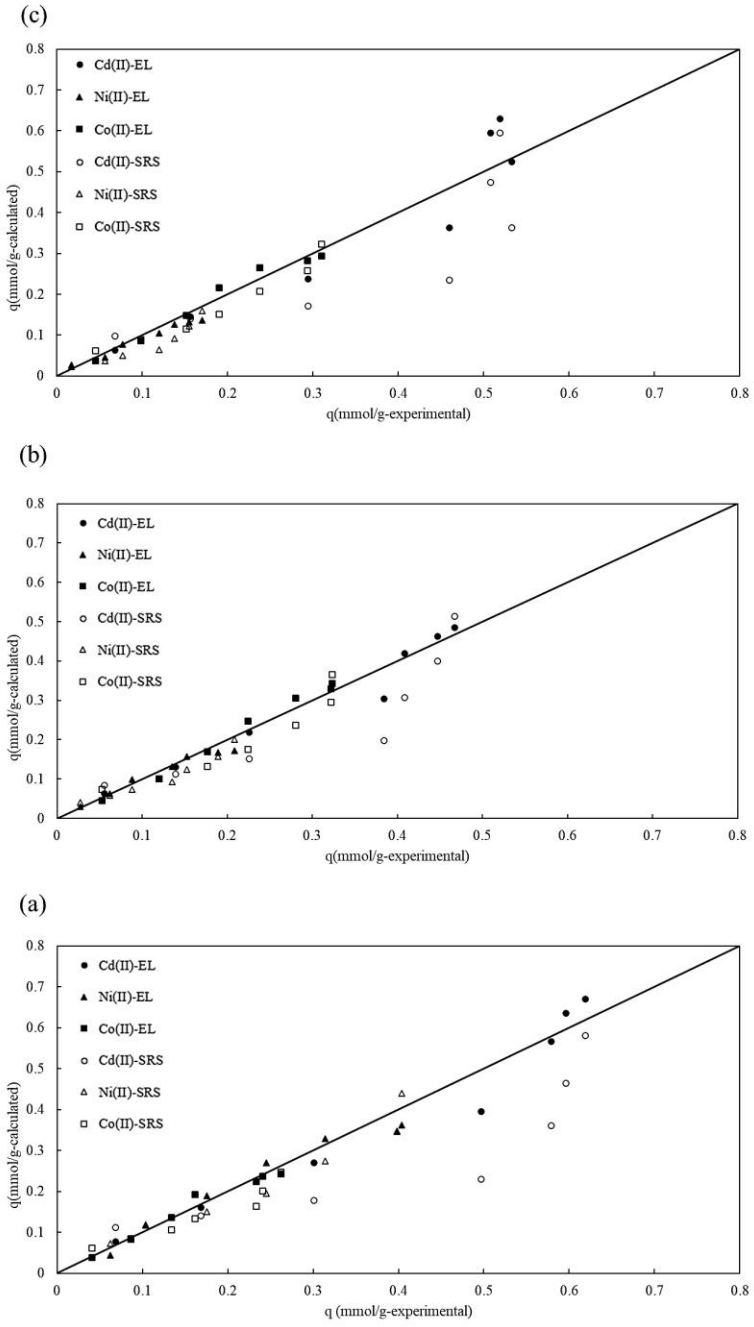

Figure 7-4. Comparison of the experimental and calculated qe values of Cd(II), Ni(II), and Co(II) ions in the ternary system on (a)CB, (b)STPP-CB, (c)IIP-STPP-CB

As presented in Table 7-4, the total metal ions uptake (q_m) onto CB, STPP-CB and IIP-STPP-CB in the ternary system were estimated by EL as 1.33, 1.04 and 1.11 mmol/g. It is worth noting that the estimated q_m values by the EL model were noticeably lower than the sum of the maximum adsorption capacities of Cd(II), Ni(II), and Co(II) ions obtained from the mono-component system on CB (2.69 mmol/g), STPP-CB (2.04 mmol/g), and IIP-STPP-CB (2.12 mmol/g), which can be explained by the competition of Cd(II), Ni(II), and Co(II) over the adsorption sites in the multi-component system [313]. Figure 7-3(a) and (b) show the total metal ions uptake determined by EL onto STPP-CB and IIP-STPP-CB in the ternary system along with the Langmuir isotherm models obtained from the single-component systems of Cd(II), Ni(II) and Co(II). As seen, the total metal ions uptake (q_m) obtained from the EL model in the multi-component system was higher than the maximum adsorption capacity of each metal in the single-component solutions, which can be attributed to the large concentration gradient and driving force in the ternary system solution compared to the mono-component systems. The figure also shows that the synthesis of ion-imprinted adsorbent resulted in an adsorbent (IIP-STPP-CB) with greater adsorption capacity than conventional non-imprinted crosslinked chitosan (STPP-CB) because of the higher total metal ions uptake of the former.

7.4.3.2.1 Selectivity Studies

Qu et al. [414] reported that the order of adsorption affinity of an adsorbent for different metal ions is related to the ionic radii of the metal ions. Theoretically, higher ionic radii lead to a higher affinity of the metal ions and thus higher adsorption capacity. Smaller metal ions have greater hydration enthalpies, making their separation from water molecules more difficult. As a result, they are less likely to interact with adsorbents [415]. The literature also shows that other factors such as electronegativity, stability constant, and atomic weight could affect the adsorption behaviour [412]. Overall, the order of K_L values obtained from EL in this study was identified as Cd(II)>Ni(II)>Co(II) for their uptake by CB and Cd(II)>Co(II)>Ni(II) for their adsorption on STPP-CB and IIP-STPP-CB, which were in the same order as for the mono-component system. They can be correlated to their ionic radii in the order of Cd(II) (0.95 A°), Co(II) (0.74 A°), and Ni(II) (0.71 A°) [416]. Given the close ionic radius of Co(II) and Ni(II), their adsorption uptake may vary depending on the adsorbent used.

In this research, the relative selectivity coefficient was used to evaluate the efficiency of IIP-STPP-CB compared to STPP-CB for Cd(II) uptake in the ternary system. Distribution (D), selectivity (β), and relative selectivity coefficients (β_r) were calculated by Eq. (7-7), (7-8), and (7-9) [396]:

$$D_i = \frac{(C_{0.i} - C_{e,i})}{C_{e,i}} \times \frac{V}{W} \qquad 7\text{-}7$$

$$\beta_{i/j} = \frac{D_i}{D_j} \qquad 7\text{-}8$$

$$\beta_r = \frac{\beta_{imprinted}}{\beta_{non-imprinted}} \qquad 7\text{-}9$$

where C_0 (mmol/L) and C_e (mmol/L) are the initial and the equilibrium concentrations of adsorbate in the solution, V (L) is the solution volume, and W (g) denotes the mass of the dry adsorbent.

For this purpose, batch adsorption tests were conducted at different ratios of Cd(II):Ni(II):Co(II) in which each metal ion's concentration was 0.44 mmol/L in a 1:1:1 ratio. The selectivity coefficients were computed using Eq. (7-9), and the results are listed in Table 7-5. It can be seen that in the presence of Co(II) and Ni(II), the values of the relative selectivity coefficient of Cd(II) fluctuated between 1.35 and 2.04, indicating that IIP-STPP-CB had a higher adsorption uptake and a better selectivity for Cd(II) uptake in comparison with STPP-CB in a competitive adsorption system. In fact, the imprinting technique formed some cavities and specific binding sites for Cd(II) ions. As a result, more Cd(II) ions were sorbed on IIP-STPP-CB in the ternary system, leading to its higher adsorption capacity and better selectivity toward Cd(II).

Table 7-5. Relative selectivity coefficients for Cd(II) uptake in the ternary system of Cd(II)-Ni(II)-Co(II)

	Cd(II):Ni(II):Co(II)					
	2:1:1	1:2:1	1:1:2	2:2:1	2:1:2	1:2:2
β_r (Cd(II)-Ni(II))	1.90	1.51	1.57	1.51	1.96	1.35
β_r (Cd(II)-Co(II))	2.04	1.71	1.37	1.88	1.62	1.38

7.4.4 Adsorption mechanism

Different mechanisms have been suggested in the literature for heavy metal ions adsorption on chitosan derivatives [153,381]. In general, metal adsorption on chitosan derivatives is thought to happen by a combination of single or mixed interactions, including chemical bonding (i.e. complexation and chelation), electrostatic attraction or ion exchange, and ion pair formation, depending on the metal ions, their chemistry, the pH of the solution, and the chemical and physical properties of the adsorbent [98,417]. However, some researchers have suggested that the adsorption mechanism of heavy metal cations onto chitosan derivatives is mainly governed by chemical bonding [366]. The O and N of the respective hydroxyl and amino groups present in the chitosan tend to donate lone pair of electrons to a metal ion to fill the empty atomic orbital of M^{2+}. As a result, the chitosan–metal complex forms on the surface of the adsorbent [418]. The possible mechanism of adsorption in this study was investigated by evidence from Scanning Electron Microscopy Coupled With Energy-Dispersive X-ray Spectroscopy (SEM-EDS) and Fourier Transform Infrared Spectroscopy (FTIR) [200].

Figure 7-5 shows the SEM-EDS analysis of CB after adsorption of (a)Cd(II), (b)Ni(II), and (c)Co(II) in a single metal system. The EDS spectra verified the presence of carbon and oxygen originated from CB structure, and the Au peaks seen in the spectra were because of the sample coating. The EDS data showed the presence of Cd(II), Ni(II), and Co(II) signals, and the intensity of each signal is correlated to the number of atoms of a given element interacting with the electron beam, which were in the order of Cd(II) > Ni(II) > Co(II). This observation can be explained by CB's affinity for each metal ion, which supported the isotherm study results in the single-solute system, indicating the order Cd(II) > Ni(II) > Co(II).

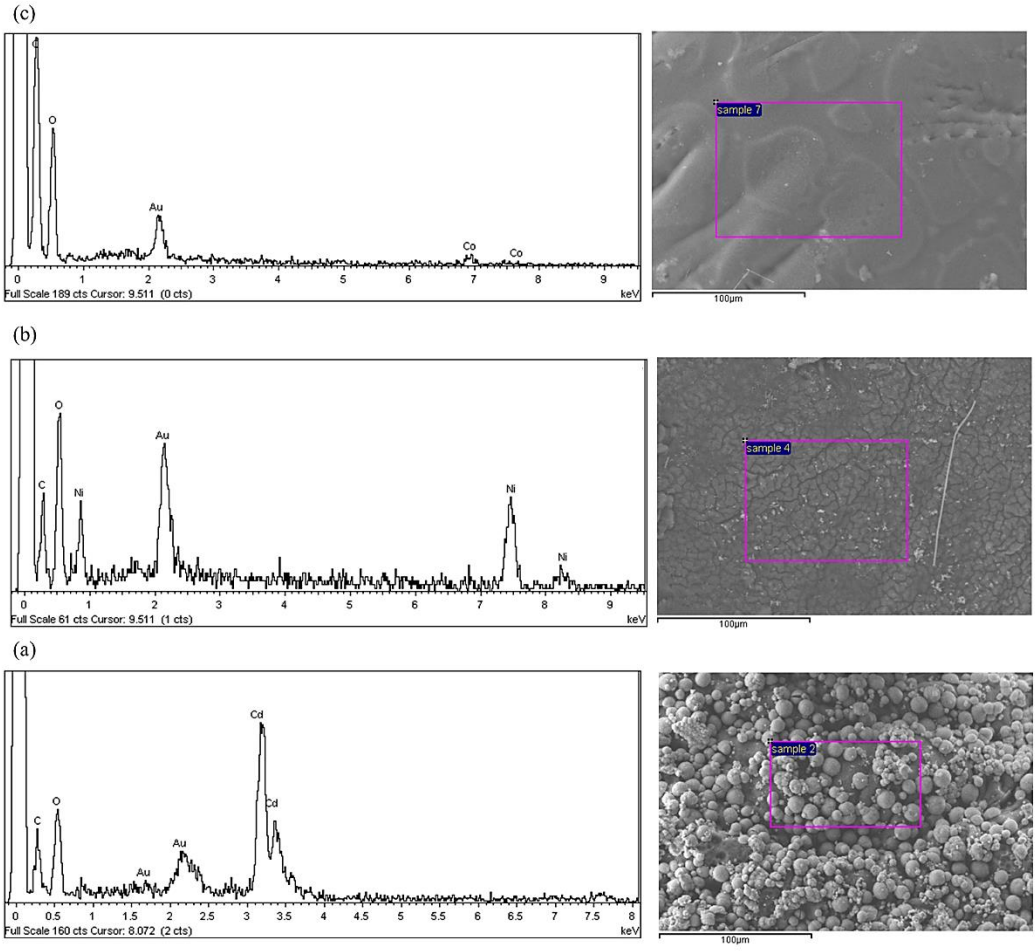

Figure 7-5. SEM-EDS element distribution images of CB after adsorption of (a)Cd(II), (b)Ni(II), and Co(II) in the monocomponent system

SEM-EDS analysis of IIP-STPP-CB after adsorption in the ternary system is shown in Figure 7-6. The presence of P signal on IIP-STPP-CB confirmed the occurrence of crosslinking by sodium tripolyphosphate. As seen, Cd(II) and Ni(II) peaks intensity was relatively lower in the EDS spectra of IIP-STPP-CB compared to CB, implying the competition in the system and better adsorption efficiency of CB for their uptake because of a higher number of amino groups accessible on its surface. In contrast, the intensity of Co(II) signals was somewhat greater in the EDS spectrum of IIP-STPP-CB in comparison with CB, which is consistent with the isotherm study findings, indicating that chitosan crosslinked with sodium tripolyphosphate had a better affinity to Co(II), and phosphate groups might contribute to Co(II) adsorption [419].

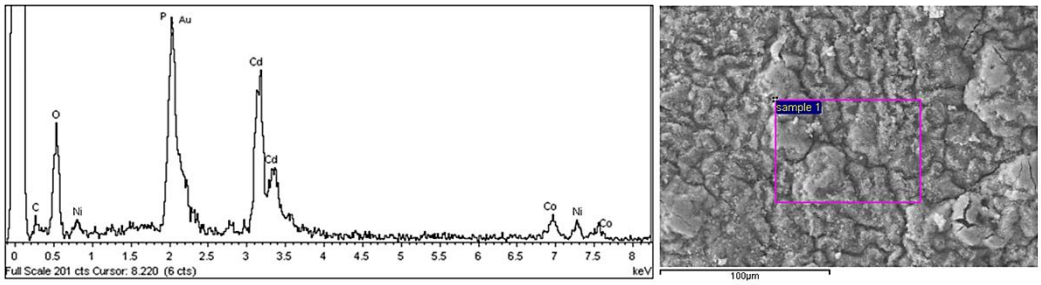

Figure 7-6. SEM-EDS element distribution image of IIP-STPP-CB after adsorption in the ternary system

The FTIR spectroscopy can provide valuable information about the active sites on the adsorbent surface engaged in the adsorption of metal ions in a multi-component system. FTIR spectra of CB, STPP-CB and IIP-STPP-CB before adsorption, as well as IIP-STPP-CB after adsorption in the ternary system, were recorded and shown in Figure 7-7. The peaks identified on CB at ~2975 and 1525 cm^{-1} (Fig7-7.(a)) were attributed to the asymmetric and symmetric stretching vibrations of C-H and bending vibration of N−H; these peaks vanished in the spectra of STPP-CB (Fig.7-7(b)). Two additional peaks appeared on the spectra of chitosan after crosslinking by sodium tripolyphosphate at ~775 and ~1050 cm^{-1} ascribed to the stretching vibration of P-O, confirming the presence of phosphate group in the structure STPP-CB [359]. This observation implied the interaction between phosphoric and ammonium and the consumption of chitosan amino groups as the main binding sites by the crosslinker in ionic crosslinking, which can explain the lower adsorption efficiency STPP-CB toward Cd(II) and Ni(II) compared to CB. CB and IIP-STPP-CB spectra were found to be almost identical with a few minor changes, shown in Fig.7-7(a) and (c), interpreting that the fabrication of ion-imprinted crosslinked chitosan successfully protected some of the functional groups of chitosan. As seen, the amine peak was shifted from 1525 cm^{-1} in CB to ~1500 cm^{-1} in the IIP-STPP-CB spectra because of N-H deformation as a result of the ionic crosslinking reaction. The simultaneous presence of the stretching vibration of P-O and the bending vibration of N-H characteristic peaks at ~900/1050 and 1500 cm^{-1} in the spectrum of IIP-STPP-CB confirmed the occurrence of partial crosslinking as well as protection of amino groups due to the imprinting technique [226].

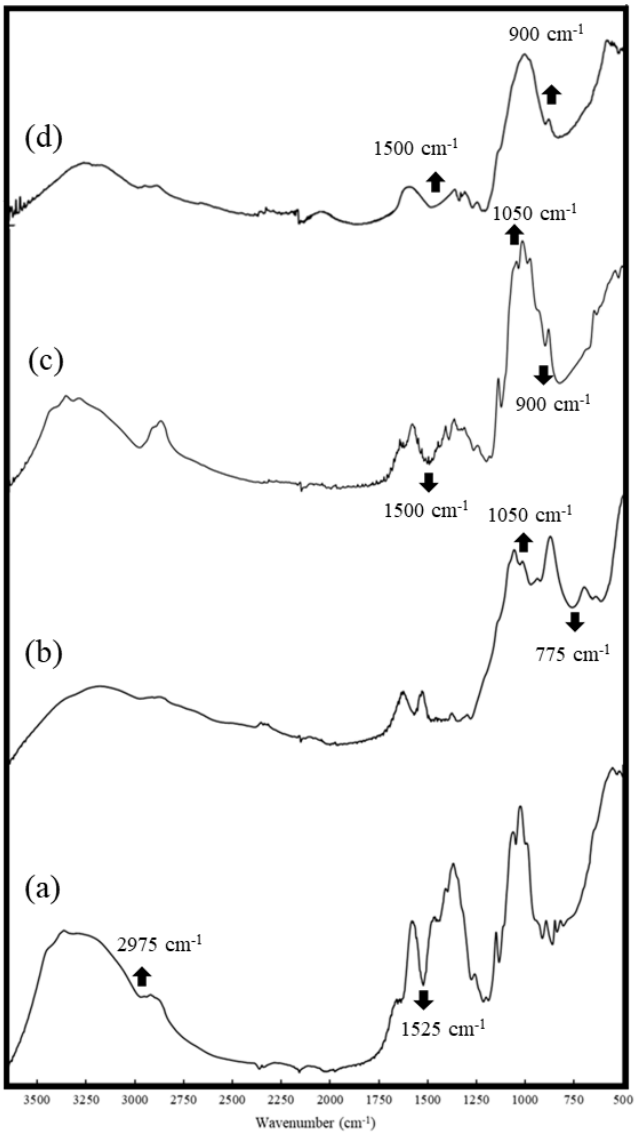

Figure 7-7. FTIR spectra of (a)CB, (b)STPP-CB, and (c)IIP-STPP-CB before adsorption and (d)IIP-STPP-CB after adsorption in the ternary system

A comparison between loaded and unloaded FTIR spectra of IIP-STPP-CB (Fig.7-7(C) and (d)) can reveal valuable information regarding the mechanism of adsorption in the ternary system. Unloaded IIP-STPP-CB spectra showed a peak at ~900 cm^{-1} corresponding to P-O stretching vibration, which was shifted and weakened after the adsorption of metal ions in the ternary system, suggesting that phosphate groups were involved in the adsorption process. Moreover, loaded IIP-STPP-CB spectra showed a weaker peak at 1500 cm^{-1} attributed to N−H vibration than unloaded

IIP-STPP-CB spectra, implying that the nitrogen atoms were affected during the adsorption. With respect to the results from the previous sections, it was assumed that phosphate groups participated in Co(II) adsorption because of the higher adsorption efficiency of STPP-CB compared to CB. On the other hand, amine groups were the primary sites for Cd(II) and Ni(II) adsorption considering the lower adsorption capacity of chitosan after crosslinking. These findings suggest that two mechanisms governed the adsorption of metal ions on IIP-STPP-CB in the ternary system: chemical binding and ion exchange, happening on two different binding sites, including the residual amino groups and phosphate groups, respectively, shown in Figure 7-8.

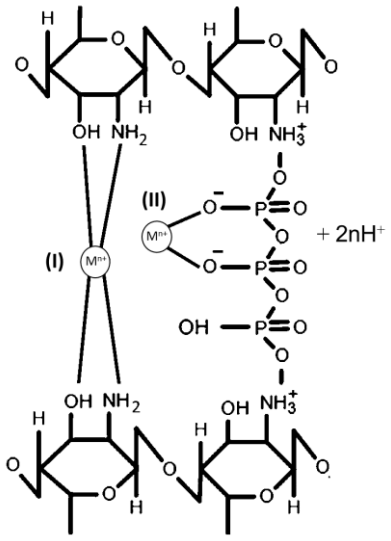

Figure 7-8. The possible mechanism of metal ions adsorption on IIP-STPP-CB in the ternary system of Cd(II)/Ni(II)/Co(II)

7.5 Conclusions

Chitosan (CB), crosslinked chitosan (STTP-CB), and ion-imprinted crosslinked chitosan (IIP-STPP-CB) were synthesized and characterized by XRD and BET techniques in this study, showing higher BET surface area and total pore volume of IPP-STPP-CB compared to STPP-CB. The adsorption efficiency of the fabricated adsorbents was investigated in the mono- and multi-component systems of Cd(II)-Ni(II)-Co(II), and the results showed the systems followed the Langmuir isotherm and the extended Langmuir models, respectively. The order of metal ions adsorption was Cd(II)>Ni(II)>Co(II) on CB and Cd(II)>Co(II)>Ni(II) on STPP-CB and IIP-STPP-

CB. The total metal ions uptake estimated by EL showed better adsorption capacity of IPP-STPP-CB (1.11 mmol/g) compared to STPP-CB (1.04 mmol/g). The relative selectivity coefficient indicated that IIP-STPP-CB had a higher selectivity for Cd(II) uptake than STPP-CB, validating the efficiency of the ion imprinting process. The mechanism investigation showed that two binding sites were involved in metal ions uptake, including amino and phosphate groups, and the adsorption process was governed by chemical binding and ion exchange.

7.6 References

The references are merged with those of the other chapters' references and presented at the end of the thesis.

Chapter 8

8 Synthesis, Integration and General Discussion of Results

Finding a cost-effective and ecologically friendly method to recover heavy metals found in spent batteries is becoming important for moving towards sustainability. Adsorption appears to be a practical method for this purpose, and chitosan has garnered considerable attention as a good adsorbent for metal sorption purposes. This would also offer a sustainable management option for wastes from fisheries industries. However, chitosan modification is unavoidable to increase its physical, chemical, and mechanical properties. Sodium tripolyphosphate is a non-toxic crosslinker that can modify chitosan, followed by an ion-imprinting technique to enhance crosslinked chitosan adsorption efficiency and selectivity. Considering the above, this research investigated the adsorption of cadmium, nickel, and cobalt on chitosan-based adsorbents in five phases.

In the first and second phases (Chapter 3 and 4), chitosan and sodium tripolyphosphate crosslinked chitosan beads were synthesized for Cd(II) and Ni(II) uptake from aqueous media in single-component adsorption systems, and response surface methodology (RSM) was applied to model and optimize cadmium(II) and nickel(II) adsorption onto crosslinked chitosan beads. In the third phase (Chapter 5), the adsorption of Ni(II) and Cd(II) ions from binary metal ions solutions onto chitosan and crosslinked chitosan beads was studied. In the fourth (Chapter 6) and fifth phase (Chapter 7), crosslinked chitosan beads went under another modification step to prepare Cd-imprinted crosslinked chitosan beads to improve the capacity and selectivity for Cd(II) uptake.

The effect of some adsorption parameters, including pH, adsorbent dosage, temperature and contact time, was examined in batch adsorption systems. Adsorption tests results were modelled using common adsorption isotherm models. Also, the synthesized adsorbents were characterized by different techniques, including FTIR spectroscopy, XRD, swelling test, BET, TGA, SEM, and SEM-EDS. The main findings of this research are synthesized and discussed below.

8.1 Investigation of adsorption parameters

8.1.1 Effect of pH

The effect of pH was investigated in single-component adsorption systems of Cd(II), Ni(II), Co(II) on different adsorbents, including chitosan, crosslinked chitosan and ion-imprinted

crosslinked chitosan beads. The results indicated that increasing the pH enhanced the adsorption efficiency of the adsorbents regardless of the metal ions type and the adsorbent used in the system. The pH was not studied beyond 8.5 because of metal ions' precipitation as hydroxide, and pHs below 4.0 were not evaluated due to low adsorption efficiency.

8.1.2 Effect of adsorbent dosage

The effect of adsorbent dosage was studied in single-component adsorption systems of Ni(II) and Cd(II). Irrespective of the adsorbent type applied, the percentage of metal ions removal increased with increasing the adsorbent dosage. On the other hand, the apparent adsorption capacity in the batch adsorption system decreased with an increase in adsorbent dosage. As a result, an optimal dosage of adsorbent, in the range of 0.45 to 0.65 g/L, was selected for each metal ion to balance adsorption capacity as well as removal percentage.

8.1.3 Effect of contact time

The preliminary batch adsorption tests were conducted in a single component system of Cd(II) and Ni(II), indicating that the adsorption of metal ions on chitosan and crosslinked chitosan beads reached equilibrium after 18h. However, evaluating the effect of time on Cd(II) adsorption on ion-imprinted crosslinked chitosan indicated that the equilibrium was achieved in 48h. So this period was selected for examining the efficiency of ion-imprinted crosslinked chitosan. Different kinetics models were examined to study the kinetics of Cd(II) adsorption on crosslinked chitosan and ion-imprinted crosslinked chitosan beads, and the results indicated that the second-order rate equation governed the kinetics adsorption of Cd(II), suggesting that chemisorption was the rate-controlling.

8.1.4 Effect of temperature

Effect of temperature was investigated for Cd(II) and Ni(II) uptake in a single-component adsorption system onto chitosan, crosslinked chitosan, and ion-imprinted crosslinked chitosan beads. These results indicated that increasing temperature improved the adsorption uptake of Cd(II) and Ni(II). The computed thermodynamic parameters at three temperatures, including 25, 40, 55 °C, showed that Cd(II) and Ni(II) adsorption processes were endothermic, and randomness increased irrespective of adsorbents type used in the system. Moreover, it was found that Cd(II)

adsorption onto chitosan, crosslinked chitosan, and ion-imprinted crosslinked chitosan beads were spontaneous except for chitosan crosslinked in 15% (w/v) sodium tripolyphosphate solution at room temperature. On the other hand, Ni(II) adsorption was only spontaneous on chitosan hydrogel beads at 40 and 55 ℃.

8.2 Investigation of synthesized adsorbents in single-component systems

8.2.1 Chitosan

The adsorption capacity of Cd(II), Ni(II), and Co(II) on chitosan was investigated and compared by varying their initial concentration from 0.089 to 8.89 mmol/L. Among the different isotherm models used, the Langmuir model best fitted the experimental data of the metal ions on chitosan hydrogel beads, and the maximum adsorption capacity followed the order of Cd(II) (1.17 mmol/g) > Ni(II) (0.90 mmol/g) > Co(II) (0.61 mmol/g).

8.2.2 Crosslinked chitosan

The effect of crosslinking and its degree was evaluated for Cd(II), Ni(II), and Co(II) uptake in single-component adsorption systems. The initial concentration of metal ions changed in the range of 0.089 to 8.89 mmol/L, and the Langmuir isotherm model was selected as the best fit. It was observed that the adsorption uptake of Cd(II) and Ni(II) decreased by crosslinking and increasing the sodium tripolyphosphate solution concentration. On the contrary, Co(II) adsorption capacity increased after crosslinking chitosan with sodium tripolyphosphate, implying that new adsorption sites originated from sodium tripolyphosphate were involved in Co(II) adsorption onto cross-linked chitosan beads. The metal ions uptake by crosslinked chitosan followed the order Cd(II) (0.86 mmol/g) > Co(II) (0.73 mmol/g) > Ni(II) (0.44 mmol/g).

The Central Composite Design (CCD) of experiments was used to analyze the effect of two independent variables on Cd(II) and Ni(II) adsorption on crosslinked chitosan beads. A reduced quadratic model with good agreement with experimental data ($R^2 = 0.95$) was determined to formulate the adsorption capacity of Cd(II) as a function of the crosslinking extent and temperature. The optimization based on the reduced model indicated that the maximum adsorption capacity of 99.87 (mg/g) is feasible at the temperature of 55.17 ℃ when sodium tripolyphosphate

solution concentration is 2.92% (w/v). Ni(II) adsorption capacity was correlated to pH and the crosslinking degree using RSM with a simple linear model with a high magnitude of the correlation coefficient between the experimental and model-predicted values (R^2=0.96). The model showed that an adsorption capacity of 31.94 mg/g is feasible at pH 7.21 and sodium tripolyphosphate solution concentration of 2.92% (w/v).

8.2.3 Ion-imprinted crosslinked

The ion-imprinting technique using Cd(II) as a template ion was employed in this study to improve the adsorption uptake of crosslinked chitosan beads. The synthesized adsorbent was employed and evaluated in the single-component system of Cd(II), Ni(II), and Co(II). The initial concentration of metal ions changed within the range of 0.089 to 8.89 mmol/L, and the Langmuir model showed the best fit to the experimental data. The results indicated that Cd(II) uptake improved by 25% after applying the ion-imprinting technique on chitosan beads crosslinked in 5% (w/v) sodium tripolyphosphate solution. On the other hand, Ni(II) and Co(II) adsorption capacity decreased after ion-imprinting the crosslinked chitosan beads by Cd(II) templates. The order of metal ions adsorption on ion-imprinted-crosslinked chitosan was in the order of Cd(II) (1.06 mmol/g) > Co(II) (0.68 mmol/g) > Ni(II) (0.38 mmol/g). This observation showed that ion-imprinting using Cd(II) as templates improved the adsorption uptake of crosslinked chitosan for Cd(II) adsorption.

8.3 Investigation of synthesized adsorbents in multi-component systems

The adsorption capacity of chitosan, crosslinked chitosan, and ion-imprinted crosslinked chitosan beads was evaluated in the multi-component systems of metal ions. It was observed that the presence of co-ions in the multi-component system diminished the adsorption capacity of the individual metal ions compared to results from single-component systems. However, the total adsorption capacity of metal ions in multi-component systems was higher than the maximum adsorption capacity of each metal ion in single-component systems. In the binary system of Cd(II) and Ni(II), the extended Freundlich model interpreted the experimental data on chitosan and crosslinked chitosan beads better than the other investigated models. However, the results from the ternary system showed that the experimental data of Cd(II), Ni(II), and Co(II) on chitosan,

crosslinked chitosan, and ion-imprinted crosslinked chitosan could be fitted better by the extended Langmuir model. The overall adsorbates uptake obtained from the extended Langmuir model followed the order of chitosan>ion-imprinted crosslinked chitosan>crosslinked chitosan beads. The relative selectivity coefficients of ion-imprinted to non-imprinted crosslinked chitosan were computed for Cd(II) adsorption at different ratios of Cd(II):Ni(II):Co(II), showing values greater than 1.00. This observation showed that the ion-imprinted adsorbent had more affinity compared to crosslinked chitosan beads for adsorbing Cd(II) rather than Ni(II) and Co(II) in a multi-component system.

8.4 Characterization of synthesized adsorbents before and after adsorption

Different characterization techniques have been employed in this study to examine the properties of the synthesized adsorbents and the mechanism of crosslinking and adsorption. TGA profiles of synthesized adsorbents demonstrated better thermal stability of crosslinked chitosan compared to chitosan due to crosslinking. The XRD pattern of chitosan and crosslinked chitosan beads showed that the crystalline structure of chitosan changed after crosslinking with sodium tripolyphosphate. The XRD spectrum of ion-imprinted crosslinked chitosan indicated a crystalline structure similar to chitosan. The SEM of crosslinked chitosan and ion-imprinted crosslinked chitosan showed the non-granular surface of the former and porous surface morphology of the latter. The BET characterization revealed that the BET surface area of chitosan beads decreased from 6.50 to 5.60 m^2/g after crosslinking. However, the ion-imprinted crosslinked chitosan beads showed a higher BET surface area (6.20 m^2/g) than crosslinked chitosan beads, explaining the higher adsorption capacity of ion-imprinted crosslinked chitosan. FTIR characterization helped understand the groups involved in crosslinking; it was revealed that ionic crosslinking of chitosan occurred on the amine groups of chitosan due to the interaction between the positively charged amino groups and negatively charged phosphoric ions originating from sodium tripolyphosphate. FTIR characterization of loaded adsorbents showed that amine groups were the main biding sites for uptake of metal ions via chemical reactions. Phosphate groups originating from sodium tripolyphosphate also participated in the uptake of metal ions via ion-exchange reaction. SEM-EDS examination of loaded chitosan beads in single-component systems showed intensity in the

order of Cd(II)>Ni(II)>Co(II), which changed to Cd(II)>Co(II)>Ni(II) for ion-imprinted crosslinked chitosan beads in the multi-component system.

Chapter 9

9 Conclusions and Future Works

9.1 Conclusions

Adsorption was employed in this study for the recovery of Cd(II), Ni(II) and Co(II) found in used Ni-Cd batteries. Among different adsorbents, chitosan as a low-cost adsorbent, which can be extracted from seafood industry waste, was selected in this research to move toward sustainable waste management. Therefore, chitosan in the form of hydrogel beads was synthesized and used in a batch adsorption system of synthetic solution of heavy metal ions. Despite the good adsorption properties of chitosan hydrogel beads, they had low chemical and physical properties, confirmed by solubility and swelling tests. Hence, chitosan hydrogel beads were crosslinked by a non-toxic crosslinker, sodium tripolyphosphate, to form more rigid and insoluble beads in acidic conditions, confirmed by TGA, solubility, and swelling tests. The use of sodium tripolyphosphate for chitosan modification had the advantage of forming and crosslinking beads in a single step in a sodium tripolyphosphate solution and eliminating the use of chemicals (i.e., NaOH) for beads formation. Crosslinking chitosan by sodium tripolyphosphate consumed the amino groups of chitosan and altered chitosan crystal structure, confirmed by the FTIR and XRD tests. The characterization of the crosslinked chitosan beads also indicated that increasing crosslinking degree reduced the BET surface area and total pore volume of the adsorbents. This could be due to the fact that crosslinking chitosan reduced the adsorption efficiency of chitosan for heavy metal ions uptake, which was confirmed by the isotherm study results. The isotherm study in single-and multi-component adsorption systems showed that Cd(II) and Ni(II) uptake decreased after crosslinking chitosan. Considering the decrease in Cd(II) adsorption, the ion-imprinting technique using Cd(II) as a template was employed to counteract the negative impact of crosslinking on adsorption uptake. The characterization of the prepared adsorbents showed an increase in BET surface area and total pore volume of the hydrogel beads after ion imprinting the crosslinked chitosan. The isotherm study in mono- and multi-component systems of Cd(II)-Ni(II)-Co(II) showed an increase in adsorption capacity and selectivity of crosslinked chitosan after ion imprinting for Cd(II) uptake. Based on the results, Cd(II)-imprinted crosslinked chitosan adsorption capacity followed the order of Cd(II)>Co(II)>Ni(II) in the ternary system. Contrary to Cd(II) and Ni(II), Co(II) adsorption improved after crosslinking chitosan beads, suggesting the involvement of phosphate groups in

Co(II) adsorption, which was confirmed by FTIR and SEM-EDS characterizations. The characterization implied that two mechanisms on two different binding sites governed the adsorption of metal ions on ion-imprinted crosslinked chitosan beads in the ternary system, including the amino groups for Cd(II)/Ni(II)/Co(II) uptake and phosphate groups for Co(II) uptake.

9.2 Recommendations for future work

- Using a real leach solution from used Ni-Cd batteries and evaluating the efficiency of the synthesized adsorbents.
- Studying the adsorption efficiency of the synthesized beads in a continuous adsorption system.
- Using other non-toxic crosslinkers which use -OH groups instead of -NH groups of chitosan.
- Modifying the ion-imprinting process used in this research to enhance its selectivity for Cd(II) uptake in a competitive adsorption system.
- Synthesizing ion-imprinted crosslinked chitosan using Ni(II)/Co(II) as a template and investigating the selectivity of the prepared beads for Ni(II)/Co(II) uptake.
- Using RSM to model the adsorption capacity of ion-imprinted crosslinked chitosan as a function of the most influential parameters and optimize them.
- Employing other characterization techniques (i.e., XPS) to understand adsorption and crosslinking mechanisms better.
- Synthesizing magnetic ion-imprinted crosslinked chitosan beads to facilitate the beads' separation from the solution in the adsorption-desorption cycle.
- Using other desorption effluents such as acidic reagents and evaluating the adsorbent capacity in the adsorption-desorption cycle.

Appendices

Appendix 1: Laboratory equipment used for heavy metal ions concentration measurement

The concentration of Cd(II), Ni(II), and Co(II) was measured using a flame atomic absorption spectrometer (PinAAcle 500, PerkinElmer, Waltham), following standard methods 3111B [420]. This measurement procedure involves aspirating a liquid sample into a flame and atomizing it, then measuring the amount of the light absorbed when the flame passes through the emission of a hollow cathode elemental lamp. For each measurement, a calibration curve must be established. Therefore, standard solutions were prepared and used for calibration prior to each analytical measurement. Generally, a blank sample must be analyzed first, followed by the analysis of the standard solutions to obtain the calibration curve. Once the calibration curve is constructed, the samples can be analyzed. It should be noted that 1% concentrated nitric acid must be added to all solutions, including blanks, standards, and samples, to guarantee that the heavy metal ions remain dissolved in the solution; moreover, to clean the capillary tube, spray chamber, and burner head and prevent any residual metals from becoming stuck inside the instrument and causing analytical mistakes. A picture of AAS is shown below.

Figure AP1. 1. *PerkinElmer PinAAcle 500 Flame Atomic Adsorption Spectroscopy*

Appendix 2: Complementary Results

Equilibrium time

The following figures show the equilibrium time for Cd(II) and Ni(II) adsorption on chitosan in a monocomponent system.

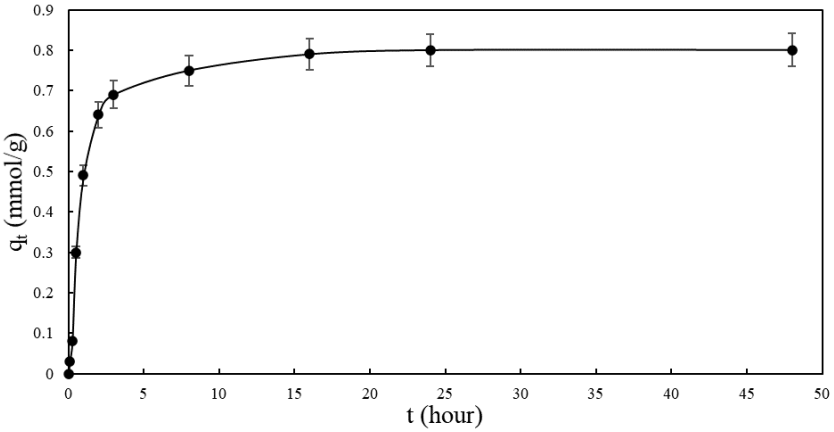

Figure AP2. 1. *Equilibrium time for the adsorption of Cd(II) onto CB at 25°C, dosage 0.45 g/L, Cd(II) concentration 50 mg/L, and pH 7*

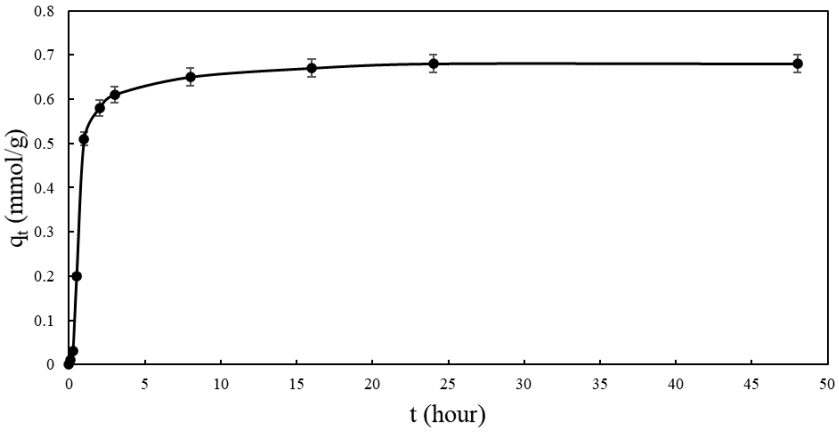

Figure AP2.2. *Equilibrium time for the adsorption of Ni(II) onto CB at 25°C, dosage 0.55 g/L, Ni(II) concentration 50 mg/L, and pH 7*

Effect of adsorbent dosage

The following figure shows the effect of adsorbent dosage on Ni(II) adsorption on CB.

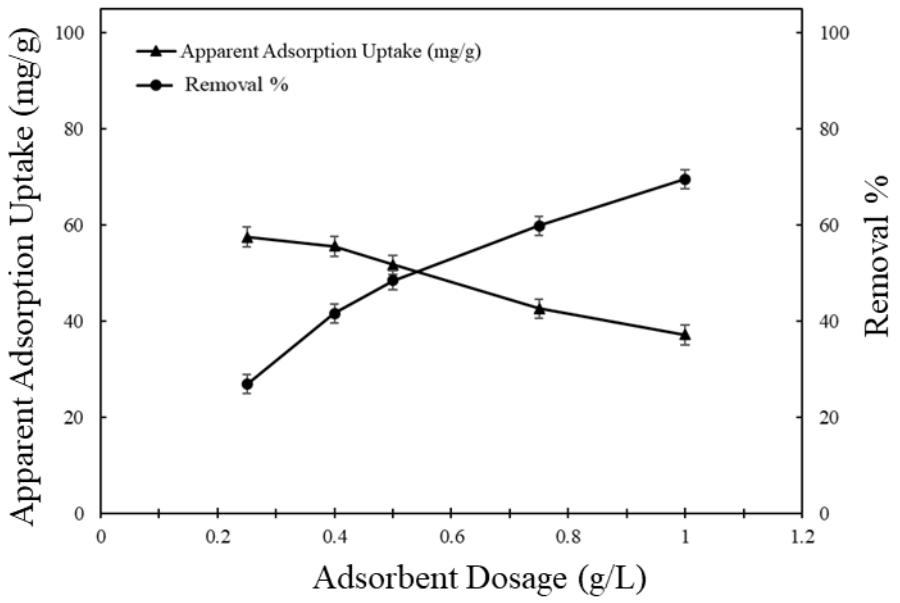

Figure AP2. 3. *Effect of adsorbent dosage on the adsorption of Ni(II) onto CB at 25℃, Ni(II) concentration 50 mg/L, and pH 7*

References

The references are merged with those of the other chapters' references and presented at the end of the thesis.

References

1. Zhang, X. *et al.* Toward sustainable and systematic recycling of spent rechargeable batteries. *Chemical Society Reviews* **47**, 7239–7302 (2018).

2. Lacerda, V. G., Mageste, A. B., Santos, I. J. B., da Silva, L. H. M. & da Silva, M. do C. H. Separation of Cd and Ni from Ni-Cd batteries by an environmentally safe methodology employing aqueous two-phase systems. *Journal of Power Sources* **193**, 908–913 (2009).

3. Blumbergs, E., Serga, V., Platacis, E., Maiorov, M. & Shishkin, A. Cadmium Recovery from Spent Ni-Cd Batteries: A Brief Review. *Metals (Basel)* **11**, 1714 (2021).

4. Kaya, M. Recovery of metals and nonmetals from electronic waste by physical and chemical recycling processes. *Waste Management* **57**, 64–90 (2016).

5. Dave, G. & Lidman, U. Biological and toxicological effects of solvent extraction chemicals. *Hydrometallurgy* **3**, 201–216 (1978).

6. Rotuska, K. & Chmielewski, T. Growing role of solvent extraction in copper ores processing. *Physicochemical Problems of Mineral Processing* **42**, 29–36 (2008).

7. Innocenzi, V. *et al.* Purification of residual leach liquors from hydrometallurgical process of NiMH spent batteries through micellar enhanced ultra filtration. *Journal of Environmental Management* (2018) doi:10.1016/j.jenvman.2018.03.073.

8. Bonilla-Petriciolet, A., Mendoza-Castillo, D. I. & Reynel-Avila, H. E. *Adsorption Processes for Water Treatment and Purification*. (Springer International Publishing, 2017). doi:10.1007/978-3-319-58136-1.

9. Babel, S. & Kurniawan, T. A. Low-cost adsorbents for heavy metals uptake from contaminated water: a review. *J Hazard Mater* **97**, 219–43 (2003).

10. Wang, J. & Chen, C. Biosorbents for heavy metals removal and their future. *Biotechnology Advances* **27**, 195–226 (2009).

11. Kumari, S., Rath, P., Sri Hari Kumar, A. & Tiwari, T. N. Extraction and characterization of chitin and chitosan from fishery waste by chemical method. *Environmental Technology & Innovation* **3**, 77–85 (2015).

12. Yadav, M. *et al.* Seafood waste: a source for preparation of commercially employable chitin/chitosan materials. *Bioresources and Bioprocessing* **6**, 8 (2019).

13. Pillai, C. K. S., Paul, W. & Sharma, C. P. *Chitosan: manufacture, properties and uses*. *Chitosan: manufacture, properties, and usage* (2011).

14. Liu, B., Wang, D., Yu, G. & Meng, X. Adsorption of heavy metal ions, dyes and proteins by chitosan composites and derivatives - A review. *Journal of Ocean University of China* **12**, 500–508 (2013).

15. Mourya, V. K. & Inamdar, N. N. Chitosan-modifications and applications: Opportunities galore. *Reactive and Functional Polymers* **68**, 1013–1051 (2008).

16. Wang, J. & Chen, C. Chitosan-based biosorbents: Modification and application for biosorption of heavy metals and radionuclides. *Bioresource Technology* **160**, 129–141 (2014).

17. Kaur, S. & Dhillon, G. S. Recent trends in biological extraction of chitin from marine shell wastes: a review. *Crit Rev Biotechnol* **8551**, 44–61 (2013).

18. Miretzky, P. & Cirelli, A. F. Hg(II) removal from water by chitosan and chitosan derivatives: A review. *Journal of Hazardous Materials* **167**, 10–23 (2009).

19. Chen, C.-Y., Yang, C.-Y. & Chen, A.-H. Biosorption of Cu(II), Zn(II), Ni(II) and Pb(II) ions by cross-linked metal-imprinted chitosans with epichlorohydrin. *Journal of Environmental Management* **92**, 796–802 (2011).

20. Sankararamakrishnan, N., Sharma, A. K. & Sanghi, R. Novel chitosan derivative for the removal of cadmium in the presence of cyanide from electroplating wastewater. *Journal of Hazardous Materials* **148**, 353–359 (2007).

21. Jóźwiak, T., Filipkowska, U., Szymczyk, P., Rodziewicz, J. & Mielcarek, A. Effect of ionic and covalent crosslinking agents on properties of chitosan beads and sorption effectiveness of Reactive Black 5 dye. *Reactive and Functional Polymers* **114**, 58–74 (2017).

22. Wang, H. *et al.* A Novel Magnetic Cd(II) Ion-Imprinted Polymer as a Selective Sorbent for the Removal of Cadmium Ions from Aqueous Solution. *Journal of Inorganic and Organometallic Polymers and Materials* **29**, 1874–1885 (2019).

23. Dąbrowski, A., Hubicki, Z., Podkościelny, P. & Robens, E. Selective removal of the heavy metal ions from waters and industrial wastewaters by ion-exchange method. *Chemosphere* **56**, 91–106 (2004).

24. Borah, R., Hughson, F. R., Johnston, J. & Nann, T. On battery materials and methods. *Materials Today Advances* **6**, 100046 (2020).

25. Meshram, P., Pandey, B. D. & Abhilash. Perspective of availability and sustainable recycling prospects of metals in rechargeable batteries – A resource overview. *Resources Policy* **60**, 9–22 (2019).

26. Zeng, X., Li, J. & Singh, N. Recycling of spent lithium-ion battery: A critical review. *Critical Reviews in Environmental Science and Technology* **44**, 1129–1165 (2014).

27. Bernardes, A. M., Espinosa, D. C. R. & Tenório, J. A. S. Recycling of batteries: A review of current processes and technologies. *Journal of Power Sources* **130**, 291–298 (2004).

28. Espinosa, D. C. R. & Mansur, M. B. Recycling batteries. *Waste Electrical and Electronic Equipment (WEEE) Handbook* 365–384 (2012) doi:10.1533/9780857096333.3.365.

29. Tanong, K., Coudert, L., Mercier, G. & Blais, J. F. Recovery of metals from a mixture of various spent batteries by a hydrometallurgical process. *Journal of Environmental Management* **181**, 95–107 (2016).

30. Morrow, H. Environmental and human health impact assessments of battery systems. in *Industrial Chemistry Library* vol. 10 1–34 (2001).

31. Wiaux, J.-P. *Used Battery Collection and Recycling*. *Industrial Chemistry Library* vol. 10 (2001).

32. Xu, J. *et al.* A review of processes and technologies for the recycling of lithium-ion secondary batteries. *Journal of Power Sources* **177**, 512–527 (2008).

33. Tanong, K., Tran, L.-H., Mercier, G. & Blais, J.-F. Recovery of Zn (II), Mn (II), Cd (II) and Ni (II) from the unsorted spent batteries using solvent extraction, electrodeposition and precipitation methods. *Journal of Cleaner Production* **148**, 233–244 (2017).

34. Wilberforce, T., Thompson, J. & Olabi, A.-G. Classification of Energy Storage Materials. in *Encyclopedia of Smart Materials* 8–14 (Elsevier, 2022). doi:10.1016/B978-0-12-803581-8.11762-X.

35. Rudnik, E. & Nikiel, M. Hydrometallurgical recovery of cadmium and nickel from spent Ni-Cd batteries. *Hydrometallurgy* **89**, 61–71 (2007).

36. Nogueira, C. A. & Margarido, F. Chemical and physical characterization of electrode materials of spent sealed Ni-Cd batteries. *Waste Management* **27**, 1570–1579 (2007).

37. Huang, K., Li, J. & Xu, Z. A Novel Process for Recovering Valuable Metals from Waste Nickel−Cadmium Batteries. *Environmental Science & Technology* **43**, 8974–8978 (2009).

38. Georgi-Maschler, T., Friedrich, B., Weyhe, R., Heegn, H. & Rutz, M. Development of a recycling process for Li-ion batteries. *Journal of Power Sources* **207**, 173–182 (2012).

39. Espinosa, D. C. R., Bernardes, A. M. & Tenório, J. A. S. An overview on the current processes for the recycling of batteries. *Journal of Power Sources* **135**, 311–319 (2004).

40. Hung, Y. Y. *et al.* Recycling of spent nickel–cadmium battery using a thermal separation process. *Environmental Progress and Sustainable Energy* **37**, 645–654 (2018).

41. Yadav, P., Jie, C. J., Tan, S. & Srinivasan, M. Recycling of cathode from spent lithium iron phosphate batteries. *Journal of Hazardous Materials* **399**, 123068 (2020).

42. Huang, K., Li, J. & Xu, Z. Characterization and recycling of cadmium from waste nickel-cadmium batteries. *Waste Management* **30**, 2292–2298 (2010).

43. Sayilgan, E. *et al.* A review of technologies for the recovery of metals from spent alkaline and zinc–carbon batteries. *Hydrometallurgy* **97**, 158–166 (2009).

44. Freitas, M. B. J. G. & Rosalém, S. F. Electrochemical recovery of cadmium from spent Ni-Cd batteries. *Journal of Power Sources* **139**, 366–370 (2005).

45. Nogueira, C. A. & Margarido, F. Leaching behaviour of electrode materials of spent nickel-cadmium batteries in sulphuric acid media. *Hydrometallurgy* (2004) doi:10.1016/S0304-386X(03)00123-3.

46. Mahandra, H., Singh, R. & Gupta, B. Recycling of Zn-C and Ni-Cd spent batteries using Cyphos IL 104 via hydrometallurgical route. *Journal of Cleaner Production* **172**, 133–142 (2018).

47. Freitas, M. B. J. G., Penha, T. R. & Sirtoli, S. Chemical and electrochemical recycling of the negative electrodes from spent Ni-Cd batteries. *Journal of Power Sources* **163**, 1114–1119 (2007).

48. Fernandes, A., Afonso, J. C. & Bourdot Dutra, A. J. Hydrometallurgical route to recover nickel, cobalt and cadmium from spent Ni-Cd batteries. *Journal of Power Sources* **220**, 286–291 (2012).

49. Fernandes, A., Afonso, J. C. & Dutra, A. J. B. Separation of nickel(II), cobalt(II) and lanthanides from spent Ni-MH batteries by hydrochloric acid leaching, solvent extraction and precipitation. *Hydrometallurgy* **133**, 37–43 (2013).

50. Chen, X. *et al.* Recovery of valuable metals from mixed types of spent lithium ion batteries. Part II: Selective extraction of lithium. *Waste Management* **80**, 198–210 (2018).

51. Hazotte, C., Leclerc, N., Diliberto, S., Meux, E. & Lapicque, F. End-of-life nickel-cadmium accumulators: Characterization of electrode materials and industrial Black Mass. *Environmental Technology (United Kingdom)* **36**, 796–805 (2015).

52. Reddy, B. R. & Priya, D. N. Chloride leaching and solvent extraction of cadmium, cobalt and nickel from spent nickel-cadmium, batteries using Cyanex 923 and 272. *Journal of Power Sources* (2006) doi:10.1016/j.jpowsour.2006.05.044.

53. Nogueir, C. A. & Margarido, F. Nickel-cadmium batteries: Effect of electrode phase composition on acid leaching process. *Environmental Technology* **33**, 359–366 (2012).

54. Zhang, L. *et al.* Microwave and ultrasound augmented leaching of complicated zinc oxide ores in ammonia and ammonium citrate solutions. *Metals (Basel)* (2017) doi:10.3390/met7060216.

55. Hazotte, C., Leclerc, N., Meux, E. & Lapicque, F. Direct recovery of cadmium and nickel from Ni-Cd spent batteries by electroassisted leaching and electrodeposition in a single-cell process. *Hydrometallurgy* **162**, 94–103 (2016).

56. Agrawal, A., Pathak, P., Mishra, D. & Sahu, K. K. Solvent mediated interactions for the selective recovery of Cadmium from Ni-Cd battery waste. *Journal of Molecular Liquids* (2012) doi:10.1016/j.molliq.2012.06.017.

57. Bartolozzi, M., Braccini, G., Bonvini, S. & Marconi, P. F. Hydrometallurgical recovery process for nickel-cadmium spent batteries. *Journal of Power Sources* (1995) doi:10.1016/0378-7753(95)02180-O.

58. Mauchauffée, S., Meux, E. & Schneider, M. Selective precipitation of cadmium from nickel cadmium sulphate solutions using sodium decanoate. *Separation and Purification Technology* **62**, 394–400 (2008).

59. Jha, M. K., Kumar, V., Jeong, J. & Lee, J. C. Review on solvent extraction of cadmium from various solutions. *Hydrometallurgy* **111–112**, 1–9 (2012).

60. Laki, S., Shamsabadi, A. A. & Kargari, A. Comparative solvent extraction study of silver(I) by MEHPA and Cyanex 302 as acidic extractants in a new industrial diluent (MIPS). *Hydrometallurgy* **160**, 38–46 (2016).

61. Fröhlich, S. & Sewing, D. The BATENUS process for recycling mixed battery waste. *Journal of Power Sources* (1995) doi:10.1016/0378-7753(95)02234-1.

62. Babakhani, A., Rashchi, F., Zakeri, A. & Vahidi, E. Selective separation of nickel and cadmium from sulfate solutions of spent nickel-cadmium batteries using mixtures of D2EHPA and Cyanex 302. *Journal of Power Sources* **247**, 127–133 (2014).

63. Peng, C. hong, Bai, B. shuai & Chen, Y. feng. Study on the preparation of Mn-Zn soft magnetic ferrite powders from waste Zn-Mn dry batteries. *Waste Management* (2008) doi:10.1016/j.wasman.2007.03.020.

64. Salgado, A. L. *et al.* Recovery of zinc and manganese from spent alkaline batteries by liquid–liquid extraction with Cyanex 272. *Journal of Power Sources* **115**, 367–373 (2003).

65. Burakov, A. E. *et al.* Adsorption of heavy metals on conventional and nanostructured materials for wastewater treatment purposes: A review. *Ecotoxicology and Environmental Safety* **148**, 702–712 (2018).

66. Attia, A. A., Khedr, S. A. & Elkholy, S. A. Adsorption of chromium ion (VI) by acid activated carbon. *Brazilian Journal of Chemical Engineering* (2010) doi:10.1590/S0104-66322010000100016.

67. Motsi, T., Rowson, N. A. & Simmons, M. J. H. Adsorption of heavy metals from acid mine drainage by natural zeolite. *International Journal of Mineral Processing* **92**, 42–48 (2009).

68. Rao, R. A. K. & Kashifuddin, M. Adsorption studies of Cd(II) on ball clay: Comparison with other natural clays. *Arabian Journal of Chemistry* (2016) doi:10.1016/j.arabjc.2012.01.010.

69. Black, R., Sartaj, M., Mohammadian, A. & Qiblawey, H. A. M. Biosorption of Pb and Cu using fixed and suspended bacteria. *Journal of Environmental Chemical Engineering* **2**, 1663–1671 (2014).

70. Zhou, Y. T., Branford-White, C., Nie, H. L. & Zhu, L. M. Adsorption mechanism of Cu2+ from aqueous solution by chitosan-coated magnetic nanoparticles modified with α-ketoglutaric acid. *Colloids and Surfaces B: Biointerfaces* **74**, 244–252 (2009).

71. Raval, N. P., Shah, P. U. & Shah, N. K. Adsorptive removal of nickel(II) ions from aqueous environment: A review. *Journal of Environmental Management* **179**, 1–20 (2016).

72. Kakavandi, B. *et al.* Efficient adsorption of cobalt on chemical modified activated carbon: characterization, optimization and modeling studies. *DESALINATION AND WATER TREATMENT* **111**, 310–321 (2018).

73. Islam, Md. A., Awual, Md. R. & Angove, M. J. A review on nickel(II) adsorption in single and binary component systems and future path. *Journal of Environmental Chemical Engineering* **7**, 103305 (2019).

74. Abdulrazak, S., Hussaini, K. & Sani, H. M. Evaluation of removal efficiency of heavy metals by low-cost activated carbon prepared from African palm fruit. *Applied Water Science* (2017) doi:10.1007/s13201-016-0460-x.

75. Khaleque, A. *et al.* Zeolite synthesis from low-cost materials and environmental applications: A review. *Environmental Advances* **2**, 100019 (2020).

76. Taamneh, Y. & Sharadqah, S. The removal of heavy metals from aqueous solution using natural Jordanian zeolite. *Applied Water Science* **7**, 2021–2028 (2017).

77. Vengris, T., Binkiene, R. & Sveikauskaite, A. Nickel, copper and zinc removal from waste water by a modified clay sorbent. *Applied Clay Science* (2001) doi:10.1016/S0169-1317(00)00036-3.

78. Tripathi, A. & Rawat Ranjan, M. Heavy Metal Removal from Wastewater Using Low Cost Adsorbents. *Journal of Bioremediation & Biodegradation* **06**, (2015).

79. Uddin, M. K. A review on the adsorption of heavy metals by clay minerals, with special focus on the past decade. *Chemical Engineering Journal* **308**, 438–462 (2017).

80. Uddin, M. K. A review on the adsorption of heavy metals by clay minerals, with special focus on the past decade. *Chemical Engineering Journal* **308**, 438–462 (2017).

81. Gupta, V. K., Carrott, P. J. M., Ribeiro Carrott, M. M. L. & Suhas. Low-Cost Adsorbents: Growing Approach to Wastewater Treatment—a Review. *Critical Reviews in Environmental Science and Technology* **39**, 783–842 (2009).

82. Apiratikul, R. & Pavasant, P. Batch and column studies of biosorption of heavy metals by Caulerpa lentillifera. *Bioresource Technology* (2008) doi:10.1016/j.biortech.2007.06.036.

83. Tianwei, T., Xiaojing, H. & Weixia, D. Adsorption behaviour of metal ions on imprinted chitosan resin. *Journal of Chemical Technology & Biotechnology* **76**, 191–195 (2001).

84. Kurita, K. Chitin and chitosan: Functional biopolymers from marine crustaceans. *Marine Biotechnology* **8**, 203–226 (2006).

85. Abdou, E. S., Nagy, K. S. A. & Elsabee, M. Z. Extraction and characterization of chitin and chitosan from local sources. *Bioresource Technology* **99**, 1359–1367 (2008).

86. Wang, J. & Zhuang, S. Removal of various pollutants from water and wastewater by modified chitosan adsorbents. *Critical Reviews in Environmental Science and Technology* **47**, 2331–2386 (2017).

87. Felse, P. A. & Panda, T. Studies on applications of chitin and its derivatives. *Bioprocess Engineering* **20**, 505–512 (1999).

88. Tokura, S. & Tamura, H. Chitin and Chitosan. in *Comprehensive Glycoscience* 449–475 (Elsevier, 2007). doi:10.1016/B978-044451967-2/00127-6.

89. Crini, G. & Badot, P.-M. Application of chitosan, a natural aminopolysaccharide, for dye removal from aqueous solutions by adsorption processes using batch studies: A review of recent literature. *Progress in Polymer Science* **33**, 399–447 (2008).

90. Gimeno, L. *et al.* Oceanic and terrestrial sources of continental precipitation. *Reviews of Geophysics* (2012) doi:10.1029/2012RG000389.

91. el Knidri, H., Belaabed, R., Addaou, A., Laajeb, A. & Lahsini, A. Extraction, chemical modification and characterization of chitin and chitosan. *International Journal of Biological Macromolecules* **120**, 1181–1189 (2018).

92. No, H. K. & Meyers, S. P. Application of chitosan for treatment of wastewaters. *Reviews of environmental contamination and toxicology* (2000) doi:10.1007/978-1-4757-6429-1_1.

93. Yong, S. K., Bolan, N. S., Lombi, E., Skinner, W. & Guibal, E. Sulfur-Containing Chitin and Chitosan Derivatives as Trace Metal Adsorbents: A Review. *Critical Reviews in Environmental Science and Technology* **43**, 1741–1794 (2013).

94. Kyzas, G. & Bikiaris, D. Recent Modifications of Chitosan for Adsorption Applications: A Critical and Systematic Review. *Marine Drugs* **13**, 312–337 (2015).

95. Andrade, F. *et al.* Chitosan Formulations as Carriers for Therapeutic Proteins. *Current Drug Discovery Technologies* (2011) doi:10.2174/157016311796799035.

96. Babakhani, A. & Sartaj, M. Removal of Cadmium (II) from aqueous solution using tripolyphosphate cross-linked chitosan. *Journal of Environmental Chemical Engineering* **8**, 103842 (2020).

97. Salehi, E., Daraei, P. & Arabi Shamsabadi, A. A review on chitosan-based adsorptive membranes. *Carbohydrate Polymers* **152**, 419–432 (2016).

98. Guibal, E. Interactions of metal ions with chitosan-based sorbents: a review. *Separation and Purification Technology* **38**, 43–74 (2004).

99. Wang, J. & Zhuang, S. Removal of various pollutants from water and wastewater by modified chitosan adsorbents. *Critical Reviews in Environmental Science and Technology* **47**, 2331–2386 (2017).

100. Abou El-Reash, Y. G. Magnetic chitosan modified with cysteine-glutaraldehyde as adsorbent for removal of heavy metals from water. *Journal of Environmental Chemical Engineering* **4**, 3835–3847 (2016).

101. Zhang, L., Zeng, Y. & Cheng, Z. Removal of heavy metal ions using chitosan and modified chitosan: A review. *Journal of Molecular Liquids* **214**, 175–191 (2016).

102. Reyna-Urrutia, V. A., Mata-Haro, V., Cauich-Rodriguez, J. v., Herrera-Kao, W. A. & Cervantes-Uc, J. M. Effect of two crosslinking methods on the physicochemical and biological properties of the collagen-chitosan scaffolds. *European Polymer Journal* **117**, 424–433 (2019).

103. Dang, M. Y., Guo, H. M. & Tan, Y. K. Adsorption Kinetics of Zn(II) from Aqueous Solutions onto Epichlorohydrin Crosslinked Chitosan. *Advanced Materials Research* **463–464**, 7–11 (2012).

104. Monteiro, O. A. C. & Airoldi, C. Some studies of crosslinking chitosan-glutaraldehyde interaction in a homogeneous system. *International Journal of Biological Macromolecules* **26**, 119–128 (1999).

105. Wan Ngah, W. S., Endud, C. S. & Mayanar, R. Removal of copper(II) ions from aqueous solution onto chitosan and cross-linked chitosan beads. *Reactive and Functional Polymers* **50**, 181–190 (2002).

106. Giraldo, J. D., Rivas, B. L., Elgueta, E. & Mancisidor, A. Metal ion sorption by chitosan-tripolyphosphate beads. *Journal of Applied Polymer Science* **134**, 45511 (2017).

107. Mao, C., Imtiaz, S. A. & Zhang, Y. Competitive adsorption of Ag (I) and Cu (II) by tripolyphosphate crosslinked chitosan beads. *Journal of Applied Polymer Science* **132**, n/a-n/a (2015).

108. Vakili, M. *et al.* Application of chitosan and its derivatives as adsorbents for dye removal from water and wastewater: A review. *Carbohydrate Polymers* **113**, 115–130 (2014).

109. Stranges, S. *et al.* The valence electronic structure and conformational flexibility of epichlorohydrin. *Physical Chemistry Chemical Physics* (2011) doi:10.1039/c0cp02730h.

110. Gutha, Y., Zhang, Y., Zhang, W. & Jiao, X. Magnetic-epichlorohydrin crosslinked chitosan schiff's base (m-ECCSB) as a novel adsorbent for the removal of Cu(II) ions from aqueous environment. *International Journal of Biological Macromolecules* **97**, 85–98 (2017).

111. Abdulhameed, A. S., Jawad, A. H. & Mohammad, A.-T. Synthesis of chitosan-ethylene glycol diglycidyl ether/TiO2 nanoparticles for adsorption of reactive orange 16 dye using a response surface methodology approach. *Bioresource Technology* **293**, 122071 (2019).

112. Jolibois, B., Guerbet, M. & Vassal, S. Glutaraldehyde in hospital wastewater. *Archives of Environmental Contamination and Toxicology* (2002) doi:10.1007/s00244-001-0011-8.

113. Sano, L. L., Krueger, A. M. & Landrum, P. F. Chronic toxicity of glutaraldehyde: Differential sensitivity of three freshwater organisms. *Aquatic Toxicology* (2005) doi:10.1016/j.aquatox.2004.12.001.

114. Shu, X. Z. & Zhu, K. J. A novel approach to prepare tripolyphosphate/chitosan complex beads for controlled release drug delivery. *International Journal of Pharmaceutics* (2000) doi:10.1016/S0378-5173(00)00403-8.

115. Gurses, M. S., Erkey, C., Kizilel, S. & Uzun, A. Characterization of sodium tripolyphosphate and sodium citrate dehydrate residues on surfaces. *Talanta* **176**, 8–16 (2018).

116. Yang, Z. & Yuan, Y. Studies on the synthesis and properties of hydroxyl azacrown ether-grafted chitosan. *Journal of Applied Polymer Science* (2001) doi:10.1002/app.2026.

117. Wang, J. *et al.* Recent progress on synthesis, property and application of modified chitosan: An overview. *International Journal of Biological Macromolecules* **88**, 333–344 (2016).

118. Ma, G., Yang, D., Kennedy, J. F. & Nie, J. Synthesize and characterization of organic-soluble acylated chitosan. *Carbohydrate Polymers* (2009) doi:10.1016/j.carbpol.2008.07.035.

119. Flores-Ramírez, N. *et al.* Characterization and degradation of functionalized chitosan with glycidyl methacrylate. *Journal of Biomaterials Science, Polymer Edition* (2005) doi:10.1163/1568562053700174.

120. Wan Ngah, W. S. & Hanafiah, M. A. K. M. Removal of heavy metal ions from wastewater by chemically modified plant wastes as adsorbents: A review. *Bioresource Technology* **99**, 3935–3948 (2008).

121. Bailey, S. E., Olin, T. J., Bricka, R. M. & Adrian, D. D. A review of potentially low-cost sorbents for heavy metals. *Water Research* **33**, 2469–2479 (1999).

122. Zhang, Y. *et al.* Ion imprinted adsorbent for the removal of Ni(II) from waste water: preparation, characterization, and adsorption. (2019) doi:10.1080/01932691.2018.1538883.

123. Liu, B., Wang, D., Xu, Y. & Huang, G. Adsorption properties of Cd(II)-imprinted chitosan resin. *Journal of Materials Science* **46**, 1535–1541 (2011).

124. Wang, L. *et al.* Green multi-functional monomer based ion imprinted polymers for selective removal of copper ions from aqueous solution. *Journal of Colloid and Interface Science* **541**, 376–386 (2019).

125. Sun, S. & Wang, A. Adsorption properties and mechanism of cross-linked carboxymethyl-chitosan resin with Zn(II) as template ion. *Reactive and Functional Polymers* (2006) doi:10.1016/j.reactfunctpolym.2005.11.008.

126. Zhu, Y., Bai, Z., Luo, W., Wang, B. & Zhai, L. A facile ion imprinted synthesis of selective biosorbent for Cu2+ via microfluidic technology. *Journal of Chemical Technology and Biotechnology* (2017) doi:10.1002/jctb.5193.

127. Zhang, Y. *et al.* Ion imprinted adsorbent for the removal of Ni(II) from waste water: preparation, characterization, and adsorption. *Journal of Dispersion Science and Technology* **40**, 1751–1760 (2019).

128. Sun, S., Wang, L. & Wang, A. Adsorption properties of crosslinked carboxymethyl-chitosan resin with Pb(II) as template ions. *Journal of Hazardous Materials* **136**, 930–937 (2006).

129. Yoshida, W., Oshima, T., Baba, Y. & Goto, M. Cu(II)-imprinted chitosan derivative containing carboxyl groups for the selective removal of Cu(II) from aqueous solution. *Journal of Chemical Engineering of Japan* **49**, 630–634 (2016).

130. Rangel-Mendez, J. R., Monroy-Zepeda, R., Leyva-Ramos, E., Diaz-Flores, P. E. & Shirai, K. Chitosan selectivity for removing cadmium (II), copper (II), and lead (II) from aqueous phase: pH and organic matter effect. *Journal of Hazardous Materials* **162**, 503–511 (2009).

131. Yang, G. *et al.* Cd(II) removal from aqueous solution by adsorption on α-ketoglutaric acid-modified magnetic chitosan. *Applied Surface Science* **292**, 710–716 (2014).

132. Kamari, A., Pulford, I. D. & Hargreaves, J. S. J. Binding of heavy metal contaminants onto chitosans e An evaluation for remediation of metal contaminated soil and water. *Journal of Environmental Management* **92**, 2675–2682 (2011).

133. Repo, E., Warchol, J. K., Kurniawan, T. A. & Sillanpää, M. E. T. Adsorption of Co(II) and Ni(II) by EDTA- and/or DTPA-modified chitosan: Kinetic and equilibrium modeling. *Chemical Engineering Journal* **161**, 73–82 (2010).

134. Chen, A.-H., Yang, C.-Y., Chen, C.-Y., Chen, C.-Y. & Chen, C.-W. The chemically crosslinked metal-complexed chitosans for comparative adsorptions of Cu(II), Zn(II), Ni(II) and Pb(II) ions in aqueous medium. *J Hazard Mater* **163**, 1068–75 (2009).

135. Monier, M., Ayad, D. M., Wei, Y. & Sarhan, A. A. Adsorption of Cu(II), Co(II), and Ni(II) ions by modified magnetic chitosan chelating resin. *Journal of Hazardous Materials* **177**, 962–970 (2010).

136. Motaghi, H., Arabkhani, P., Parvinnia, M. & Asfaram, A. Simultaneous adsorption of cobalt ions, azo dye, and imidacloprid pesticide on the magnetic chitosan/activated carbon@UiO-66 bio-nanocomposite: Optimization, mechanisms, regeneration, and application. *Separation and Purification Technology* **284**, 120258 (2022).

137. Dragan, E. S. & Loghin, D. F. A. Fabrication and characterization of composite cryobeads based on chitosan and starches-g-PAN as efficient and reusable biosorbents for removal of Cu2+, Ni2+, and Co2+ ions. *Int J Biol Macromol* **120**, 1872–1883 (2018).

138. Zhang, Q., Zhuang, S. & Wang, J. Biosorptive removal of cobalt(II) from aqueous solutions using magnetic cyanoethyl chitosan beads. *Journal of Environmental Chemical Engineering* **8**, 104531 (2020).

139. Hadi, P., Xu, M., Ning, C., Sze Ki Lin, C. & McKay, G. A critical review on preparation, characterization and utilization of sludge-derived activated carbons for wastewater treatment. *Chemical Engineering Journal* (2015) doi:10.1016/j.cej.2014.08.088.

140. Agrawal, A. & Sahu, K. K. Kinetic and isotherm studies of cadmium adsorption on manganese nodule residue. *Journal of Hazardous Materials* **137**, 915–924 (2006).

141. Al-Ghouti, M. A. & Da'ana, D. A. Guidelines for the use and interpretation of adsorption isotherm models: A review. *Journal of Hazardous Materials* **393**, 122383 (2020).

142. Shaker, M. A. Thermodynamics and kinetics of bivalent cadmium biosorption onto nanoparticles of chitosan-based biopolymers. *J Taiwan Inst Chem Eng* **47**, 79–90 (2015).

143. Ahmaruzzaman, M. Industrial wastes as low-cost potential adsorbents for the treatment of wastewater laden with heavy metals. *Advances in Colloid and Interface Science* **166**, 36–59 (2011).

144. Gerente, C., Lee, V. K. C., Cloirec, P. Le & McKay, G. Application of Chitosan for the Removal of Metals From Wastewaters by Adsorption—Mechanisms and Models Review. *Critical Reviews in Environmental Science and Technology* **37**, 41–127 (2007).

145. Boddu, V. M., Abburi, K., Talbott, J. L. & Smith, E. D. Removal of hexavalent chromium from wastewater using a new composite chitosan biosorbent. *Environmental Science and Technology* **37**, 4449–4456 (2003).

146. Maleki, A., Pajootan, E. & Hayati, B. Ethyl acrylate grafted chitosan for heavy metal removal from wastewater: Equilibrium, kinetic and thermodynamic studies. *J Taiwan Inst Chem Eng* **51**, 127–134 (2015).

147. Miller, J. W. Adsorption Technology: A Step-by-Step Approach to Process Evaluation and Application. *Journal of Environment Quality* **15**, 94 (1986).

148. Miller, J. W. Adsorption Technology: A Step-by-Step Approach to Process Evaluation and Application. *Journal of Environment Quality* **15**, 94 (1986).

149. Hu, C., Zhu, P., Cai, M., Hu, H. & Fu, Q. Comparative adsorption of Pb(II), Cu(II) and Cd(II) on chitosan saturated montmorillonite: Kinetic, thermodynamic and equilibrium studies. *Applied Clay Science* **143**, 320–326 (2017).

150. Moosavian, M. A. & Moazezi, N. Removal of cadmium and zinc ions from industrial wastewater using nanocomposites of PANI/ZnO and PANI/CoHCF: a comparative study. *Desalination and Water Treatment* **57**, 20817–20836 (2016).

151. Heidari, A., Younesi, H., Mehraban, Z. & Heikkinen, H. Selective adsorption of Pb(II), Cd(II), and Ni(II) ions from aqueous solution using chitosan–MAA nanoparticles. *International Journal of Biological Macromolecules* **61**, 251–263 (2013).

152. Ngah, W. S. W. & Fatinathan, S. Adsorption characterization of Pb(II) and Cu(II) ions onto chitosan-tripolyphosphate beads: Kinetic, equilibrium and thermodynamic studies. *Journal of Environmental Management* **91**, 958–969 (2010).

153. Zhou, Y.-T., Branford-White, C., Nie, H.-L. & Zhu, L.-M. Adsorption mechanism of Cu2+ from aqueous solution by chitosan-coated magnetic nanoparticles modified with α-ketoglutaric acid. *Colloids and Surfaces B: Biointerfaces* **74**, 244–252 (2009).

154. Zur Theorie der sogenannten Adsorption gelöster Stoffe. *Zeitschrift für Chemie und Industrie der Kolloide* **2**, 15–15 (1907).

155. Ho, Y. S. & McKay, G. Pseudo-second order model for sorption processes. *Process Biochemistry* (1999) doi:10.1016/S0032-9592(98)00112-5.

156. Chien, S. H. & Clayton, W. R. Application of Elovich Equation to the Kinetics of Phosphate Release and Sorption in Soils1. *Soil Science Society of America Journal* (1980) doi:10.2136/sssaj1980.03615995004400020013x.

157. Langmuir, I. THE ADSORPTION OF GASES ON PLANE SURFACES OF GLASS, MICA AND PLATINUM. *J Am Chem Soc* **40**, 1361–1403 (1918).

158. Freundlich, H. M. F. Adsorption in solution. *Z. Phys. Chem.* (1906).

159. Brunauer, S., Emmett, P. H. & Teller, E. Adsorption of Gases in Multimolecular Layers. *J Am Chem Soc* (1938) doi:10.1021/ja01269a023.

160. Redlich, O. & Peterson, D. L. A useful adsorption isotherm. *Journal of Physical Chemistry* (1959) doi:10.1021/j150576a611.

161. Do, D. D. *Adsorption Analysis: Equilibria and Kinetics*. *Chemical Engineering* vol. 2 (Imperial College Press, 1998).

162. Vasconcelos, H. L., Guibal, E., Laus, R., Vitali, L. & Fávere, V. T. Competitive adsorption of Cu(II) and Cd(II) ions on spray-dried chitosan loaded with Reactive Orange 16. *Materials Science and Engineering C* **29**, 613–618 (2009).

163. Al-Asheh, S., Banat, F., Al-Omari, R. & Duvnjak, Z. Predictions of binary sorption isotherms for the sorption of heavy metals by pine bark using single isotherm data. *Chemosphere* **41**, 659–665 (2000).

164. Adamson, a W. & Gast, a P. *Physical Chemistry of Surfaces Sixth Edition*. *SubStance* (1997). doi:10.1149/1.2133374.

165. Fritz, W. & Schluender, E.-U. Simultaneous adsorption equilibria of organic solutes in dilute aqueous solutions on activated carbon. *Chemical Engineering Science* **29**, 1279–1282 (1974).

166. Bellot, J. C. & Condoret, J. S. Modelling of liquid chromatography equilibria. *Process Biochemistry* **28**, 365–376 (1993).

167. Choy, K. K. H., Porter, J. F. & McKay, G. Langmuir isotherm models applied to the multicomponent sorption of acid dyes from effluent onto activated carbon. *Journal of Chemical and Engineering Data* **45**, 575–584 (2000).

168. Abdulaziz, M. & Musayev, S. Multicomponent biosorption of heavy metals from aqueous solutions: A review. *Polish Journal of Environmental Studies* **26**, 1433–1441 (2017).

169. Kirkby, N. Gas Separation by Adsorption Processes. *Gas Separation & Purification* **2**, 41 (1988).

170. Salvador, F., Martin-Sanchez, N., Sanchez-Hernandez, R., Sanchez-Montero, M. J. & Izquierdo, C. Regeneration of carbonaceous adsorbents. Part I: Thermal Regeneration. *Microporous and Mesoporous Materials* (2015) doi:10.1016/j.micromeso.2014.02.045.

171. Salvador, F., Martin-Sanchez, N., Sanchez-Hernandez, R., Sanchez-Montero, M. J. & Izquierdo, C. Regeneration of carbonaceous adsorbents. Part II: Chemical, Microbiological and Vacuum Regeneration. *Microporous and Mesoporous Materials* (2015) doi:10.1016/j.micromeso.2014.08.019.

172. Vakili, M. *et al*. Regeneration of chitosan-based adsorbents used in heavy metal adsorption: A review. *Separation and Purification Technology* **224**, 373–387 (2019).

173. Vijayaraghavan, K. & Yun, Y. S. Bacterial biosorbents and biosorption. *Biotechnology Advances* (2008) doi:10.1016/j.biotechadv.2008.02.002.

174. Zhu, R., Zhu, J., Ge, F. & Yuan, P. Regeneration of spent organoclays after the sorption of organic pollutants: A review. *Journal of Environmental Management* (2009) doi:10.1016/j.jenvman.2009.06.015.

175. Sabio, E. *et al.* Thermal regeneration of activated carbon saturated with p-nitrophenol. *Carbon N Y* (2004) doi:10.1016/j.carbon.2004.05.007.

176. Momina, Shahadat, M. & Isamil, S. Regeneration performance of clay-based adsorbents for the removal of industrial dyes: A review. *RSC Advances* (2018) doi:10.1039/c8ra04290j.

177. Liao, B., Sun, W., Guo, N., Ding, S. & Su, S. Equilibriums and kinetics studies for adsorption of Ni(II) ion on chitosan and its triethylenetetramine derivative. *Colloids and Surfaces A: Physicochemical and Engineering Aspects* **501**, 32–41 (2016).

178. Fan, W. & Xu, Z. Biosorption of nickel ion by chitosan-immobilized brown algae Laminaria japonica. *Chemical and Biochemical Engineering Quarterly* (2011).

179. Iordache, M. L. *et al.* Magnetic chitosan grafted (alkyl acrylate) composite particles: Synthesis, characterization and evaluation as adsorbents. *Arabian Journal of Chemistry* **11**, 1032–1043 (2018).

180. Monier, M., Ayad, D. M. & Abdel-Latif, D. A. Adsorption of Cu(II), Cd(II) and Ni(II) ions by cross-linked magnetic chitosan-2-aminopyridine glyoxal Schiff's base. *Colloids and Surfaces B: Biointerfaces* **94**, 250–258 (2012).

181. Futalan, C. M. *et al.* Copper, nickel and lead adsorption from aqueous solution using chitosan-immobilized on bentonite in a ternary system. *Sustainable Environment Research* (2012).

182. Laus, R. & De Fávere, V. T. Competitive adsorption of Cu(II) and Cd(II) ions by chitosan crosslinked with epichlorohydrin-triphosphate. *Bioresource Technology* **102**, 8769–8776 (2011).

183. Wu, S. *et al.* Fabrication of xanthate-modified chitosan/poly(N-isopropylacrylamide) composite hydrogel for the selective adsorption of Cu(II), Pb(II) and Ni(II) metal ions. *Chemical Engineering Research and Design* **139**, 197–210 (2018).

184. Petrova, Y. S., Kapitanova, E. I., Neudachina, L. K. & Pestov, A. V. Sorption isotherms of metal ions onto an N-(2-sulfoethyl)chitosan-based material from single- and multi-component solutions. *Separation Science and Technology (Philadelphia)* **52**, 2385–2394 (2017).

185. Humelnicu, D. *et al.* Removal of heavy metal ions from multi-component aqueous solutions by eco-friendly and low-cost composite sorbents with anisotropic pores. *Journal of Hazardous Materials* **381**, 120980 (2020).

186. Kong, A. *et al.* A novel route for the removal of Cu(II) and Ni(II) ions via homogeneous adsorption by chitosan solution. *Journal of Cleaner Production* **192**, 801–808 (2018).

187. Deng, J. *et al.* Competitive adsorption of Pb(II), Cd(II) and Cu(II) onto chitosan-pyromellitic dianhydride modified biochar. *Journal of Colloid and Interface Science* **506**, 355–364 (2017).

188. Cai, Y., Zheng, L. & Fang, Z. Selective adsorption of Cu(<scp>ii</scp>) from an aqueous solution by ion imprinted magnetic chitosan microspheres prepared from steel pickling waste liquor. *RSC Advances* **5**, 97435–97445 (2015).

189. Montazer-Rahmati, M. M., Rabbani, P., Abdolali, A. & Keshtkar, A. R. Kinetics and equilibrium studies on biosorption of cadmium, lead, and nickel ions from aqueous solutions by intact and chemically modified brown algae. *Journal of Hazardous Materials* **185**, 401–407 (2011).

190. Ghosh, D., Saha, R., Ghosh, A., Nandi, R. & Saha, B. A review on toxic cadmium biosorption from contaminated wastewater. *Desalination and Water Treatment* **53**, 413–420 (2015).

191. Purkayastha, D., Mishra, U. & Biswas, S. A comprehensive review on Cd(II) removal from aqueous solution. *Journal of Water Process Engineering* **2**, 105–128 (2014).

192. Xu, L. *et al.* Fast and effective removal of cadmium ion from water using chitosan encapsulated magnetic Fe3O4 nanoparticles. *Desalination and Water Treatment* (2016) doi:10.1080/19443994.2015.1019369.

193. Fu, F. & Wang, Q. Removal of heavy metal ions from wastewaters: A review. *Journal of Environmental Management* **92**, 407–418 (2011).

194. Abdalbake, M. & Shino, O. Removing the cadmium, arsenic and sulfate ions from wet process phosphoric acid. *Periodica Polytechnica Chemical Engineering* (2004).

195. Kaewsarn, P. & Yu, Q. Cadmium(II) removal from aqueous solutions by pre-treated biomass of marine alga Padina sp. *Environmental Pollution* (2001) doi:10.1016/S0269-7491(00)00114-7.

196. Mohammadi, A., Ataie, A. & Sheibani, S. Chromium (VI) ions adsorption onto barium hexaferrite magnetic nano-adsorbent. *Advanced Materials Letters* **7**, 579–586 (2016).

197. Rahangdale, D. & Kumar, A. Acrylamide grafted chitosan based ion imprinted polymer for the recovery of cadmium from nickel-cadmium battery waste. *Journal of Environmental Chemical Engineering* **6**, 1828–1839 (2018).

198. Carolin, C. F., Kumar, P. S., Saravanan, A., Joshiba, G. J. & Naushad, M. Efficient techniques for the removal of toxic heavy metals from aquatic environment: A review. *Journal of Environmental Chemical Engineering* **5**, 2782–2799 (2017).

199. Ali, I., Asim, M. & Khan, T. A. Low cost adsorbents for the removal of organic pollutants from wastewater. *Journal of Environmental Management* **113**, 170–183 (2012).

200. Plaza Cazón, J., Viera, M., Donati, E. & Guibal, E. Zinc and cadmium removal by biosorption on Undaria pinnatifida in batch and continuous processes. *Journal of Environmental Management* **129**, 423–434 (2013).

201. Zeng, L. *et al.* Adsorption of Cd(II), Cu(II) and Ni(II) ions by cross-linking chitosan/rectorite nano-hybrid composite microspheres. *Carbohydrate Polymers* **130**, 333–343 (2015).

202. Zhao, F., Repo, E., Yin, D. & Sillanpää, M. E. T. Adsorption of Cd(II) and Pb(II) by a novel EGTA-modified chitosan material: Kinetics and isotherms. *Journal of Colloid and Interface Science* **409**, 174–182 (2013).

203. Rouibah, K., Meniai, A. H., Rouibah, M. T., Deffous, L. & Lehocine, M. B. Chromium VI and cadmium II removal from aqueous solutions by olive stones. *Desalination and Water Treatment* (2010) doi:10.5004/dwt.2010.1690.

204. Singh, K. K., Rastogi, R. & Hasan, S. H. Removal of cadmium from wastewater using agricultural waste "rice polish." *Journal of Hazardous Materials* (2005) doi:10.1016/j.jhazmat.2004.11.002.

205. Awwad, N. S., Daifuallah, A. A. M. & Ali, M. M. S. Removal of Pb2+, Cd2+, Fe3+, and Sr2+ from aqueous solution by selected activated carbons derived from date pits. *Solvent Extraction and Ion Exchange* (2008) doi:10.1080/07366290802497990.

206. Vimala, R. & Das, N. Biosorption of cadmium (II) and lead (II) from aqueous solutions using mushrooms: A comparative study. *Journal of Hazardous Materials* (2009) doi:10.1016/j.jhazmat.2009.02.062.

207. Nessim, R. B., Bassiouny, A. R., Zaki, H. R., Moawad, M. N. & Kandeel, K. M. Biosorption of lead and cadmium using marine algae. *Chemistry and Ecology* (2011) doi:10.1080/02757540.2011.607439.

208. Wan Ngah, W. S., Teong, L. C. & Hanafiah, M. A. K. M. Adsorption of dyes and heavy metal ions by chitosan composites: A review. *Carbohydrate Polymers* **83**, 1446–1456 (2011).

209. Crini, G. Non-conventional low-cost adsorbents for dye removal: A review. *Bioresource Technology* (2006) doi:10.1016/j.biortech.2005.05.001.

210. Pillai, C. K. S., Paul, W. & Sharma, C. P. Chitin and chitosan polymers: Chemistry, solubility and fiber formation. *Progress in Polymer Science (Oxford)* **34**, 641–678 (2009).

211. Monier, M. & Abdel-Latif, D. A. Preparation of cross-linked magnetic chitosan-phenylthiourea resin for adsorption of Hg(II), Cd(II) and Zn(II) ions from aqueous solutions. *Journal of Hazardous Materials* **209–210**, 240–249 (2012).

212. Xu, L. *et al.* Fast and effective removal of cadmium ion from water using chitosan encapsulated magnetic Fe $_3$ O $_4$ nanoparticles. *Desalination and Water Treatment* **57**, 1–9 (2015).

213. Mahaninia, M. H. & Wilson, L. D. Modular Cross-Linked Chitosan Beads with Calcium Doping for Enhanced Adsorptive Uptake of Organophosphate Anions. *Industrial & Engineering Chemistry Research* **55**, 11706–11715 (2016).

214. Sureshkumar, M. K., Das, D., Mallia, M. B. & Gupta, P. C. Adsorption of uranium from aqueous solution using chitosan-tripolyphosphate (CTPP) beads. *Journal of Hazardous Materials* **184**, 65–72 (2010).

215. Ding, Y. & Sartaj, M. Statistical analysis and optimization of ammonia removal from aqueous solution by zeolite using factorial design and response surface methodology. *Journal of Environmental Chemical Engineering* **3**, 807–814 (2015).

216. Aydin, Y. A. & Aksoy, N. D. Adsorption of chromium on chitosan: Optimization, kinetics and thermodynamics. *Chemical Engineering Journal* **151**, 188–194 (2009).

217. Mi, F.-L., Shyu, S.-S., Lee, S.-T. & Wong, T. B. Kinetic Study of Chitosan Tripolyphosphate Complex Reaction and Acid-Resistive Properties of the Chitosan Tripolyphosphate Gel Beads Prepared by in-Liquid Curing Method . *Journal of Polymer Science: Part B: Polymer Physics*, **37**, 1551–1564 (1999).

218. Annadurai, G. Design of optimum response surface experiments for adsorption of direct dye on chitosan. *Bioprocess Engineering* **23**, 451–455 (2000).

219. Salah, T. A., Mohammad, A. M., Hassan, M. A. & El-Anadouli, B. E. Development of nano-hydroxyapatite/chitosan composite for cadmium ions removal in wastewater treatment. *J Taiwan Inst Chem Eng* (2014) doi:10.1016/j.jtice.2013.10.008.

220. Ren, Y., Abbood, H. A., He, F., Peng, H. & Huang, K. Magnetic EDTA-modified chitosan/SiO2/Fe3O4 adsorbent: Preparation, characterization, and application in heavy metal adsorption. *Chemical Engineering Journal* **226**, 300–311 (2013).

221. Hydari, S., Sharififard, H., Nabavinia, M. & Parvizi, M. reza. A comparative investigation on removal performances of commercial activated carbon, chitosan biosorbent and chitosan/activated carbon composite for cadmium. *Chemical Engineering Journal* **193–194**, 276–282 (2012).

222. Pal, P. & Pal, A. Surfactant-modified chitosan beads for cadmium ion adsorption. *International Journal of Biological Macromolecules* **104**, 1548–1555 (2017).

223. Saeed, A., Iqbal, M. & Akhtar, M. W. Removal and recovery of lead(II) from single and multimetal (Cd, Cu, Ni, Zn) solutions by crop milling waste (black gram husk). *Journal of Hazardous Materials* **117**, 65–73 (2005).

224. Moussout, H., Ahlafi, H., Aazza, M. & Bourakhouadar, M. Kinetics and mechanism of the thermal degradation of biopolymers chitin and chitosan using thermogravimetric analysis. *Polymer Degradation and Stability* (2016) doi:10.1016/j.polymdegradstab.2016.05.016.

225. Dahmane, E. M., Taourirte, M., Eladlani, N. & Rhazi, M. Extraction and Characterization of Chitin and Chitosan from Parapenaeus longirostris from Moroccan Local Sources. *International Journal of Polymer Analysis and Characterization* (2014) doi:10.1080/1023666X.2014.902577.

226. Aydın, H., Yerlikaya, Ç. & Uzan, S. Equilibrium and kinetic studies of copper (II) ion uptake by modified wheat shells. *Desalination and Water Treatment* **44**, 296–305 (2012).

227. Laus, R., Costa, T. G., Szpoganicz, B. & Fávere, V. T. Adsorption and desorption of Cu(II), Cd(II) and Pb(II) ions using chitosan crosslinked with epichlorohydrin-triphosphate as the adsorbent. *Journal of Hazardous Materials* **183**, 233–241 (2010).

228. Sila, A., Mlaik, N., Sayari, N., Balti, R. & Bougatef, A. Chitin and Chitosan Extracted from Shrimp Waste Using Fish Proteases Aided Process: Efficiency of Chitosan in the Treatment of Unhairing Effluents. *Journal of Polymers and the Environment* **22**, 78–87 (2014).

229. Li, X. *et al.* Studies of heavy metal ion adsorption on Chitosan/Sulfydryl-functionalized graphene oxide composites. *Journal of Colloid and Interface Science* **448**, 389–397 (2015).

230. Matet, M., Heuzey, M. C., Pollet, E., Ajji, A. & Avérous, L. Innovative thermoplastic chitosan obtained by thermo-mechanical mixing with polyol plasticizers. *Carbohydrate Polymers* (2013) doi:10.1016/j.carbpol.2013.02.052.

231. Jingou, J. *et al.* Preparation, characterization of hydrophilic and hydrophobic drug in combine loaded chitosan/cyclodextrin nanoparticles and in vitro release study. *Colloids and Surfaces B: Biointerfaces* (2011) doi:10.1016/j.colsurfb.2010.11.005.

232. Bhumkar, D. R. & Pokharkar, V. B. Studies on effect of pH on cross-linking of chitosan with sodium tripolyphosphate: A technical note. *AAPS PharmSciTech* **7**, E138–E143 (2006).

233. Horsfall, M., Abia, A. A. & Spiff, A. I. Kinetic studies on the adsorption of Cd2+, Cu2+ and Zn2+ ions from aqueous solutions by cassava (Manihot sculenta Cranz) tuber bark waste. *Bioresource Technology* (2006) doi:10.1016/j.biortech.2005.02.016.

234. Kołodyńska, D. Adsorption characteristics of chitosan modified by chelating agents of a new generation. *Chemical Engineering Journal* **179**, 33–43 (2012).

235. Dubinin, M. M. The potential theory of adsorption of gases and vapors for adsorbents with energetically nonuniform surfaces. *Chemical Reviews* (1960) doi:10.1021/cr60204a006.

236. Edwards, A. Decontamination of nebulisers. *Nurs Times* **97**, III–IV (2012).

237. Guibal, E., Dambies, L., Milot, C. & Roussy, J. Influence of polymer structural parameters and experimental conditions on metal anion sorption by chitosan. *Polymer International* **48**, 671–680 (1999).

238. Xu, C. *et al.* Adsorption of uranium by amidoximated chitosan-grafted polyacrylonitrile, using response surface methodology. *Carbohydrate Polymers* **121**, 79–85 (2015).

239. Ding, Y. & Sartaj, M. Optimization of ammonia removal by ion-exchange resin using response surface methodology. *International Journal of Environmental Science and Technology* **13**, 985–994 (2016).

240. Chen, Y. *et al.* Understanding the adsorption mechanism of Ni(II) on graphene oxides by batch experiments and density functional theory studies. *Science China Chemistry* **59**, 412–419 (2016).

241. Guohua, Y., Elshkaki, A. & Xiao, X. Dynamic analysis of future nickel demand, supply, and associated materials, energy, water, and carbon emissions in China. *Resources Policy* **74**, 102432 (2021).

242. Nancharaiah, Y. V., Venkata Mohan, S. & Lens, P. N. L. Metals removal and recovery in bioelectrochemical systems: A review. *Bioresource Technology* **195**, 102–114 (2015).

243. Noori, M., Rashchi, F., Babakhani, A. & Vahidi, E. Selective recovery and separation of nickel and vanadium in sulfate media using mixtures of D2EHPA and Cyanex 272. *Separation and Purification Technology* **136**, 265–273 (2014).

244. Saad, A. H. A., Azzam, A. M., El-Wakeel, S. T., Mostafa, B. B. & Abd El-latif, M. B. Removal of toxic metal ions from wastewater using ZnO@Chitosan core-shell nanocomposite. *Environmental Nanotechnology, Monitoring & Management* **9**, 67–75 (2018).

245. Saleh, T. A., Mustaqeem, M. & Khaled, M. Developing water treatment technologies in removing heavy metals from wastewater: A review. *Environmental Nanotechnology, Monitoring & Management* 100617 (2021) doi:10.1016/j.enmm.2021.100617.

246. Barakat, M. A. New trends in removing heavy metals from industrial wastewater. *Arabian Journal of Chemistry* **4**, 361–377 (2011).

247. Vardhan, K. H., Kumar, P. S. & Panda, R. C. A review on heavy metal pollution, toxicity and remedial measures: Current trends and future perspectives. *Journal of Molecular Liquids* **290**, 111197 (2019).

248. Al-Omair, M. A. & El-Sharkawy, E. A. Removal of Heavy Metals Via Adsorption on Activated Carbon Synthesized from Solid Wastes. *Environmental Technology* **28**, 443–451 (2007).

249. Mohd Yusof, A., Ahmad Nizam Nik Malek, N., Asyikin Kamaruzaman, N. & Adil, M. Environmental Technology Removal of Ca 2+ and Zn 2+ from aqueous solutions by zeolites NaP and KP. (2010) doi:10.1080/09593330903313794.

250. Santos, O. S. *et al.* The use of sugar and alcohol industry waste in the adsorption of potentially toxic metals. *Environmental Technology* **37**, 279–291 (2016).

251. Mudhoo, A., Garg, V. K. & Wang, S. Removal of heavy metals by biosorption. *Environmental Chemistry Letters* **10**, 109–117 (2012).

252. Vieira, T. *et al.* Chitosan-based hydrogels for the sorption of metals and dyes in water: isothermal, kinetic, and thermodynamic evaluations. *Colloid and Polymer Science* **299**, 649–662 (2021).

253. Ahmed, S. & Ikram, S. *Chitosan: Derivatives, Composites and Applications*. (2017). doi:10.1002/9781119364849.

254. Xu, L. *et al.* Simultaneous removal of cadmium, zinc and manganese using electrocoagulation: Influence of operating parameters and electrolyte nature. *Journal of Environmental Management* **204**, 394–403 (2017).

255. Ge, H., Hua, T. & Chen, X. Selective adsorption of lead on grafted and crosslinked chitosan nanoparticles prepared by using Pb2+ as template. *Journal of Hazardous Materials* **308**, 225–232 (2016).

256. Şahan, T. Application of RSM for Pb(II) and Cu(II) adsorption by bentonite enriched with SH groups and a binary system study. *Journal of Water Process Engineering* **31**, 100867 (2019).

257. Marzouk Trifi, I., Trifi, B., ben Souissi, E. & Hamrouni, B. Response surface methodology for dyes removal by adsorption onto alginate calcium. *https://doi.org/10.1080/09593330.2019.1612470* **41**, 3473–3482 (2019).

258. Çiçek, E., Cojocaru, C., Zakrzewska-Trznadel, G., Harasimowicz, M. & Miskiewicz, A. Response surface methodology for the modelling of 85Sr adsorption on zeolite 3A and pumice. *http://dx.doi.org/10.1080/09593330.2010.549514* **33**, 51–59 (2011).

259. Naga Babu, A., Raja Sree, T., Srinivasa Reddy, D., Suresh Kumar, G. & Krishna Mohan, G. v. Experimental and statistical analysis of As(III) adsorption from contaminated water using activated red mud doped calcium-alginate beads. *https://doi.org/10.1080/09593330.2019.1681520* **42**, 1810–1825 (2019).

260. Sips, R. On the Structure of a Catalyst Surface. *The Journal of Chemical Physics* **16**, 490–495 (1948).

261. Hoseinian, F. S., Rezai, B., Kowsari, E. & Safari, M. A hybrid neural network/genetic algorithm to predict Zn(II) removal by ion flotation. *Separation Science and Technology* **55**, 1197–1206 (2020).

262. Biswas, S., Sharma, S., Mukherjee, S., Meikap, B. C. & Sen, T. K. Process modelling and optimization of a novel Semifluidized bed adsorption column operation for aqueous phase divalent heavy metal ions removal. *Journal of Water Process Engineering* **37**, 101406 (2020).

263. Rasoulzadeh, H. *et al.* Parametric modelling of Pb(II) adsorption onto chitosan-coated Fe3O4 particles through RSM and DE hybrid evolutionary optimization framework. *Journal of Molecular Liquids* **297**, 111893 (2020).

264. Dong, S. & Sartaj, M. Statistical analysis and optimization of ammonia removal from landfill leachate by sequential microwave/aeration process using factorial design and response surface methodology. *Journal of Environmental Chemical Engineering* **4**, 100–108 (2016).

265. Chen, A.-H., Liu, S.-C., Chen, C.-Y. & Chen, C.-Y. Comparative adsorption of Cu(II), Zn(II), and Pb(II) ions in aqueous solution on the crosslinked chitosan with epichlorohydrin. *Journal of Hazardous Materials* **154**, 184–191 (2008).

266. Zhang, Y. *et al.* Ion imprinted adsorbent for the removal of Ni(II) from waste water: preparation, characterization, and adsorption. *Journal of Dispersion Science and Technology* **40**, 1751–1760 (2019).

267. Mishra, S. & Tripathi, A. Adsorptive removal of Pb(II) via green route using magnetic iron nanoparticle sprinkled graphene oxide-chitosan beads in aqueous medium. *Environmental Nanotechnology, Monitoring & Management* **17**, 100632 (2022).

268. Sethy, T. R., Pradhan, A. K. & Sahoo, P. K. Simultaneous studies on kinetics, bio-adsorption behaviour of chitosan grafted thin film nanohydrogel for removal of hazardous metal ion from water. *Environmental Nanotechnology, Monitoring & Management* **12**, 100262 (2019).

269. Babakhani, A. & Sartaj, M. Competitive adsorption of nickel(II) and cadmium(II) ions by chitosan cross-linked with sodium tripolyphosphate. *Chemical Engineering Communications* 1–19 (2021) doi:10.1080/00986445.2021.1966424.

270. Moeini, A. *et al.* Effect of pH and TPP concentration on chemico-physical properties, release kinetics and antifungal activity of Chitosan-TPP-Ungeremine microbeads. *Carbohydr Polym* **195**, 631–641 (2018).

271. Rouhi Broujeni, B., Nilchi, A. & Azadi, F. Adsorption modeling and optimization of thorium (IV) ion from aqueous solution using chitosan/TiO2 nanocomposite: Application of artificial neural network and genetic algorithm. *Environmental Nanotechnology, Monitoring & Management* **15**, 100400 (2021).

272. Qu, J. *et al.* Multi-component adsorption of Pb(II), Cd(II) and Ni(II) onto microwave-functionalized cellulose: Kinetics, isotherms, thermodynamics, mechanisms and application for electroplating wastewater purification. *Journal of Hazardous Materials* **387**, 121718 (2020).

273. Cheraghipour, E. & Pakshir, M. Environmentally friendly magnetic chitosan nano-biocomposite for Cu(II) ions adsorption and magnetic nano-fluid hyperthermia: CCD-RSM design. *Journal of Environmental Chemical Engineering* **9**, 104883 (2021).

274. VIJAYARAGHAVAN, K., PADMESH, T., PALANIVELU, K. & VELAN, M. Biosorption of nickel(II) ions onto Sargassum wightii: Application of two-parameter and three-parameter isotherm models. *Journal of Hazardous Materials* **133**, 304–308 (2006).

275. Hamza, M. F., Wei, Y., Mira, H. I., Abdel-Rahman, A. A. H. & Guibal, E. Synthesis and adsorption characteristics of grafted hydrazinyl amine magnetite-chitosan for Ni(II) and Pb(II) recovery. *Chemical Engineering Journal* **362**, 310–324 (2019).

276. Eser, A., Nüket Tirtom, V., Aydemir, T., Becerik, S. & Dinçer, A. Removal of nickel(II) ions by histidine modified chitosan beads. *Chemical Engineering Journal* **210**, 590–596 (2012).

277. Tirtom, V. N., Dinçer, A., Becerik, S., Aydemir, T. & Çelik, A. Comparative adsorption of Ni(II) and Cd(II) ions on epichlorohydrin crosslinked chitosan–clay composite beads in aqueous solution. *Chemical Engineering Journal* **197**, 379–386 (2012).

278. Liu, W. *et al.* Preparation of Surface Ion-Imprinted Materials Based on Modified Chitosan for Highly Selective Recognition and Adsorption of Nickel Ions in Aqueous Solutions. *Industrial & Engineering Chemistry Research* **59**, 6033–6042 (2020).

279. Kameda, T., Honda, R., Kumagai, S., Saito, Y. & Yoshioka, T. Adsorption of Cu2+ and Ni2+ by tripolyphosphate-crosslinked chitosan-modified montmorillonite. *Journal of Solid State Chemistry* **277**, 143–148 (2019).

280. Peligro, F. R., Pavlovic, I., Rojas, R. & Barriga, C. Removal of heavy metals from simulated wastewater by in situ formation of layered double hydroxides. *Chemical Engineering Journal* **306**, 1035–1040 (2016).

281. Papageorgiou, S. K., Katsaros, F. K., Kouvelos, E. P. & Kanellopoulos, N. K. Prediction of binary adsorption isotherms of Cu2+, Cd2+ and Pb2+ on calcium alginate beads from single adsorption data. *Journal of Hazardous Materials* **162**, 1347–1354 (2009).

282. Denkhaus, E. & Salnikow, K. Nickel essentiality, toxicity, and carcinogenicity. *Critical Reviews in Oncology/Hematology* **42**, 35–56 (2002).

283. Godt, J. *et al.* The toxicity of cadmium and resulting hazards for human health. *Journal of Occupational Medicine and Toxicology* **1**, (2006).

284. Randhawa, N. S., Gharami, K. & Kumar, M. Leaching kinetics of spent nickel–cadmium battery in sulphuric acid. *Hydrometallurgy* **165**, 191–198 (2016).

285. Brahmi, K. *et al.* Treatment of heavy metal polluted industrial wastewater by a new water treatment process: ballasted electroflocculation. *Journal of Hazardous Materials* **344**, 968–980 (2018).

286. Landaburu-Aguirre, J., Pongrácz, E., Perämäki, P. & Keiski, R. L. Micellar-enhanced ultrafiltration for the removal of cadmium and zinc: Use of response surface methodology to improve understanding of process performance and optimisation. *Journal of Hazardous Materials* **180**, 524–534 (2010).

287. Chang, Q. & Wang, G. Study on the macromolecular coagulant PEX which traps heavy metals. *Chemical Engineering Science* **62**, 4636–4643 (2007).

288. Polat, H. & Erdogan, D. Heavy metal removal from waste waters by ion flotation. *Journal of Hazardous Materials* **148**, 267–273 (2007).

289. Kabdaşlı, I., Arslan, T., Ölmez-Hancı, T., Arslan-Alaton, I. & Tünay, O. Complexing agent and heavy metal removals from metal plating effluent by electrocoagulation with stainless steel electrodes. *Journal of Hazardous Materials* **165**, 838–845 (2009).

290. Provazi, K., Campos, B. A., Espinosa, D. C. R. & Tenório, J. A. S. Metal separation from mixed types of batteries using selective precipitation and liquid–liquid extraction techniques. *Waste Management* **31**, 59–64 (2011).

291. Thakur, A. K. *et al.* Polyethylenimine-modified mesoporous silica adsorbent for simultaneous removal of Cd(II) and Ni(II) from aqueous solution. *Journal of Industrial and Engineering Chemistry* **49**, 133–144 (2017).

292. Luo, X. *et al.* Synergic adsorption of acid blue 80 and heavy metal ions (Cu2+/Ni2+) onto activated carbon and its mechanisms. *Journal of Industrial and Engineering Chemistry* **27**, 164–174 (2015).

293. Hong, M. *et al.* Heavy metal adsorption with zeolites: The role of hierarchical pore architecture. *Chemical Engineering Journal* **359**, 363–372 (2019).

294. Khaligh, N. G. & Johan, M. R. Recent Application of the Various Nanomaterials and Nanocatalysts for the Heavy Metals' Removal from Wastewater. *Nano* **13**, 1830006 (2018).

295. Georgieva, V. G., Tavlieva, M. P., Genieva, S. D. & Vlaev, L. T. Adsorption kinetics of Cr(VI) ions from aqueous solutions onto black rice husk ash. *Journal of Molecular Liquids* **208**, 219–226 (2015).

296. Yang, S. *et al.* Mono/competitive adsorption of Arsenic(III) and Nickel(II) using modified green tea waste. *J Taiwan Inst Chem Eng* **60**, 213–221 (2016).

297. Khawar, A., Aslam, Z., Javed, S. & Abbas, A. Pb (II) biosorption using DAP / EDTA-modified biopolymer (Chitosan). *Chemical Engineering Communications* **205**, 1555–1567 (2018).

298. Muzzarelli, R. Chitin and chitosan as chromatographic supports and adsorbents for collection of metal ions from organic and aqueous solutions and sea-water. *Talanta* **16**, 1571–1577 (1969).

299. Xiao, X., Yu, Y., Sun, Y., Zheng, X. & Chen, A. Heavy metal removal from aqueous solutions by chitosan-based magnetic composite flocculants. *Journal of Environmental Sciences* **108**, 22–32 (2021).

300. Song, X., Li, L., Zhou, L. & Chen, P. Magnetic thiolated / quaternized-chitosan composites design and application for various heavy metal ions removal , including cation and anion. *Chemical Engineering Research and Design* **136**, 581–592 (2018).

301. Ebisike, K., Okoronkwo, A. E. & Alaneme, K. K. Adsorption of Cd (II) on chitosan–silica hybrid aerogel from aqueous solution. *Environmental Technology and Innovation* (2019) doi:10.1016/j.eti.2019.100337.

302. Duan, L. *et al.* Removal of Copper and Lead from Aqueous Solution by Adsorption onto Cross-Linked Chitosan/Montmorillonite Nanocomposites in the Presence of Hydroxyl–Aluminum Oligomeric Cations: Equilibrium, Kinetic, and Thermodynamic Studies. *Chemical Engineering Communications* **203**, 28–36 (2016).

303. Premakshi, H. G., Ramesh, K. & Kariduraganavar, M. Y. Modification of crosslinked chitosan membrane using NaY zeolite for pervaporation separation of water – isopropanol mixtures. *Chemical Engineering Research and Design* **94**, 32–43 (2014).

304. Laus, R. *et al.* Competitive adsorption of Cu(II) and Cd(II) ions by chitosan crosslinked with epichlorohydrin-triphosphate. *Bioresource Technology* **102**, 8769–8776 (2011).

305. Liu, T., Yang, X., Wang, Z. L. & Yan, X. Enhanced chitosan beads-supported Fe0-nanoparticles for removal of heavy metals from electroplating wastewater in permeable reactive barriers. *Water Research* **47**, 6691–6700 (2013).

306. Radke, C. J. & Prausnitz, J. M. Thermodynamics of multi-solute adsorption from dilute liquid solutions. *AIChE Journal* (1972) doi:10.1002/aic.690180417.

307. Mirzaei, A., Chen, Z., Haghighat, F. & Yerushalmi, L. Enhanced adsorption of anionic dyes by surface fluorination of zinc oxide: A straightforward method for numerical solving of the ideal adsorbed solution theory (IAST). *Chemical Engineering Journal* **330**, 407–418 (2017).

308. Chemical Equilibrium Diagrams | KTH. https://www.kth.se/che/medusa/.

309. Das, D., Sureshkumar, M. K., Radhakrishnan, K., Nuwar, J. & Pillai, C. G. S. Adsorptive removal of Cr(III) from aqueous solution using tripolyphosphate cross-linked chitosan beads. *Journal of Radioanalytical and Nuclear Chemistry* **289**, 275–285 (2011).

310. Wang, Q. *et al.* The adsorption behavior of metals in aqueous solution by microplastics effected by UV radiation. *Journal of Environmental Sciences* **87**, 272–280 (2019).

311. Tirtom, V. N., Dinçer, A., Becerik, S., Aydemir, T. & Çelik, A. Comparative adsorption of Ni(II) and Cd(II) ions on epichlorohydrin crosslinked chitosan–clay composite beads in aqueous solution. *Chemical Engineering Journal* **197**, 379–386 (2012).

312. Srivastava, V. C., Mall, I. D. & Mishra, I. M. Competitive adsorption of cadmium(II) and nickel(II) metal ions from aqueous solution onto rice husk ash. *Chemical Engineering and Processing: Process Intensification* **48**, 370–379 (2009).

313. Srivastava, V. C., Mall, I. D. & Mishra, I. M. Modelling individual and competitive adsorption of cadmium(II) and zinc(II) metal ions from aqueous solution onto bagasse fly ash. *Separation Science and Technology* **41**, 2685–2710 (2006).

314. Hilbrandt, I., Lehmann, V., Zietzschmann, F., Ruhl, A. S. & Jekel, M. Quantification and isotherm modelling of competitive phosphate and silicate adsorption onto micro-sized granular ferric hydroxide. *RSC Advances* **9**, 23642–23651 (2019).

315. Mende, M., Schwarz, D., Steinbach, C., Boldt, R. & Schwarz, S. Simultaneous adsorption of heavy metal ions and anions from aqueous solutions on chitosan—Investigated by spectrophotometry and SEM-EDX analysis. *Colloids and Surfaces A: Physicochemical and Engineering Aspects* **510**, 275–282 (2016).

316. Wang, X. S., Miao, H. H., He, W. & Shen, H. L. Competitive adsorption of Pb(II), Cu(II), and Cd(II) ions on wheat-residue derived black carbon. *Journal of Chemical and Engineering Data* **56**, 444–449 (2011).

317. Şengil, İ. A. & Özacar, M. Competitive biosorption of Pb2+, Cu2+ and Zn2+ ions from aqueous solutions onto valonia tannin resin. *Journal of Hazardous Materials* **166**, 1488–1494 (2009).

318. Padilla-Ortega, E., Leyva-Ramos, R. & Flores-Cano, J. V. Binary adsorption of heavy metals from aqueous solution onto natural clays. *Chemical Engineering Journal* **225**, 535–546 (2013).

319. Martín-Lara, M. A., Blázquez, G., Calero, M., Almendros, A. I. & Ronda, A. Binary biosorption of copper and lead onto pine cone shell in batch reactors and in fixed bed columns. *International Journal of Mineral Processing* (2016) doi:10.1016/j.minpro.2016.01.017.

320. Borhade, A. V., Kshirsagar, T. A., Dholi, A. G. & Agashe, J. A. Removal of Heavy Metals Cd 2+ , Pb 2+ , and Ni 2+ From Aqueous Solutions Using Synthesized Azide Cancrinite, Na 8 [AlSiO 4] 6 (N 3) 2.4 (H 2 O) 4.6. *Journal of Chemical & Engineering Data* **60**, 586–593 (2015).

321. Guo, H. *et al.* Separation of Cd(II) and Ni(II) in a binary mixture through competitive adsorption and acid leaching. *RSC Advances* **5**, 92885–92892 (2015).

322. Pelekani, C. & Snoeyink, V. L. Competitive adsorption in natural water: role of activated carbon pore size. *Water Research* **33**, 1209–1219 (1999).

323. Oyetade, O. A., Nyamori, V. O., Jonnalagadda, S. B. & Martincigh, B. S. Removal of Cd2+ and Hg2+ from aqueous solutions by adsorption onto nitrogen-functionalized carbon nanotubes. *Desalination and Water Treatment* **108**, 253–267 (2018).

324. Villarín, M. C. & Merel, S. Paradigm shifts and current challenges in wastewater management. *Journal of Hazardous Materials* **390**, 122139 (2020).

325. Zambrano-Monserrate, M. A., Ruano, M. A. & Sanchez-Alcalde, L. Indirect effects of COVID-19 on the environment. *Science of The Total Environment* **728**, 138813 (2020).

326. Joseph, L., Jun, B.-M., Flora, J. R. V., Park, C. M. & Yoon, Y. Removal of heavy metals from water sources in the developing world using low-cost materials: A review. *Chemosphere* **229**, 142–159 (2019).

327. Kim, J.-J., Kim, Y.-S. & Kumar, V. Heavy metal toxicity: An update of chelating therapeutic strategies. *Journal of Trace Elements in Medicine and Biology* **54**, 226–231 (2019).

328. Wang, Q. *et al.* Non-thermal plasma oxidation of Cu(II)-EDTA and simultaneous Cu(II) elimination by chemical precipitation. *Journal of Environmental Management* **248**, 109237 (2019).

329. Zou, Z. *et al.* A modified coagulation-ultrafiltration process for silver nanoparticles removal and membrane fouling mitigation: The role of laminarin. *International Journal of Biological Macromolecules* **172**, 241–249 (2021).

330. Bashir, A. *et al.* Removal of heavy metal ions from aqueous system by ion-exchange and biosorption methods. *Environmental Chemistry Letters* **17**, 729–754 (2019).

331. Gupta, B., Mishra, A., Singh, R. & Thakur, I. S. Fabrication of calcite based biocomposites for catalytic removal of heavy metals from electroplating industrial effluent. *Environmental Technology & Innovation* **21**, 101278 (2021).

332. Sunil, K. *et al.* Al-Ti2O6 a mixed metal oxide based composite membrane: A unique membrane for removal of heavy metals. *Chemical Engineering Journal* **348**, 678–684 (2018).

333. Shahrokhi-Shahraki, R., Benally, C., El-Din, M. G. & Park, J. High efficiency removal of heavy metals using tire-derived activated carbon vs commercial activated carbon: Insights into the adsorption mechanisms. *Chemosphere* **264**, 128455 (2021).

334. Zamora-Ledezma, C. *et al.* Heavy metal water pollution: A fresh look about hazards, novel and conventional remediation methods. *Environmental Technology & Innovation* **22**, 101504 (2021).

335. Omer, A. M., Dey, R., Eltaweil, A. S., Abd El-Monaem, E. M. & Ziora, Z. M. Insights into recent advances of chitosan-based adsorbents for sustainable removal of heavy metals and anions. *Arabian Journal of Chemistry* **15**, 103543 (2022).

336. Ramalingam, B., Parandhaman, T., Choudhary, P. & Das, S. K. Biomaterial Functionalized Graphene-Magnetite Nanocomposite: A Novel Approach for Simultaneous Removal of Anionic Dyes and Heavy-Metal Ions. *ACS Sustainable Chemistry & Engineering* **6**, 6328–6341 (2018).

337. Aigbe, U. O. *et al.* Fly ash-based adsorbent for adsorption of heavy metals and dyes from aqueous solution: a review. *Journal of Materials Research and Technology* **14**, 2751–2774 (2021).

338. Ma, J. *et al.* Rice husk derived double network hydrogel as efficient adsorbent for Pb(II), Cu(II) and Cd(II) removal in individual and multicomponent systems. *Bioresource Technology* **290**, 121793 (2019).

339. Shrestha, R. *et al.* Technological trends in heavy metals removal from industrial wastewater: A review. *Journal of Environmental Chemical Engineering* **9**, 105688 (2021).

340. Pyrzynska, K. Removal of cadmium from wastewaters with low-cost adsorbents. *Journal of Environmental Chemical Engineering* **7**, 102795 (2019).

341. Almasi, A., Omidi, M., Khodadadian, M., Khamutian, R. & Gholivand, M. B. Lead(II) and cadmium(II) removal from aqueous solution using processed walnut shell: kinetic and equilibrium study. *Toxicological & Environmental Chemistry* **94**, 660–671 (2012).

342. Gupta, V. K. & Nayak, A. Cadmium removal and recovery from aqueous solutions by novel adsorbents prepared from orange peel and Fe2O3 nanoparticles. *Chemical Engineering Journal* **180**, 81–90 (2012).

343. Jaishankar, M. *et al.* Toxicity, mechanism and health effects of some heavy metals. (2014) doi:10.2478/intox-2014-0009.

344. Guibal, E., Van Vooren, M., Dempsey, B. A. & Roussy, J. A Review of the Use of Chitosan for the Removal of Particulate and Dissolved Contaminants. *Separation Science and Technology* **41**, 2487–2514 (2006).

345. Mirabedini, M., Kassaee, M. Z. & Poorsadeghi, S. Novel Magnetic Chitosan Hydrogel Film, Cross-Linked with Glyoxal as an Efficient Adsorbent for Removal of Toxic Cr(VI) from Water. *Arabian Journal for Science and Engineering* **42**, 115–124 (2017).

346. Abdulhameed, A. S., Jawad, A. H. & Mohammad, A. K. T. Synthesis of chitosan-ethylene glycol diglycidyl ether/TiO2 nanoparticles for adsorption of reactive orange 16 dye using a response surface methodology approach. *Bioresource Technology* **293**, 122071 (2019).

347. Chiou, M. S. & Li, H. Y. Adsorption behavior of reactive dye in aqueous solution on chemical cross-linked chitosan beads. *Chemosphere* **50**, 1095–1105 (2003).

348. Nishad, P. A., Bhaskarapillai, A., Velmurugan, S. & Narasimhan, S. V. Cobalt (II) imprinted chitosan for selective removal of cobalt during nuclear reactor decontamination. *Carbohydrate Polymers* **87**, 2690–2696 (2012).

349. Zhang, M., Helleur, R. & Zhang, Y. Ion-imprinted chitosan gel beads for selective adsorption of Ag^{+} from aqueous solutions. *Carbohydrate Polymers* **130**, 206–212 (2015).

350. Elsayed, N. H., Monier, M. & Alatawi, R. A. S. Thiosemicarbazide-modified/ion-imprinted phenolic resin for selective uptake of cadmium ions. *Materials Chemistry and Physics* **264**, 124433 (2021).

351. Takezawa, N. & Mezaki, R. Langmuir-temkin-pyzhev rate models for ammonia decomposition reaction. *The Canadian Journal of Chemical Engineering* **48**, 428–431 (1970).

352. Collins, F. & Sanjayan, J. G. Effect of pore size distribution on drying shrinking of alkali-activated slag concrete. *Cement and Concrete Research* **30**, 1401–1406 (2000).

353. Monier, M. & Abdel-Latif, D. A. Fabrication of Au(III) ion-imprinted polymer based on thiol-modified chitosan. *International Journal of Biological Macromolecules* **105**, 777–787 (2017).

354. Loutfy, S. A. *et al.* Synthesis, Characterization and Cytotoxic Evaluation of Graphene Oxide Nanosheets: In Vitro Liver Cancer Model. *Asian Pac J Cancer Prev* **18**, 955–961 (2017).

355. Rodrigues, S., Costa, A. M. R. Da & Grenha, A. Chitosan/carrageenan nanoparticles: Effect of cross-linking with tripolyphosphate and charge ratios. *Carbohydrate Polymers* **89**, 282–289 (2012).

356. Yong, S. K., Bolan, N., Lombi, E. & Skinner, W. Synthesis and Characterization of Thiolated Chitosan Beads for Removal of Cu(II) and Cd(II) from Wastewater. *Water, Air, & Soil Pollution* **224**, 1720 (2013).

357. Cho, A. R., Chun, Y. G., Kim, B. K. & Park, D. J. Preparation of Chitosan-TPP Microspheres as Resveratrol Carriers. *Journal of Food Science* **79**, E568–E576 (2014).

358. Lee, S.-T., Mi, F.-L., Shen, Y.-J. & Shyu, S.-S. Equilibrium and kinetic studies of copper(II) ion uptake by chitosan-tripolyphosphate chelating resin. *Polymer (Guildf)* **42**, 1879–1892 (2001).

359. Vimal, S. *et al.* Synthesis and characterization of CS/TPP nanoparticles for oral delivery of gene in fish. *Aquaculture* **358–359**, 14–22 (2012).

360. Sutirman, Z. A., Sanagi, M. M., Abd Karim, K. J. & Wan Ibrahim, W. A. Preparation of methacrylamide-functionalized crosslinked chitosan by free radical polymerization for the removal of lead ions. *Carbohydrate Polymers* **151**, 1091–1099 (2016).

361. França, D., Medina, Â. F., Messa, L. L., Souza, C. F. & Faez, R. Chitosan spray-dried microcapsule and microsphere as fertilizer host for swellable − controlled release materials. *Carbohydrate Polymers* **196**, 47–55 (2018).

362. Ma, J. *et al.* Efficient removal of heavy metal ions with EDTA functionalized chitosan/polyacrylamide double network hydrogel. *ACS Sustainable Chemistry & Engineering* acssuschemeng.6b02181 (2016) doi:10.1021/acssuschemeng.6b02181.

363. Laus, R. *et al.* Competitive adsorption of Cu(II) and Cd(II) ions by chitosan crosslinked with epichlorohydrin-triphosphate. *Bioresource Technology* **102**, 8769–8776 (2011).

364. Swayampakula, K., Boddu, V. M., Nadavala, S. K. & Abburi, K. Competitive adsorption of Cu (II), Co (II) and Ni (II) from their binary and tertiary aqueous solutions using chitosan-coated perlite beads as biosorbent. *Journal of Hazardous Materials* **170**, 680–689 (2009).

365. Green-Ruiz, C., Rodriguez-Tirado, V. & Gomez-Gil, B. Cadmium and zinc removal from aqueous solutions by Bacillus jeotgali: pH, salinity and temperature effects. *Bioresource Technology* **99**, 3864–3870 (2008).

366. Kumar, M., Tripathi, B. P. & Shahi, V. K. Crosslinked chitosan/polyvinyl alcohol blend beads for removal and recovery of Cd(II) from wastewater. *Journal of Hazardous Materials* **172**, 1041–1048 (2009).

367. Sousa Neto, V. O. *et al.* Use of coconut bagasse as alternative adsorbent for separation of copper (II) ions from aqueous solutions: Isotherms, kinetics, and thermodynamic studies. *BioResources* **6**, 3376–3395 (2011).

368. Xiang, J., Lin, Q., Yao, X. & Yin, G. Removal of Cd from aqueous solution by chitosan coated MgO-biochar and its in-situ remediation of Cd-contaminated soil. *Environmental Research* **195**, 110650 (2021).

369. Wu, D. *et al.* Phosphorylated chitosan/CoFe2O4 composite for the efficient removal of Pb(II) and Cd(II) from aqueous solution: Adsorption performance and mechanism studies. *Journal of Molecular Liquids* **277**, 181–188 (2019).

370. Elanchezhiyan, S. S., Karthikeyan, P., Rathinam, K., Hasmath Farzana, M. & Park, C. M. Magnetic kaolinite immobilized chitosan beads for the removal of Pb(II) and Cd(II) ions from an aqueous environment. *Carbohydrate Polymers* **261**, 117892 (2021).

371. Pal, P. & Pal, A. Treatment of real wastewater: Kinetic and thermodynamic aspects of cadmium adsorption onto surfactant-modified chitosan beads. *International Journal of Biological Macromolecules* **131**, 1092–1100 (2019).

372. Chen, A. *et al.* Novel thiourea-modified magnetic ion-imprinted chitosan/TiO2 composite for simultaneous removal of cadmium and 2,4-dichlorophenol. *Chemical Engineering Journal* **191**, 85–94 (2012).

373. Abou El-Reash, Y. G., Otto, M., Kenawy, I. M. & Ouf, A. M. Adsorption of Cr(VI) and As(V) ions by modified magnetic chitosan chelating resin. *International Journal of Biological Macromolecules* **49**, 513–522 (2011).

374. Li, M., Zhang, Z., Li, R., Wang, J. J. & Ali, A. Removal of Pb(II) and Cd(II) ions from aqueous solution by thiosemicarbazide modified chitosan. *International Journal of Biological Macromolecules* **86**, 876–884 (2016).

375. da Cunha, J. M. *et al.* Cobalt recovery from leached solutions of lithium-ion batteries using waste materials as adsorbents. *Canadian Journal of Chemical Engineering* **93**, 2198–2204 (2015).

376. Arulkumar, M., Sathishkumar, P. & Palvannan, T. Optimization of Orange G dye adsorption by activated carbon of Thespesia populnea pods using response surface methodology. *Journal of Hazardous Materials* **186**, 827–834 (2011).

377. Chen, A. *et al.* Carbon disulfide-modified magnetic ion-imprinted chitosan-Fe(III): A novel adsorbent for simultaneous removal of tetracycline and cadmium. *Carbohydrate Polymers* **155**, 19–27 (2017).

378. Repo, E., Warchoł, J. K., Bhatnagar, A. & Sillanpää, M. Heavy metals adsorption by novel EDTA-modified chitosan–silica hybrid materials. *Journal of Colloid and Interface Science* **358**, 261–267 (2011).

379. Donia, A. M., Yousif, A. M., Atia, A. A. & Elsamalehy, M. F. Selective Separation of Hg^{2+} on Modified Crosslinked Chitosan Beads Enriched with Amine Groups. *Separation Science and Technology* **46**, 1638–1646 (2011).

380. Gerçel, Ö., Özcan, A., Özcan, A. S. & Gerçel, H. F. Preparation of activated carbon from a renewable bio-plant of Euphorbia rigida by H2SO4 activation and its adsorption behavior in aqueous solutions. *Applied Surface Science* **253**, 4843–4852 (2007).

381. Sutirman, Z. A., Sanagi, M. M., Abd Karim, K. J., Wan Ibrahim, W. A. & Jume, B. H. Equilibrium, kinetic and mechanism studies of Cu(II) and Cd(II) ions adsorption by modified chitosan beads. *International Journal of Biological Macromolecules* **116**, 255–263 (2018).

382. Vold, I. M. N., Vårum, K. M., Guibal, E. & Smidsrød, O. Binding of ions to chitosan—selectivity studies. *Carbohydrate Polymers* **54**, 471–477 (2003).

383. Huang, K., Li, J. & Xu, Z. Enhancement of the recycling of waste Ni-Cd and Ni-MH batteries by mechanical treatment. *Waste Management* **31**, 1292–1299 (2011).

384. Madala, S., Nadavala, S. K., Vudagandla, S., Boddu, V. M. & Abburi, K. Equilibrium, kinetics and thermodynamics of Cadmium (II) biosorption on to composite chitosan biosorbent. *Arabian Journal of Chemistry* **10**, S1883–S1893 (2017).

385. Tabelin, C. B. *et al.* Towards a low-carbon society: A review of lithium resource availability, challenges and innovations in mining, extraction and recycling, and future perspectives. *Minerals Engineering* **163**, 106743 (2021).

386. Piątek, J. *et al.* Toward Sustainable Li-Ion Battery Recycling: Green Metal-Organic Framework as a Molecular Sieve for the Selective Separation of Cobalt and Nickel. *ACS Sustainable Chemistry and Engineering* **9**, 9770–9778 (2021).

387. Kumar, A., Holuszko, M. & Espinosa, D. C. R. E-waste: An overview on generation, collection, legislation and recycling practices. *Resources, Conservation and Recycling* **122**, 32–42 (2017).

388. Reddy, B. R., Priya, D. N. & Park, K. H. Separation and recovery of cadmium(II), cobalt(II) and nickel(II) from sulphate leach liquors of spent Ni-Cd batteries using phosphorus based extractants. *Separation and Purification Technology* **50**, 161–166 (2006).

389. Yao, Y. *et al.* Hydrometallurgical Processes for Recycling Spent Lithium-Ion Batteries: A Critical Review. *ACS Sustainable Chemistry & Engineering* **6**, 13611–13627 (2018).

390. Wu, F.-C., Tseng, R.-L. & Juang, R.-S. A review and experimental verification of using chitosan and its derivatives as adsorbents for selected heavy metals. *J Environ Manage* **91**, 798–806 (2010).

391. Lü, H., An, H. & Xie, Z. Ion-imprinted carboxymethyl chitosan–silica hybrid sorbent for extraction of cadmium from water samples. *International Journal of Biological Macromolecules* **56**, 89–93 (2013).

392. Bhatnagar, A. & Sillanpää, M. Applications of chitin- and chitosan-derivatives for the detoxification of water and wastewater — A short review. *Advances in Colloid and Interface Science* **152**, 26–38 (2009).

393. Monier, M., Bukhari, A. A. H. & Elsayed, N. H. Designing and characterization of copper (II) ion-imprinted adsorbent based on isatin functionalized chitosan. *International Journal of Biological Macromolecules* **155**, 795–804 (2020).

394. Mao, J. *et al.* Ion-imprinted chitosan fiber for recovery of Pd(II): Obtaining high selectivity through selective adsorption and two-step desorption. *Environ Res* **182**, 108995 (2020).

395. Qin, L. *et al.* Preparation of ion-imprinted montmorillonite nanosheets/chitosan gel beads for selective recovery of Cu(II) from wastewater. *Chemosphere* **252**, 126560 (2020).

396. Monier, M., Bukhari, A. A. H. & Elsayed, N. H. Designing and characterization of copper (II) ion-imprinted adsorbent based on isatin functionalized chitosan. *International Journal of Biological Macromolecules* **155**, 795–804 (2020).

397. Babakhani, A. & Sartaj, M. Synthesis, characterization, and performance evaluation of ion-imprinted crosslinked chitosan (with sodium tripolyphosphate) for cadmium biosorption. *Journal of Environmental Chemical Engineering* **10**, 107147 (2022).

398. Ali, M. E. A., Aboelfadl, M. M. S., Selim, A. M., Khalil, H. F. & Elkady, G. M. Chitosan nanoparticles extracted from shrimp shells, application for removal of Fe(II) and Mn(II)

from aqueous phases. *Separation Science and Technology (Philadelphia)* **53**, 2870–2881 (2018).

399. Peng, J., Wang, X. & Lou, T. Preparation of chitosan/gelatin composite foam with ternary solvents of dioxane/acetic acid/water and its water absorption capacity. *Polymer Bulletin* **77**, 5227–5244 (2020).

400. Kaur, I., Goyal, D. & Agnihotri, S. Formulation of cartap hydrochloride crosslinked chitosan tripolyphosphate nanospheres and its characterization. *Colloid and Polymer Science* **299**, 1407–1418 (2021).

401. Monier, M. & Abdel-Latif, D. A. Fabrication of Au(III) ion-imprinted polymer based on thiol-modified chitosan. *International Journal of Biological Macromolecules* **105**, 777–787 (2017).

402. Bouhamed, F., Elouear, Z., Bouzid, J. & Ouddane, B. Multi-component adsorption of copper, nickel and zinc from aqueous solutions onto activated carbon prepared from date stones. *Environmental Science and Pollution Research* **23**, 15801–15806 (2016).

403. Chiban, M., Soudani, A., Sinan, F. & Persin, M. Single, binary and multi-component adsorption of some anions and heavy metals on environmentally friendly Carpobrotus edulis plant. *Colloids and Surfaces B: Biointerfaces* **82**, 267–276 (2011).

404. Gutierrez, M. & Fuentes, H. R. Modeling adsorption in multicomponent systems using a Freundlich-type isotherm. *Journal of Contaminant Hydrology* **14**, 247–260 (1993).

405. Vilela, P. B., Matias, C. A., Dalalibera, A., Becegato, V. A. & Paulino, A. T. Polyacrylic acid-based and chitosan-based hydrogels for adsorption of cadmium: Equilibrium isotherm, kinetic and thermodynamic studies. *Journal of Environmental Chemical Engineering* **7**, 103327 (2019).

406. Zhou, G., Liu, C., Chu, L., Tang, Y. & Luo, S. Rapid and efficient treatment of wastewater with high-concentration heavy metals using a new type of hydrogel-based adsorption process. *Bioresource Technology* **219**, 451–457 (2016).

407. Kong, X. *et al.* Evaluation of zeolite-supported microscale zero-valent iron as a potential adsorbent for Cd2+ and Pb2+ removal in permeable reactive barriers. *Environmental Science and Pollution Research 2017 24:15* **24**, 13837–13844 (2017).

408. Huang, Z., Wu, Q., Liu, S., Liu, T. & Zhang, B. A novel biodegradable β-cyclodextrin-based hydrogel for the removal of heavy metal ions. *Carbohydrate Polymers* **97**, 496–501 (2013).

409. Tran, H. N., You, S.-J. & Chao, H.-P. Thermodynamic parameters of cadmium adsorption onto orange peel calculated from various methods: A comparison study. *Journal of Environmental Chemical Engineering* **4**, 2671–2682 (2016).

410. Zhu, Y., Hu, J. & Wang, J. Competitive adsorption of Pb(II), Cu(II) and Zn(II) onto xanthate-modified magnetic chitosan. *Journal of Hazardous Materials* **221–222**, 155–161 (2012).

411. Futalan, C. M. *et al.* Comparative and competitive adsorption of copper, lead, and nickel using chitosan immobilized on bentonite. *Carbohydrate Polymers* **83**, 528–536 (2011).

412. Hadi, P., Barford, J. & McKay, G. Selective toxic metal uptake using an e-waste-based novel sorbent–Single, binary and ternary systems. *Journal of Environmental Chemical Engineering* **2**, 332–339 (2014).

413. Tran, H. N., You, S.-J., Hosseini-Bandegharaei, A. & Chao, H.-P. Mistakes and inconsistencies regarding adsorption of contaminants from aqueous solutions: A critical review. *Water Research* **120**, 88–116 (2017).

414. Qu, J. *et al.* Multi-component adsorption of Pb(II), Cd(II) and Ni(II) onto microwave-functionalized cellulose: Kinetics, isotherms, thermodynamics, mechanisms and application for electroplating wastewater purification. *Journal of Hazardous Materials* **387**, (2020).

415. Ricordel, S., Taha, S., Cisse, I. & Dorange, G. Heavy metals removal by adsorption onto peanut husks carbon: characterization, kinetic study and modeling. *Separation and Purification Technology* **24**, 389–401 (2001).

416. Sidhu, P. S., Gilkes, R. J. & Posner, A. M. The synthesis and some properties of Co, Ni, Zn, Cu, Mn and Cd substituted magnetites. *Journal of Inorganic and Nuclear Chemistry* **40**, 429–435 (1978).

417. Muzzarelli, R. A. A. Potential of chitin/chitosan-bearing materials for uranium recovery: An interdisciplinary review. *Carbohydrate Polymers* **84**, 54–63 (2011).

418. Ng, J. C. Y., Cheung, W. H. & McKay, G. Equilibrium Studies of the Sorption of Cu(II) Ions onto Chitosan. *Journal of Colloid and Interface Science* **255**, 64–74 (2002).

419. Zhou, L., Jia, Y., Peng, J., Liu, Z. & Al-Zaini, E. Competitive adsorption of uranium(VI) and thorium(IV) ions from aqueous solution using triphosphate-crosslinked magnetic chitosan resins. *Journal of Radioanalytical and Nuclear Chemistry* **302**, 331–340 (2014).

420. Walter, William. G. STANDARD METHODS FOR THE EXAMINATION OF WATER AND WASTEWATER (11th ed.). *American Journal of Public Health and the Nations Health* **51**, 940–940 (1961).